FINAL REPORT FOR NASA RESEARCH GRANT NAG-1-1134

by

John W. Norbury

Physics Department
Rider College
Lawrenceville, NJ 08648

This report describes the work that was performed on NASA research grant NAG-1-1134 at Rider College during the years 1990 - 1992. The report consists of a collection of papers (both published, unpublished and in progress) that were written during this period.

Most of the papers deal with electromagnetic processes in nucleus-nucleus collisions which are of concern in the space radiation program. In particular the removal of one and two nucleons via both electromagnetic and strong interaction processes has been extensively investigated. Also preliminary work has been completed concerning the creation of large numbers of electron-positron pairs that are created via two-photon processes in nucleus-nucleus collisions. The theory of relativistic Coulomb fission has also been developed.

Several papers on quark models also appear. These are of relevance because it has been discovered by the present author that in the cases where heavy-ion experiments disagree with theory a non-perturbative approach to QED is required. The method of dealing with the singularities that occur in quark models can be immediately applied to the non-perturbative QED problem.

Finally note that the theoretical methods developed in this work have been directly applied to the task of radiation protection of astronauts. This has been done by paramterizing the theoretical formalism in such a fashion that it can be used in cosmic ray transport codes. In particular these parameterizations now reside in the NUCFRAG code developed at NASA Langley Research Center.

The following papers are collected herein:

RESEARCH PUBLICATIONS

1. *Cross Section Parametrizations for Cosmic Ray Nuclei I. Single Nucleon Removal* (J.W. Norbury and L.W. Townsend)
   to be submitted to **Astrophysical Journal.**
2. *Solution of Two-Body Relativistic Bound State Equations with Confining plus Coulomb Interactions* (K.M. Maung, D.E. Kahana and J.W. Norbury)
   submitted to **Physical Review D.**
3. *Do Recent Observations of Very Large Electromagnetic Dissociation Cross Sections Signify a Transition to Non-Perturbative QED ?* (J.W. Norbury)
   submitted to **Physical Review Letters.**
4. *Effects of Retardation in Relativistic Equations with Confining Interaction*
   (K.M. Maung, D.E. Kahana and J.W. Norbury)
   preprint number **CEBAF-TH-91-21.**
5. *Two Neutron Removal in Relativistic Nucleus-Nucleus Reactions*
   (J.W. Norbury) **Physical Review C 45 3024 (1992).**
6. *Confining Potential in Momentum Space*
   (J.W. Norbury, D.E. Kahana and K.M. Maung)
   preprint number **CEBAF-TH-91-02, Canadian J. Physics 70 86 (1992).**
7. *Calculations of Hadronic Dissociation of ^{28}Si Projectiles at 14.6 AGeV by Nucleon Emission* (L.W. Townsend, J.W. Norbury and F. Khan)
   Physical Review C 43 R2045 (1991).
8. *Relativistic Coulomb Fission* (J.W. Norbury)
   Physical Review C 43 R368 (1991).
9. *Higgs Boson Production in Nucleus-Nucleus Collisions* (J.W. Norbury)
   Physical Review D 42 3696 (1990).
10. *Charge Dependence and Electric Quadrupole Effects on Single Nucleon Removal in Relativistic and Intermediate Energy Nuclear Collisions*
    (J.W. Norbury) **Physical Review C 42 2259 (1990).**
11. *Single Nucleon Emission in Relativistic Nucleus-Nucleus Collisions*
    (J.W. Norbury and L.W. Townsend) **Physical Review C 42 1775 (1990).**
12. *Electric Quadrupole Excitations in Relativistic Nucleus-Nucleus Collisions*
    (J.W. Norbury) **Physical Review C 42 711 (1990).**

NASA PUBLICATIONS

1. *Stopping Powers and Cross Sections due to Two-Photon Processes in Relativistic Nucleus-Nucleus Collisions* (W. Cheung and J.W. Norbury) **NASA Technical Paper** , submitted.
2. *Corrections to the Participant-Spectator Model of High Energy Alpha Particle Fragmentation* (F.A. Cucinotta, L.W. Townsend, J.W. Wilson and J.W. Norbury) **NASA Technical Memorandum 4262 (1991).**

BOOKS

1. *Transport Methods and Interactions for Space Radiations* (J.W. Wilson, L.W. Townsend, W.S. Schimmerling, G.S. Khandelwal, F. Khan, J.E. Nealy, F.A. Cucinotta, L.C. Simonsen, J.L. Shinn and J.W. Norbury) **NASA Reference Publication 1257 (1991).**

OTHER

1. An Introduction to using the Fortran codes provided with "Computational Nucelar Physics I" (M. Boytos and J.W. Norbury)

2. An Experiment to Study Strong Electromagnetic Fields at RHIC (M. Fatyga and J.W. Norbury) Proc. Fourth Workshop on Experiments and Detectors for a Relativistic Heavy Ion Collider p.345 (1990) edited by M. Fatyga and B. Moskowitz

3. A Letter of Intent for an Experiment to study Strong Electromagnetic Fields at RHIC via Multiple Electromagnetic Processes (M. Fatyga and J.W. Norbury) Letter of Intent submitted to RHIC management (1992).

Acknowledgements:

The following students and staff at Rider College have contributed to the work listed in this report: Dr. W. Cheung, Mr. M. Boytos and Mr. D. Goldstein. I also wish to thank the following individuals who have helped in many ways: Drs. L. Townsend, F. Cucinotta, K. Maung Maung, D. Kahana, W. Buck, F. Khan, J. Wilson, R. Tripathi, E. Conway, F. Gross, H. Takai, W. Llope, P. Braun-Munzinger, M. Fatyga, G. Baur, C. Bertulani, J. Hill, P. Deutchman, G. Satchler, J. Vary, C. Benesh and F. Wohn

CROSS SECTION PARAMETRIZATIONS FOR COSMIC RAY NUCLEI I. SINGLE NUCLEON REMOVAL.

by

John W. Norbury

Physics Department
Rider College
Lawrenceville, NJ 08648

and

Lawrence W. Townsend

NASA Langley Research Center
Hampton, VA 23665

ABSTRACT

Paramterizations of single nucleon removal from the electromagnetic and strong interactions of cosmic rays with nuclei are presented. These parametrizations are based upon the most accurate theoretical calculations available to date. They should be very suitable for use in cosmic ray propogation through interstellar space, the Earth's atmosphere, lunar samples, meteorites, spacecraft walls and lunar and martian habitats.

PACS: 97.70.S, 96.40.De

I. INTRODUCTION

Galactic cosmic rays (Shapiro 1983, Friedlander 1989) are very high energy particles confined to the region of our Milky Way galaxy. They consist of about 98% fully stripped nuclei including protons and alpha particles, and about 2% electrons and positrons (Simpson 1983). Of the nuclear component, about 87% is hydrogen, about 12% is helium and the other 1% consists of heavier nuclei. Of these heavier nuclei, the CNO group and Fe are the most abundant with a typical energy of about 1 GeV/N. Even though these heavy nuclei are not very abundant, they are very penetrating due to their large mass and high speed.

An understanding of the interactions of galactic cosmic ray nuclei with not only hydrogen and helium but also with heavier nuclei is important for several reasons:

!. Knowledge of the cosmic ray spectrum at the top of the Earth's atmosphere and knowledge of the composition of the interstellar medium and heliosphere enables one to determine the cosmic ray spectrum at the source (Simpson 1983). The interstellar medium (Field 1986) consists primarily of hydrogen and helium so that cosmic ray interactions with these nuclei are the most important (Austin 1981; Ferrando et al 1988). However carbon, nitrogen and oxygen are also present in the interstellar medium (Morton 1975; Karttunen, Kroger, Oja, Poutanen and Donner 1987) and one anticipates that the understanding of cosmic ray interactions with these heavier nuclei may be needed in the future.

2. Knowledge of the spectrum at high altitude and knowledge of the composition of the Earth's atmosphere enables one to determine the cosmic ray spectrum at the top of the

atmosphere (Wilson, Townsend and Badavi 1987a).

3. The radiation environment inside a spacecraft, due to solar and galactic cosmic rays may be determined (Wilson and Townsend 1988). Such knowledge is important for lunar and martian habitats and other long duration space flights (National Council on Radiation Protection and Measurements 1989; Joselyn and Whipple 1990; Rester and Trombka 1989).

4. Studies of the history of extraterrestrial matter (such as lunar samples, meteorites and cosmic spherules and dust found in deep sea sediments) and also of the history of cosmic rays themselves can be made with the knowledge of the production rate of various nuclides (Reedy 1987; Reedy, Arnold and Lal 1983).

5. Cross section parametrizations of cosmic ray nuclei interacting with arbitrary target nuclei including those targets heavier than helium are required in the interpretation of emulsion data and in the the interactions of cosmic rays with air. (Gaisser 1990; Gaisser, Stanev, Freier and Waddington 1982; Gaisser and Stanev 1983, Shapiro and Silberberg 1970).

The basic nucleus-nucleus interaction that a cosmic ray undergoes can occur mainly via the Strong or Electromagnetic (EM) force. (Actually the study of nucleus-nucleus collisions *began* in cosmic ray studies (Goldhaber and Heckman 1978; Bradt and Peters 1948, 1949, 1950; Kaplan, Peters, Reynolds, and Ritson 1952).) Strong interaction processes (Goldhaber and Heckman 1978; Gyulassy 1981; Benesh, Cook and Vary 1989) have been studied extensively and quite recently the study of Electromagnetic processes in

high energy collisions has begun (Bertulani and Baur 1988).

To study the propagation of cosmic rays through interstellar space, the Earth's atmosphere or a spacecraft wall it is not enough to have a good understanding of the nucleus-nucleus interaction cross section as input to a transport computer code (Wilson, Townsend, Schimmerling, Khandelwal, Khan, Nealy, Cucinotta, Simonsen, Shinn and Norbury 1991). These codes can be very complex and therefore require simple expressions for the cross sections rather than the use of large data bases or complicated theoretical models (Wilson and Townsend 1988). Thus there has been a considerable effort to parameterize the cross section expressions so that the only required inputs are the nuclear energies and charge and mass numbers (Letaw, Silberberg and Tsao 1983; Silberberg and Tsao 1973, 1990; Townsend and Wilson 1986; Norbury, Cucinotta, Townsend and Badavi 1988; Wilson, Townsend and Badavi 1987a,b).

In order to understand cosmic ray transport through the interstellar medium, the early work on parametrizations (Rudstam 1966; Letaw, Silberberg and Tsao 1983; Silberberg and Tsao 1973, 1990) concentrated primarily on proton-nucleus interactions due to the fact that the interstellar medium consists primarily of hydrogen. However based on the 5 items listed above it would also be very useful for a wide variety of cosmic ray studies to have accurate parametrizations for *any* nucleus-nucleus interaction. It is the aim of the present work to provide such a parametrization. Actually such parametrizations (Wilson, Townsend and Badavi 1987b) have already been formulated and give good results for the removal of *many* nucleons. However for removal of only a *few* nucleons from heavy nuclei, the parametrizations (Wilson, Townsend and Badavi 1987b) sometimes give poor results. In fact *a whole new approach to the parametrization of few-nucleon removal cross sections in nucleus-nucleus interactions is required. In the present paper an*

accurate parametrization of single-nucleon removal cross sections is presented. Future work will discuss the removal of more nucleons. When this program is completed we will have available accurate parametrizations of few-nucleon removal cross sections in nucleus-nucleus interactions. When combined with the many-nucleon removal paramterizations (Silberberg, Tsao and Shapiro 1976; Wilson, Townsend and Badavi 1987b) and proton-nucleus parametrizations (Letaw, Silberberg and Tsao 1983; Silberberg and Tsao 1973, 1990), there will be available accurate cross section parametrizations for arbitrary cosmic ray species interacting with arbitrary media. See also the work of Webber et al (1990).

One approach to the parametrization of cross sections is to simply take all the available experimental data and fit a curve through it. However such an approach often requires a large number of adjustable parameters and may not be applicable to regimes where experiments have not been performed. A much more satisfying approach is to base one's parametrization on a physical theory or model that successfully describes the experimental data as well. This will be the approach of the present work. The various models and theories that have been developed will be collected together and parameterized. The whole method will require only *one* adjustable parameter (x_d in equation 29). Furthermore this parameter is not essential. Good results are obtained without it. It is only introduced to provide some fine tuning.

A preliminary parametrization of the EM process has already been presented (Norbury, Cucinotta, Badavi 1988), which utilizes the Weizsacker-Williams (WW) method of virtual quanta (Bertulani and Baur 1988; Jackson 1975). However, since then the theory has been improved to include the effects of both electric dipole (E1) and electric quadrupole (E2) interactions (Bertulani and Baur 1988; Norbury 1990a,b), which will henceforth be referred to as multipole theory in contrast to WW theory. In addition Benesh, Cook and

Vary (1989) have recently provided a parametrization of the strong interaction single nucleon removal cross section.

II. STRONG INTERACTION PARAMETRIZATION

The parametrization due to Benesh, Cook and Vary (1989) is

$$\sigma(N) = \frac{N}{A} \sigma_G P_{esc} \tag{1a}$$

for single neutron removal where N is the number of neutrons and A is the number of nucleons and

$$\sigma(Z) = \frac{Z}{A} \sigma_G P_{esc} \tag{1b}$$

for single proton removal where Z is the number of protons. See also Norbury and Townsend (1990). σ_G is the reaction cross section given by

$$\sigma_G = 2\pi (b_c - \frac{\Delta b}{2}) \Delta b \tag{2}$$

where

$$\Delta b = 0.5 \text{ fm} \tag{3}$$

and the critical impact parameter for single nucleon removal is

$$b_c = 1.34 \text{ fm } [A_P^{1/3} + A_T^{1/3} - 0.75(A_P^{-1/3} + A_T^{-1/3})] \quad (4)$$

with A_P and A_T being the projectile and target nucleon numbers respectively. The single nucleon escape probability is

$$P_{esc} = (1 - f) + f \exp^{-\nu} \quad (5)$$

with

$$f = \frac{1}{2}(1 - \cos \theta_{max}) \quad (6)$$

and

$$\sin \theta_{max} = \frac{b_c' - \Delta b}{b_c'} \quad (7)$$

and

$$\nu = \frac{A \sigma_{NN}}{\pi b_c'^2} \quad (8)$$

where A is the nucleon number of the nucleus from which the nucleon is being removed, and b_c' is the critical impact parameter for the single nucleon escaping and is given by b_c in equation (4) but with $A_T = 1$ (or $A_P = 1$) if the nucleon is escaping from the projectile (or target). Thus the escape probability is independent of A_T (or A_P) as one would expect. σ_{NN} is the nucleon-nucleon cross section which has been parameterized as (Wilson, Townsend, Nealy, Chun, Hong, Buck, Lamkin, Ganapol, Khan and Cucinotta 1989)

$$\sigma_{NN} = (1 + \frac{5}{T_{lab}}) \{40 + 109 \cos(0.199\pi\sqrt{E}/180) \exp[-0.451(T_{lab} - 25)^{0.258}] \} \text{ mb} \quad (9)$$

for $T_{lab} \geq 25$ MeV and as

$$\sigma_{NN} = \exp [6.51 \exp (T_{lab}/134)^{0.7}] \qquad \text{mb} \tag{10}$$

for $T_{lab} < 25$ MeV.

Note that the energy dependence of the strong interaction cross section is totally contained in equation (9). Because of the exponential factor in (5) this energy dependence is rather weak as one would expect.

III. ELECTROMAGNETIC THEORY

The EM theory has already been discussed extensively (Bertulani and Baur 1988; Norbury 1989, 1990a,b) and only a few relevant details will be given here. The total nucleus-nucleus EM cross section is written as

$$\sigma = \sigma_{E1} + \sigma_{E2} = \int [N_{E1}(E)\sigma_{E1}(E) + N_{E2}(E)\sigma_{E2}(E)] \, dE \tag{11}$$

where $N_{Ei}(E)$ is the virtual photon spectrum (of energy E) of a particular multipolarity i due to the projectile nucleus and $\sigma_{E1}(E) + \sigma_{E2}(E)$ is the photonuclear reaction cross section of the target nucleus. (In principle the above equation should include other EM multipoles, but their effect is much less important.) A less exact expression is given by WW theory as

$$\sigma_{WW} = \int N_{WW}(E)\,[\sigma_{E1}(E) + \sigma_{E2}(E)]\,dE \qquad (12)$$

where $N_{WW}(E)$ is the WW virtual photon spectrum. Bertulani and Baur (1988) have shown that

$$N_{WW}(E) = N_{E1}(E) = \frac{1}{E}\frac{2}{\pi} Z^2 \alpha \frac{1}{\beta^2}\left[\xi K_0 K_1 - \frac{1}{2}\xi^2 \beta^2 (K_1^2 - K_0^2)\right] \qquad (13)$$

and

$$N_{E2}(E) = \frac{1}{E}\frac{2}{\pi} Z^2 \alpha \frac{1}{\beta^4}\left[\, 2(1-\beta^2)K_1^2 + \xi(2-\beta^2)^2 K_0 K_1 - \frac{1}{2}\xi^2\beta^4(K_1^2 - K_0^2)\right] \qquad (14)$$

with

$$\xi = \frac{E\, b_{min}}{\gamma \beta\, (\hbar c)} \qquad (15)$$

where all of the modified Bessel functions K are functions of ξ. In the above equations E is the virtual photon energy, Z is the nuclear charge, α is the EM fine structure constant, and b_{min} is the minimum impact parameter, below which the collision occurs via the Strong interaction. Also $\beta = \frac{v}{c}$ and $\gamma = \frac{1}{\sqrt{1-\beta^2}}$ where c is the speed of light and v is the speed of the cosmic ray. The minimum impact parameter is given by

$$b_{min} = b_c + \frac{\pi\, a_0}{2\gamma} \qquad (16)$$

where

$$a_0 = \frac{Z_P Z_T e^2}{m_0 v^2} \tag{17}$$

allows for deviation of the trajectory from a straight line (Aleixo and Bertulani 1989).

In equation (11) the photonuclear cross sections satisfy the following sum rules (Bertulani and Baur 1988):

$$\int \sigma_{E1}(E)\, dE = 60 \frac{N Z}{A} \text{ MeV mb} \tag{18}$$

and

$$\int \sigma_{E2}(E) \frac{dE}{E^2} = F\, 0.22\, Z\, A^{2/3} \quad \frac{\mu b}{MeV} \tag{19}$$

where F is the fractional exhaustion of this energy-weighted sum rule. The latter expression is the sum rule for the *isoscalar* E2 giant resonance. The *isovector* E2 resonance is ignored as it decays mainly by 2-nucleon emission (Bertulani and Baur 1988).

IV. ELECTROMAGNETIC PARAMETRIZATION

Because the photonuclear cross sections $\sigma_{E1}(E)$ and $\sigma_{E2}(E)$ are Lorentzian shaped, they behave somewhat like delta functions. The integrals of equation (11) can be approximated by taking $N_{E1}(E)$ and $N_{E2}(E)$ outside the integrals as (Bertulani and Baur 1988):

$$\sigma \approx N_{E1}(E_{GDR}) \int \sigma_{E1}(E)\, dE + N_{E2}(E_{GQR})\, E_{GQR}^2 \int \sigma_{E2}(E)\, \frac{dE}{E^2} \qquad (20)$$

and the integrals are evaluated using the sum rules in equations (18) and (19). In the above equation E_{GDR} and E_{GQR} are the central energies of the E1 and E2 photonuclear cross sections given by (Westfall, Wilson, Lindstrom, Crawford, Greiner and Heckman 1979)

$$E_{GDR} = \bar{h}c \left[\frac{m^* c^2 R_0^2}{8 J} (1 + u - \frac{1 + \varepsilon + 3u}{1 + \varepsilon + u} \varepsilon) \right]^{-1/2} \qquad (21)$$

with

$$u = \frac{3 J}{Q'} A^{-1/3} \qquad (22)$$

and

$$R_0 = r_0 A^{1/3} \qquad (23)$$

where $\varepsilon = 0.0768$, $Q' = 17$ MeV, $J = 36.8$ MeV, $r_0 = 1.18$ fm, and m^* is 7/10 of the nucleon mass. Note that other expressions for E_{GDR} such as $80\ A^{-1/3}$ (Bertulani and Baur 1988) provide very inaccurate results for light nuclei. Equation (21) is accurate for all mass regions. The central energy of the E2 resonance is simply

$$E_{GQR} = \frac{63}{A^{1/3}} \text{ MeV} \qquad (24)$$

In addition the fractional exhaustion of the Energy-Weighted Sum Rule in equation (19) is given by (Bertrand 1976)

$$f = 0.9 \text{ for } A > 100$$
$$= 0.6 \text{ for } 40 < A \leq 100$$
$$= 0.3 \text{ for } 40 \leq A \qquad (25)$$

Finally, to obtain the reaction cross section for proton or neutron removal the above cross sections must be multiplied by the proton or neutron branching ratios. The proton branching ratio has been parameterized by Westfall, Wilson, Lindstrom, Crawford, Greiner and Heckman (1979) as

$$g_p = \min \left[\frac{Z}{A}, 1.95 \exp(- 0.075 Z) \right] \qquad (26)$$

where Z is the number of protons and the minimum value of the two quantities in square brackets is to be taken. Assuming that only single nucleon removal occurs, the neutron braching ratio is

$$g_n = 1 - g_p \qquad (27)$$

For light nuclei however the following branching ratios are used instead of equation (26)

$$g_p = 0.5 \quad \text{for} \quad Z < 6$$
$$= 0.6 \quad \text{for} \quad 6 \leq Z \leq 8$$
$$= 0.7 \quad \text{for} \quad 8 < Z < 14 \qquad (28)$$

Lastly, an adjustable parameter (the only one in the whole parametrization!) is introduced as $x_d = 0.25$ where

$$b_{min} = (1 + x_d)\, b_c + \frac{\pi\, a_0}{2\,\gamma} \qquad (29)$$

in place of equation (16).

Finally, if one is interested in a very quick calculation for estimation purposes we shall write down an approximate "pocket" formula which does not require the evaluation of the Bessel functions in (13) and (14). Using the low and high frequency approximations for the dipole photon spectrum (Jackson, 1975) and ignoring quadrupole effects, equation (20) can be written approximately as

$$\sigma \approx \frac{1}{E_{GDR}} \frac{2}{\pi} Z^2 \alpha \frac{1}{\beta^2} \left[\ln \left(\frac{1.123 \gamma \bar{\hbar} c \beta}{E_{GDR}\, b_{min}} \right) - \frac{1}{2} \beta^2 \right] \qquad \text{for } E_{GDR} < \frac{\gamma \bar{\hbar} c \beta}{b_{min}}$$

$$\approx \frac{1}{E_{GDR}} Z^2 \alpha \frac{1}{\beta^2} \left(1 - \frac{1}{2} \beta^2 \right) \exp(-2 E_{GDR} b_{min} / \gamma \bar{\hbar} c \beta) \qquad \text{for } E_{GDR} \geq \frac{\gamma \bar{\hbar} c \beta}{b_{min}} \qquad (30)$$

This EM formula, combined with the Strong interaction parameterization, gives a very simple "pocket" formula which may also be useful in complicated versions of transport codes that have CPU time at a premium. However to get a good fit to data one must use $x_d = -0.1$ in (30).

V. RESULTS AND CONCLUSIONS

The cross section parametrizations are compared with the existing nucleus-nucleus experimental data in Tables I - III. It can be seen that the overall agreement is extremely good for a very wide variety of projectiles, targets and energies. There are however a few notable discrepancies particularly for ^{197}Au targets in Table II. It should be

noted however that these discrepancies are not due to the parametrization per se. Similar discrepancies are observed in comparisons between the original theory and experiment (Norbury 1989, 1990a, 1990b, Norbury and Townsend 1990, Benesh, Cook and Vary 1989, Hill, Wohn, Schwellenbach and Smith 1991). It is not clear whether these discrepancies are due to theoretical or experimental problems and their resolution is a matter of ongoing research.

In summary a parametrization of single nucleon removal cross sections for nucleus-nucleus collisions has been developed which accurately reproduces the experimental data for a wide range of nuclear species and energies. Future work will be devoted to few nucleon removal. Combining this with the many nucleon removal parametrizations (Wilson, Townsend and Badavi 1987b) and the proton-nucleus parametrizations (Letaw, Silberberg and Tsao 1983; Silberberg and Tsao 1973, 1990) provides a very useful parametrization of arbitrary cosmic ray species interacting with an arbitrary medium.

Acknowledgements

This work was supported in part by NASA grant number NAG-1-1134. We wish to thank F. Cucinotta for many useful discussions. JWN would also like to thank W. Cheung, M. Boytos and D. Goldstein who have participated in various aspects of this work.

REFERENCES

Aleixo, A.N.F., and Bertulani, C.A. 1989, Nucl. Phys. A **505**, 448.

Austin, S.M. 1981, Prog. Part. Nucl. Phys. **7**, 1.

Barrette, J., Braun-Munzinger, P., Cleland, W.E., David, G., Duek, E., Fatyga, M., Fox, M., Greene, S.V., Hall, J.R., Heifetz, R., Hemmick, T.K., Herrmann, N., Hogue, R.W., Ingold, G., Jayananda, K., Kraus, D., Legault, A., Lissauer, D., Muthuswamy, M., O'Brien, E., Olsen, L.H., Polychronakos, V., Rawool-Sullivan, M., Rotondo, F.S., Sandweiss, J., Shivakumar, B., Simon, J., Sonnodara, U., Stachel, J., Sunier, J., Takai, H., Throwe, T.G., VanHecke, H., Waters, L., Willis, W.J., Wolf, K., Wolfe, D., and Woody, C.L. 1990, Phys. Rev. C **41**,1512.

Benesh, C.J., Cook, B.C., and Vary, J.P. 1989, Phys. Rev. C **40**, 1198.

Bertrand, F.E. 1976, Ann. Rev. Nucl. Sci., **26**, 457.

Bertulani, C.A., and Baur, G. 1988, Phys. Rep.,**163**, 299.

Bradt, H.L., and Peters, B. 1948, Phys. Rev., **74** , 1828.

Bradt, H.L., and Peters, B. 1949, Phys. Rev., **75**, 1779.

Bradt, H.L., and Peters, B. 1950, Phys. Rev., **77**, 54; **80**, 943.

Ferrando, P., Webber W.R., Goret, P., Kish, J.C., Schrier, D.A., Soutoul, A., and Testard, O. 1988, Phys. Rev. C **37**, 1490.

Field, G.B. 1986, in *Highlights of Modern Astrophysics: Concepts and Controversies*, Shapiro, S.L., and Teukolsky, S.A. (editors), Wiley, New York.

Friedlander, M.W. 1989, *Cosmic Rays*, Harvard University Press, Cambridge, Massachusetts.

Gaisser, T.K. 1990, *Cosmic Rays and Particle Physics*, Cambridge University Press, New York.

Gaisser, T.K., Stanev, T., Freier, P., and Waddington, C.J. 1982, Phys. Rev. D **25**, 2341.

Gaisser, T.K., and Stanev, T. 1983, Phys. Rev. D **28**, 464.

Goldhaber, A.S., and Heckman, H.H. 1978, Ann. Rev. Nucl. Part. Sci., **28**, 161.

Gyulassy, M. 1981, Nucl. Phys. A **354**, 395.

Heckman, H.H., and Lindstrom, P.J., 1976, Phys. Rev. Lett. **37**, 56.

Hill, J.C., Wohn, F.K., Schwellenbach, D.D., and Smith, A.R. 1991, Phys. Lett. B **273**, 371.

Hill, J.C., Wohn, F.K., Winger, J.A., and Smith, A.R. 1988, Phys. Rev. Lett. **60**, 999.

Hill, J.C., Wohn, F.K., Winger, J.A., Khayat, M., Leininger, K., and Smith, A.R. 1988, Phys. Rev. C **38**, 1722.

Hill, J.C. 1988 in *Current Issues in Hadron Physics* edited by J.Tran Thanh Van, Proc. XX111 rd Recontre de Moriond (Editions Frontieres, 1988).

Jackson, J.D. 1975, *Classical Electrodymanics*, Wiley, New York.

Joselyn, J.A., and Whipple, E.C. 1990, American Scientist **78**, 126.

Kaplan, M.F., Peters, B., Reynolds, H.L., and Ritson, D.M. 1952, Phys. Rev. **85**, 295.

Karttunen, H., Kroger, P., Oja, H., Poutanen, M., and Donner, K.J. (editors) 1987, *Fundamental Astronomy*, Springer-Verlag, New York.

Letaw, J.R., Silberberg, R., and Tsao, C.H. 1983, Ap. J. Suppl., **51**, 271.

Levinger, J.S. 1960, *Nuclear Photo-Disintegration*, Oxford University Press, London.

Loveland, W., Xu, Z., Casey, C., Aleklett, K., Liljenzin, J.D., Lee, D., and Seaborg, G.T. 1988, Phys. Rev. C **38**, 2094.

Mercier, M.T., Hill, J.C., Wohn, F.K., McCullough, C.M., Nieland, M.E., Winger, J.A., Howard, C.B., Renwick, S., and Matheis, D.K.1986, Phys. Rev. C **33**, 1655.

Morton, D.C. 1975, Ap. J. **197**, 85.

National Council on Radiation Protection and Measurements 1989, *Guidance on Radiation*

Received in Space Activities, NCRP Report No. 98, Bethesda, Maryland.

Norbury, J.W. 1989, Phys. Rev. C **40**, 2621.

Norbury, J. W. 1990a, Phys. Rev. C **41**, 372.

Norbury, J. W. 1990b, Phys. Rev. C **42**, 711, 2259.

Norbury, J. W., and Townsend, L.W. 1990, Phys. Rev. C **42**, 1775.

Norbury, J.W., Cucinotta, F.A., Townsend , L.W., and Badavi, F.F. 1988, Nucl. Inst. Meth. Phys. Res. B **31**, 535.

Olson, D.L., Berman, B.L., Greiner, D.E., Heckman, H.H., Lindstrom, P.J., Westfall, G.D., and Crawford, H.J. 1981, Phys. Rev. C **24**, 1529.

Reedy, R.C. 1987, Nucl. Inst. Meth. Phys. Res. B **29**, 251.

Reedy, R.C., Arnold, J.R., and Lal, D. 1983, Ann. Rev. Nucl. Part. Sci. **33**, 505.

Rester, A.C., and Trombka, J.I. 1989, *High-Energy Radiation Background in Space*, AIP Conference Proceedings 186, American Institute of Physics, New York.

Rudstam, G. 1966, *Zs. Naturforschung*, **21a**, 1027.

Shapiro, M.M. (editor) 1983, *Composition and Origin of Cosmic Rays*, NATO ASI Series, D. Reidel Publishing Company, Dordrecht, Holland.

Shapiro, M.M., and Silberberg, R. 1970, Ann. Rev. Nucl. Sci. **20**, 323.

Silberberg, R., and Tsao, C.H. 1973, Ap. J. Suppl. **25**, 315, 335.

Silberberg, R., Tsao, C.H. and Shapiro, M.M. 1976, Semiempirical Cross Sections and Applications to Nuclear Interactions of Cosmic Rays. *Spallation Nuclear Reactions and Their Applications*, B.S.P. Shen and M. Merker, eds., D. Reidel Publ. Co., pp.49 - 81.

Silberberg, R., Tsao, C.H., and Letaw, J.R. 1985, Ap. J. Suppl. **58**, 873.

Silberberg, R., and Tsao, C.H. 1990, Phys. Rep. **191**, 351.

Simpson, A.R. 1983, Ann. Rev. Nucl. Part. Sci., **33**, 323.

Smith, A.R., Hill, J.C., Winger, J.A., and Karol, P.J. 1988, Phys. Rev. C **38**, 210.

Townsend, L.W., and Wilson, J.W. 1986, Radiation Research, **106**, 283.

Webber, W.R., Kish,J.C. 1990, and Schrier, D.A. Phys Rev. C **41**, 520, 533, 547, 566.

Westfall, G.D., Wilson, L.W., Lindstrom, P.J., Crawford, H.J., Greiner, D.E., and Heckman, H.H. 1979, Phys. Rev. C**19**, 1309.

Wilson, J.W., and Townsend, L.W. 1988, Radiation Research, **114**, 201.

Wilson, J.W., Townsend, L.W., and Badavi, F.F. 1987a, Radiation Research, **109**, 173.

Wilson, J.W., Townsend, L.W., and Badavi, F.F. 1987b, Nucl. Inst. Meth. Phys. Res. B **18**, 225.

Wilson, J.W., Townsend, L.W., Nealy, J.E., Chun, S.Y., Hong, B.S., Buck, W.W., Lamkin, S.L., Ganapol, B.D., Khan, F., and Cucinotta, F.A. 1989 NASA Technical Paper 2887.

Wilson, J.W., Townsend, L.W., Schimmerling, W., Khandelwal, G.S., Khan, F., Nealy, J.E., Cucinotta, F.A., Simonsen, L.C., Shinn, J.L., and Norbury, J.W. 1991, NASA Reference Publication 1257.

Table I Electromagnetic (EM) Cross Sections for single neutron and single proton removal. σ^{EM}_{expt} are the experimental EM cross sections from Olson et al 1981, Heckman and Lindstrom 1976, Barrette et al 1990 and Hill 1988. σ^{EM}_{param} is the parameterized EM cross section discussed in the text. Values in parentheses use the EM pocket formula.

Projectile	Target	T_{lab} (GeV/N)	Final State	σ^{EM}_{expt} (mb)	σ^{EM}_{param} (mb)
^{12}C	Pb	2.1	^{11}C	51 ± 18	48 (57)
^{12}C	Pb	2.1	^{11}B	50 ± 25	72 (86)
^{12}C	Pb	1.05	^{11}C	39 ± 24	26 (17)
^{12}C	Pb	1.05	^{11}B	50 ± 25	39 (26)
^{16}O	Pb	2.1	^{15}O	50 ± 24	71 (85)
^{16}O	Pb	2.1	^{15}N	96 ± 26	106 (127)
^{12}C	Ag	2.1	^{11}C	21 ± 10	20 (24)
^{12}C	Ag	2.1	^{11}B	18 ± 13	30 (36)
^{12}C	Ag	1.05	^{11}C	21 ± 10	12 (12)
^{12}C	Ag	1.05	^{11}B	25 ± 19	18 (18)
^{16}O	Ag	2.1	^{15}O	26 ± 13	29 (35)
^{16}O	Ag	2.1	^{15}N	30 ± 16	43 (53)
^{12}C	Cu	2.1	^{11}C	10 ± 7	9 (11)
^{12}C	Cu	2.1	^{11}B	4 ± 8	13 (16)
^{12}C	Cu	1.05	^{11}C	9 ± 8	6 (6)
^{12}C	Cu	1.05	^{11}B	5 ± 8	8 (10)
^{16}O	Cu	2.1	^{15}O	9 ± 8	13 (16)
^{16}O	Cu	2.1	^{15}N	15 ± 8	19 (23)

Table I continued

Projectile	Target	T_{lab} (GeV/N)	Final State	σ^{EM}_{expt} (mb)	σ^{EM}_{param} (mb)
^{12}C	Al	2.1	^{11}C	0 ± 5	2 (3)
^{12}C	Al	2.1	^{11}B	0 ± 5	3 (4)
^{12}C	Al	1.05	^{11}C	1 ± 6	2 (2)
^{12}C	Al	1.05	^{11}B	1 ± 7	2 (3)
^{16}O	Al	2.1	^{15}O	0 ± 5	3 (4)
^{16}O	Al	2.1	^{15}N	-1 ± 9	5 (6)
^{12}C	C	2.1	^{11}C	-2 ± 5	1 (1)
^{12}C	C	2.1	^{11}B	-1 ± 4	1 (1)
^{12}C	C	1.05	^{11}C	-2 ± 5	0 (1)
^{12}C	C	1.05	^{11}B	-2 ± 5	1 (1)
^{16}O	C	2.1	^{15}O	-1 ± 4	1 (1)
^{16}O	C	2.1	^{15}N	-1 ± 4	1 (1)
^{18}O	Ti	1.7	^{17}O	8.7 ± 2.7	8 (10)
^{18}O	Ti	1.7	^{17}N	-0.5 ± 1.0	12 (15)
^{18}O	Pb	1.7	^{17}O	136 ± 2.9	69 (79)
^{18}O	Pb	1.7	^{17}N	20.2 ± 1.8	103 (118)
^{18}O	U	1.7	^{17}O	140.8 ± 4.1	82 (92)
^{18}O	U	1.7	^{17}N	25.1 ± 1.6	123 (138)
^{32}S	^{197}Au	200	^{196}Au	1120 ± 160	1274 (1297)
^{28}Si	^{27}Al	13.7	1p	37 ± 5	25 (28)
^{28}Si	^{27}Al	13.7	1n	15 ± 4	12 (13)
^{28}Si	^{120}Sn	13.7	1p	313 ± 4	325 (370)
^{28}Si	^{120}Sn	13.7	1n	136 ± 6	151 (172)
^{28}Si	^{208}Pb	13.7	1p	743 ± 27	822 (942)
^{28}Si	^{208}Pb	13.7	1n	347 ± 18	383 (438)

Table II Total (= EM + Nuclear) Cross Sections for single neutron removal. σ^{Tot}_{expt} are the experimental total cross sections from Hill, Wohn, Winger and Smith 1988, Hill, Wohn, Winger, Khayat, Leininger and Smith 1988, Hill, Wohn, Schwellenbach and Smith 1991, Smith et al 1988 and Loveland et al 1988. σ^{Tot}_{param} is the parameterized total cross section discussed in the text. Values in parentheses use the EM pocket formula.

Projectile	Target	T_{lab} (GeV/N)	Final State	σ^{Tot}_{expt} (mb)	σ^{Tot}_{param} (mb)
^{12}C	^{238}U	2.1	^{237}U	173 ± 22	191 (195)
^{20}Ne	^{238}U	2.1	^{237}U	192 ± 16	286 (300)
^{12}C	^{197}Au	2.1	^{196}Au	178 ± 7	172 (175)
^{20}Ne	^{197}Au	2.1	^{196}Au	268 ± 11	249 (260)
^{40}Ar	^{197}Au	1.8	^{196}Au	463 ± 30	458 (491)
^{56}Fe	^{197}Au	1.7	^{196}Au	707 ± 52	748 (812)
^{139}La	^{197}Au	1.26	^{196}Au	2130 ± 120	2187 (2295)
^{139}La	^{197}Au	0.15	^{196}Au	765 ± 48	729 (883)
^{238}U	^{197}Au	0.96	^{196}Au	3440 ± 210	3997 (3486)
^{16}O	^{197}Au	60	^{196}Au	400 ± 20	383 (389)
^{16}O	^{197}Au	200	^{196}Au	560 ± 30	458 (462)
^{12}C	^{89}Y	2.1	^{88}Y	115 ± 6	117 (119)
^{20}Ne	^{89}Y	2.1	^{88}Y	160 ± 7	148 (154)
^{40}Ar	^{89}Y	1.8	^{88}Y	283 ± 11	223 (240)
^{56}Fe	^{89}Y	1.7	^{88}Y	353 ± 14	319 (351)
^{12}C	^{59}Co	2.1	^{58}Co	89 ± 5	99 (101)
^{20}Ne	^{59}Co	2.1	^{58}Co	132 ± 7	119 (122)
^{56}Fe	^{59}Co	1.7	^{58}Co	194 ± 9	212 (229)
^{139}La	^{59}Co	1.26	^{58}Co	450 ± 30	433 (461)

Table II continued

Projectile	Target	T_{lab} (GeV/N)	Final State	σ^{Tot}_{expt} (mb)	σ^{Tot}_{param} (mb)
^{12}C	^{12}C	2.1	^{11}C	61 ± 1	65 (66)
^{20}Ne	^{12}C	1.05	^{11}C	78 ± 2	73 (73)
^{56}Fe	^{12}C	1.7	^{11}C	94 ± 2	100 (101)
^{139}La	^{12}C	1.26	^{11}C	148 ± 2	134 (135)
^{28}Si	^{12}C	13.7	^{11}C	73.5 ± 3.5	85 (85)

Table III Nuclear Cross Sections for single neutron and single proton removal. σ^{nuc}_{expt} are the experimental nuclear cross sections from Fig. 4 of Barrette et al 1990. σ^{nuc}_{param} is the parameterized nuclear cross section discussed in the text.

Projectile	Target	T_{lab} (GeV/N)	Final State	σ^{nuc}_{expt} (mb)	σ^{nuc}_{param} (mb)
^{28}Si	Al	13.7	1p	140 ± 14	87
^{28}Si	Al	13.7	1n	100 ± 10	87
^{28}Si	Sn	13.7	1p	220 ± 22	120
^{28}Si	Sn	13.7	1n	145 ± 15	120
^{28}Si	Pb	13.7	1p	300 ± 30	136
^{28}Si	Pb	13.7	1n	180 ± 18	136

Solution of Two-Body Relativistic Bound State Equations with Confining plus Coulomb Interactions

by

Khin Maung Maung
Department of Physics
Hampton University
Hampton, Virginia 23668

David E. Kahana
Continuous Electron Beam Accelerator Facility
12000 Jefferson Ave., Newport News, Virginia 23606

John W. Norbury
Department of Physics
Rider College
Lawrenceville, New Jersey 08648

Abstract

Studies of meson spectroscopy have often employed a non-relativistic Coulomb plus Linear Confining potential in position space. However because the quarks in mesons move at an appreciable fraction of the speed of light, it is necessary to use a relativistic treatment of the bound state problem. Such a treatment is most easily carried out in momentum space. However the position space Linear and Coulomb potentials lead to singular kernels in momentum space. Using a subtraction procedure we show how to remove these singularities *exactly* and thereby solve the Schrödinger equation in momentum space for *all* partial waves. Furthermore, we generalize the Linear and Coulomb potentials to relativistic kernels in 4-dimensional momentum space. Again we use a subtraction procedure to remove the relativistic singularities exactly for all partial waves. This enables us to solve 3-dimensional reductions of the Bethe-Salpeter equation. We solve six such equations for Coulomb plus Confining interactions for all partial waves.

PACS numbers: 11.10.St, 11.10.Qr, 14.80.Dq

1. INTRODUCTION

Meson spectroscopy[1] has been one of the most interesting and fundamental subjects in elementary particle physics for the last two decades. It has provided one of the basic testing grounds for our understanding of both the symmetries and the dynamics of the strong interaction between quarks, mediated by gluons. Future studies are also of great interest, particularly as they may provide evidence of constituent glue. Given the important role of meson spectroscopy it is vital that our theoretical descriptions of these relativistic $q\bar{q}$ systems be as accurate and consistent as possible. Thus one would ideally like to be able to connect the theoretical description of mesons to the fundamental theory of the strong interactions, namely Quantum Chromodynamics (QCD). However the non-abelian nature of QCD leads to strong self-interactions between the gluons resulting in field equations that are highly nonlinear and are unable to be solved by standard diagrammatic methods except in the perturbative regime. In the region of large distances , lattice gauge calculations[2], which provide the most direct link to QCD, have led to the conclusion that in the static quark limit the force between quarks can be very well described with a Linearly rising plus Coulomb potential. Nonrelativistic models which use such a potential have been very successful in accounting for both the masses and decays of mesons, particularly those containing heavy quarks.

However the pure non-relativistic model calculations have limitations. Firstly for systems containing one light quark the use of pure nonrelativistic formalism is obviously unjustified. Secondly the nonrelativistic formalism has intrinsic problems such as the incorrect dependence of the meson mass on the quark mass, i.e. the mesons with light quarks can become heavier than the mesons with heavier quarks[3,4]. Also the nonrelativistic Linear potential does not lead to Linear Regge trajectories[3]. None of these problems occur in semirelativistic treatments where the relativistic expression for the energy is used. Clearly then one must also introduce relativistic effects. Such studies have been made and good descriptions of the entire meson family have been obtained[5]. However, if one incorporates relativity into a position space calculation then many different relativistic

effects must be put in "by hand" leading to a significant number of adjustable parameters[5]. A much more satisfactory approach can be made by doing calculations in momentum space where relativistic effects can be handled in a much more economic way.

Such calculations immediately present two difficulties. Firstly, because one would like to retain a manifestly covariant approach it is natural to transform the Linear plus Coulomb potentials to momentum space. The problem is however, that both potentials lead to singular kernels. Secondly, because many mesons of interest contain quarks of comparable mass, one should ideally solve the two-body Bethe-Salpeter (BS) equation[6] and certainly not consider only the one-body Klein-Gordon or Dirac equations. Although the best way to do meson physics in the two-body framework would be to solve the Bethe-Salpeter(BS) equation, it is more practical to solve a three-dimensional[7-11] reduction of it. However there exist in principle infinitely many possible three-dimensional reductions[7-11] of the BS equation and generally there is no reason to prefer one reduction to another, although in some cases the physical problem itself might suggest a particular reduction scheme. Therefore for the general $q\bar{q}$ problem it is useful to carry out a systematic study of the various reductions of the BS equation.

In this paper we present a complete study of how to solve relativistic two-body bound state equations in momentum space with kernels which are a generalization of Coulomb plus Linear potentials. A method for treating linear and Coulomb potentials in momentum space for the nonrelativistic case was presented by Spence and Vary[18] but their method is not easily generalizable for the relativistic case if one retains retardation in the interaction. We present a systematic treatment of how to deal with the momentum space singularities for both Coulomb and Confining interactions for all partial waves and for both the non-relativstic Schrödinger equation and for six different 3-dimensional reductions[7-11] of the Bethe-Salpeter equation. The only parameters that our method permits are the quark masses and the Coulomb and Confining couplings. Our study is a comprehensive treatment of relativistic effects but with a very restrictive parameter set and should thus eventually provide a definitive description of the entire meson spectrum. *The main purpose of the present paper is to present the theoretical subtraction techniques necessary to solve two-body relativistic bound state equations in momentum space.*

2. SCHRÖDINGER EQUATION AND POTENTIALS IN MOMENTUM SPAC

The nonrelativistic power law potential in r-space can be written as

$$V^N(r) = \lambda_N \lim_{\eta \to 0} r^N e^{-\eta r} \tag{2.1}$$

Where λ_N is the strength of the potential and η is the screening parameter. The index N indicates the type of potential under consideration, i.e $N = -1$ corresponds to Coulomb potential ($\lambda_N = \lambda_C$) and $N = 1$ corresponds to a Linear potential ($\lambda_N = \lambda_L$). In the present paper we shall be considering only these two types of potential. For the bound state problem of two particles with masses m_1 and m_2 interacting via $V^N(\mathbf{q})$ the Schrödinger equation in momentum space is

$$\frac{\mathbf{p}^2}{2\mu}\phi(\mathbf{p}) + \int V^N(\mathbf{q})\phi(\mathbf{p}')d\mathbf{p}' = E\phi(\mathbf{p}) \tag{2.2}$$

where μ is the reduced mass. The momentum space potential is given by the Fourier transform of Eq.(2.1) namely

$$V^N(\mathbf{q}) = \frac{\lambda_N}{2\pi^2} \lim_{\eta \to 0}(-1)^{N+1} \frac{\partial^{N+1}}{\partial \eta^{N+1}}[\frac{1}{\mathbf{q}^2 + \eta^2}] \tag{2.3}$$

Where $\mathbf{q} = \mathbf{p}' - \mathbf{p}$. The Schrödinger equation for the l^{th} partialwave is given by

$$\frac{p^2}{2\mu}\phi_{nl}(p) + \int_0^\infty V_l^N(p', p)\phi_{nl}(p')p'^2 dp' = E_{nl}\phi_{nl}(p) \tag{2.4}$$

where $p = |\mathbf{p}|$, n is the principal quantum number and l is the orbital quantum number. The partial wave components of the potential is readily obtained as

$$\begin{aligned} V_l^N(p', p) &= 2\pi \int_{-1}^{1} V^N(\mathbf{q})P_l(x)dx \\ &= \frac{\lambda_N}{\pi} \lim_{\eta \to 0}(-1)^{N+1} \frac{\partial^{N+1}}{\partial \eta^{N+1}} \frac{Q_l(y)}{pp'} \end{aligned} \tag{2.5}$$

where $x = cos\theta_{\mathbf{pp}'}$ and y is defined as

$$y = \frac{p^2 + p'^2 + \eta^2}{2pp'} \tag{2.6}$$

The exact $\lim_{\eta\to 0}$ will be taken shortly. Special cases of interest are the Coulomb case ($N=-1$) and the Linear potential ($N=1$) and they are readily obtained from Eq(2.5) as

$$V_l^C(p',p) = \frac{\lambda_C}{\pi} \lim_{\eta\to 0} \frac{Q_l(y)}{pp'} \tag{2.7}$$

and

$$V_l^L(p',p) = \frac{\lambda_L}{\pi} \lim_{\eta\to 0} \frac{\partial^2}{\partial\eta^2} \frac{Q_l(y)}{pp'} \tag{2.8a}$$

$$= \frac{\lambda_L}{\pi} \lim_{\eta\to 0} \left[\frac{Q'_l(y)}{(pp')^2} + \frac{\eta^2}{(pp')^3} Q''_l(y) \right] \tag{2.8b}$$

Here $Q_l(y)$ are the Legendre polynomials of the second kind and their first and second derivatives are taken with respect to y, i.e.

$$Q'_l(y) = \frac{\partial Q_l(y)}{\partial y} \tag{2.9a}$$

$$Q''_l(y) = \frac{\partial^2 Q_l(y)}{\partial y^2} \tag{2.9b}$$

We note here that these potentials (at $\eta = 0$) have singularities when $p' = p$ which corresponds to $y = 1$. In order to see the singularity structure explicitly we rewrite $Q_l(y)$ in terms of $Q_0(y)$ as

$$Q_l(y) = P_l(y)Q_0(y) - w_{l-1}(y) \tag{2.10a}$$

where

$$w_{l-1}(y) = \sum_{m=1}^{l} \frac{1}{m} P_{l-m}(y) P_{m-1}(y) \tag{2.10b}$$

Note also that

$$Q_0(y) = 1/2\ ln|(y+1)/(y-1)| = 1/2\ ln\left[\frac{(p'+p)^2+\eta^2}{(p'-p)^2+\eta^2}\right] \tag{2.11a}$$

$$Q'_0(y) = \frac{1}{1-y^2} = pp'\left[\frac{-1}{(p'-p)^2+\eta^2} + \frac{1}{(p'+p)^2+\eta^2}\right] \tag{2.11b}$$

and

$$\frac{\eta^2}{pp'}Q''_0(y) = \eta^2(p^2+p'^2+\eta^2)\left[\frac{-1}{(p'-p)^2+\eta^2}+\frac{1}{(p'+p)^2+\eta^2}\right]^2. \qquad (2.11c)$$

In the expression for $Q_l(y)$ the only term that is singular (at $\eta = 0$) is $Q_0(y)$. Therefore the Coulomb potential has a logarithmic singularity from $Q_0(y)$ and the Linear potential has higher order singularities from $Q'_0(y)$ and $Q''_0(y)$. We note that the singularity structure of these potentials are the same for all partial waves.

As mentioned above the potentials we are interested in have singularities at $p' = p$ and in the following sections we will show how to take care of these singularities in the momentum space Schrödinger equation. There are two useful integrals which will be used repeatedly in the following sections. They are

$$\int_0^\infty \frac{Q_0(y,\eta=0)}{p'}dp' = \frac{\pi^2}{2} \qquad (2.12)$$

$$\int_0^\infty [\frac{\eta^2}{pp'}Q''_0(y) + Q'_0(y)]dp' = 0 \qquad (2.13)$$

2.1 NON-RELATIVISTIC COULOMB PROBLEM

In this subsection we will present a subtraction method which will treat the Coulomb singularity properly. For the pure Coulomb problem in momentum space the exact analytic bound state solutions were found by Fock[12], but our aim is to solve the Schrödinger equation and later relativistic equations for a combined Linear plus Coulomb interaction. Thus we need to be able to implement a numerical subtraction procedure in momentum space. Apart from the rearrangement of terms this method is identical to the one developed in references 13 and 14, but we reproduce it here for completeness. With the potential given in Eq.(2.7) and using the expression (2.10a) for $Q_l(y)$ the Schrödinger equation (2.4), with $\eta = 0$ becomes

$$\frac{p^2}{2\mu}\phi_{nl}(p) + \frac{\lambda_C}{\pi p}\int_0^\infty P_l(y)\frac{Q_0(y)}{p'}\phi_{nl}(p')p'^2dp' - \frac{\lambda_C}{\pi p}\int_0^\infty w_{l-1}(y)\phi_{nl}(p')p'dp' = E_{nl}\phi_{nl}(p) \tag{2.14}$$

Since $w_{l-1}(y)$ contains no singularity the second integral needs no special treatment. In order to remove the singularity arising from the $Q_0(y)$ term we subtract and add a term from the integrand fo the first integral of Eq(2.13). The added term is propotional to the integral of Eq(2.12) and we obtain a singularity free equation

$$\frac{p^2}{2\mu}\phi_{nl}(p) + \frac{\lambda_C}{\pi p}\int_0^\infty P_l(y)\frac{Q_0(y)}{p'}\left[p'^2\phi_{nl}(p') - \frac{p^2\phi_{nl}(p)}{P_l(y)}\right]dp'$$
$$+ \frac{\lambda_C}{\pi p}\left[\frac{\pi^2}{2}p^2\phi_{nl}(p)\right] - \frac{\lambda_C}{\pi p}\int_0^\infty w_{l-1}(y)\phi_{nl}(p')p'dp' = E_{nl}\phi_{nl}(p) \tag{2.15}$$

Note that at the singular point we have $p = p'$, $y = 1$ and $P_l(1) = 1$. Therefore the terms in the square brackets cancel exactly and removes the singularity arising from $Q_0(y)$. The numerical solution of this equation is discussed in the section on Numerical Methods (Sec. 2.3).

2.2 NON-RELATIVISTIC CONFINING PROBLEM

In the case of the Linear potential there are singularities arising from $Q_0(y)$, $Q'_0(y)$ and $Q''_0(y)$. We are interested in solving the Schrödinger equation in the limit $\eta = 0$. For the sake of clarity we will first consider the $l = 0$ case. For $l = 0$ the potential is

$$V_0^L(p',p) = \frac{\lambda_L}{\pi}\lim_{\eta\to 0}\left(\frac{\eta^2}{(pp')^3}Q''_0(y) + \frac{Q'_0(y)}{(pp')^2}\right) \tag{2.16}$$

Therefore the s-wave Schrödinger equation is

$$\frac{p^2}{2\mu}\phi_{n0}(p) + \frac{\lambda_L}{\pi p^2}\lim_{\eta\to 0}\int_0^\infty\left(\frac{\eta^2}{pp'}Q''_0(y) + Q'_0(y)\right)\phi_{n0}(p')dp' = E_{n0}\phi_{n0}(p) \tag{2.17}$$

Now by adding and subtracting a term in the integral we obtain

$$\frac{p^2}{2\mu}\phi_{n0}(p) + \frac{\lambda_L}{\pi p^2}\lim_{\eta\to 0}\int_0^\infty (\frac{\eta^2}{pp'}Q''_0(y) + Q'_0(y))\Big(\phi_{n0}(p') - \phi_{n0}(p)\Big)dp'$$

$$+ \frac{\lambda_L}{\pi p^2}\phi_{n0}(p)\lim_{\eta\to 0}\int_0^\infty (\frac{\eta^2}{pp'}Q''_0(y) + Q'_0(y)) = E_{n0}\phi_{n0}(p) \qquad (2.18)$$

From Eq(2.13) we see that the last integral is identically zero. Now we can take the $\eta = 0$ limit explicitly[15,16] and we finally get

$$\frac{p^2}{2\mu}\phi_{n0}(p) + \frac{\lambda_L}{\pi p^2}\int_0^\infty Q'_0(y)\Big(\phi_{n0}(p') - \phi_{n0}(p)\Big)dp' = E_{n0}\phi_{n0}(p) \qquad (2.19)$$

In the above equation $Q'_0(y)$ has a double pole singularity at $p = p'$ (see Eq2.11b). By Taylor series expansion of $\phi_{n0}(p')$ around the point $p' = p$ we can see that only a principal value singularity is left, which can be treated by conventional means.(see section on numerical methods and reference 17. Next we consider the case for general l. After removing the terms which can be shown to vanish when the $\eta = 0$ limit is taken the form of the potential is

$$V_l^L(p',p) = \frac{\lambda_L}{\pi}\lim_{\eta\to 0}\left[P_l(y)\left(\frac{\eta^2}{(pp')^3}Q''_0(y) + \frac{Q'_0(y)}{(pp')^2}\right) + \frac{P'_l(y)Q_0(y) - w'_{l-1}(y)}{(pp')^2}\right] \qquad (2.20)$$

Substituting this into the Schrödinger equation (2.4) we have

$$\frac{p^2}{2\mu}\phi_{nl}(p) + \frac{\lambda_L}{\pi p^2}\lim_{\eta\to 0}\int_0^\infty \Big[P_l(y)\Big(\frac{\eta^2}{pp'}Q''_0(y) + Q'_0(y)\Big)$$

$$+ P'_l(y)Q_0(y) - w'_{l-1}(y)\Big]\phi_{nl}(p')dp' = E_{nl}\phi_{nl}(p) \qquad (2.21)$$

In order to remove the singularities now we must perform two separate subtractions. The first subtraction is for the singularities coming from $Q'_0(y)$ and $Q''_0(y)$ and the second subtraction is for $Q_0(y)$. For the singularities arising from Q' and Q'', by using Eq.(2.13) we can make a subtraction without having to add anything back and for the singularity

arising from Q_0, by using Eq.(2.12) we subtract and add a term as for the Coulomb case. In addition, we have shown previously[15] how to take the explicit $\eta = 0$ limit. Thus our singularity free equation, in the exact $\eta = 0$ limit is

$$\frac{p^2}{2\mu}\phi_{nl}(p) + \frac{\lambda_L}{\pi p^2}\int_0^\infty P_l(y)Q'_0(y)\left(\phi_{nl}(p') - \frac{\phi_{nl}(p)}{P_l(y)}\right)dp'$$
$$+ \frac{\lambda_L}{\pi p^2}\int_0^\infty P'_l(y)\frac{Q_0(y)}{p'}\left(p'\phi_{nl}(p') - \frac{l(l+1)}{2}\frac{p\phi_{nl}(p)}{P'_l(y)}\right)dp'$$
$$+ \frac{\lambda_L}{\pi p^2}\frac{l(l+1)}{2}\left[\frac{\pi^2}{2}p\phi_{nl}(p)\right]$$
$$- \frac{\lambda_L}{\pi p^2}\int_0^\infty w'_{l-1}(y)\phi_{nl}(p')dp' = E_{nl}\phi_{nl}(p) \qquad (2.22)$$

At the singular point ($p' = p$; $y = 1$) we have $P_l(y = 1) = 1$ and the bracketed term in the first integral vanishes. Therefore, as in the $l = 0$ case we are left a pricipal value singularity. In the second integral at the singular point $P'_l(y = 1) = l(l + 1)/2$ and the term in the bracket again vanishes and kills the logarithmic singularity arising from $Q_0(y)$. Note that for $l = 0$ Eq(2.22) reduces to Eq(2.19). Now we are in a position to solve Eq.(2.15) for the pure Coulomb or Eq.(2.22) for the pure Linear potential for all partial waves. It is also obvious how to treat the combined Coulomb plus Linear potentials together.

2.3 NUMERICAL METHODS

Consider first the Coulomb equation (2.15). An important point to note is that at the singular point $p' = p$ the term in the square brackets of the first integral goes to zero *faster* than the logarithmic singularity in $Q_0(y)$, and therefore the integrand of the first term is *identically zero* at $p' = p$. By using Gaussian quadrature one can easily write the whole equation (2.15) as a matrix equation with $\phi_{nl}(p)$ as the eigenvectors and E_{nl} as the eigenvalues. Because the kernel of the first integral is zero when $p' = p$, the diagonal term of

the corresponding matrix will vanish; i.e. the matrix coefficients of the matrix eigenvectors will vanish at $p' = p$. However there remain non-zero terms multiplying $\phi_{nl}(p)$. These can be used as non-zero diagonal coefficient terms for the eigenvectors. The result is that one can obtain eigenvalues *and eigenvectors* directly from one's matrix equation. As we shall see later this is no longer possible for the Linear potential. These techniques for the pure Coulomb case are also very well explained in references 13 and 14.

However for the Linear potential this method does not work. (For the sake of simplicity let us discuss the $l = 0$ Linear potential equation only. The methods are identical for the higher l equation.) The reason that the above method does not work in Eq.(2.19) is because $Q'_0(y)$ has a double pole singularity and even after the subtraction, a principal value singularity is left. *Thus the integral must be evaluated explicitly.* However to do this we must know what the functions $\phi_{n0}(p)$ are before we solve the problem ! The way around this dilemma is to expand $\phi_{n0}(p)$ in a suitable set of basis functions:

$$\phi_{n0}(p) = \sum_i^M C_i g_i(p) \tag{2.23}$$

Inserting this expansion in Eq(2.19), multiplying by $p^2 g_j(p)$ and integrating over p, we obtain:

$$\sum_i^M C_i [\int_0^\infty \frac{p^4}{2\mu} g_j(p) g_i(p) dp + \frac{\lambda_L}{\pi} \int_0^\infty \int_0^\infty Q'_0(y) g_j(p) \Big(g_i(p') - g_i(p) \Big) dp' dp]$$
$$= E_{n0} \sum_i^M C_i \int_0^\infty p^2 g_j(p) g_i(p) dp \tag{2.24}$$

which is just the matrix equation:

$$\sum_i A_{ji} C_i = E_{n0} \sum_i G_{ji} C_i \tag{2.25}$$

which is symmetric under interchange of i and j (equivalent to symmetry under interchange of p and p') thus ensuring that the eigenvalues are all real.

The double integral still contains a principal value singularity. In order to treat this, the integral over p' is performed by integrating from 0 to $2p$ and then $2p$ to ∞ with

the singularity at the midpoint of the first region, which is carried out using Gaussian quadrature with an even number of points. This type of integration yields the Cauchy principal value automatically[17]. When we solve (2.25) we get M eigenvalues E_{10} to E_{M0} and a corresponding set of M eigenvectors C_1 to C_M. Thus Eq.(2.25) is solved for the energies E_{n0} and the coefficients C_i, which yield the wave function when substituted back into Eq.(2.23) Convergence is obtained by increasing the number of basis functions M and integration points. In order to obtain the wave function in coordinate space, one simply takes the Fourier transform $g_i(r)$ of the basis functions $g_i(p)$ and uses the same set of coefficients C_i but now multiplying $g_i(r)$ to obtain the coordinate space wave function. (Thus it is very convenient to pick $g_i(p)$ so that they have a simple Fourier transform.) For the masses and couplings considered in this paper a convenient set of functions $g_i(p)$ is

$$g_i(p) = exp[-p^2 i^2/M] \tag{2.26}$$

where M is the maximum number of functions used in the expansion Eq(2.23). Note however that for different masses and couplings[15], a different set of basis functions is necessary to achieve rapid convergence.

When solving the general Coulomb plus Linear problem one cannot take advantage of the simplicity of the Coulomb numerical procedure[13,14] by itself. One must employ the basis function expansion method described above. The basis functions appropriate to the Linear potential alone also turn out to be suitable for the general Linear plus Coulomb problem for the masses and couplings of this paper.

2.4 NON-RELATIVISTIC RESULTS

We have carried out many different tests of our methods. Firstly, for the pure Coulomb case we solved the problem with the method of references 13 and 14, which does not require any basis function expansion. We compared to the exact Coulomb energies and found that we could easily generate over 20 eigenvalues very accurately. Secondly, as an additional

check we also solved the pure Coulomb case using an appropriate set of basis expansion functions and were able to obtain about 10 eigenvalues quite accurately. Thirdly, the pure Linear problem was solved for $l = 0$ (see reference 15 for details) and compared to the exact results. (For the $l = 0$, pure Linear potential case, the exact eigenvalues can be obtained in terms of the roots of the Airy function). The calculated eigenfunctions also agreed with the exact results. Fourthly, the combined Coulomb plus Linear problem was solved with the expansion functions in Eq.(2.26) for $l = 0, 1, 2, 3$ and compared to a coordinate space calculation. (The coordinate space code integrates the Schrödinger equation out from the origin at $r = 0$ and in from large r, and matches the logarithmic derivatives at the classical turning point). Fifthly, the combined Coulomb plus Linear results were also compared to those listed in reference 18 and also with a coordinate space code. Excellent agreement was obtained.

In summary, we have very thoroughly tested our methods for Coulomb plus Linear potentials for many partial waves against results from exact calculations, coordinate space codes and the results of other authors for both eigenvalues and wave functions.

3. RELATIVISTIC TWO-BODY EQUATIONS AND INTERACTION KERNELS

In traditional nuclear physics, the deuteron is the only two particle bound state system. It has been studied in both the nonrelativistic framework and also in numerous relativistic frameworks. Compared to the deuteron the $q\bar{q}$ system is a very rich system and its spectra provides an ideal testing ground in which a systematic study of the 3-dimensional relativistic equations can be made.

The Bethe-Salpeter(BS) equation for the bound state problem in the center of mass frame is given by

$$\Psi(\mathbf{p}, P_0) = \frac{i}{(2\pi)^4} \int V(p, p') G(p', P_0) \Psi(\mathbf{p}, P_0) d^4p' \tag{3.1}$$

As mentioned above, there are infinitely many 3-dimensional reductions of the BS

equation. In this section we are going to work with six particular reductions which we believe to be a fair representative sample of the most commonly used 3-dimensional reductions of the BS equation. In order to reduce Eq(3.1) in to a 3-dimensional equation, we replace the propagator G by a 3-dimensional propagator g which has the same elastic cut. A systematic study of these 3-dimensional relativistic equations for the problem of scattering of scalar particles has been performed in reference 11. As stated in the introduction, in this paper we will make a similar study of the bound state of two particles interacting via a confining interaction. Some results have already been previously discussed[16]. The choice of the 3-dimensional propagator can be categorized into two types in general. One which renders the interaction to be instantaneous and one which does not. In this paper we study six 3-dimensional reductions, three of each type. Minimal Relativity (MR) equation[8?], Kadyshevsky (K) equation[9], and Gross (G) equation[7] all of which retain the retardation in the interaction. The equations with instantaneous interaction(no retardation) are the Blankenbecler-Sugar (BBS)equation[8], Kadyshevsky (K0) (without retardation)[9] and Thompson (T) equation[10]. All six equations can be generically written as (compare to Eq.2.2)

$$D_i\phi(\mathbf{p}) = -\int d\mathbf{p}' V_i(p,p')\phi(\mathbf{p}') \tag{3.2}$$

where $\phi(\mathbf{p})$ is a Schrödinger like wave function. We will neglect the couplings to the negative energy channels since the subtraction method is the same for the coupled channel case. The D_i are given in table I and the index i can be MR, K, G, BBS, K0 and T. Note that for MR, K and G equations the interaction V_i has retardation and for the other three equations it does not. We will choose to use MR, BBS, K and K0 equations to study the bound states of two scalar particles interacting via a confining interaction and G and T equations to study the bound state of spinor quarks[7].

The confining interaction to be used in these relativistic equations is a straightforward generalization of the Linearly rising potential discussed in section 2. We simply replace the three vector $\mathbf{q}$ of Eq(2.2) by a four-vector q. Now q^2 is given by

$$q^2 = (\mathbf{p}-\mathbf{p}')^2 - (E_{\mathbf{p}} - E_{\mathbf{p}'})^2 \tag{3.3}$$

In this generalization the form of the Coulomb type interaction and the confining interaction remain the same as in the nonrelativistic case but now $\mathbf{q}^2$ is replaced by q^2 and the partial wave components of these interactions will be given by Eq(2.5) but for the equations that include retardation (MR, K, G) the variable y is now replaced by $\bar{y}$ (instead of Eq.2.6 with $\eta = 0$) where

$$\bar{y} = \frac{p'^2 + p^2 - (E_p - E_{p'})^2}{2pp'} \tag{3.4}$$

Equations without retardation (BBS, K0, T) retain the original form of y in Eq.(2.6) with $\eta = 0$. Here p and p' are only the magnitude of the three vectors. Again we note that these relativistic interactions will introduce singularities as in the nonrelativistic case at $q^2 = 0$ or at $\bar{y} = 1$. Note also that although the variables are different the singularity structures are similar to the nonrelativistic case; i.e. the Coulomb interaction will have a logarithmic singularity and the confining interacting has higher order singularities. For the equations without retardation the interaction $V_i(p, p')$ is instantaneous and it is exactly the same as the nonrelativistic case. For the instantaneous interaction, relativistic effects come in to the equation only through the kinematics; i.e. only through the operator D_i. The singularities in this interaction can be handled exactly the same way as in the nonrelativistic case.

In the following subsections we will discuss how the singularities in the relativistic confining and Coulomb interactions can be treated properly.

3.1 RELATIVISTIC COULOMB PROBLEM

The relativistic generalization of the Coulomb interaction in the partial wave form is given by

$$V_l^C(p', p) = \frac{\lambda_C}{\pi} \lim_{\eta \to 0} \frac{Q_l(\bar{y})}{pp'} \tag{3.5}$$

and by using the expression for Q_l Eq(3.2) becomes

$$D_i\phi_{nl}(p) + \frac{\lambda_C}{\pi p}\int_0^\infty P_l(\bar{y})\frac{Q_0(\bar{y})}{p'}\phi_{nl}(p')p'^2dp' - \frac{\lambda_C}{\pi p}\int_0^\infty w_{l-1}(\bar{y})\phi_{nl}(p')p'dp' = 0 \qquad (3.6)$$

for the MR, K and G equations only. For the instantaneous equations BBS, K0, T instead of the above Eq.(3.6), we have simply the Schrödinger equation (2.14) but with the operator D_i replacing the Schrödinger propagator. Note that the only singularity in equation (3.6) arises from $Q_0(\bar{y})$. We want to handle this singularity in a similar fasion as in the nonrelativistic case; i.e. by adding and subtracting a term. But we must also be able to handle the added term analytically or numerically. Unfortunately because of the presense of retardation we cannot just subtract a ϕ_{nl} and use Eq.(2.12) as in the nonrelativistic case. In order to take advantage of Eq(2.12), we subtract a term propotional to the nonrelativistic interaction and obtain (compare to Eq. 2.15)

$$D_i\phi_{nl}(p) + \frac{\lambda_C}{\pi p}\int_0^\infty \Big[Q_0(\bar{y})\phi_{nl}(p')p' - Q_0(y)\frac{p^2\phi_{nl}(p)}{p'P_l(\bar{y})}\Big]P_l(\bar{y})dp'$$
$$+ \frac{\lambda_C}{\pi p}\big[p^2\phi_{nl}(p)\frac{\pi^2}{2}\big] - \frac{\lambda_C}{\pi p}\int_0^\infty w_{l-1}(\bar{y})\phi_{nl}(p')p'dp' = 0 \qquad (3.7)$$

for the MR, K and G equations only. Again for the instantaneous equations BBS, K0, T instead of the above Eq.(3.7), we have simply the Schrödinger equation (2.15) but with the operator D_i replacing the Schrödinger propagator. Note that we again have at the singular point $p' = p$, $\bar{y} = 1$ and $P_l(\bar{y} = 1) = 1$ and by Taylor expanding $Q_0(\bar{y})$ around $p' = p$, one can show that the term in the square brackets vanishes at the singular point.

3.2 RELATIVISTIC CONFINING PROBLEM

In the case of the relativistic confining interaction, the functional structure of the interaction is again the same as the nonrelativistic case but y replaced by $\bar{y}$. We therefore use

the same type of subtraction used in the relativistic Coulomb case. That is, we subtract and add a term propotional to the nonrelativistic confining interaction. We obtain (compare to Eq. 2.22)

$$D_i\phi_{nl}(p) + \frac{\lambda_L}{\pi p^2}\int_0^\infty \Big[{Q'}_0(\bar{y})\phi_{nl}(p') - (\frac{E_p}{m})^2 {Q'}_0(y)\frac{\phi_{nl}(p)}{P_l(\bar{y})}\Big]P_l(\bar{y})dp'$$

$$\frac{\lambda_L}{\pi p^2}\int_0^\infty \Big[Q_0(\bar{y})\phi_{nl}(p') - \frac{p}{p'}\frac{l(l+1)}{2{P'}_l(\bar{y})}Q_0(y)\phi_{nl}(p)\Big]{P'}_l(\bar{y})dp'$$

$$-\frac{\lambda_L}{\pi p^2}\int_0^\infty {W'}_{l-1}(\bar{y})\phi_{nl}(p')dp' + \frac{\lambda_L}{\pi p^2}\frac{l(l+1)}{2}p\frac{\pi^2}{2}\phi_{nl}(p) = 0 \qquad (3.8)$$

for the MR, K and G equations only. Once more for the instantaneous equations BBS, K0, T instead of the above Eq.(3.8), we have the Schrödinger equation (2.22) but with the operator D_i replacing the Schrödinger propagator. The factor E_p^2/m^2 in the subtracted term of the first integral in Eq(3.8) is necessary in order to cancel the singularity arising from ${Q'}_0(\bar{y})$ exactly at the singular point. This can easily be seen by Taylor expanding ${Q'}_0(\bar{y})$ at $p' = p$. Equation (3.8) is now ready to be solved for various choices of D_i when there is retardation in the interaction. For cases without retardation V_i is identical to the nonrelativistic problem and the subtraction technique developed in the nonrelativistic section can be used.

3.3 RELATIVISTIC RESULTS AND CONCLUSIONS

The main purpose of the present paper is to present the theoretical subtraction techniques necessary to solve two-body relativistic bound state equations in momentum space. Therefore equations (3.7) and (3.8) are our major results.

Nevertheless for the sake of illustration we shall present some numerical solutions for the pure confining problem with equation (3.8) written in terms of a single channel. Such results will at least allow us to see whether our theoretical methods give reasonable results.

The usefulness of these relativistic equations depends on the extent to which they reproduce global properties of the spectrum characterized by the dependence of the energy E_{nl} on the principal quantum number n. This dependence is most easily revealed by studying the ratio E_{nl}/E_{1l}. E_{nl} is related to the total energy W_{nl} through $E_{nl} = W_{nl} - 2m$. Tables 2, 3 and 4 contain the results for the ratio E_{nl}/E_{1l} for the equations listed above for a reasonable choice of mass and coupling parameters. l values range from 0 to 2.

There are three observations to make from these tables. First all of the energy ratios are reasonably close to the non-relativistic results for heavy quark masses. Second the difference between the relativistic results and the non-relativistic results gets bigger for smaller quark mass. Third, the higher radial excitations show more pronounced relativistic corrections, which is consistent with the virial theorem[3] for a positive power law potential which requires larger kinetic energies for orbits with greater average radii. These results lead us to conclude that our theoretical methods are valid and give us confidence that the methods developed herein will be suitable when a full coupled channels calculation is performed and compared to experimental data.

In conclusion we have presented the theoretical subtraction techniques necessary to solve two-body relativistic bound state equations in momentum space with Coulomb plus Confining interactions. Future work will be devoted to including spinors and coupling to the negative energy channels in all six equations so that detailed comparisons to experiment can be carried out.

Acknowledgements

We would like to extend our sincere thanks to Franz Gross, Nathan Isgur and Warren Buck for many useful discussions. We are also grateful to the CEBAF theory group for its continuing hospitality. JWN was supported in part by NASA grant NAG-1-1134.

Table 1

D_i operators for relativistic equations

G and T equations are describing pseudoscalar mesons with spinor quarks

The other four relativistic equations are for scalar quarks

i	Name	D_i	Retardation
MR	Minimal Relativity	$4E_k(E_k{}^2 - W^2/4)$	Yes
BBS	Blanckenbecler Sugar	*same as MR*	No
K	Kadyshevsky	$2E_k{}^2(E_k - W/2)$	Yes
K0	Kadyshevsky	*same as K*	No
G	Gross	$2E_k - W$	Yes
T	Thompson	*same as G*	No

Table 2

Energy ratios $\frac{E_{n+1}}{E_1}$ for pure Confining interaction with $l = 0$.

G and T equations are for spinor quarks with $k = 0.2GeV^2$. The other four relativistic equations are for scalar quarks with $k = 0.2GeV^4$. The nonrelativistic(NR) equation is with $k = 0.2GeV^2$. All masses are in units of GeV.

n	MR	BBS	K	K0	G	T	NR	Mass
1	1.73	1.71	1.74	1.72	1.79	1.72	1.75	1.5
2	2.31	2.27	2.34	2.30	2.47	2.30	2.36	1.5
3	2.81	2.75	2.87	2.80	3.09	2.80	2.90	1.5
1	1.58	1.50	1.68	1.54	1.90	1.67	1.75	0.5
2	2.00	1.82	2.21	1.89	2.73	2.18	2.36	0.5
3	2.35	2.08	2.65	2.16	3.52	2.62	2.90	0.5
1	1.51	1.41	1.66	1.44	1.98	1.63	1.75	0.3
2	1.87	1.65	2.13	1.69	2.92	2.11	2.36	0.3
3	2.17	1.84	2.52	1.89	3.84	2.51	2.90	0.3

Table 3

Energy ratios $\frac{E_{n+1}}{E_1}$ for pure Confining interaction with $l = 1$.

Notation and units are the same as Table 2.

n	MR	BBS	K	K0	G	T	NR	Mass
1	1.44	1.43	1.45	1.44	1.49	1.43	1.45	1.5
2	1.82	1.79	1.85	1.81	1.92	1.80	1.85	1.5
3	2.16	2.11	2.20	2.15	2.33	2.13	2.20	1.5
1	1.38	1.31	1.47	1.35	1.56	1.39	1.45	0.5
2	1.67	1.54	1.84	1.59	2.09	1.71	1.85	0.5
3	1.92	1.72	2.17	1.79	2.60	2.00	2.20	0.5
1	1.37	1.27	1.52	1.30	1.61	1.36	1.45	0.3
2	1.64	1.45	1.90	1.50	2.21	1.67	1.85	0.3
3	1.87	1.60	2.22	1.65	2.80	1.93	2.20	0.3

Table 4

Energy ratios $\frac{E_{n+1}}{E_1}$ for pure Confining interaction with $l = 2$.

Notation and units are the same as Table 2.

n	MR	BBS	K	K0	G	T	NR	Mass
1	1.32	1.31	1.33	1.31	1.35	1.31	1.33	1.5
2	1.59	1.57	1.62	1.59	1.68	1.58	1.62	1.5
3	1.84	1.81	1.88	1.84	1.99	1.82	1.89	1.5
1	1.29	1.23	1.37	1.26	1.41	1.27	1.33	0.5
2	1.52	1.40	1.67	1.45	1.80	1.51	1.62	0.5
3	1.71	1.55	1.94	1.61	2.19	1.72	1.89	0.5
1	1.30	1.20	1.44	1.23	1.45	1.25	1.33	0.3
2	1.52	1.35	1.78	1.39	1.89	1.47	1.62	0.3
3	1.72	1.47	2.06	1.52	2.33	1.67	1.89	0.3

References

1) E. Eichten, K. Gottfried, T. Kinoshita, K.D. Lane and T.M. Yan, Phys. Rev. D **17** 3090 (1978); ibid **21** 203 (1980); W. Kwong, J.L. Rosner and C. Quigg, Ann. Rev. Nucl. Part. Sci. **37** 325 (1987).

2) J.D. Stack, Phys. Rev. D **27** 412 (1983); H.Q. Ding, Phys. Rev. D **44** 2200 (1991); A. Hasenfratz and P. Hasenfratz, Ann. Rev. Nucl. Part. Sci. **35** 559 (1985).

3) W. Lucha, F.F. Schöberl and D. Gromes, Phys. Rep. **200** 127 (1991).

4) D. Flamm, F. Schöberl and H. Uematsu, Phys. Rev. D **36** 2176 (1987).

5) S. Godfrey and N. Isgur, Phys. Rev. D **32** 189 (1985).

6) H. A. Bethe and E. E. Salpeter, Phys. Rev. **82**(1951)309; Phys. Rev. **84**(1951)1232.

7) F. Gross, Phys. Rev. **186**(1969)1448, F. Gross and J. Milana, Phys. Rev. D **43** 2401 (1991).

8) R. Blankenbecler and R. Sugar, Phys. Rev. **142**(1966)1051.

9) V. G. Kadyshevsky, Nucl. Phys. **B6**(1968)125.

10) R. H. Thompson, Phys. Rev. D **1**(1970) 110.

11) R.M. Woloshyn and A.D. Jackson, Nucl. Phys. B **64** 269 (1973).

12) V. Fock, Z. Phys. **98** 145 (1935); H. A. Bethe and E. E. Salpeter, *Quantum Mechanics of One and Two Electron Atoms* (Plenum, New York, 1977)

13) R.H. Landau, *Quantum Mechanics II; A Second Course in Quantum Theory*, Wiley, New York (1990).

14) Y.R. Kwon and F. Tabakin, Phys. Rev. C **18** 932 (1978); R.H. Landau, Phys. Rev. C **27** 2191 (1983).

15) D.E. Kahana, J.W. Norbury and K. Maung Maung, Canadian J. Physics **xx** xxx (1992).

16) K. Maung Maung, D.E. Kahana and J.W. Norbury, CEBAF preprint number CEBAF-TH-91-21 (1991).

17) I.H. Sloan, J. Computational Phys. **3** 332 (1968).

18) J.R. Spence and J.P. Vary, Phys. Rev. D **35** 2191 (1987); L. Durand, B. Durand and J.B. Whitenton, Phys. Rev. D **28** 607 (1983).

Do Recent Observations of Very Large Electromagnetic Dissociation Cross Sections signify a transition towards Non-Perturbative QED ?

John W. Norbury
Physics Department, Rider College,
Lawrenceville, NJ 08648

The very large electromagnetic dissociation (emd) cross section recently observed by Hill, Wohn, Schwellenbach and Smith do not agree with Weizsacker-Williams (WW) theory or any simple modification thereof. Calculations are presented for the reaction probabilities for this experiment and the entire single and double nucleon removal emd data set. It is found that for those few reactions where theory and experiment disagree, the probabilities are exceptionally large. This indicates that WW theory is not valid for these reactions and that one must consider higher order corrections and perhaps even a non-perturbative approach to QED.

PACS: 25.70.Np

In nucleus-nucleus collisions when the impact parameter is larger than the sum of the nuclear radii the interaction proceeds via the electromagnetic (em) force. Measurements of electromagnetic dissociation (emd) cross sections have been carried out for many years [1-6]. The main theoretical tool employed in the interpretation of this data has been the Weizsacker-Williams (WW) method [7-9] of virtual quanta in which one replaces the incident nucleus by an equivalent photon field $n_{WW}(E)$ which specifies the number spectrum of photons with energies E. To obtain the emd nucleus-nucleus cross section σ_{WW} one integrates this photon spectrum over the photonuclear cross section $\sigma(E)$ of the nucleus in which particles are emitted as in [1-13]

$$\sigma_{WW} = \int n_{WW}(E)\, \sigma(E)\, \frac{dE}{E} \qquad (1)$$

$n_{WW}(E)$ is given in Ref. [7] and includes an integral over the impact parameter from b_{min} to infinity where b_{min} is the value below which the reaction proceeds via the nuclear force, and is approximately the sum of the nuclear radii. The parametrization of Refs. [3,4,10] is used herein.

The WW method has been applied to em processes in relativistic nuclear collisions involving such diverse topics as beam lifetime limitations [14], relativistic Coulomb fission [15], measuring the W boson magnetic moment [16] and em properties of the τ lepton [17], exotic neutron rich nuclei [18,19], production of radioactive beams [18,19], measurement of

astrophysically relevant cross sections [20], photonuclear physics [21], and production of Higgs bosons [22,23], lepton pairs [23], intermediate vector bosons [24], supersymmetric particles [25] and toponium [26] and in two-photon processes in e^+e^- reactions [9,27]. Clearly then it is important to understand the regions of applicability of the WW method.

Comparison of WW theory to experiment. - There has been very little effort devoted to a systematic experimental test of the validity of the WW method in nuclear collisions. Such tests are crucial if the theoretical calculations are to be believed. The most thorough investigations of the WW method for nucleon removal in nuclear collisions has been carried out by Hill, Wohn and collaborators [3,4]. Their data and that of other authors [1-6] is presented in Table I.

The theoretical cross sections σ_{WW} listed in Table I were calculated by numerically integrating equation (1) using *experimental* photonuclear data for $\sigma(E)$. (Details are described in Refs. [11] and [12]). There are some large differences between theory and experiment (highlighted in **bold face** in Table I) as first noted in Reference [11]. These differences have been extensively studied [3,10-13] and most of them can be plausibly explained if one takes into account the following 6 items: **1)** The experimental em cross section is actually derived from the total measured cross section by subtracting off the nuclear component. Some differences are accounted for by using a more realistic model

for the nuclear contribution [10,13]. **2)** The WW virtual photon spectrum assumes that all of the radiation is electric dipole in character [7]. When including the effect of electric quadrupole contributions [7,12,13] better agreement with experiment is obtained. **3)** The WW calculations assume a straight line trajectory for the incident nucleus. One should also include Rutherford bending [13,28] of the orbit. **4)** The experimental error in the photonuclear cross section $\sigma(E)$ used as input to the WW calculations must be considered as well as uncertainties in the quadrupole parameters. **5)** The value used for b_{min} may need modification. **6)** For the case of double nucleon removal it has been found that discrepancies can be plausibly resolved using cross section systematics from other reactions [29]. Therefore in Table I the "revised" experimental numbers from Ref. [29] are quoted.

Consider how these effects account for the single nucleon removal discrepancies of Table I: **^{18}O + Target -> ^{17}O** : The calculations of σ_{WW} in Table I use b_{min} from Refs. [3,4,10] which was derived [10] for single nucleon removal from stable nuclei such as ^{16}O. There is no guarantee that this form should work for ^{18}O which has two valence neutrons. In fact when discussing the original data, Olson et al [1] used a much larger value of b_{min} and were able to obtain satisfactory agreement with all of the ^{18}O data. (item 5 above) **^{12}C + ^{197}Au -> ^{196}Au; ^{16}O + ^{197}Au -> ^{196}Au (60 GeV/nucleon); ^{139}La + ^{59}Co -> ^{58}Co** : As discussed in Ref. [13] these reactions are satisfactorily explained if one considers items 1, 2 and 4 above. **^{16}O + ^{197}Au -> ^{196}Au (200**

GeV/nucleon) : Including the 6 items above one still does not obtain agreement between theory and experiment for this reaction [13]. Nevertheless if one simply replaces the ^{16}O projectile with ^{32}S then agreement occurs (see Table I). Thus there might be a problem with the experimental error bars. **$^{139}La + ^{197}Au \rightarrow ^{196}Au$ (150 MeV/nucleon)** : As pointed out in Ref. [13] this reaction cannot be explained even with the inclusion of all 6 items. **$^{238}U + ^{197}Au \rightarrow ^{196}Au$** : This is the recent data of Hill et al [4] who report the largest emd cross section ever observed. Calculating the cross section including items 2, 3 and 4 above one obtains a theoretical value of 4.8 $\pm$ 0.5 barn. This gives even worse disagreement with the experimental value of 3.16 $\pm$ 0.23 barn. Considering the effect of item 1 the experimental total cross section [4] was reported as 3.44 $\pm$ 0.21 barn compared to the present calculated value of 5.0 $\pm$ 0.5 barn.

In conclusion so far, the reactions $^{139}La + ^{197}Au \rightarrow ^{196}Au$ at 150 MeV/nucleon (measured by Loveland et al[10]) and $^{238}U + ^{197}Au \rightarrow ^{196}Au$ at 960 MeV/nucleon (measured by Hill et al [4]) cannot be accounted for by the 6 simple modifications. These reactions show a genuine discrepancy between WW theory and experiment.

Probabilities.-- *The present paper aims to explain the above failure of WW theory.* In calculations of e^+e^- production [29] unitarity violation occurs for small impact parameters thus indicating that WW theory is not valid. It is natural

to see if a similar unitarity violation occurs for the single-nucleon removal cross sections. The probability of interaction P(b) is related to the cross section [7] via

$$\sigma_{WW} = \int_{b_{min}}^{\infty} 2\pi\, b\, P(b)\, db \qquad (2)$$

Equating this with equation (1) implies that

$$P(b) = \int N_{WW}(E,b)\, \sigma(E)\, \frac{dE}{E} \qquad (3)$$

$N_{WW}(E,b)$ is the photon spectrum [7] dependent on impact parameter.

The probabilities have been calculated by numerically integrating equation (3) using experimental data [11] for the photonuclear cross section $\sigma(E)$. It is found that the probability $P(b)$ is a maximum when $b = b_{min}$ and then drops steadily for larger b. This probability function was numerically integrated a second time according to equation (2) to check that the results from equation (1) were obtained. Bertulani and Baur have previously calculated some probabilites [7], but *this is the first time that probabilities have been calculated using experimental photonuclear data as input and the first time that these probabilities have been directly compared to the entire emd data set. Also it is the first time that both single and double nucleon probabilities have been calculated and compared.*

The place to look for unitarity violation is the (maximum) value of the probability $P(b=b_{min})$. Referring to Table I, unitarity is clearly *not* violated for any of these reactions. Thus, in

contrast to e^+e^- production [30], unitarity violation is not the cause for the failure of WW theory as applied to single nucleon removal. However, note the remarkable result in which the probabilities are *small* for all reactions *except* the very reactions mentioned above where genuine discrepancies between theory and experiment occur. The experiment of Hill et al [4] where the discrepancy is worst has the largest probability of 0.4.

Budnev et al [9] have shown that the WW approximation results from the first order Feynman amplitude when the mass of the virtual photon can be neglected. Therefore the large value of the calculated probability indicates that higher order diagrams cannot be neglected and this suggests the reason for the failure of WW theory in predicting the recent data [4]. **(See the footnote[1] below for an important comment.)** In em nucleus-nucleus reactions the coupling constant is Z/137 which for light nuclei is still small enough for the first order diagram to be dominant. However for virtual photons emanating from ^{238}U the coupling Z/137 is about 0.7 indicating that many diagrams or even a non-perturbative approach might be needed. Thus the recent data [4] lie somewhere between the perturbative and non-perturbative regime and the complete data set in Table I is significant because by varying Z it provides experimental evidence of the transition from perturbative towards non-perturbative QED.

Finally note the very interesting behaviour of the double nucleon removal probabilities and cross sections. (Final

states in Table I are ^{195}Au and ^{57}Co.) Based on the statements above one would guess that WW theory should also fail for double nucleon removal in the $^{139}La + ^{197}Au \rightarrow ^{195}Au$ reaction because the coupling Z/137 is 0.4 and WW theory does not work for the single nucleon reaction. However looking at Table I good agreement is obtained. It is surprising that WW theory does work for this large coupling reaction ! However the minimum impact parameter probability is 0.03 compared to 0.2 for the single nucleon case and this is seen to be the explanation as to why WW theory works for double nucleon removal and not for single nucleon removal despite the coupling being the same for both reactions. Clearly the probability is a much more reliable indicator of the validity of WW theory than is the coupling Z/137 alone.

Hill and Wohn [31] are planning to measure the $^{197}Au + ^{197}Au$ reaction at 11 GeV/N. Using WW theory I have calculated the minimum impact parameter probabilities (and cross sections) as 0.35 (11 barn) and 0.07 (1.8 barn) for one and two neutron removal respectively. I therefore predict that when these measurements are made the two neutron removal cross section will agree with my WW calculation but that the experimental one neutron cross section will be considerably smaller than the WW calculation. This is in spite of the fact that the coupling Z/137 is the same for both reactions.

I am very grateful to Drs. Mirek Fatyga (Brookhaven) and Wang Cheung (Rider College) for useful discussions.

This work was supported in part by NASA grant NAG-1-1134.

Footnote: [1]One may think that the apparently good agreement between theory and experiment for $^{139}La + ^{197}Au \rightarrow ^{196}Au$ at 1.26 GeV/nucleon (Table I) also with a large probability value of 0.2 invalidates this hypothesis. As mentioned a more correct calculation incorporates the 6 items above. This is done in Ref. [13] where the total (nuclear plus em) theoretical value is 2534 ± 237 mb compared with the total experimental value of 2130 ± 120 mb. Despite the large error bars, this more accurate calculation indicates that this large probability reaction also has the theoretical value larger than the experimental number.

Table I Electromagnetic (em) Cross Sections for single and double nucleon removal. σ_{expt} are the experimental em cross sections from Refs. [1-6]. Where σ_{expt} for double nucleon removal is given without experimental error it means that the "revised" experimental numbers from Ref. [29] are quoted. σ_{WW} is the theoretical cross section and $P(b=b_{min})$ is the probability calculated at the minimum impact parameter. **Large** discrepancies between σ_{expt} and σ_{WW} are shown in **bold face**. (σ_{WW} for double nucelon removal is slightly different to the values in Ref. [29] which listed the calculations of Hill et al [3].)

Projectile	Target	T_{lab} (GeV/N)	Final State	σ_{expt} (mb)	σ_{WW} (mb)	$P(b=b_{min})$
^{12}C	Pb	2.1	^{11}C	51 ± 18	51	0.008
^{12}C	Pb	2.1	^{11}B	50 ± 25	74	0.01
^{12}C	Pb	1.05	^{11}C	39 ± 24	31	0.008
^{12}C	Pb	1.05	^{11}B	50 ± 25	47	0.01
^{16}O	Pb	2.1	^{15}O	50 ± 24	64	0.01
^{16}O	Pb	2.1	^{15}N	96 ± 26	120	0.02
^{12}C	Ag	2.1	^{11}C	21 ± 10	20	0.004
^{12}C	Ag	2.1	^{11}B	18 ± 13	29	0.006
^{12}C	Ag	1.05	^{11}C	21 ± 10	13	0.004
^{12}C	Ag	1.05	^{11}B	25 ± 19	20	0.006
^{16}O	Ag	2.1	^{15}O	26 ± 13	25	0.005
^{16}O	Ag	2.1	^{15}O	30 ± 16	46	0.008
^{12}C	Cu	2.1	^{11}C	10 ± 7	9	0.002
^{12}C	Cu	2.1	^{11}B	4 ± 8	12	0.003
^{12}C	Cu	1.05	^{11}C	9 ± 8	6	0.002
^{12}C	Cu	1.05	^{11}B	5 ± 8	9	0.003
^{16}O	Cu	2.1	^{15}O	9 ± 8	11	0.003
^{16}O	Cu	2.1	^{15}O	15 ± 8	20	0.004

Table I continued

Projectile	Target	T_{lab} (GeV/N)	Final State	σ_{expt} (mb)	σ_{ww} (mb)	$P(b=b_{min})$
^{12}C	Al	2.1	^{11}C	0 ± 5	2	0.0007
^{12}C	Al	2.1	^{11}B	0 ± 5	3	0.0009
^{12}C	Al	1.05	^{11}C	1 ± 6	2	0.0007
^{12}C	Al	1.05	^{11}B	1 ± 7	2	0.0009
^{16}O	Al	2.1	^{15}O	0 ± 5	3	0.0008
^{16}O	Al	2.1	^{15}N	-1 ± 9	5	0.001
^{12}C	C	2.1	^{11}C	-2 ± 5	1	0.0002
^{12}C	C	2.1	^{11}B	-1 ± 4	1	0.0003
^{12}C	C	1.05	^{11}C	-2 ± 5	0	0.0002
^{12}C	C	1.05	^{11}B	-2 ± 5	1	0.0003
^{16}O	C	2.1	^{15}O	-1 ± 4	1	0.0002
^{16}O	C	2.1	^{15}N	-1 ± 4	1	0.0004
^{18}O	**Ti**	**1.7**	**^{17}O**	**8.7 ± 2.7**	**16**	**0.004**
^{18}O	Ti	1.7	^{17}N	-0.5 ± 1.0	3	0.001
^{18}O	**Pb**	**1.7**	**^{17}O**	**136 ± 2.9**	**165**	**0.02**
^{18}O	**Pb**	**1.7**	**^{17}N**	**20.2 ± 1.8**	**31**	**0.006**
^{18}O	**U**	**1.7**	**^{17}O**	**140.8 ± 4.1**	**202**	**0.03**
^{18}O	**U**	**1.7**	**^{17}N**	**25.1 ± 1.6**	**37**	**0.006**
^{28}Si	^{27}Al	13.7	1p	37 ± 5	24	0.003
^{28}Si	^{27}Al	13.7	1n	15 ± 4	9	0.001
^{28}Si	^{120}Sn	13.7	1p	313 ± 4	317	0.02
^{28}Si	^{120}Sn	13.7	1n	136 ± 6	118	0.008
^{28}Si	^{208}Pb	13.7	1p	743 ± 27	806	0.04
^{28}Si	^{208}Pb	13.7	1n	347 ± 18	301	0.02

Table I continued

Projectile	Target	T_{lab} (GeV/N)	Final State	σ_{expt} (mb)	σ_{WW} (mb)	$P(b=b_{min})$
^{12}C	**^{197}Au**	**2.1**	**^{196}Au**	**75 ± 14**	**40**	**0.004**
^{12}C	^{197}Au	2.1	^{195}Au	9 ± 17	6	0.0008
^{20}Ne	^{197}Au	2.1	^{196}Au	153 ± 18	105	0.01
^{20}Ne	^{197}Au	2.1	^{195}Au	19	15	0.002
^{40}Ar	^{197}Au	1.8	^{196}Au	348 ± 34	297	0.03
^{40}Ar	^{197}Au	1.8	^{195}Au	42	42	0.005
^{56}Fe	^{197}Au	1.7	^{196}Au	601 ± 54	578	0.05
^{56}Fe	^{197}Au	1.7	^{195}Au	73 ± 13	80	0.01
^{139}La	^{197}Au	1.26	^{196}Au	1970 ± 130	2089	0.2
^{139}La	^{197}Au	1.26	^{195}Au	239	260	0.03
^{139}La	**^{197}Au**	**0.15**	**^{196}Au**	**447 ± 28**	**666**	**0.2**
^{238}U	**^{197}Au**	**0.96**	**^{196}Au**	**3160 ± 230**	**4205**	**0.4**
^{16}O	**^{197}Au**	**60**	**^{196}Au**	**280 ± 30**	**218**	**0.007**
^{16}O	**^{197}Au**	**200**	**^{196}Au**	**440 ± 40**	**281**	**0.007**
^{32}S	^{197}Au	200	^{196}Au	1120 ± 160	1104	0.03
^{12}C	^{89}Y	2.1	^{88}Y	9 ± 12	13	0.002
^{20}Ne	^{89}Y	2.1	^{88}Y	43 ± 12	35	0.006
^{40}Ar	^{89}Y	1.8	^{88}Y	132 ± 17	96	0.01
^{56}Fe	^{89}Y	1.7	^{88}Y	217 ± 20	185	0.03
^{12}C	^{59}Co	2.1	^{58}Co	6 ± 9	8	0.002
^{12}C	^{59}Co	2.1	^{57}Co	6 ± 4	1	0.0003
^{20}Ne	^{59}Co	2.1	^{58}Co	32 ± 11	20	0.004
^{20}Ne	^{59}Co	2.1	^{57}Co	3 ± 5	3	0.0006
^{56}Fe	^{59}Co	1.7	^{58}Co	88 ± 14	105	0.02
^{56}Fe	^{59}Co	1.7	^{57}Co	13 ± 6	13	0.003
^{139}La	**^{59}Co**	**1.26**	**^{58}Co**	**280 ± 40**	**358**	**0.05**
^{139}La	^{59}Co	1.26	^{57}Co	32 ± 16	39	0.007

1) D.L. Olson, B.L. Berman, D.E. Greiner, H.H. Heckman, P.J. Lindstrom, G.D. Westfall and H.J. Crawford, Phys. Rev. C **24**, 1529 (1981).

2) H.H. Heckman and P.J. Lindstrom, Phys. Rev. Lett. **37**, 56 (1976).

3) M.T. Mercier et al, Phys. Rev. C **33**, 1655 (1986); J.C. Hill et al, Phys. Rev. Lett. **60**, 999 (1988); Phys. Rev. C **38**, 1722 (1988); ibid. **39**, 524 (1989); J.C. Hill, in *Current Issues in Hadron Physics*, edited by J. Tran Thanh Van (Editions Frontieres, Gif-sur-Yvette, France, 1988); J.W. Norbury, Phys. Rev. C **39**, 2472 (1989); J.C. Hill and F.K. Wohn, ibid. 2474 (1989).

4) J.C. Hill, F.K. Wohn, D.D. Schwellenbach and A.R. Smith, Phys. Lett. B **273**, 371 (1991).

5) W. Loveland et al, Phys. Rev. C **38**, 2094 (1988).

6) J. Barrette et al, Phys. Rev. C **41**, 1512 (1990).

7) C.A. Bertulani and G. Baur, Phys. Rep. **163**, 299 (1988).

8) J.D. Jackson, *Classical Electrodynamics*, 2nd Ed. (Wiley, New York, 1975).

9) V.W. Budnev et al, Phys. Rep. **15**, 181 (1975).

10) C.J. Benesh, B.C. Cook, and J.P. Vary, Phys. Rev. C **40**, 1198 (1989); J.W. Norbury and L.W. Townsend, ibid. **42**, 1775 (1990).

11) J.W. Norbury, Phys. Rev. C **40**, 2621 (1989).

12) J.W. Norbury, Phys. Rev. C **41**, 372 (1990); ibid. **42**, 711 (1990).

13) J.W. Norbury, Phys. Rev. C **42**, 2259 (1990).

14) G. Baur and C.A. Bertulani, Nucl. Phys. A **505**, 835 (1989).

15) J.W. Norbury, Phys. Rev. C **43**, R368 (1991).

16) F. Cornet and J.I. Illana, Phys. Rev. Lett. **67**, 1705 (1991); G. Couture, Phys. Rev. D **44**, 2755 (1991).

17) F. del Aguila, F. Cornet and J.I. Illana, Phys. Lett. B **271**, 256 (1991).

18) I. Tanihata, Nucl.Phys. A**520**, 411c (1990); ibid. **522**, 275c (1991).

19) C.A. Bertulani, G. Baur and M.S. Hussein, Nucl.Phys.A **526**,751(1991).

20) G. Baur and M.Weber, Nucl. Phys. A **504**, 352 (1989); R. Shyam, G. Baur and P. Banerjee, Phys. Rev. C **44**, 915 (1991); J. Kiener et al, ibid., 2195 (1991); J. Hesselbarth and K.T. Knopfle, Phys. Rev. Lett. **67**, 2773 (1991).

21) D.L. Olson et al, Phys. Rev. C **44**, 1862 (1991).

22) E. Papageorgiu, Phys. Rev. D **40**, 92 (1989); Phys. Lett. B **250**, 155 (1990); R.N. Cahn and J.D. Jackson, Phys. Rev. D **42**, 3690 (1990); J.W. Norbury, ibid., 3696 (1990).

23) G. Baur and L.G. Ferreira Filho, Nucl. Phys. A **518**, 786 (1990); Phys. Lett. B **254**, 30 (1991).

24) M. Grabiak et al, J. Phys. G **15**, L25 (1989); M. Greiner et al, J. Phys. G **17**, L45 (1991).

25) J. Rau et al, J. Phys. G **16**, 211 (1990).

26) S. Schneider et al, J. Phys. G **17**, L149 (1991).

27) S. Cooper, Ann. Rev. Nucl. Part. Sci. **38**, 705 (1988); H.Terazawa, Rev.Mod.Phys.**45**, 615(1973);M.Poppe, Int.J.Mod.Phys. A**1**,545 (1986).

28) A.N.F. Aleixo and C.A. Bertulani, Nucl. Phys. A **505**, 448 (1989).

29) J.W. Norbury, Phys. Rev. C **45**, xxx (1992).

30) M. Fatyga, M.J. Rhoades-Brown and M.J. Tannenbaum (editors), *Can RHIC be used to test QED?* BNL report no. 52247 (1990).

31) F. Wohn, private communication

CEBAF
The Continuous Electron Beam Accelerator Facility
Theory Group Preprint Series

Additional copies are available from the authors.

The Southeastern Universities Research Association (SURA) operates the Continuous Electron Beam Accelerator Facility for the United States Department of Energy under contract DE-AC05-84ER40150

Effects of Retardation in Relativistic Equations with Confining Interaction

by

Khin Maung Maung
Department of Physics
Hampton University
Hampton, Virginia 23668
and
NASA Langley Research Center
Hampton, Virginia 23665

David E. Kahana
Continuous Electron Beam Accelerator Facility
12000 Jefferson Ave., Newport News, Virginia 23606

John W. Norbury
Department of Physics
Rider College
Lawrenceville, New Jersey 08648

Abstract

A method has been developed for solving two-body relativistic bound state equations in momentum space with a confining interaction. A total of six different three-dimensional reductions of the Bethe-Salpeter equation are studied with particular emphasis placed on the competing roles of relativistic kinematics and retardation. The results indicate that these two effects counteract each other and this sheds some light on why non-relativistic models of meson spectroscopy have been quite successful.

Many theoretical studies of meson spectroscopy[1,2] have been performed in a non-relativistic framework with a confining plus Coulomb-like potential. The confining term prevents the quarks from escaping to large distances and the Coulomb term simulates the short range behavior of the one gluon exchange force. Motivated by the studies of lattice gauge theories[3], most work in this area uses a linearly rising potential to provide confinement. Relativity has also been introduced into the problem by different authors with various prescriptions[4,5]. Although the best way to do meson physics in the two-body framework would be to solve the Bethe-Salpeter(BS)[6] equation, it is more practical and economical to solve a three-dimensional reduction of it. However it is well known that there exist, in principle, infinitely many possible three-dimensional reductions of the BS equation[7] and generally speaking there is no reason to prefer one reduction to another, although in some special cases the physical problem itself suggests the use of a particular reduction scheme. For example, in the case of a system of one heavy quark and one light quark one might prefer the Gross equation[8] since the heavy quark can be put on mass-shell with some justification. Therefore for the general $q\bar{q}$ problem it would seem useful to carry out a systematic study of the various reductions of the BS equation. We have developed a method for solving bound state equations in momentum space with the singular kernel that arises from the linear confining potential[9] and in this letter we generalize the nonrelativistic linear potential to the relativistic case, and compare solutions for the scalar and spinor $q\bar{q}$ system obtained using six representative three dimensional reductions of the BS equation.

The nonrelativistic linear confining potential can be written as

$$V(r) = \lim_{\eta \to 0} kre^{-\eta r} \tag{1}$$

In momentum space this becomes

$$V(\mathbf{q}) = \lim_{\eta \to 0} \frac{k}{2\pi^2} \frac{\partial^2}{\partial \eta^2} \frac{1}{\mathbf{q}^2 + \eta^2} \tag{2}$$

The relativistic generalization of this potential has been obtained by replacing 3-vector $\mathbf{q} = \mathbf{p}' - \mathbf{p}$ by 4-vector q, so that $q^2 = \mathbf{q}^2 - q_0^2$. This would appear to be the most natural generalization of the non-relativistic linear potential, and indeed yields the non-relativistic

potential exactly when retardation effects are neglected. One can see that the momentum space potential has a singularity in the limit of $\eta \to 0$. One way of avoiding this singularity problem [5] is to carry out the calculation for a small finite value of eta. However this does not produce true confinement. We have previously studied how to extract the *exact* $\eta \to 0$ limit for the nonrelativistic case[9]. We have also generalized this limiting procedure to the relativistic case. Complete mathematical details of this procedure will be communicated elsewhere. In this letter we describe the main ideas concentrating rather on a discussion of the results and the effects of retardation and relativistic kinematics.

In the following we study these effects in two model systems, one containing scalar particles and the other containing spinors. For scalar " quarks " we consider the Minimal Relativity(MR) equation,the Blankenbecler-Sugar(BBS) equation[10] and the Kadyshevsky equation[11] with and without retardation (K and K0). For spinor quarks the Gross equation[8](G) (with retardation) and the Thompson (T) equation[12] (without retardation) are studied. These equations are the same set that were considered in the work of Woloshyn and Jackson[7] where the scattering of scalar particles was studied.

All six equations can be written in the generic form in C.M. frame as

$$D_i\phi(\mathbf{p}) = -\int V(p',p)\phi(\mathbf{p}')d\mathbf{p}' \tag{3}$$

where the operators D_i are listed in Table I.

The singularity that arises from the non-relativistic confining potential in momentum space has been handled by a subtraction procedure [9] similar in spirit, but very different in detail, to that developed for the Coulomb potential[10]. For the relativistic generalization of the linear potential considered herein, the singularity structure of the relativistic kernel remains the same as the non-relativistic case. Thus we obtain the extremely useful result that the relativistic singularity can be handled by subtracting a term propotional to the nonrelativistic kernel. The $\eta \to 0$ limit is taken in the same way as the non-relativistic case[9], so that we obtain in the case of $l = 0$ and for equal mass particles:

$$D_i\phi_0(p) = \frac{-k}{\pi p^2} \mathrm{P} \int_0^\infty |Q_0'(\bar{y})\phi_0(p') - (\frac{E_p}{m})^2 Q_0'(y)\phi_0(p)|dp'. \tag{4}$$

Here $\bar{y}$ and y are defined as

$$\bar{y} = \frac{p^2 + p'^2}{2pp'} - \frac{(E_p - E_{p'})^2}{2pp'} \tag{5}$$

$$y = \frac{p^2 + p'^2}{2pp'} \qquad (6)$$

P denotes the principal value integral, Q_0 and Q_0' are the Legendre function of the second kind and its first derivative respectively and $E_p = \sqrt{m^2 + p^2}$.

Using the relativistic generalization of the method developed in reference 9, these equations are solved for the total energy W for the s-wave and particles of equal mass m. Only coupling to the positive energy channels is retained. The usefulness of these relativistic equations depends on the extent to which they reproduce global properties of the spectrum characterized by the dependence of the energy E_n on the principal quantum number n. This dependence is most easily revealed by studying the ratio E_n/E_1. E_n is related to the total energy W_n through $E_n = W_n - 2m$. Table (2) contains the results for the ratio E_n/E_1 for the equations listed above for a reasonable choice of mass and coupling parameters.

Consider first the equations which have no retardation effect, (BBS, K0, T). One sees that in all three cases the energy ratios are significantly smaller than the non-relativistic result (which is independent of mass) and furthermore that this difference is more important for small quark masses which is as one would expect for a purely kinematic effect. In addition, the higher radial excitations show more pronounced relativistic corrections, which is consistent with the virial theorem [2] for a positive power law potential which requires larger kinetic energies for orbits with greater average radii.

A result of considerable interest is that when retardation is included, as in equations (MR, K, G), the effect of relativistic kinematics described above is counteracted, in that the energy ratios move back towards the non-relativistic values rather than continuing to become smaller. This provides one possible explanation as to why non-relativistic equations have been quite successful in describing meson spectroscopy. Notice that the differences between MR and BBS, K and K0 equations is retardation. By comparing the differences between MR column and BBS column to the differences between K and K0 coulmn in table 2 we notice that the effect of retardation is more pronounced in the Kadyshevsky equation than in the Minimal Relativity equation.

In conclusion we have solved the two-body relativistic bound state problem for a

relativistic confining interaction which is a generalization of the non-relativistic linear potential. We have considered six different 3-dimensional relativistic equations, four for scalars particles and two for spinor quarks. In all cases we have studied, we have found that the effects of relativistic kinematics and retardation counteract each other. Future work will be devoted to including spinors and coupling to the negative energy channels in all six equations so that detailed comparisons to experiment can be carried out.

Acknowledgements

We would like to thank Franz Gross and Warren Buck for useful discussions and also Wang Cheung for providing a matrix code. KMM and JWN were supported in part by NASA grants NAG-1-477 and NAG-1-1134. DEK would like to thank Martin Lavelle and Jim Beaver for a private communication received in Santa Fé. We are also grateful to the CEBAF theory group for its continuing hospitality.

Table 1

D_i operators for relativistic equations

G and T equations are describing pseudoscalar mesons with spinor quarks

The other four relativistic equations are for scalar quarks

i	Name	D_i	Retardation
MR	Minimal Relativity	$4E_p(E_p^2 - W^2/4)$	Yes
BBS	Blankenbecler Sugar	*same as MR*	No
K	Kadyshevsky	$2E_p^2(E_p - W/2)$	Yes
K0	Kadyshevsky	*same as K*	No
G	Gross	$2E_p - W$	Yes
T	Thompson	*same as G*	No

Table 2

Energy ratios $\frac{E_{n+1}}{E_1}$

for the six relativistic equations discussed in the text

G and T equations are for spinor quarks with $k = 0.2GeV^2$

The other four relativistic equations are for scalar quarks with $k = 0.2GeV^4$

The nonrelativistic(NR) equation is with $k = 0.2GeV^2$

n	MR	BBS	K	K0	G	T	NR	mass (GeV)
1	1.73	1.71	1.74	1.72	1.79	1.72	1.75	1.5
2	2.31	2.27	2.35	2.30	2.47	2.30	2.36	1.5
3	2.81	2.75	2.88	2.80	3.09	2.80	2.90	1.5
1	1.58	1.50	1.68	1.54	1.90	1.67	1.75	0.5
2	2.00	1.82	2.21	1.89	2.73	2.18	2.36	0.5
3	2.35	2.08	2.65	2.16	3.52	2.62	2.90	0.5
1	1.51	1.41	1.66	1.44	1.98	1.63	1.75	0.3
2	1.87	1.65	2.13	1.69	2.91	2.11	2.36	0.3
3	2.18	1.84	2.52	1.89	3.83	2.51	2.90	0.3

References

1) E. Eichten, K. Gottfried, T. Kinoshita, K.D. Lane and T.M. Yan, Phys. Rev. D **17** 3090 (1978); ibid **21** 203 (1980); W. Kwong, J.L. Rosner and C. Quigg, Ann. Rev. Nucl. Part. Sci. **37** 325 (1987).

2) W. Lucha, F.F. Schoberl and D. Gromes, Phys. Rep. **200** 127 (1991).

3) J.D. Stack, Phys. Rev. **27** 412 (1983); A. Hasenfratz and P. Hasenfratz, Ann. Rev. Nucl. Part. Sci. **35** 559 (1985).

4) S. Godfrey and N. Isgur, Phys. Rev. D **32** 189 (1985); T. Zhang and R. Koniuk, Phys. Rev. D **43** 1688 (1991).

5) A.B. Henriques, B.H. Kellet and R.G. Moorehouse, Phys. Lett. B **64** 85 (1976).

6) H. A. Bethe and E. E. Salpeter, Phys. Rev. **82**(1951)309; Phys. Rev. **84**(1951)1232.

7) R.M. Woloshyn and A.D. Jackson, Nucl. Phys. B **64** 269 (1973).

8) F. Gross, Phys. Rev. **186**(1969)1448, F. Gross and J. Milana, Phys. Rev. D **43** 2401 (1991).

9) D.E. Kahana, J.W. Norbury and K. Maung Maung, CEBAF preprint number CEBAF-TH-91-02 (1991).

10) R. Blankenbecler and R. Sugar, Phys. Rev. **142**(1966)1051.

11) V. G. Kadyshevsky, Nucl. Phys. **B6**(1968)125.

12) R. H. Thompson, Phys. Rev. D **1**(1970) 110.

13) Y.R. Kwon and F. Tabakin, Phys. Rev. C 18 932 (1978); R.H. Landau, Phys. Rev. C 27 2191 (1983).

PHYSICAL REVIEW C VOLUME 45, NUMBER 6 JUNE 1992

Two neutron removal in relativistic nucleus-nucleus reactions

John W. Norbury
Department of Physics, Rider College, Lawrenceville, New Jersey 08648
(Received 8 January 1992)

Significant discrepancies between theory and experiment have previously been noted for double neutron removal via electromagnetic processes in relativistic nucleus-nucleus collisions. The present work examines the cause of these discrepancies and systematically investigates whether the problem might be due to electromagnetic theory, nuclear contributions, or an underestimate of experimental error. Using cross-section systematics from other reactions it is found that the discrepancies can be resolved in a plausible manner.

PACS number(s): 25.75.+r

In recent studies [1–6] of electromagnetic (EM) dissociation in relativistic nucleus-nucleus collisions, the cross sections measured are total cross sections $\sigma_{\rm tot}$, which actually comprise both the nuclear $\sigma_{\rm nuc}$ and EM cross sections $\sigma_{\rm EM}$ via

$$\sigma_{\rm tot}=\sigma_{\rm nuc}+\sigma_{\rm EM}\ . \tag{1}$$

Thus, in extracting $\sigma_{\rm nuc}$ (or $\sigma_{\rm EM}$) one has to know the EM (or nuclear) cross section.

The pioneering experimental work on separating nuclear and EM cross sections for one [1–5] and two [6] nucleon removal from nuclear beams was done by Hill, Wohn, and collaborators [1–6]. Their work has provided an extremely important and useful set of data with which to compare theoretical studies of EM processes in nuclear collisions [7]. They used the concept of limiting fragmentation [1–6] to estimate the nuclear cross section (denoted by $\sigma^F_{\rm nuc}$) and thereby deduced experimental values for the EM cross section (denoted by $\sigma^{\rm expt}_{\rm EM}$). It was found that significant discrepancies between theory and experiment occurred for these EM cross sections [1–6,8,9], particularly [9] for ^{197}Au. This discrepancy was interpreted by Benesh, Cook, and Vary (BCV) [10] (and confirmed in Ref. [11]) as being due to an underestimate of the $\sigma_{\rm nuc}$ contribution.

Hill, Wohn, and collaborators have recently extended their work on single neutron removal to a very interesting study of two neutron removal [16] from ^{59}Co and ^{197}Au targets. Their results [6] are reproduced in Tables I and II. It can be seen that they find a deviation between Weizsacker-Williams (WW) theory and experiment for ^{20}Ne, ^{40}Ar, and ^{139}La projectiles for two neutron removal from ^{197}Au targets (compare $\sigma^{\rm WW}_{\rm EM}$ with $\sigma^{\rm expt}_{\rm EM}$). This discrepancy was also noted in Ref. [9]. In Ref. [10] and [11] deviations between theory and experiment were studied only for *single* neutron removal. It is the aim of the present work to use the BCV methods [10] and cross-section systematics to study the above two neutron removal discrepancies.

When deviations between theory and experiment occur, the problem can be due to any of the cross sections in Eq. (1). (BCV have shown [10] that interference terms are negligible.) Hill, Wohn, and collaborators [1–6] have discussed possible problems with $\sigma_{\rm EM}$, in contrast to Refs. [10] and [11] that have investigated problems with $\sigma_{\rm nuc}$. Of course, the third possibility is problems with the experimental cross section $\sigma^{\rm exp}_{\rm tot}$. These three possibilities will be discussed below for the two neutron removal experiments [6].

Electromagnetic cross sections. In Ref. [6] it was suggested that the discrepancy between theory and experiment might be due to problems with the WW calculation. (This calculation is discussed extensively in Refs. [1–10] and will not be repeated here.) Possible problems in the use of WW theory might be (i) neglect of electric quadrupole excitations [7,12,13], (ii) large experimental errors [13] in the photonuclear cross sections used as input, (iii) neglect of Rutherford bending of the trajectory [14], (iv) multiple Coulomb excitations [15], (v) incorrect choice of the impact parameter [9,11], or (vi) finite-size effects [7]. All of these possibilities have been thoroughly studied [1–15], and most previous discrepancies have been resolved [13], leading one to the conclusion that WW theory should be an excellent approximation for the two neutron removal studies [6]. Furthermore, it is somewhat mysterious that all the ^{59}Co target cross sections, as well as the ^{12}C and ^{56}Fe projectiles for ^{197}Au targets, are in good agreement, yet ^{20}Ne, ^{40}Ar, and ^{139}La projectiles on ^{197}Au targets are in poor agreement. One might expect that, if there really is a problem, all of the ^{197}Au target cross sections would be problematic because the neutrons are being removed from the target. Thus, one is led to consider the possibility that the trouble might be elsewhere, and not with WW theory. This was the conclusion reached in Refs. [10–11] for the case of *one* neutron removal.

Nuclear cross sections. In Refs. [10] and [11] it was claimed that an optical model for one neutron removal $\sigma^{\rm opt}_{\rm nuc}$ provided better agreement between theory and experiment. In other words $\sigma^{\rm opt}_{\rm nuc}+\sigma^{\rm WW}_{\rm EM}$ provided better agreement with $\sigma^{\rm expt}_{\rm tot}$ than did $\sigma^F_{\rm nuc}+\sigma^{\rm WW}_{\rm EM}$, where $\sigma^F_{\rm nuc}$ is the nuclear contribution calculated by Hill, Wohn, and collaborators [1–6] from limiting fragmentation. Thus, it is natural to try the same explanation for the case of two neutron removal.

TABLE I. Cross sections for the ^{59}Co$(P,X)^{57}$Co and ^{59}Co$(P,X)^{58}$Co reactions, where P is the projectile and X is anything. Values listed are for two neutron removal, and values in parentheses are for one neutron removal [6,11]. Symbols are $\sigma_{\rm tot}^{\rm expt}$ (total experimental cross section), $\sigma_{\rm nuc}^{F}$ (nuclear cross section determined from factorization), $\sigma_{\rm EM}^{\rm expt}\equiv\sigma_{\rm tot}^{\rm expt}-\sigma_{\rm nuc}^{F}$, and $\sigma_{\rm EM}^{\rm WW}$ (theoretically calculated WW cross section). $\sigma_{\rm nuc}$ is the nuclear neutron removal cross section calculated as in the text. All cross sections are in units of mb and $T_{\rm lab}$ is in units of GeV/nucleon. * denotes that $P_{\rm esc}^{(2N)}$ was fitted to data.

Projectile	$T_{\rm lab}$	$\sigma_{\rm tot}^{\rm expt}$ [a]	$\sigma_{\rm nuc}^{F}$ [a]	$\sigma_{\rm EM}^{\rm expt}$ [a]	$\sigma_{\rm EM}^{\rm WW}$ [a]	$\sigma_{\rm nuc}$
^{12}C	2.1	46±3(89)	38±3(83)	6±4(6)	1.1(8.1)	45*(111)
^{20}Ne	2.1	49±3(132)	46±4(100)	3±5(32)	2.9(21)	49(121)
^{56}Fe	1.7	62±4(194)	49±4(106)	13±6(88)	14(111)	60(122)
^{139}La	1.26	110±11(450)	82±10(170)	32±16(280)	44(376)	72(142)

[a]Reference [6].

In Ref. [10] the single *nucleon* removal cross section was parametrized as

$$\sigma_G(1N)=2\pi(b_c-\tfrac{1}{2}\Delta b)\Delta b\ , \tag{2}$$

where b_c is the critical impact parameter [10] and $\Delta b\approx 0.5$ fm. Thus, one can write the two nucleon removal cross section as

$$\sigma_G(2N)=2\pi(b_c-\tfrac{1}{2}\Delta b)\Delta b\ . \tag{3}$$

The cross section for one *neutron* removal is

$$\sigma_{\rm nuc}^{1N}=\frac{N}{A}P_{\rm esc}^{(1N)}\sigma_G(1N)\ , \tag{4}$$

where N/A is the ratio of neutrons to nucleons and $P_{\rm esc}^{(1N)}$ is the escape probability for that neutron. In Ref. [11] it was noted that $P_{\rm esc}^{(1N)}$ is the most uncertain part of the calculation. For two neutron removal

$$\sigma_{\rm nuc}^{2N}=\left[\frac{N}{A}\right]^2 P_{\rm esc}^{(2N)}\sigma_G(2N)\ , \tag{5}$$

where $P_{\rm esc}^{(2N)}$ is the two neutron escape probability. Given the difficulties in determining this probability, the approach that we take here is to fit it to one experimental data point (e.g., for the ^{12}C projectile) by making sure that $\sigma_{\rm nuc}+\sigma_{\rm EM}^{\rm WW}$ fits the value $\sigma_{\rm tot}^{\rm expt}$ and then use that value for the calculation of the other reactions. (Such an approach also works very well for single nucleon removal, although the results are not presented here.) For ^{59}Co the fitted value of $P_{\rm esc}^{(2N)}$ is 0.71, whereas for ^{197}Au it is 0.58.

Final model cross sections are listed in Tables I and II in the column labeled $\sigma_{\rm nuc}$. (The single nucleon values are from Ref. [11].) It can be seen that, whereas for one neutron removal there existed significant differences between $\sigma_{\rm nuc}^{F}$ and $\sigma_{\rm nuc}$ (as discussed previously in Refs. [10] and [11]), the situation for two neutron removal seems to be quite acceptable. In other words, the present model calculation for the nuclear contribution seems to agree reasonably well with the cross section $\sigma_{\rm nuc}^{F}$ derived from the factorization by Hill, Wohn, and collaborators [6].

Given our reluctance to find fault with WW theory, and given the above good agreement between the nuclear cross section as determined from factorization [6] and the present calculation, one is led to consider a third alternative.

Total experimental cross sections. Quite apart from the above considerations, is there any other evidence to suggest that the discrepancies for ^{20}Ne, ^{40}Ar, and ^{139}La projectiles on ^{197}Au targets may be due to an underestimate of the experimental error bars?

First, note that the $\sigma_{\rm tot}^{\rm expt}$ for one and two neutron removal from ^{59}Co and for one neutron removal from ^{197}Au all increase as the mass of the projectile increases. (The exception is two neutron removal from ^{59}Co for ^{12}C and ^{20}Ne projectiles.) One would surely also expect this behavior for two neutron removal from ^{197}Au, yet a *drop* (or more accurately a constant value within experimental error) is observed from ^{40}Ar to ^{56}Fe. Given that the EM discrepancy (compare $\sigma_{\rm EM}^{\rm expt}$ with $\sigma_{\rm EM}^{\rm WW}$) for two neutron removal occurs for ^{40}Ar, one suspects that the ^{40}Ar value of $\sigma_{\rm tot}^{\rm expt}$ might be too large. This would explain why $\sigma_{\rm EM}^{\rm WW}$ is smaller than the experimental EM cross section $\sigma_{\rm EM}^{\rm expt}$.

Second, note that the $\sigma_{\rm tot}^{\rm expt}$ for two neutron removal from ^{59}Co are equal (within experimental error) for ^{12}C and ^{20}Ne projectiles. One should therefore also expect this to be the case for two neutron removal from ^{197}Au, yet the ^{20}Ne cross section is nearly *double* the ^{12}C cross

TABLE II. Same as Table I, except now the reactions are for ^{197}Au$(P,X)^{195}$Au and ^{197}Au$(P,X)^{196}$Au. $\sigma_{\rm EM}^{\rm rev}$ is the revised EM "experimental" cross section as explained in the text.

Projectile	$T_{\rm lab}$	$\sigma_{\rm tot}^{\rm expt}$ [a]	$\sigma_{\rm nuc}^{F}$ [a]	$\sigma_{\rm EM}^{\rm expt}$ [a]	$\sigma_{\rm EM}^{\rm WW}$ [a]	$\sigma_{\rm nuc}$	$\sigma_{\rm EM}^{\rm rev}$
^{12}C	2.1	67±15(178)	58±8(103)	9±17(75)	5(39)	62*(140)	
^{20}Ne	2.1	114±12(268)	65±9(115)	49±15(153)	14(103)	66(152)	19
^{40}Ar	1.8	141±15(463)	65±10(115)	76±18(348)	38(292)	73(149)	42
^{56}Fe	1.7	133±9(707)	60±9(106)	73±13(601)	73(569)	77(147)	
^{139}La	1.26	424±47(2130)	89±18(160)	335±49(1970)	238(2058)	89(167)	239

[a]Reference [6].

section. Again, given that the two neutron EM discrepancy occurs for ^{20}Ne, one suspects that the ^{20}Ne value of $\sigma_{\rm tot}^{\rm expt}$ might be too large. Again, this would explain why $\sigma_{\rm EM}^{\rm WW}$ is smaller than the $\sigma_{\rm EM}^{\rm expt}$ cross section.

Third, note that the $\sigma_{\rm tot}^{\rm expt}$ for two neutron removal from ^{59}Co are roughly doubled when one goes from ^{56}Fe to ^{139}La, but for two neutron removal from ^{197}Au the value is roughly quadrupled rather than doubled as one would expect. Again, this explains why $\sigma_{\rm EM}^{\rm WW}$ is smaller than experiment for ^{139}La.

The above considerations have led to the hypothesis that perhaps the two neutron $\sigma_{\rm tot}^{\rm expt}$ values for ^{20}Ne, ^{40}Ar, and ^{139}La projectiles on ^{197}Au targets are overestimated. Can one use $\sigma_{\rm EM}^{\rm expt}$ cross-section systematics on the remaining reactions to deduce "revised"' values of $\sigma_{\rm EM}^{\rm expt}$ for the above three projectiles on ^{197}Au? Let us assume that the $\sigma_{\rm EM}^{\rm expt}$ values for *one* neutron removal from ^{197}Au are correct for all five projectiles. (In fact they are not quite correct [10,11], but their ratios, discussed below, do scale correctly.) Also assume that the two neutron values are correct for ^{12}C and ^{56}Fe on ^{197}Au. The two neutron values should scale exactly as the one neutron values. Thus, to determine the "revised" EM experimental value for two neutron removal from projectile P using one neutron values for projectiles P and ^{56}Fe, we write

$$\sigma_{\rm EM}^{\rm rev}(P)_{2N}=\sigma_{\rm EM}^{\rm expt}(P)_{1N}\frac{\sigma_{\rm EM}^{\rm expt}(^{56}{\rm Fe})_{2N}}{\sigma_{\rm EM}^{\rm expt}(^{56}{\rm Fe})_{1N}}\ . \tag{6}$$

Thus, for example, for the ^{20}Ne projectile we have $19=153\times73/601$. (^{56}Fe is used rather than ^{12}C because the relative experimental error is much smaller. Nevertheless, one obtains nearly identical results using ^{12}C. One could also use the theoretical $\sigma_{\rm EM}^{\rm WW}$ numbers. The results are not that different.) When these revised "experimental" values $\sigma_{\rm EM}^{\rm rev}$ are compared to $\sigma_{\rm EM}^{\rm WW}$ (see Table II) excellent agreement is found, thus providing a plausible explanation for the previous discrepancies.

The foregoing arguments do not prove absolutely that the experimental error bars are too small. They simply suggest that the discrepancies between theory and experiment for two neutron removal from ^{197}Au are not *necessarily* the fault of WW theory. The conclusion from this study is that cross-section systematics provide a possible explanation for previously observed discrepancies.

This work was supported in part by NASA Research Grant No. NAG-1-1134. I wish to thank Wang Cheung, Lawrence Townsend, and Frank Cucinotta for useful discussions.

[1] M. T. Mercier, J. C. Hill, F. K. Wohn, and A. R. Smith, Phys. Rev. Lett. **52**, 898 (1984).
[2] M. T. Mercier, J. C. Hill, F. K. Wohn, C. M. McCullough, M. E. Nieland, J. A. Winger, C. B. Howard, S. Renwick, D. K. Matheis, and A. R. Smith, Phys. Rev. C **33**, 1655 (1986).
[3] J. C. Hill, F. K. Wohn, J. A. Winger, and A. R. Smith, Phys. Rev. Lett. **60**, 999 (1988).
[4] A. R. Smith, J. C. Hill, J. A. Winger, and P. J. Karol, Phys. Rev. C **38**, 210 (1988).
[5] J. C. Hill, F. K. Wohn, J. A. Winger, M. Khayat, K. Leininger, and A. R. Smith, Phys. Rev. C **38**, 1722 (1988).
[6] J. C. Hill, F. K. Wohn, J. A. Winger, M. Khayat, M. T. Mercier, and A. R. Smith, Phys. Rev. C **39**, 524 (1989).
[7] C. A. Bertulani and G. Baur, Phys. Rep. **163**, 299 (1988).
[8] J. W. Norbury, Phys. Rev. C **39**, 2472 (1989); J. C. Hill and F. K. Wohn, *ibid.* **39**, 2474 (1989).
[9] J. W. Norbury, Phys. Rev. C **40**, 2621 (1989).
[10] C. J. Benesh, B. C. Cook, and J. P. Vary, Phys. Rev. C **40**, 1198 (1989).
[11] J. W. Norbury and L. W. Townsend, Phys. Rev. C **42**, 1775 (1990).
[12] J. W. Norbury, Phys. Rev. C **41**, 372 (1990); **42**, 711 (1990).
[13] J. W. Norbury, Phys. Rev. C **42**, 2259 (1990).
[14] A. N. F. Aleixo and C. A. Bertulani, Nucl. Phys. **A505**, 448 (1982).
[15] W. J. Llope and P. Braun-Munzinger, Phys. Rev. C **41**, 2644 (1990).

Confining potential in momentum space

JOHN W. NORBURY
Department of Physics, Rider College, Lawrenceville, NJ 08648, U.S.A.
DAVID E. KAHANA
Continuous Electron Beam Accelerator Facility, Newport News, VA 23606, U.S.A.
AND
KHIN MAUNG MAUNG
Department of Physics, Hampton University, Hampton, VA 23668, U.S.A. and NASA Langley Research Center, Hampton, VA 23665, U.S.A.

Received September 4, 1991

A method is presented for the solution in momentum space of the bound-state problem with a linear potential in r space. The potential is unbounded at large r leading to a singularity at small q. The singularity is integrable, when regulated by exponentially screening the r-space potential, and is removed by a subtraction technique. The limit of zero screening is taken analytically, and the numerical solution of the subtracted integral equation gives eigenvalues and wave functions in good agreement with position space calculations.

On présente une méthode pour la résolution dans l'espace des impulsions du problème des états liés, avec un potentiel linéaire dans l'espace r. Ce potentiel n'étant pas borné pour les grandes valeurs de r, on a une singularité pour les faibles valeurs de q. Ce potentiel est intégrable et peut être enlevé par une technique de soustraction, si on ajoute un écran exponentiel au potentiel dans l'espace r. La limite d'écran zéro est prise analytiquement, et la solution numérique de l'équation intégrale soustraite donne des valeurs propres et des fonctions d'onde qui sont en bon accord avec les calculs effectués dans l'espace des positions. La méthode peut facilement être généralisée pour des potentiels variant selon une loi de puissance arbitraire.
[Traduit par la rédaction]

Can. J. Phys. 70, 86 (1992)

Lattice gauge calculations (1) for static (heavy) quarks support the notion that the interquark potential in quantum chromodynamics (QCD) behaves as $V(r) \sim \lambda r$ for large r. Indeed, the linear potential has long been used in phenomenological nonrelativistic quark models of baryons and mesons (2, 3). Meson spectroscopy in particular is successfully described by a linear potential at large r, modified by spin- and colour-dependent Coulomb forces at small r. Most calculations with the linear potential are carried out in coordinate space. This is the simplest procedure for heavy-quark systems, which can perhaps be considered as nonrelativistic; however for light-quark systems it would be desirable to have a relativistic treatment. Bound-state equations in relativistic systems (4) are generally much easier to solve in momentum space, and thus we are led to consider, as a starting point for the relativistic case, the Schrödinger equation for two scalar particles interacting by a linear potential. The methods developed will generalize relatively straightforwardly to relativistic treatments.

To summarize: here, we treat the Schrödinger equation for a linear r-space potential. The method is for the most part straightforward, the only difficulty arising from the singularity of the kernel at the origin of momentum space. Previous treatments (5) have usually been approximate in the sense that the singularity was handled by screening the r-space pontential:

$$[1] \quad V(r) \sim \lambda r\, e^{-\eta r}$$

What has perhaps not been generally appreciated is that the limit $\eta \to 0$ can be taken analytically. Previous treatments keep the parameter η finite, leading to some uncertainty as to the nature of the calculated eigenvalues and wave functions. In this connection, recall that the screened linear potential does not, strictly speaking, possess true bound states, instead it has scattering resonances, which for low energy approximate the bound states of the unscreened potential. We will extract the limit of zero screening analytically, using a subtraction technique. The resulting subtracted integral equation is relatively easy to handle numerically. An alternative procedure, not employing any subtraction, and leading to a different integrodifferential equation is presented in ref. 6. Our approach is easy to implement and generalizes without difficulty to higher partial waves. The Schrödinger equation for the lth partial wave is (with the inhomogeneous term already omitted, as it will not contribute to the bound states in the limit of zero screening)

$$[2] \quad \frac{p^2}{2\mu}\phi_l(p) + \int V_l(p,p')\,\phi_l(p')\,p'^2\,dp' = E\phi_l(p)$$

Here $\mu = m_1 m_2/(m_1 + m_2)$ is the reduced mass and V_l, given by

$$[3] \quad V_l(p,p') = \frac{\lambda}{\pi}\left[\frac{Q_l'(y)}{(pp')^2} + \eta^2\frac{Q_l''(y)}{(pp')^3}\right]$$

is the lth partial-wave component of the Fourier transform of [1]:

$$[4] \quad \hat{V}(p,p') = -\frac{\lambda}{2\pi^2}\left[\frac{2}{[(p'-p)^2+\eta^2]^2} - \frac{8\eta^2}{[(p'-p)^2+\eta^2]^3}\right]$$

The variable y is given by:

$$[5] \quad y = \frac{p^2 + p'^2 + \eta^2}{2pp'}$$

$Q_l'(y)$ and $Q_l''(y)$ are the first and second derivatives (with respect to y) of the Legendre function of the second kind. To illustrate the method we specialize to s-waves, where we find by contour integration

$$[6] \quad \int V_l(p,p')\,p'^2\,dp' = \frac{\lambda}{\pi}\int dp'\left[Q_0'(y) + \frac{\eta^2}{pp'}Q_0''(y)\right]$$

$$= \frac{\lambda}{\pi}\left[-\frac{\pi p^2}{\eta} + \frac{\pi p^2}{\eta}\right] = 0$$

Note that when $\eta = 0$, $Q_0'(y)$ and $Q_0''(y)$ have double and quadruple poles, respectively, at $p' = p$, so that their integrals do not exist separately. Nevertheless, the two terms added together produce a function with an integrable singularity. This is illustrated in Fig. 1, which shows the kernel as a function of p' for fixed p. One observes that there is a central maximum at $p' = p$ with height scaling as $1/\eta^2$, flanked by two minima at $p' \sim p \pm 2\eta$ whose heights also scale with $1/\eta^2$. The integral vanishes [6] and this allows us to rewrite the Schrödinger equation in subtracted form

$$[7] \quad \frac{p^2}{2\mu}\phi_0(p) + \frac{\lambda}{\pi}\int\left[\frac{Q_0'(y)}{(pp')^2} + \eta^2\frac{Q_0''(y)}{(pp')^3}\right]$$

$$\times\,[\phi_0(p') - \phi_0(p)]\,p'^2\,dp' = E\phi_0(p)$$

The limit $\eta \to 0$ now exists, and may be extracted by splitting the region of integration to isolate the singularity. We write

$$[8] \quad \int dp'\left[Q_0'(y) + \frac{\eta^2}{pp'}Q_0''(y)\right][\phi_0(p') - \phi_0(p)]$$

$$= \int_0^{p-4\eta} + \int_{p-4\eta}^{p+4\eta} + \int_{p+4\eta}^{\infty}$$

$$= A + B + C$$

The limits $p \pm 4\eta$ are chosen so that all three extrema of the kernel lie in the middle region B. The explicit forms of the Legendre functions are

$$Q_0'(y) = \frac{1}{1-y^2}$$

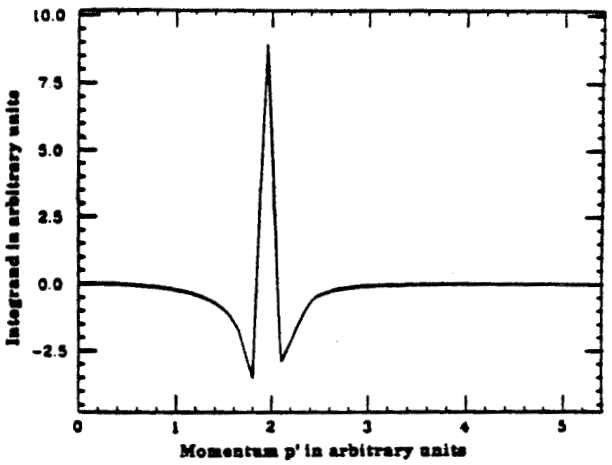

FIG. 1. The singularity structure of the kernel is shown for finite $\eta = 0.075$ with fixed $p = 2$.

$$= pp'\left[\frac{-1}{(p'-p)^2+\eta^2} + \frac{1}{(p'+p)^2+\eta^2}\right]$$

and

$$\frac{\eta^2}{pp'}Q_0''(y) = \eta^2(p^2 + p'^2 + \eta^2)$$

$$\times\left[\frac{-1}{(p'-p)^2+\eta^2} + \frac{1}{(p'+p)^2+\eta^2}\right]^2$$

It is clear that for $p' \neq p$, as is the case in the integrals A and C, the limit $\eta \to 0$ is innocuous, and may be taken immediately, indeed one has

$$[9] \quad \lim_{\eta\to 0}[A + C]$$

$$= P\int_0^{\infty} dp'\left[\frac{-4p^2p'^2}{(p'^2-p^2)^2}\right][\phi_0(p') - \phi_0(p)]$$

where P denotes as usual, the Cauchy principal value of the integral, which has been made well defined by the subtraction. The term B must be handled with care, however, since $p' = p$ inside the region of integration. Assuming $\phi(p')$ is analytic in the neighborhood of p, and making an obvious change of variable we find

$$[10] \quad \lim_{\eta\to 0} B = \lim_{\eta\to 0}\int_{-4\eta}^{4\eta} dx\left\{\left[p(p+x)\left[\frac{-1}{x^2+\eta^2} + \frac{1}{(x+2p)^2+\eta^2}\right]\left[x\phi' + \frac{x^2}{2}\phi'' + \ldots\right]\right]\right.$$

$$\left. + \left[\eta^2[(x+p)^2 + p^2 + \eta^2]\left[\frac{-1}{x^2+\eta^2} + \frac{1}{(x+2p)^2+\eta^2}\right]^2\left[x\phi' + \frac{x^2}{2}\phi'' + \ldots\right]\right]\right\} = \lim_{\eta\to 0} B1 + \lim_{\eta\to 0} B2$$

Scaling out 4η then results in

$$[11] \quad \lim_{\eta\to 0} B1 = \lim_{\eta\to 0}\int_{-1}^{1}(4\eta)\,dy\,\frac{p}{4\eta}\left(\frac{p}{4\eta} + y\right)\left(\frac{-16}{1+16y^2}\right)\left[(4\eta)y\phi' + \frac{(4\eta)^2y^2}{2}\phi'' + \ldots\right]$$

$$= [p^2\phi'(p)]\int_{-1}^{1} dy\left(\frac{-16y}{1+16y^2}\right) = 0$$

TABLE 1. Energy eigenvalues in GeV for $l = 0$, $m_1 = m_2 = 1.5$ GeV, and $\lambda = 5$ GeV^2

	N						
	8	10	12	14	16	18	Exact
E_1	5.973	5.972	5.972	5.972	5.972	5.972	5.971
E_2	10.468	10.444	10.443	10.443	10.443	10.443	10.441
E_3	14.389	14.114	14.111	14.104	14.104	14.104	14.101
E_4	18.646	17.452	17.378	17.341	17.335	17.335	17.335
E_5	23.402	21.125	20.397	20.351	20.294	20.293	20.291
E_6	27.206	25.683	23.440	23.281	23.072	23.053	23.046
E_7	33.032	31.269	27.274	26.059	25.842	25.648	25.646
E_8	44.374	36.224	32.113	29.032	28.789	27.947	28.119
E_9		40.519	38.146	33.051	31.561	30.194	30.488
E_{10}		51.774	45.309	38.067	34.428	33.340	32.769
E_{11}			49.940	44.286	38.517	36.489	34.972
E_{12}			58.588	51.893	43.615	37.309	37.109

The contribution of the second term in $B1$ clearly vanishes since it is not singular at $p' = p$, the analysis of $B2$ is similar, and we conclude that B tends to zero. Therefore the limiting form of the equation is

$$[12]\quad \frac{p^2}{2\mu}\phi_0(p) - \frac{\lambda}{\pi p^2} P \int_0^\infty dp' \left[\frac{4p^2p'^2}{(p'^2 - p^2)^2}\right][\phi_0(p') - \phi_0(p)] = E\phi_0(p)$$

We now discuss the numerical solution of [12], which is not yet a completely trivial matter, since care must be taken to obtain the Cauchy principal value. In this respect there is a difference between the linear potential and the Coulomb potential, the latter giving rise to a logarithmic singularity. For the Coulomb potential, the method used in the literature (7) is to write the Coulomb analog of [12] directly, for example, using Gaussian quadrature, as a matrix equation. Since the singularity is only logarithmic this method is successful for the Coulomb potential. Here, such an approach is not feasible. Instead, we expand ϕ_0 in a suitable set of basis functions

$$[13]\quad \phi_0(p) = \sum_n^N C_n g_n(p)$$

Inserting this expansion in [12], multiplying by $p^2 g_m(p)$ and integrating over p, we obtain

$$[14]\quad \sum_n C_n \left\{ \int \frac{p^4}{2\mu} g_m(p) g_n(p)\, dp + \frac{\lambda}{\pi} \int \left[\frac{4p^2p'^2}{(p'^2 - p^2)^2}\right] g_m(p)[g_n(p') - g_n(p)]\, dp'\, dp \right\} = E \sum_n C_n \int p^2 g_m(p) g_n(p)\, dp$$

which is just the matrix equation

$$[15]\quad \sum_n A_{mn} C_n = E \sum_n G_{mn} C_n$$

The double integral over p and p' is performed by changing to variables $(p' + p)$ and $(p' - p)$. The singularity is in the integral over $(p' - p)$, so this is carried out first using Gaussian quadrature with an even number of points. This type of integration yields the Cauchy principal value automatically (8). A convenient set of functions $g(p)$ is

$$[16]\quad g_n(p) = \frac{1}{(n^2/N)^2 + p^4}$$

where N is the maximum number of functions used in expansion [13]. Figure 2 is a $3D$ plot of the kernel of [14], showing clearly the cancellation that leads to the principal value. Using the above method, we have calculated both eigenvalues and eigenvectors. In Table 1 the first 12 eigenvalues are listed. We used $m_1 = m_2 = 1.5$ GeV and the string tension $\lambda = 5$ GeV^2. One can see that the lower eigenvalues converge nicely as the number of functions is increased. We compare these with the eigenvalues obtained from a coordinate space calculation (integrating the equation out from $r = 0$ and in from large r, and matching the logarithmic derivatives at the classical turning point), in Table 1. The calculated eigenfunctions also agree with the coordinate-space calculation.

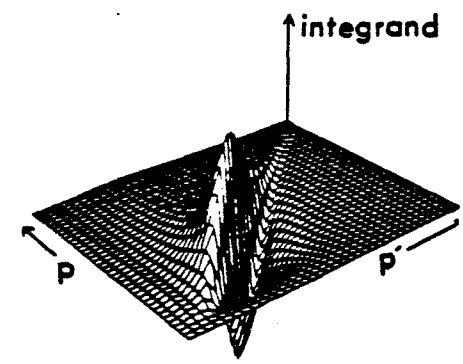

FIG. 2. A three-dimensional figure of the subtracted, regulated integrand; $\eta = 0.075$. The cancellation that produces the Cauchy principle value is evident.

In conclusion, we have treated the problem of two nonrelativistic, scalar particles interacting via a linear potential in momentum space. The relevant Schrödinger equation has a singular kernel. We have shown how after regulating the singularity by exponentially screening the r-space potential, the severity of the singularity can be reduced by a suitable subtraction, and the limit of zero screening extracted analytically. To the best of our knowledge, this point has not been generally understood in the literature. The limiting form of the equation has been treated numerically, and the results are in good agreement with more straightforward coordinate space calculations. Relativistic equations involving linear potentials involve similar singularities, so that the methods developed here will be applicable. We intend to study the relativistic quark–antiquark problem in the future. The method presented here can be generalized to higher partial waves without undue difficulty.

Acknowledgements

We are extremely grateful to Franz Gross for his generous contribution of essential ideas during all stages of this work. We would also like to thank Warren Buck and J.W.N. would like to thank Frank Cucinotta and Barry Ganapol for useful conversations. K.M.M. and J.W.N. would like to thank the Continuous Electron Beam Accelerator Facility for its hospitality. This work was supported in part by the Department of Energy through Continuous Electron Beam Accelerator Facility (D.E.K.), and by NASA grants NAG-1-1134 (J.W.N.) and NAG-1-477 (K.M.M.).

1. J. D. Stack. Phys. Rev. D: Part. Fields, **27**, 412 (1983); A. Hasenfratz and P. Hasenfratz. Ann. Rev. Nucl. Part. Sci. **35**, 559 (1985).
2. E. Eichten, K. Gottfried, T. Kinoshita, K. D. Lane, and T. M. Yan. Phys. Rev. D: Part. Fields, **17**, 3090 (1978); **21**, 203 (1980).
3. S. Godfrey and N. Isgur. Phys. Rev. D: Part. Fields, **32**, 189 (1985)
4. W. W. Buck and F. Gross. Phys. Rev. C: Nucl. Phys. **20**, 2361 (1979); F. Gross. Phys. Rev. **186**, 1448 (1969); H. Crater and P. Van Alstine. Phys. Rev. D: Part. Fields **37**, 1982 (1988).
5. A. B. Henriques, B. H. Kellett, and R. G. Moorhouse. Phys. Lett. **64B**, 85 (1976).
6. J. R. Spence and J. P. Vary. Phys. Rev. D: Part. Fields **35**, 2191 (1987).
7. Y. R. Kwon and F. Tabakin. Phys. Rev. C: Nucl. Phys. **18**, 932 (1978); R. H. Landau. **27**, 2191 (1983).
8. I. H. Sloan. J. Comput. Phys. **3**, 332 (1968).

PHYSICAL REVIEW C VOLUME 43, NUMBER 5 MAY 1991

Calculations of hadronic dissociation of ^{28}Si projectiles at 14.6A GeV by nucleon emission

Lawrence W. Townsend
National Aeronautics and Space Administration Langley Research Center, Hampton, Virginia 23665-5225

John W. Norbury
Department of Physics, Rider College, Lawrenceville, New Jersey 08648
and National Aeronautics and Space Administration Langley Research Center, Hampton, Virginia 23665-5225

Ferdous Khan
Department of Physics, Old Dominion University, Norfolk, Virginia 23529
(Received 15 November 1990)

An optical potential abrasion-ablation collision model is used to calculate hadronic dissociation cross sections for one, two, and three nucleon removal for the first time for a 14.6A GeV ^{28}Si beam fragmenting in aluminum, tin, and lead targets. These estimates are compared with recent semi-inclusive measurements. Significant differences between some calculated and measured semi-inclusive cross sections exist which cannot be resolved without measurements of the exclusive channel hadronic cross sections. Calculations for each exclusive reaction channel contributing to the semi-inclusive cross sections are presented and discussed.

Recently, the E814 Collaboration at Brookhaven National Laboratory (BNL) made a very detailed experimental study of the breakup of silicon beams at relativistic energies ($E_{\rm lab}=14.6A$ GeV or $T_{\rm lab}=13.7A$ GeV) using the Alternating-Gradient Synchrotron.[1] They reported cross-section measurements of one, two, and three nucleon removal by aluminum, tin, and lead targets from both electromagnetic and hadronic dissociation processes. For the electromagnetic dissociation (EMD) process, measurements of individual exclusive channel contributions were reported. Comparisons of measurements for $1p$ and $1n$ removal with calculated values obtained using the Weizsacker-Williams method of virtual quanta[2] were made, and good agreement was obtained. More recently, Llope and Braun-Munzinger[3] extended the EMD analysis to include multiple excitations of the giant dipole resonance coupled with fragmentation probabilities obtained from the standard statistical model of nuclear decay. They then use this extended calculational framework to predict exclusive EMD cross sections for many of the channels measured by the E814 Collaboration.

For the measured hadronic dissociation channels, however, no detailed analyses have been reported. In Ref. 1, simple comparisons between semi-inclusive measurements and a recent parametrization[4] of $1p$ and $1n$ geometrical calculation of single nucleon removal[5] were made. In this work, we analyze the hadronic dissociation of silicon projectile nuclei by aluminum, tin, and lead targets using an optical potential abrasion-ablation collision model which includes contributions from frictional-spectator interactions.[6] This model is used to calculate exclusive cross sections. Although no exclusive experimental hadronic cross sections were reported in Ref. 1 (the only exclusive cross sections reported were due to EMD), these calculated results are presented to stimulate interest in their experimental measurement and to facilitate further discussion in the semi-inclusive cross-section analysis.

The abrasion portion of this formalism was recently used to successfully describe single nucleon emission in relativistic nucleus-nucleus collisions.[7] Predictions of hadronic cross sections for the exclusive reaction channels measured in Ref. 1 are presented. Semi-inclusive cross sections, obtained by summing the appropriate exclusive channels, are presented and compared with the measured values reported in Ref. 1. Reasonably good agreement is obtained for the xp ($x=1, 2, 3$) channels. However, for the yn ($y=1, 2$) channels, the agreement is not as good, with the calculations generally overestimating the experimental data. Comments concerning the difficulties in resolving these differences are made, and the need for exclusive measurements of these hadronic cross sections is pointed out.

In the optical potential formalism,[6] the abrasion cross section for removal of m nucleons is

$$\sigma_{\rm abr}(A_{\rm PF})=\binom{A_p}{m}\int d^2b[1-P(b)]^m[P(b)]^{A_{\rm PF}}, \quad (1)$$

where

$$P(b)=\exp[-A_T\sigma(e)I(b)], \quad (2)$$

with

$$I(b)=[2\pi B(e)]^{-3/2}\int dz_0\int d^3\xi_T\rho_T(\xi_T)\int d^3y\,\rho_p(b+z_0+y+\xi_T)\exp[-y^2/2B(e)]\ . \quad (3)$$

In Eqs. (2) and (3), b is the impact parameter, e is the two-nucleon kinetic energy in their center-of-mass frame, z_0 is the target center-of-mass position in the projectile rest frame, ξ_T denotes the target-nucleus internal coordinates, and y is the projectile-nucleon–target-nucleon relative coordinate. Methods for obtaining the appropriate nuclear distributions ρ_i $(i=P, T)$ and constituent-averaged nucleon-nucleon cross sections $\sigma(e)$ are given in Ref. 8. Values for the diffractive nucleon-nucleon scattering slope parameter $B(e)$ are obtained from the parametrization in Ref. 9. The Pauli correlation correction derived in Ref. 8 is neglected here because it is negligible for the peripheral collisions[6] being considered in this work.

Since the abraded nucleons consist of protons and neutrons, a prescription for calculating the prefragment charge dispersion is needed. The three available choices are completely correlated,[10] hypergeometric (completely uncorrelated),[11] and a model based upon the zero-point vibrations of the giant dipole resonance.[12] For the present work, we have chosen to implement the hypergeometric model, which assumes that there is no correlation at all between the neutron and proton distributions. For few nucleon removal processes, such as are being investigated here, the calculated results are not particularly sensitive to any of these particular charge dispersion methods.[13] For example, all three methods yield identical charge dispersion results for single nucleon abrasions from self-conjugate nuclei. If z out of the original Z projectile nucleus protons are abraded along with n out of the original N projectile neutrons, then the abrasion cross section becomes

$$\sigma_{\rm abr}(Z_{\rm PF},A_{\rm PF})=\frac{\binom{N}{n}\binom{Z}{z}}{\binom{A_p}{m}}\sigma_{\rm abr}(A_{\rm PF})\,, \tag{4}$$

where

$$m=n+z\,, \tag{5}$$

$$Z_{\rm PF}=Z-z\,, \tag{6}$$

$$A_{\rm PF}=A_p-m\,, \tag{7}$$

and $\binom{A_p}{m}$ denotes the usual binomial coefficient expression from probability theory. To complete the abrasion portion of the calculation, prefragment excitation energies $E_{\rm exc}$ must be estimated. We use

$$E_{\rm exc}=E_s+E_{\rm FSI}\,, \tag{8}$$

where the surface energy term (E_s) is calculated using the usual clean-cut abrasion formalism.[14] The frictional-spectator interaction (FSI) contribution $(E_{\rm FSI})$ is estimated using the methods of Ref. 11. To compute the probability that p FSI's have occurred for each abrasion of m nucleons, we use an extension of the Benesh, Cook, and Vary (BCV) prescription for estimating escape probabilities of abraded nucleons rather than the usual assumed value of one-half.[6,11] Therefore, the abrasion cross section for a prefragment of isotopic species $(Z_{\rm PF},A_{\rm PF})$ which has undergone p FSI's is given by

$$\sigma_{\rm abr}(Z_{\rm PF},A_{\rm PF},p)=\binom{m}{p}(1-P_{\rm esc})^p(P_{\rm esc})^{m-p}\times\sigma_{\rm abr}(Z_{\rm PF},A_{\rm PF})\,, \tag{9}$$

where $P_{\rm esc}$ is the BCV probability that an abraded nucleon escapes without undergoing any frictional-spectator interactions.[5] For the reactions considered herein, $P_{\rm esc}\approx 0.7$.

Depending upon the excitation energy, the excited prefragment will decay by emitting one or more nucleons, composites, or gamma rays. The probability $a_{ij}(p)$ for formation of a specific final fragment of type i as a result of the deexcitation of a prefragment of type j which has undergone p frictional-spectator interactions is obtained using the EVA-3 computer code.[12] For $m=1$ or 2 and $p=0$ (no FSI), the values of $E_{\rm exc}$ are less than 3 MeV for all targets and no particle emission occurs. Hence, the calculated cross sections for ^{27}Si$+n$, ^{26}Si$+2n$, ^{27}Al$+p$, and ^{26}Mg$+2p$ arise solely from the abrasion process. Whenever one or more FSI's ($p=1$, 2) occur for a fragmenting silicon nucleus, an additional (average) excitation energy of 31 MeV per FSI (computed using the methods of Ref. 11) is deposited in the prefragment. When these resultant excitation energies are used as inputs into the EVA-3 code, the cross sections for the ^{25}Mg$+2p+n$ and the ^{25}Al$+p+2n$ final states are so large that all calculated xn or xp ($x=1$, 2) semi-inclusive cross sections significantly overestimate the present experimental measurements. In earlier work[15] on a semiempirical fragmentation code which used this same FSI model, it was noted that improved agreement between calculations and all available experimental data were obtained if values of excitation energy were increased above those obtained from the methods of Ref. 11. In this work, we observed that treating $E_{\rm FSI}$ as a free parameter and increasing its value by 15 MeV reduced the cross sections for the ^{25}Mg$+2p+n$ and ^{25}Al$+p+2n$ channels—thereby improving the semi-inclusive cross-section predictions. Therefore, the final hadronic cross section for production of the type i isotope is given by

$$\sigma_{\rm nuc}(Z_i,A_i)=\sum_j\sum_{p=0}^{m}a_{ij}(p)\sigma_{\rm abr}(Z_j,A_j,p)\,, \tag{10}$$

where the summation over j accounts for the contributions to i from different prefragment species j, and the summation over p accounts for the effects of the different excitation energies resulting from FSI's.

Estimated exclusive cross sections obtained using the fragmentation model described herein are separately listed in Table I for each target. To compare our predictions with the semi-inclusive hadronic cross-section measurements (Fig. 4 of Ref. 1), we sum the exclusive channels listed in Table I for each of the relevant nucleon emission reactions. For example, the $1p$ semi-inclusive calculation is the sum of the exclusive channel cross sections for the ^{27}Al$+p$, ^{26}Al$+p+n$, ^{25}Al$+p+2n$, and the ^{24}Al$+p+3n$ reactions. Similarly, the $1n$ semi-inclusive calculation is the sum of the ^{27}Si$+n$, ^{26}Al$+p+n$, ^{25}Mg$+2p+n$, and ^{24}Na$+3p+n$ exclusive channels. The calculated results for xn ($x=1$, 2) and yp ($y=1$, 2, 3) semi-inclusive cross sections are plotted in Fig. 1 along with the BNL experimental measurements from Fig. 4 of Ref. 1. Except for the $1p$ datum for the lead target, all calculated proton cross sections are in reasonably good agreement with the experimental data. Comparing the calculated and experi-

TABLE I. Exclusive channel hadronic dissociation cross-section calculations.

	Cross section (mb) with target nucleus		
Channel	Aluminum	Tin	Lead
^{27}Si+n	99.1	126.4	134.4
^{27}Al+p	99.1	126.4	134.4
^{26}Si+2n	17.9	22.3	23.9
^{26}Al+p+n^-	38.9	48.2	51.7
^{26}Mg+2p	17.9	22.3	23.9
^{25}Al+p+2n	1.5	2.1	2.3
^{25}Mg+2p+n	13.8	20.1	21.8
^{25}Na+3p	0.3	0.4	0.4
^{24}Al+p+3n	0.1	0.2	0.2
^{24}Mg+2p+2n	30.7	44.2	47.5
^{24}Na+3p+n	10.2	14.5	15.6

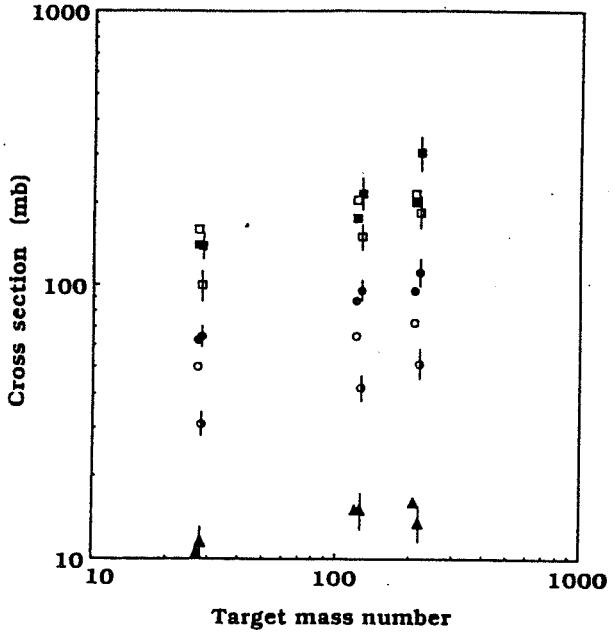

FIG. 1. Hadronic dissociation cross sections vs target mass number. The experimental data point symbols include error bars; the theoretical calculation point symbols do not. 1p is represented by a solid square, 1n by an open square, 2p by a solid circle, 2n by an open circle, and 3p by a solid triangle.

mental neutron removal cross sections, however, we note that the agreement is not as good. There the calculations systematically overestimate the measurements by nearly 50%. Since the experimental data were not corrected for detector acceptance limitations,[16] the observed trend for calculated cross sections to generally be larger than measured ones is expected because the experimental data are likely to underestimate the actual cross sections by an as yet unknown amount. Resolution of these discrepancies is therefore hampered by the lack of exclusive channel measurements and detector acceptance corrections, which would enable the source(s) of any differences to be pinpointed.

For the 1n removal calculations, the main contribution (nearly half) to these cross sections for each target arises from the ^{27}Si+n exclusive channel when no FSI occur. Simple modifications to the current calculation model, such as using the Rasmussen[11] FSI escape probability ($P_{esc}\equiv 0.5$), would reduce the neutron cross-section differences; however, the calculated proton removal cross sections would also be reduced, destroying the agreement that presently exists between theory and experiment. A potential source for part of the difference between neutron and proton removal cross sections, not accounted for by the theory, is the difference in removal threshold energies. A proton, being less tightly bound, should have a larger removal cross section than a neutron. To test this hypothesis, we turn to the earlier fragmentation measurement of carbon and oxygen beams by Lindstrom *et al.*[17] which provide a fairly complete data set. Correcting their measurements for EMD contributions using Ref. 18, we find that the exclusive 1p removal channel (^{15}N or ^{11}B formation) is only 10%–20% larger than the exclusive 1n removal channel (^{15}O or ^{11}C). Adding the other 1n and 1p exclusive channels (^{14}N, ^{13}N, ^{13}C, ^{10}C, etc.) to estimate experimental 1n and 1p inclusive cross sections yields much smaller differences between them—unlike the recent ^{28}Si measurements[1] where the 1p semi-inclusive cross sections are substantially larger than the 1n cross sections. From a binding energy point of view, this may result from the fact that the ^{11}C-^{11}B binding-energy difference is smaller than that for ^{27}Si-^{27}Al. A way to incorporate proton-neutron binding-energy differences into the present model may be to use different nuclear distributions for the proton and neutron densities. Such efforts are considered in Refs. 19 and 20. Recent work[21,22] has shown how the binding energy is directly influenced by the nuclear density. In principle, then, one could model the proton-neutron densities of ^{28}Si to fit the observed binding-energy differences. However, this particular method is beyond the scope of the present treatment. Instead, possible changes to the calculated cross sections, resulting from neutron-proton density differences, were modeled by reducing the half-density radius of the ^{28}Si neutron distribution by 0.5 fm. The calculated neutron cross sections were reduced, as anticipated, but by only a few millibarns (less than 10 mb for all targets). These reductions were not large enough to account for the reported differences between measured semi-inclusive proton and neutron removal channels. Clearly, exclusive channel experimental measurements for ^{28}Si hadronic cross sections, which are presently being analyzed,[16] would substantially aid efforts to resolve the differences between calculation and experimental measurements.

The authors wish to thank Dr. H. Takai and Dr. P. Braun-Munzinger for useful discussions. This work was partly supported by NASA Grants No. NCCI-42 and No. NAG-1-1134.

[1]E814 Collaboration, J. Barrette *et al.*, Phys. Rev. C **41**, 1512 (1990).

[2]J. D. Jackson, *Classical Electrodynamics* (Wiley, New York, 1975).

[3]W. J. Llope and P. Braun-Munzinger, Phys. Rev. C **41**, 2644 (1990).

[4]C. Brechtmann, W. Heinrich, and E. V. Benton, Phys. Rev. C **39**, 2222 (1989).

[5]C. J. Benesh, B. C. Cook, and J. P. Vary, Phys. Rev. C **40**, 1198 (1989).

[6]L. W. Townsend, J. W. Wilson, F. A. Cucinotta, and J. W. Norbury, Phys. Rev. C **34**, 1491 (1986).

[7]John W. Norbury and Lawrence W. Townsend, Phys. Rev. C **42**, 1775 (1990).

[8]L. W. Townsend, Can. J. Phys. **61**, 93 (1983); L. W. Townsend, J. W. Wilson, and J. W. Norbury, *ibid.* **63**, 135 (1985).

[9]F. E. Ringia, T. Dobrowolski, H. R. Gustafson, L. W. Jones, M. J. Longo, E. F. Parker, and Bruck Cork, Phys. Rev. Lett. **28**, 185 (1972).

[10]J. D. Bowman, W. J. Swiatecki, and C. F. Tsang, Lawrence Berkeley Laboratory Report No. LBL-2908, 1973 (unpublished).

[11]Luiz F. Oliveira, Raul Donangelo, and John O. Rasmussen, Phys. Rev. C **19**, 826 (1979).

[12]D. J. Morrissey, L. F. Oliveira, J. O. Rasmussen, G. T Seaborg, Y. Yariv, and Z. Fraenkel, Phys. Rev. Lett. **43**, 113 (1979).

[13]Lawrence W. Townsend and John W. Norbury, Nationa Aeronautics and Space Administration Technical Memorandum No. TM-86340, 1985 (unpublished).

[14]J. Gosset, H. H. Gutbrod, W. G. Meyer, A. M. Poskanzer, A. Sandoval, R. Stock, and G. D. Westfall, Phys. Rev. C **16**, 629 (1977).

[15]John W. Wilson, Lawrence W. Townsend, and Forooz F. Badavi, Nucl. Instrum. Methods Phys. Res. Sect. B **18**, 225 (1987).

[16]H. Takai (private communication).

[17]P. J. Lindstrom, D. E. Greiner, H. H. Heckman, Bruce Cork, and F. S. Bieser, Lawrence Berkeley Laboratory Report No. LBL-3650, 1975 (unpublished).

[18]J. W. Norbury, Phys. Rev. C **40**, 2621 (1989).

[19]G. Bertsch, H. Esbensen, and A. Sustich, Phys. Rev. C **42**, 758 (1990).

[20]G. Bertsch, B. A. Brown, and H. Sagawa, Phys. Rev. C **39**, 1154 (1989).

[21]J. W. Negele, Phys. Rev. C **1**, 1260 (1970), see Fig. 5.

[22]X. Campi and D. W. Sprung, Nucl. Phys. A **194**, 401 (1972), see Fig. 12.

RAPID COMMUNICATIONS

PHYSICAL REVIEW C VOLUME 43, NUMBER 2 FEBRUARY 1991

Relativistic Coulomb fission

John W. Norbury
Department of Physics, Rider College, Lawrenceville, New Jersey 08648
(Received 28 June 1990)

Nuclear fission reactions induced by the electromagnetic field of relativistic nuclei are studied for energies relevant to present and future relativistic heavy-ion accelerators. Cross sections are calculated for ^{238}U and ^{239}Pu fission induced by ^{12}C, ^{28}Si, ^{197}Au, and ^{238}U projectiles. It is found that some of the cross sections can exceed 10 b.

Considerable interest in the use of electromagnetic (em) probes to study nuclear fission in recent years can be found by discussions of photofission by Bohr and Mottleson,[1] Huizenga and Britt,[2] and Berman and coworkers.[3,4]

In a detailed study of photofission in the actinide region using monoenergenic photon beams, Berman and coworkers[3,4] find that the photofission cross section in the region of the giant dipole resonance (GDR) is of a magnitude comparable to the photoneutron cross section.

Complementary em studies also have been made using electron beams. For example Arruda-Neto *et al.*[5] have made detailed studies of electrofission in which they separate out effects due to separate em multipolarities such as electric dipole ($E1$), quadrupole ($E2$), and magnetic dipole ($M1$). They relate the electrofission cross section $\sigma_{e,F}$ to the photofission cross section $\sigma_{\gamma,F}$ via

$$\sigma_{e,F}=\sum_{\lambda L}\int\sigma_{\gamma,F}^{\lambda L}(\omega)N^{\lambda L}(\omega)\frac{d\omega}{\omega}, \tag{1}$$

where λL refers to a particular em multipolarity (such as $E2$), and $N^{\lambda L}(\omega)$ is the number spectrum of virtual photons of frequency ω radiated by the electron. The total photofission cross section $\sigma_{\gamma,F}(\omega)$ is the sum of all multipolarities

$$\sigma_{\gamma,F}(\omega)=\sum_{\lambda L}\sigma_{\gamma,F}^{\lambda L}(\omega). \tag{2}$$

The third type of em probe that has been used in fission studies are heavy ions which have the advantage of being able to carry a very large charge, thus giving rise to large cross sections. This is often referred to as *Coulomb fission* and has been reviewed by Oberacker, Pinkston, and Kruse[6] and also briefly discussed by Eisenberg and Greiner.[7] As with much of the early work on Coulomb excitations,[8] the studies of Coulomb fission have been limited to low energies near the Coulomb barrier.[6,7]

It is the aim of the present work to broaden the study of Coulomb fission to include *relativistic* nucleus-nucleus collisions. At relativistic energies the Weizsäcker-Williams (WW) equivalent-photon method[9,10] is a very good approximation where one replaces the incident nucleus with its equivalent virtual photon field given by[10]

$$N_{WW}(\omega)=\frac{2}{\pi}Z^2\alpha\left[\frac{c}{v}\right]^2\left[\xi K_0K_1-\frac{v^2\xi^2}{2c^2}(K_1^2-K_0^2)\right], \tag{3}$$

where α is the fine-structure constant, ω is the photon frequency, v is the speed of the nucleus, and Z is the charge. K_1 and K_0 are modified Bessel functions which are both functions of ξ defined as

$$\xi=\frac{\omega b_{\min}}{\gamma v}, \tag{4}$$

where γ is the usual relativistic factor and $b_{\min}$ is the minimum impact parameter, below which the reaction proceeds via the hadronic interaction,

$$b_{\min}=1.2(A_T^{1/3}+A_P^{1/3})\text{ fm}, \tag{5}$$

where A_T and A_P are the target and projectile nucleon numbers. The total relativistic nuclear (N) Coulomb fission cross section is then given by

$$\sigma_{N,F}=\int\sigma_{\gamma,F}(\omega)N_{WW}(\omega)\frac{d\omega}{\omega}. \tag{6}$$

Bertulani and Baur[11,12] have shown that the WW photon spectrum is the same as the $E1$ spectrum. Also, when $v=c$, they have shown that the spectrum of *all* multipolarities is the same as WW. Thus, Eqs. (1) and (6) are identical in the high-energy limit. Clearly Eq. (6) is simpler to use because one does not need to breakup the photofission cross section into its individual multipoles, (which become important at low energy[11,12]). In Ref. 13 some detailed studies were made of the effects of electric quadrupole ($E2$) excitations for single nucleon emission and for a more exact form of $b_{\min}$. $E2$ effects on fission cross sections have not yet been examined but it is expected[13] that they would be negligible at high energies and would produce *at most* a 3% change in the cross section near 14 GeV/nucleon. $E2$ and $b_{\min}$ differences are neglected in the present work to keep the analysis simple and because they do not contribute *large* differences. Their effects will be included in later work. The use of Eq. (6) enables accurate calculations of relativistic Coulomb fission to be made because one can simply insert *experimental* photofission cross sections[3,4] for $\sigma_{\gamma,F}(\omega)$.

Berman and co-workers[3,4] have provided some very nice photofission data in the GDR region for actinides ^{232}Th, ^{233}U, ^{234}U, ^{235}U, ^{236}U, ^{238}U, ^{237}Np, and ^{239}Pu. Given the exploratory nature of the present work, calculations are presented for relativistic Coulomb fission only from ^{238}U and ^{239}Pu targets. The projectiles used are ^{12}C, ^{28}Si, ^{197}Au, and ^{238}U at a range of energies relevant to relativistic heavy-ion accelerators. These are the Bevalac at Berkeley ($T_{\text{lab}}=2.1$ GeV/nucleon), the Alternating Gra-

dient Synchrotron (AGS) at Brookhaven ($E_{lab}=14.6$ GeV/nucleon), and the Super Proton Synchrotron (SPS) at the European Center for Nuclear Research (CERN) ($E_{lab}=60$ and 200 GeV/nucleon). Results are also presented for the Relativistic Heavy Ion Collider (RHIC) to be built at Brookhaven ($E_{c.m.}=100$ GeV/nucleon per beam, corresponding to a single beam energy $T_{lab}=21$ TeV/nucleon).

The calculated cross sections are presented in Figs. 1 and 2 for the above projectiles, targets, and energies. It can be seen that many of the cross sections are enormous. For instance for ^{239}Pu fission with a ^{197}Au projectile the cross section is about 10 b for the AGS energies growing to about 50 b for RHIC energies. These large values suggest that experimental studies of relativistic Coulomb fission may be possible. For instance at the AGS one could use a ^{197}Au projectile on a ^{238}U or ^{239}Pu target.

Given the large cross sections a question arises as to whether beams would live long enough for a RHIC experiment. For definiteness consider a U-U colliding-beam experiment at RHIC with an energy per beam of 100 GeV/nucleon, corresponding to a T_{lab} of 21 TeV/nucleon (cf. Figs. 1 and 2). The fission cross section is 33 b. However the em interaction also can cause the excited ^{238}U nucleus to emit a neutron (n) or two neutrons ($2n$). Using the same technique as the present paper (see also Ref. 14) one obtains cross sections of 48 and 31 b, respectively, giving a total em cross section (fission$+n+2n$) of 112 b, which agrees well with the estimate of Baur and Bertulani,[15] who also calculate the $U+U\rightarrow(U+e^-)+e^++U$ cross section as 80 b. These processes provide the dominant beam ion cross section which is discussed in Refs. 15 and 16 (see pages 130–136).

The ^{197}Au beam parameters[16] (which would not be too different from a ^{238}U beam) for RHIC are the following: number of beam intersections $k=6$; number of particles per bunch $N_B=1.1\times10^9$; number of bunches $B=57$; and initial luminosity $L_0=9.2\times10^{26}$ cm^{-2}sec^{-1}.

The reaction rate is[16]

$$\lambda=-\frac{1}{I}\frac{dI}{dt}, \tag{7}$$

where I is the beam intensity, with the total beam initial half-life given by[16]

$$\tau=\frac{0.693}{\Sigma_i\lambda_i}, \tag{8}$$

where λ_i are the reaction rates due to various processes which are given in Ref. 16 as beam-gas nuclear reaction λ_1, beam-beam nuclear reaction λ_2, beam-beam Coulomb dissociation λ_3, and beam-beam bremstrahlung electron pair production λ_4. Only λ_3 and λ_4 contribute significantly for U-U collisions at RHIC. For the 80 b cross section[15,16] listed above λ_4 is 31.6×10^{-3} h^{-1}. For Coulomb dissociation[16]

$$\lambda_3=\frac{kL_0\sigma}{BN_B}=35.5\times10^{-3}\,h^{-1} \tag{9}$$

for $\sigma=112$ b. Thus the total initial half-file of the beam is 10 h. As mentioned in Ref. 16, the beam lifetime will actually be somewhat larger due to dilution of the phase-space density of the bunch since the beam lifetime depends on the beam dimensions. Thus U-U beams installed in RHIC appear to live long enough for fission and other measurements to be carried out.

Finally, it is of interest to consider how one might distinguish Coulomb fission from fission induced by nuclear forces. From Eq. (3) one can see the characteristic Z^2 dependence of the Coulomb cross section, although, as pointed out in the second paper of Ref. 13, this dependence becomes modified at lower energies. Nevertheless for energies greater than about 10 GeV/nucleon the dependence for all nuclei should remain as Z^2. Such a dependence would provide a clear signature for Coulomb versus nuclear processes.

A brief summary is now given. (i) The first calculations for *relativistic* Coulomb fission are presented herein. The calculations are performed using the Weizsäcker-

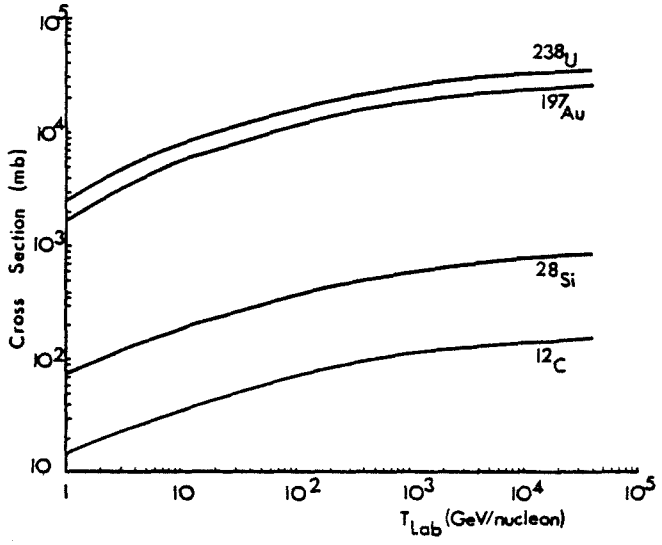

FIG. 1. Relativistic Coulomb fission cross sections as a function of laboratory kinetic energy for ^{238}U targets. The projectiles are ^{12}C, ^{28}Si, ^{197}Au, and ^{238}U.

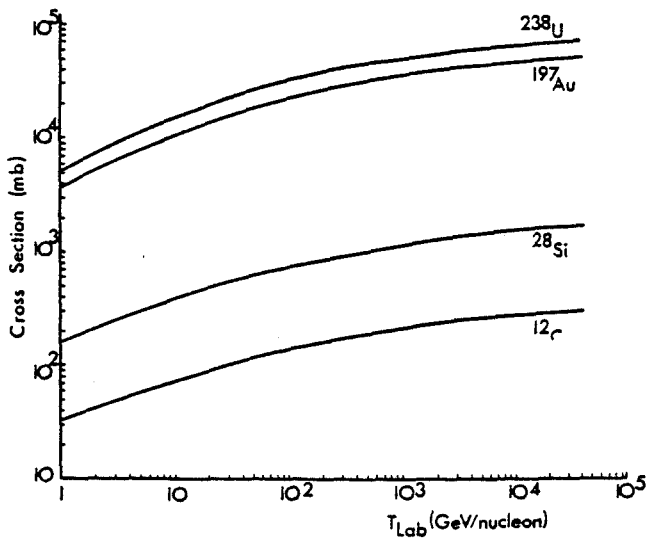

FIG. 2. Same as Fig. 1 except for ^{239}Pu targets.

Williams method of virtual quanta. (ii) The cross sections are very large and indicate that experiments may be feasible at fixed target accelerators such as the AGS. (iii) Even though the cross sections are large, it still appears that ^{238}U ions installed at RHIC would live long enough to make a useful beam. (iv) For energies greater than 10 GeV/nucleon, the Coulomb cross section will vary as Z^2 providing a clear separation from nuclear processes.

This work was supported in part by the National Aeronautics and Space Administration (NASA) under Grant No. NAG-1-1134.

[1]A. Bohr and B. Mottleson, *Nuclear Structure* (Benjamin, Reading, MA, 1975).

[2]J. R. Huizenga and H. C. Britt, in *Proceedings of the International Conference on Photonuclear Reactions and Applications*, edited by B. L. Berman (Lawrence Livermore National Laboratory, Livermore, CA, 1973), p. 833.

[3]B. L. Berman, J. T. Caldwell, E. J. Dowdy, S. S. Dietrich, P. Meyer, and R. A. Alvarez, Phys. Rev. C **34**, 2201 (1986).

[4]J. T. Caldwell, E. J. Dowdy, B. L. Berman, R. A. Alvarez, and P. Meyer, Phys. Rev. C **21**, 1215 (1980).

[5]J. D. T. Arruda-Neto, S. Simionatto, S. B. Herdade, Z. Carvalheiro, M. L. Yoneama, and B. L. Berman, Phys. Scr. **40**, 735 (1989), and references therein.

[6]V. E. Oberacker, W. T. Pinkston, and H. G. W. Krüse, Rep. Prog. Phys. **48**, 327 (1985).

[7]J. M. Eisenberg and W. Greiner, *Excitation Mechanisms of the Nucleus*, 3rd ed. (North-Holland, Amsterdam, 1988), Vol. 2, p. 239.

[8]K. Alder, A. Bohr, T. Huus, B. Mottleson, and A. Winther, Rev. Mod. Phys. **28**, 432 (1956); **30**, 353 (1958).

[9]E. J. Williams, Kgl. Dan. Vidensk. Selsk. Mat. Fys. Medd. **XIII**, No. 4 (1935); Proc. R. Soc. London Ser. A **139**, 163 (1933); C. F. von Weizsäcker, Z. Phys. **88**, 612 (1934); E. Fermi, Z. Phys. **29**, 315 (1924).

[10]J. D. Jackson, *Classical Electrodynamics*, 2nd ed. (Wiley, New York, 1975).

[11]C. A. Bertulani and G. Baur, Nucl. Phys. A **458**, 725 (1986).

[12]C. A. Bertulani and G. Baur, Phys. Rep. **163**, 299 (1988).

[13]J. W. Norbury, Phys. Rev. C **42**, 711 (1990); *ibid.* **42**, 2259 (1990).

[14]J. W. Norbury, Phys. Rev. C **40**, 2621 (1989).

[15]G. Baur and C. A. Bertulani, Nucl. Phys. A **505**, 835 (1989).

[16]*Conceptual Design of the Relativistic Heavy Ion Collider*, Brookhaven National Laboratory Report No. BNL51932 (1986).

PHYSICAL REVIEW D VOLUME 42, NUMBER 11 1 DECEMBER 199(

Higgs-boson production in nucleus-nucleus collisions

John W. Norbury
Department of Physics, Rider College, Lawrenceville, New Jersey 08648
(Received 13 June 1990; revised manuscript received 15 August 1990)

Cross-section calculations are presented for the production of intermediate-mass Higgs bosons produced in ultrarelativistic nucleus-nucleus collisions via two-photon fusion. The calculations are performed in position space using Baur's method for folding together the Weizsacker-Williams virtual-photon spectra of the two colliding nuclei. It is found that two-photon fusion in nucleus-nucleus collisions is a plausible way of finding intermediate-mass Higgs bosons at the Superconducting Super Collider or the CERN Large Hadron Collider.

The existence of the Higgs boson is one of the most important questions in physics. Of the four known interactions in our Universe, only the electromagnetic and weak interactions have been successfully unified.[1] The exchange particles responsible for the forces are the photon (γ) and the intermediate vector bosons (W^+, W^-, Z^0) with masses of zero (γ) and 80 GeV (W^+, W^-) and 91 GeV (Z^0), respectively.[2] However, in a truly unified theory all exchange particles should have the same mass. The Higgs boson was introduced[3] to account for the mass difference between the photon and the intermediate vector bosons via the mechanism of spontaneous symmetry breaking. The discovery of the Higgs boson would therefore provide the last piece of crucial experimental evidence for the unified electroweak theory. However, this theory makes no definite prediction about the mass of the Higgs boson and therefore experimental searches must cover a very large range.

The possible Higgs-boson mass M_H is often classified as light (<80 GeV), intermediate (80 GeV $< M_H <$ 160 GeV) or heavy (>160 GeV). Drees *et al.*[4] have pointed out that a light Higgs boson can be found at the Large Electron Positron (LEP) collider at the European Center for Nuclear Research (CERN), while a heavy Higgs boson can be found in proton-proton collisions at the future Superconducting Super Collider (SSC) in Texas or at the Large Hadron Collider (LHC), which will be built in the LEP tunnel at CERN. However, intermediate-mass Higgs particles are much more difficult to find.

There have been several recent suggestions[4-7] that an intermediate-mass Higgs boson could be discovered by two-photon ($\gamma\gamma$) fusion produced in nucleus-nucleus collisions in the TeV/nucleon energy range. This would be inaccessible for the highest-energy planned nucleus-nucleus collider, which is the Relativistic Heavy Ion Collider (RHIC) at Brookhaven, which will have a beam energy of 100 GeV/nucleon/beam. However, the idea has been suggested[4-7] that if one were to accelerate heavy nuclei (instead of only protons) at the LHC or SSC then the beam energies would be 3.4 TeV/nucleon and 8 TeV/nucleon, respectively. The reason for an enhanced cross section is that for nucleus-nucleus collisions the two-photon cross section is larger than that for electron-positron collisions by a factor of Z^4 where Z is the nuclear charge.

Given this very exciting possibility it is extremely important to have an accurate estimate of the expected experimental cross section. Three sets of calculations have been made using momentum-space form factors.[4-7] As an additional possibility the present work investigates a recent suggestion of Baur[8] as to how to fold together the Weizsäcker-Williams (WW) virtual-photon spectra[9] of two colliding nuclei. The advantage of this position space formalism is that one can easily impose the condition that the nuclei do not overlap (otherwise strong interactions occur). For the sake of completeness some of Baur's equations are repeated here. The WW photon spectrum[8,9] is

$$N(\omega,b)=\frac{Z^2\alpha}{\pi^2}\left[\frac{\omega}{\gamma v}\right]^2\left[\frac{c}{v}\right]^2\left[K_1^2(x)+\frac{1}{\gamma^2}K_0^2(x)\right], \quad (1)$$

where α is the fine-structure constant, ω is the photon frequency, v is the speed of the nucleus, and γ is the usual relativistic factor. K_1 and K_0 are modified Bessel functions and x is defined[8] as

$$x=\frac{\omega b}{\gamma v}, \quad (2)$$

where b is the impact parameter. For nuclei, there is a minimum value of this impact parameter, below which the $\gamma\gamma$ process will be overtaken by the strong interaction. For the $\gamma\gamma$ process one integrates from this minimum value up to infinity. The $\gamma\gamma$ cross section for two nuclei is obtained by folding the individual $\gamma\gamma$ cross section $\sigma_{\gamma\gamma}(\omega_1,\omega_2)$ with the WW photon spectrum of each nucleus as[8]

$$\sigma=\int\frac{d\omega_1}{\omega_1}\int\frac{d\omega_2}{\omega_2}F(\omega_1,\omega_2)\sigma_{\gamma\gamma}(\omega_1,\omega_2), \quad (3)$$

where the folded spectra are given by[8]

$$F(\omega_1,\omega_2)=2\pi\int_{R_1}^{\infty}b_1db_1\int_{R_2}^{\infty}b_2db_2\int_0^{2\pi}d\phi\,N_1(\omega_1,b_1)N_2(\omega_2,b_2)\times\theta(b-R_1-R_2), \quad (4)$$

where R_1 and R_2 are the nuclear radii and[8]

$$b^2=b_1^2+b_2^2-2b_1b_2\cos\phi\ . \tag{5}$$

The step function θ in Eq. (4) is zero when $b<R_1+R_2$ and unity for $b>R_1+R_2$ thus ensuring that the nuclei do not overlap.

The $\gamma\gamma$ reaction cross section for forming the Higgs boson can be related to the two-photon decay width $\Gamma_{H\to\gamma\gamma}$ as[7]

$$\sigma_{\gamma\gamma}(s)\equiv\frac{8\pi^2}{M_H}\Gamma_{H\to\gamma\gamma}\delta(s-M_H^2)\ , \tag{6}$$

where s is the square of the invariant mass W^2:

$$s=W^2=4\omega_1\omega_2\ . \tag{7}$$

An approximate expression for the width is[10]

$$\Gamma_{H\to\gamma\gamma}=3\ \text{keV}\left[\frac{M_H}{100\ \text{GeV}}\right]^3\ , \tag{8}$$

but a more accurate expression is[11]

$$\Gamma_{H\to\gamma\gamma}=\frac{\alpha^2G_FM_H^3}{8\pi^3\sqrt{2}}|I|^2\ , \tag{9}$$

where G_F is the Fermi coupling constant and $|I|^2$ is calculated according to the formulas of Papageorgiu[6] but using a W mass of 80 GeV. The use of this more exact expression for the Higgs-boson width gives substantially larger cross sections than one obtains if $|I|^2$ is simply set equal to unity, particularly when the Higgs-boson mass approaches twice the W mass.

The δ function in Eq. (6) is valid in the narrow-resonance approximation. Inserting (6) and (7) into (3), one finally obtains

$$\sigma=\frac{8\pi^2}{M_H^3}\Gamma_{H\to\gamma\gamma}\int\frac{d\omega_1}{\omega_1}F\left[\omega_1,\frac{M_H^2}{4\omega_1}\right]\ . \tag{10}$$

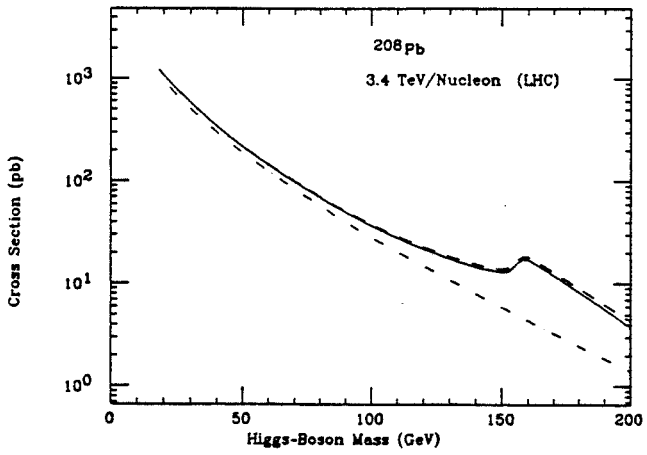

FIG. 1. Cross section in picobarns as a function of mass for Higgs-boson production via two-photon fusion with Pb-Pb collisions at 3.4 TeV/nucleon relevant to the LHC. The dash-dotted curve uses the width of Eq. (8). The solid and dashed curve uses the width of Eq. (9) corresponding to top-quark masses of 100 and 200 GeV, respectively. (These two lines merge together for a Higgs-boson mass of about 100 GeV.)

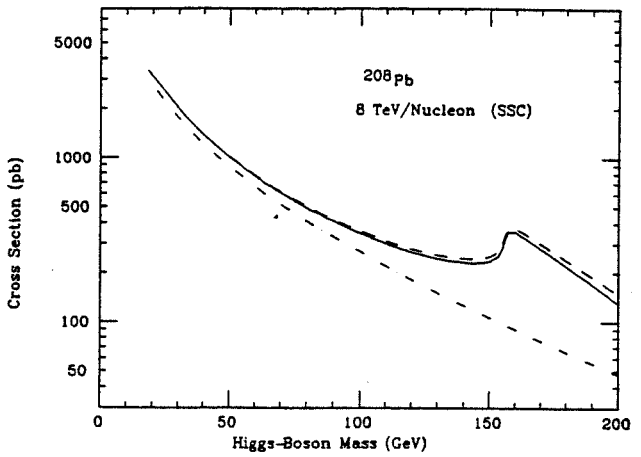

FIG. 2. Same as Fig. 1 except now for 8 TeV/nucleon relevant to the SSC.

Thus one has four nested integrals which must be evaluated numerically.

The numerical procedure can be tested very accurately because if θ is replaced by unity the three integrals in Eq. (4) can be evaluated analytically. Setting θ to unity the above equations were integrated numerically and the number of integration points and maximum energies were chosen so that the numerical answer converged to the analytical answer. These points and energies were then used in the real calculation incorporating the full θ function. (Convergence was again checked.)

The results of the present calculations appear in Figs. 1–4 for top-quark masses of 100 and 200 GeV and for Pb-Pb and U-U collisions at 3.4 TeV/nucleon (LHC) and 8 TeV/nucleon (SSC). One can see that the use of Eq. (9) gives substantially larger cross sections at larger Higgs-boson masses. Note the peak in the cross section when the Higgs-boson mass is twice the W mass, indicating the opening up of a new decay channel.

Recently Cahn and Jackson[10] and Baur and Ferreira Filho[12] have performed similar calculations. In private communications with these authors it appears that we all

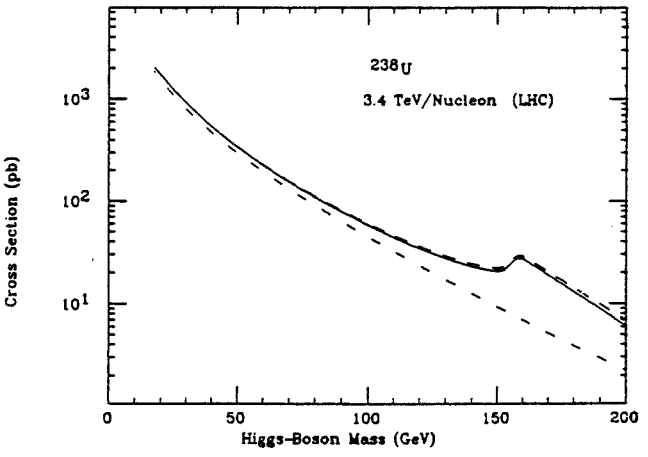

FIG. 3. Same as Fig. 1 except now for U-U collisions.

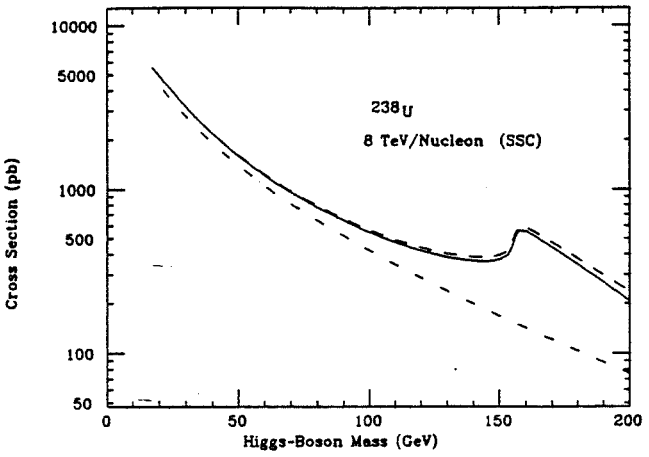

FIG. 4. Same as Fig. 2 except now for U-U collisions.

get the same results if we use the same Higgs-boson two-photon width [Eq. (8)]. However, the calculations presented in Figs. 1–4 now use both widths of Eqs. (8) and (9) above. In addition Wu *et al.*[13] have also presented calculations based upon the Monte Carlo evaluation of Feynman integrals.

In order to obtain an idea of how the present results compare with those of other authors the results obtained with Eq. (9) are now discussed. For U-U collisions at 8 TeV/nucleon (SSC) and for a Higgs-boson mass of 100 GeV, Grabiak *et al.*[7] calculate the cross section to be about 800 pb, while Papageorgiu[6] obtains about 600 pb. The present work obtains about 550 pb (roughly the same for top-quark masses of 100 and 200 GeV). Even though the differences vary as a function of Higgs-boson mass it is clear that the present position-space calculation incorporating a realistic cutoff gives smaller results than previous momentum-space calculations. Nevertheless the cross sections are still quite sizable, particularly for SSC energies, and two-photon fusion via nucleus-nucleus collisions may yet provide a way for discovering intermediate-mass Higgs bosons.

I am extremely grateful to Professor Gerhard Baur for his very encouraging comments. This work was supported in part by the National Aeronautics and Space Administration (NASA) under Grant No. NAG-1-1134.

[1]S. L. Glashow, Nucl. Phys. **22**, 579 (1961); S. Weinberg, Phys. Rev. Lett. **19**, 1264 (1967); A. Salam, in *Elementary Particle Theory: Relativistic Groups and Analyticity (Nobel Symposium No. 8)*, edited by N. Svartholm (Almqvist and Wiksell, Stockholm, 1968), p. 367.

[2]G. S. Abrams *et al.*, Phys. Rev. Lett. **63**, 2173 (1989); F. Abe *et al.*, *ibid.* **63**, 720 (1989); C. Albajar *et al.*, Z. Phys. C **44**, 15 (1989).

[3]P. W. Higgs, Phys. Lett. **12**, 132 (1964); Phys. Rev. Lett. **13**, 508 (1964); Phys. Rev. **145**, 1156 (1966).

[4]M. Drees, J. Ellis, and D. Zeppenfeld, Phys. Lett. B **223**, 454 (1989).

[5]E. Papageorgiu, Nucl. Phys. **A498**, 593c (1989).

[6]E. Papageorgiu, Phys. Rev. D **40**, 92 (1989).

[7]M. Grabiak, B. Müller, W. Greiner, G. Soff, and P. Koch, J. Phys. G **15**, L25 (1989).

[8]G. Baur, Physica Scripta **T32**, 76 (1990); in *Proceedings of the Rio de Janeiro International Workshop on Relativistic Aspects of Nuclear Physics* (World Scientific, Singapore, 1990), p. 127; and talk presented at "Can RHIC be used to test QED?" Workshop, Brookhaven National Laboratory, Upton, New York, 1990 (unpublished).

[9]J. D. Jackson, *Classical Electrodynamics*, 2nd ed. (Wiley, New York, 1975).

[10]R. N. Cahn and J. D. Jackson, this issue, Phys. Rev. D **42**, 3690 (1990).

[11]P. Renton, *Electroweak Interactions* (Cambridge University Press, Cambridge, England, 1990).

[12]G. Baur and L. G. Ferreira Filho, Nucl. Phys. A (to be published).

[13]J. S. Wu, C. Bottcher, M. R. Strayer, and A. K. Kerman (unpublished).

PHYSICAL REVIEW C VOLUME 42, NUMBER 5 NOVEMBER 1990

Charge dependence and electric quadrupole effects on single-nucleon removal in relativistic and intermediate energy nuclear collisions

John W. Norbury
Department of Physics, Rider College, Lawrenceville, New Jersey 08648
(Received 15 June 1990)

Single-nucleon removal in relativistic and intermediate energy nucleus-nucleus collisions is studied using a generalization of Weizsäcker-Williams theory that treats each electromagnetic multipole separately. Calculations are presented for electric dipole and quadrupole excitations and incorporate a realistic minimum impact parameter, Coulomb recoil corrections, and the uncertainties in the input photonuclear data. Discrepancies are discussed. The maximum quadrupole effect to be observed in future experiments is estimated and also an analysis of the charge dependence of the electromagnetic cross sections down to energies as low as 100 MeV/nucleon is made.

There has recently been considerable interest in single-nucleon removal in nucleus-nucleus reactions.[1–14] A large part of the cross section is due to electromagnetic (em) excitations which should be easily calculable by the Weiszäcker-Williams (WW) method[9] or by a simple generalization which distinguishes between electric multipoles.[4,8–11] Unfortunately, recent theoretical comparisons[3–5] to Bevalac data[7] indicated several discrepancies. Benesh, Cook, and Vary[3] have suggested that these discrepancies could be due to difficulties in subtracting the nuclear component from the total measured cross section. These authors also addressed the problem of what value to use for the minimum impact parameter which has been independently verified[12] to within a few percent. Even though the cross-section calculations of Benesh, Cook, and Vary look very promising, problems remain with ^{59}Co and ^{197}Au at energies relevant to the European Center for Nuclear Research (CERN).

A new experimental technique which attempts to avoid the above problem has been developed,[1] and new data are now available for nucleon removal from ^{28}Si at Alternating Gradient Synchrotron (AGS) energies. Other interesting work[2] has also been done on the charge dependence of the various processes in nucleus-nucleus reactions.

It is very important to fully understand em processes in nuclear collisions for all energies and all nuclei. The WW method has proven to be a useful tool in this context, but a more accurate theoretical analysis (herein referred to as "multipole theory") was developed by Bertulani and Baur,[9] Fleischhauer and Scheid,[10] and Goldberg[11] which treats each electric multipole separately.

The present paper is a continuation of previous work which used this more accurate analysis in understanding recent data.[4] The new items to be studied herein are as follows:

(1) inclusion of Coulomb recoil,[8] which Aleixo and Bertulani have shown enables the multipole theory of the virtual photon spectra[9] to be used with confidence for energies as low as 100 MeV/nucleon where the WW method breaks down;

(2) comparison of the multipole theory to new data at low energy[13] (150 MeV/nucleon), ^{28}Si data[1] at AGS energies (14.6 GeV/nucleon), and ^{32}S data[14] at CERN energy (200 GeV/nucleon);

(3) inclusion of experimental uncertainties in the photonuclear data, which is used as input into the multipole theory to arrive at a theoretical error giving better guidance in comparison to data;

(4) estimates of the maximum effect of electric quadrupole ($E2$) components in future experiments; and

(5) extension of recent WW studies of charge dependences[2] to much lower energies using multipole theory.

As pointed out in Refs. 4 and 9, the *isoscalar* component of the giant quadrupole resonance (GQR) and the isovector giant dipole resonance are expected to dominate single-nucleon removal cross sections. The isovector GQR lies at higher energy, where the virtual photon spectrum is much smaller, and decays mainly by two-nucleon emission. Note further that $E2$ transitions do *not* have the isospin selection rules found for $E1$ transitions.

The dipole and quadrupole cross sections discussed are calculated according to the method of Ref. 4 using the minimum impact parameter of Ref. 3 [which is expected to be more accurate[3,12] than the $1.2(A_P^{1/3}+A_T^{1/3})$ parametrization] and with the addition of the intermediate energy Coulomb recoil correction $\pi a_0/2\gamma$ of Ref. 8. [Note that there is a typing error in the first paper of Ref. 4. Equation (4) in that reference should have E_{GQR}^2 in the numerator and not E^2. Also, in Table I of Ref. 5, the last entry in the fifth column should read 335 ± 49 and not 73 ± 13.]

Quadrupole parameters are listed in Ref. 4 except those for ^{238}U and ^{28}Si for which the energy (MeV), width (MeV), and fractional exhaustion, respectively, are 10.2, 2.5, and 0.85 for ^{238}U and 19.7, 5.1, and 0.2 for ^{28}Si. The theoretical uncertainties based upon the uncertainties of the experimental photonuclear cross sections used as input are estimated to be 10% for ^{28}Si and ^{12}C and 5% for the heavier nuclei. The input photonuclear data are discussed in Ref. 5, and in Ref. 15 for ^{238}U and ^{28}Si. In addi-

TABLE I. Calculated cross sections $\sigma_{E1}+\sigma_{E2}$, which include the intermediate energy recoil correction of Ref. 8 and the impact parameter of Ref. 3, are added to σ_{nuclear} (Ref. 3) and compared to the total experimental cross sections of Ref. 7. The 150-MeV/nucleon data are from Ref. 13. All results refer to single-neutron removal from the target. See Ref. 16 for an important note.

Projectile	Target	T_{lab} (GeV/nucleon)	σ_{E1} (mb)	σ_{E2} (mb)	σ_{nuclear} (mb)	$\sigma_{E1}+\sigma_{E2}+\sigma_{\text{nuclear}}$ (mb)	$\sigma_{\text{total}}^{\text{expt}}$ (mb)
^{12}C	^{238}U	2.1	29	9	132	170±8	173±22
^{20}Ne	^{238}U	2.1	78	22	140	240±12	192±16
^{12}C	^{197}Au	2.1	38	7	124	169±8	178±7
^{20}Ne	^{197}Au	2.1	102	17	131	250±14	268±11
^{40}Ar	^{197}Au	1.8	286	48	142	476±34	463±30
^{56}Fe	^{197}Au	1.7	558	93	149	800±66	707±52
^{139}La	^{197}Au	1.26	2008	357	169	2534±237	2130±120
^{139}La	^{197}Au	0.15	574	566	177	1317±114	765±48
^{16}O	^{197}Au	60	211	15	128	354±24	400±20
^{16}O	^{197}Au	200	273	17	128	418±30	560±30
^{12}C	^{89}Y	2.1	13	1	98	112±5	115±6
^{20}Ne	^{89}Y	2.1	34	3	105	142±6	160±7
^{40}Ar	^{89}Y	1.8	94	9	115	218±12	283±11
^{56}Fe	^{89}Y	1.7	181	17	121	319±21	353±14
^{12}C	^{59}Co	2.1	8	1	87	96±5	89±5
^{20}Ne	^{59}Co	2.1	20	1	94	115±5	132±7
^{56}Fe	^{59}Co	1.7	103	7	110	220±13	194±9
^{139}La	^{59}Co	1.26	351	26	129	506±38	450±30
^{12}C	^{12}C	2.1	0.5	0	59	60±3	60.7±0.6
^{20}Ne	^{12}C	1.05	1	0	66	67±4	78±2
^{56}Fe	^{12}C	1.7	6	0	83	89±5	94±2
^{139}La	^{12}C	1.26	20	1	102	123±7	148±2

tion, a 5% error is included for possible uncertainties occurring in the $E2$ parameters.[4] Unlike previous work, the present electromagnetic multipole cross sections are added to the nuclear cross sections of Benesh, Cook, and Vary[3] (see Ref. 16 for an important note) and compared to the originally measured total cross section. The final theoretical uncertainty in $\sigma_{E1}+\sigma_{E2}+\sigma_{\text{nuclear}}$ incorporates the errors discussed above together with the theoretical uncertainties of Ref. 3. In addition, the em calculations are compared to newly published em data[1,13,14] for energies ranging from 150 MeV/nucleon to 14.6 GeV/nucleon to 200 GeV/nucleon (see Table I). Taken together with previous comparisons,[1,3-5,7] the results shown in Tables I and II show substantial improvement in understanding the data. The apparent disagreements between theory and experiment for ^{28}Si+^{27}Al are discussed in Ref. 1 as likely due to a remaining hadronic component. Excellent agreement between theory and experiment is obtained for ^{32}S+^{197}Au at 200 GeV/nucleon even though poor agreement is obtained for the ^{16}O projectile at the same energy. An additional measurement seems in order here. Some of the other disagreements such as ^{40}Ar+^{89}Y and ^{139}La+^{12}C may be due to uncertainties in the nuclear part of the cross section.[12] The

TABLE II. Calculated cross sections, as in Table I, are compared to experimental em cross sections of Ref. 13 (^{139}La) and Ref. 14 (^{32}S). In the case of ^{28}Si (Ref. 1) the protons or neutrons are emitted from the projectile and only the experimental semi-inclusive cross sections are listed. All energies represent total energy E, except for 0.15 GeV/nucleon (first row), which represents kinetic energy T. The experimental numbers for ^{28}Si were obtained by adding up the exclusive cross sections listed in Ref. 6.

Projectile	Target	Lab energy (GeV/nucleon)	Final state	$\sigma_{\text{em}}^{\text{expt}}$ (mb)	σ_{WW} (mb)	σ_{E1} (mb)	σ_{E2} (mb)	$\sigma_{E1}+\sigma_{E2}$ (mb)
^{139}La	^{197}Au	0.15	^{196}Au	447	603±30	574	566	1140±114
^{32}S	^{197}Au	200	^{196}Au	1120±160	1104±55	1073	60	1133±113
^{28}Si	^{27}Al	14.6	1p	37±5	24±2	24	0	24±4
^{28}Si	^{27}Al	14.6	1n	15±4	9±1	9	0	9±1
^{28}Si	^{120}Sn	14.6	1p	313±4	317±32	315	3	318±48
^{28}Si	^{120}Sn	14.6	1n	136±6	118±12	118	1	119±18
^{28}Si	^{208}Pb	14.6	1p	743±27	806±81	802	8	810±122
^{28}Si	^{208}Pb	14.6	1n	347±18	301±30	299	2	301±45

TABLE III. Calculated cross sections, as in Tables I and II, for single-neutron emission from ^{197}Au targets at a variety of laboratory and center-of-mass (c.m.) energies. The relevant accelerators are listed in parentheses. Even though ^{197}Au projectiles will not be available at all the energies below, the same ^{197}Au projectile was used simply for the sake of comparison to provide an upper limit for the importance of $E2$ effects. (AGS: alternating gradient synchrotron; RHIC: relativistic heavy ion collider.) The last column represents $(\sigma_{E1}+\sigma_{E2}-\sigma_{WW})/(\sigma_{E1}+\sigma_{E2})$ as a (rounded-off) percentage. All cross sections are in units of barn.

Energy	σ_{WW}	σ_{E1}	σ_{E2}	$\sigma_{E1}+\sigma_{E2}$	Percentage difference
$T_{lab}=100$ MeV/nucleon	0.56	0.53	0.83	1.36	60%
$T_{lab}=300$ MeV/nucleon	1.7	1.6	0.8	2.4	30%
$T_{lab}=500$ MeV/nucleon	2.3	2.2	0.7	2.9	20%
$T_{lab}=2.1$ GeV/nucleon (Bevalac)	4.9	4.7	0.6	5.3	8%
$E_{lab}=12$ GeV/nucleon (AGS)	11.1	10.8	0.7	11.5	3%
$T_{lab}=60$ GeV/nucleon (CERN)	19.3	18.7	1.0	19.7	2%
$T_{lab}=200$ GeV/nucleon (CERN)	25.5	24.7	1.1	25.8	1%
$T_{lab}=200$ GeV/nucleon (RHIC)	49.5	48.1	1.4	49.5	0%

disagreements at 150 MeV/nucleon for ^{139}La+^{197}Au are discouraging since the new theoretical additions in the present work should be more significant at lower energies (Loveland *et al.*[13] have also recognized this discrepancy). Since there is only one data point at lower energy, further experiments between 100 MeV/nucleon and 1 GeV/nucleon are particularly welcome. Finally, some light may be shed on the ^{139}La+^{197}Au disagreement by the study of ^{197}Au+^{197}Au at AGS energies.

To serve as a guide for the relative importance of $E2$ effects, the percentage differences between WW and multipole theory cross sections are shown in Table III. Calculations are presented for nucleon emission from ^{197}Au, which has one of the largest giant quadrupole resonances. Thus the cross sections listed represent the *maximum* $E2$ effect that one is ever likely to observe at the selected energies. A negligible percentage difference means that one would get just as good results using WW theory rather than multipole theory. As expected, $E2$ effects are not really relevant for energies above that of the AGS. *Note most importantly that this conclusion is only valid for single-nucleon emission.* Two-neutron removal may well be observed at high energy due to decay of the isovector giant quadrupole resonance.

Finally, the charge dependence of em processes in nucleus-nucleus collisions has been previously described by Hill *et al.*[7] and Lissauer and Takai,[2] who note that significant deviations from a simple Z^2 dependence can occur in the WW formalism. However, the WW method is limited to high energies and the advantage of the multipole theory incorporating recoil corrections is that the charge dependence studies can be taken to much lower energies. In Fig. 1 the cross section is plotted versus the charge of the incident nucleus. Note that the log plots

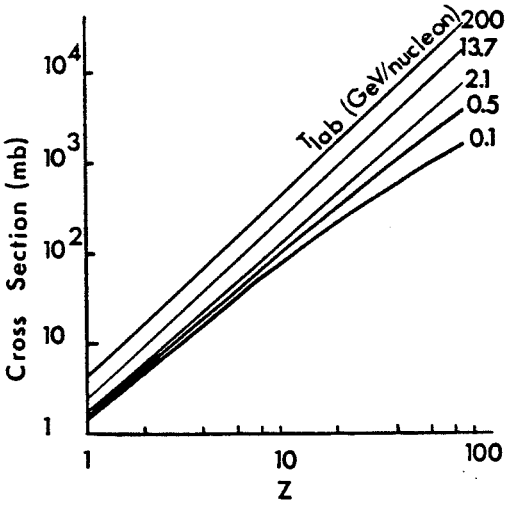

FIG. 1. ^{197}Au neutron removal cross section (mb) versus nuclear charge as a function of projectile energy.

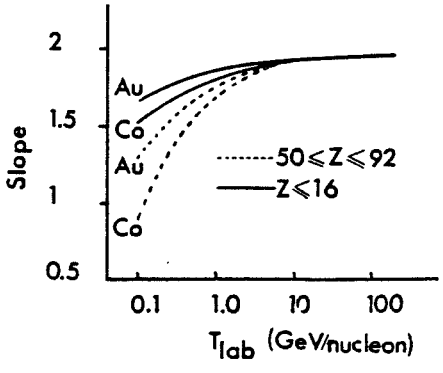

FIG. 2. Power of Z dependence (slope) versus projectile energy for neutron removal from ^{197}Au and ^{59}Co. The solid lines represent the low-Z region ($Z\leq 16$) and the dashed lines represent high-Z region ($50\leq Z\leq 92$). The dashed lines merge with the solid lines at about 10 GeV/nucleon.

are *curved* (particularly at the lower energies), indicating that there is no unique Z dependence. Nevertheless, a straight line can be fitted to the low-Z ($Z \leq 16$) region and a line of a different slope can be fitted to the high-Z ($50 \leq Z \leq 92$) region. At high energy these lines become indistinguishable from one another. To illustrate Z dependence, plots similar to Ref. 2 are shown in Fig. 2 for both high- and low-Z for single-neutron removal from ^{59}Co and ^{197}Au. Clearly, it is not possible to average out the curves into a single curve. Furthermore, one expects[2] that for processes corresponding to different photonuclear energies the corresponding plots would not overlap those of Fig. 2.

Even though one should not extend WW theory to lower energies, nevertheless if one does this, then the WW plots corresponding to Fig. 1 come out with *exactly the same shapes*, although the cross sections are all smaller. *Thus Fig. 2 is identical for both WW and multipole theory.*

In summary, the electromagnetic multipole theory[9] for nucleon emission from nucleus-nucleus reactions incorporating realistic minimum impact parameter,[3,12] Coulomb recoil correction,[8] and photonuclear data and quadrupole parameter uncertainties has been added to nuclear interaction cross sections[3] and compared to previous[7] and new data.[1,13,14] The maximum amount of $E2$ contribution has been noted and experimental discrepancies pinpointed. An analysis of charge dependence of the cross section down to energies as low as 100 MeV/nucleon has also been made.

Note added in proof. It should be noted that the $E2$ sum rule (which is strictly only valid for spin-zero nuclei) used in Refs. 4 and 9 and the present work has not been separated into its individual isoscalar and isovector parts. The reason for this is discussed by E. C. Halbert, J. B. McGrory, G. R. Satchler, and J. Speth in Nucl. Phys. **A245**, 189 (1975), where they show that the usual method of multiplying the sum rule by Z/A (to obtain the isoscalar component) can lead to an overexhaustion of the sum rule for non-self-conjugate nuclei. Given this, and the fact that most of the nuclei in Refs. 4 and 9 and the present work are not spin zero, the magnitude of the calculated electric quadrupole effects should be considered as an *approximate upper limit.*

I wish to thank Professor Gerhard Baur, Professor Carlos Bertulani, and Professor John Hill for very valuable discussions. I also thank Dr. Helio Takai for suggesting the charge dependence problem. I would also like to express my gratitude to Dr. G. R. Satchler and Dr. W. Llope. This work was supported in part by the National Aeronautics and Space Administration (NASA) under Grant No. NAG-1-1134.

[1] J. Barrette *et al.*, Phys. Rev. C **41**, 1512 (1990).
[2] D. Lissauer and H. Takai, Phys. Rev. C **41**, 2410 (1990).
[3] C. J. Benesh, B. C. Cook, and J. P. Vary, Phys. Rev. C **40**, 1198 (1989).
[4] J. W. Norbury, Phys. Rev. C **41**, 372 (1990); **42**, 711 (1990).
[5] J. W. Norbury, Phys. Rev. C **40**, 2621 (1989).
[6] W. J. Llope and P. Braun-Munzinger, Phys. Rev. C **41**, 2644 (1990).
[7] J. C. Hill, F. K. Wohn, J. A. Winger, and A. R. Smith, Phys. Rev. Lett. **60**, 999 (1988); J. C. Hill, F. K. Wohn, J. A. Winger, M. Khayat, K. Leininger, and A. R. Smith, Phys. Rev. C **38**, 1722 (1988); A. R. Smith, J. C. Hill, J. A. Winger, and P. J. Karol, *ibid.* **38**, 210 (1988); M. T. Mercier, J. C. Hill, F. K. Wohn, C. M. McCullough, M. E. Nieland, J. A. Winger, C. B. Howard, S. Renwick, and D. K. Matheis, *ibid.* **33**, 1655 (1986).
[8] A. N. F. Aleixo and C. A. Bertulani, Nucl. Phys. **A505**, 448 (1989); A. Winther and K. Alder, *ibid.* **A319**, 518 (1979).
[9] C. A. Bertulani and G. Baur, Phys. Rep. **163**, 299 (1988); B. Hoffman and G. Baur, Phys. Rev. C **30**, 247 (1984).
[10] R. Fleischhauer and W. Scheid, Nucl. Phys. **A493**, 583 (1989); *ibid.* **A504**, 855 (1989); *ibid.* **A510**, 817 (1990).
[11] A. Goldberg, Nucl. Phys. **A420**, 636 (1984).
[12] J. W. Norbury and L. W. Townsend, Phys. Rev. C **42**, 1775 (1990).
[13] W. Loveland, Z. Xu, C. Casey, K. Aleklett, J. O. Liljenzin, D. Lee, and G. T. Seaborg, Phys. Rev. C **38**, 2094 (1988).
[14] J. C. Hill, in *Current Issues in Hadron Physics*, edited by J. Tran Thanh Van (Editions Frontières, Gif-sur-Yvette, France, 1988); see also AGS Users Newsletter, Brookhaven National Laboratory, April–June 1990.
[15] R. L. Gulbranson, L. S. Cardman, A. Doron, A. Erell, K. R. Lingren, and A. I. Yavin, Phys. Rev. C **27**, 470 (1983); R. E. Pywell, B. L. Berman, J. W. Jury, J. G. Woodworth, K. G. McNeill, and M. N. Thompson, *ibid.* **27**, 960 (1983); J. T. Caldwell, E. J. Dowdy, B. L. Berman, R. A. Alvarez, and P. Meyer, *ibid.* **21**, 1215 (1980).
[16] J. P. Vary (private communication). The nuclear cross sections listed in Table I of the text are what one obtains with the formulas of Ref. 3. These differ slightly from the cross section values listed in Ref. 3 due to a small error in that work.

PHYSICAL REVIEW C VOLUME 42, NUMBER 4 OCTOBER 1990

Single nucleon emission in relativistic nucleus-nucleus reactions

John W. Norbury
Department of Physics, Rider College, Lawrenceville, New Jersey 08648
and NASA Langley Research Center, Hampton, Virginia 23665

Lawrence W. Townsend
NASA Langley Research Center, Hampton, Virginia 23665

(Received 25 June 1990)

Significant discrepancies between theory and experiment have previously been noted for nucleon emission via electromagnetic processes in relativistic nucleus-nucleus collisions. The present work investigates the hypothesis that these discrepancies have arisen due to uncertainties about how to deduce the experimental electromagnetic cross section from the total measured cross section. An optical-model calculation of single neutron removal is added to electromagnetic cross sections and compared to the total experimental cross sections. Good agreement is found thereby resolving some of the earlier noted discrepancies. A detailed comparison to the recent work of Benesh, Cook, and Vary is made for both the impact parameter and the nuclear cross section. Good agreement is obtained giving an independent confirmation of the parametrized formulas developed by those authors.

Recently Hill *et al.*[1] made a very detailed experimental study of nucleon emission induced by electromagnetic (EM) processes in relativistic nucleus-nucleus reactions. They compared the measured cross sections with theoretical calculations based upon the Weizsäcker-Williams (WW) method[2] of virtual quanta. Initial comparisons indicated[1,3] that the WW method is in serious disagreement with experiment for some projectile-target combinations, particularly[3] for nucleon emission from ^{197}Au. However, Benesh, Cook, and Vary[4] (BCV) recently speculated that the problem is due to difficulties in determining the experimental values of the EM cross section and not in the WW method.

The cross sections actually measured in experiments[1] are the total nucleon removal cross sections $\sigma_{\rm tot}$ which consist of both the nuclear and EM cross sections, $\sigma_{\rm nuc}+\sigma_{\rm EM}$. One theoretically calculates $\sigma_{\rm nuc}$ and then the experimental EM cross section is defined as

$$\sigma_{\rm EM}\equiv\sigma_{\rm tot}-\sigma_{\rm nuc}\ . \tag{1}$$

(Note that BCV have found interference effects[4] to be negligible.) Therefore, the reported $\sigma_{\rm EM}$ actually depends on the theory used to determine $\sigma_{\rm nuc}$, which, if incorrect, will lead to an incorrect experimental EM cross section. Hill *et al.* used the concept of weak factorization[1] to calculate $\sigma_{\rm nuc}$.

Benesh, Cook, and Vary[4] have recalculated $\sigma_{\rm nuc}$ using a very simple and convenient parametrization of a Glauber theory description of single nucleon removal. They added this to $\sigma_{\rm WW}$ and compared the sum to the originally measured $\sigma_{\rm tot}$. In general they find excellent agreement with experiment which strongly indicates that the discrepancies noted earlier[1,3] have more to do with nuclear reaction theory than with the WW method. However, not all problems have disappeared. The BCV calculations[4] give rather poor agreement for neutron removal from ^{59}Co. In addition the discrepancies noted[1,3] at the higher energies of 60 and 200 GeV/nucleon were not addressed.

An integral part of the BCV work[4] involved coming to grips with the problem of the impact parameter, b. In WW theory one must specify a *minimum* value $b_{\rm min}$, which is roughly the sum of the nuclear radii and then integrate from $b_{\rm min}$ to infinity. To unify the nuclear and WW theory, BCV determined the value of b necessary to remove one nucleon via the nuclear force and then used this same value as the input $b_{\rm min}$ to WW theory.

The present work has three aims: (1) to provide an independent study of whether or not the EM discrepancies between theory and experiment[1,3] are due to the way in which the nuclear contribution was subtracted from the total measured cross section; (2) to provide an independent estimate of the impact parameter for one nucleon removal which corresponds to the EM $b_{\rm min}$; and (3) to provide a detailed comparison to the recent BCV results.

The cross-section formalism, developed previously,[5] has been used in an abrasion-ablation model of nuclear fragmentation. In the present work we use only the abrasion model cross section which is simply given by a Glauber optical-model cross section for one nucleon removal but which also includes a Pauli correlation factor (neglected in the present work because it is negligible for peripheral collisions[5]) and an energy-dependent finite-range nuclear force term[5] (which *is* retained in the present work). In the absence of Pauli correlation effects and with a zero-range nuclear force, our expression for the cross section becomes identical to the BCV result [Eq. (1) of Ref. 4]. We have been very careful to use correct parametrizations of nuclear number densities, obtained by an unfolding procedure[5] from the corresponding nuclear charge densities whose parameters are from the lat-

est compilations.[6] To calculate the neutron production cross section we multiply the nucleon removal optical-model cross section by the neutron to nucleon ratio of the target nucleus and also by the final-state interaction (FSI) factor P_{esc} of BCV. Results are listed in Table I and will be discussed below.

In the above optical-model theory the cross section involves an integral over the impact parameter which is also true for the BCV optical theory.[4] Thus in order to determine b_{min} for the EM cross section, an independent method must be used to determine the most probable impact parameter for which a single nucleon is removed via the nuclear force. To calculate b we use a geometrical model based upon the methods of Ref. 7 which is described also in Ref. 8. The basic idea is that when the impact parameter takes on a certain small range of values, a

TABLE I. Impact parameters and cross sections for single neutron removal from various targets. σ represents the strong interaction nucleon removal cross section multiplied by the neutron to nucleon ratio of the target, P_{esc} is the escape probability and σ_{ww} is the Weiszäcker-Williams EM cross section. $\sigma P_{esc}+\sigma_{ww}$ is to be compared to the experimental cross section σ_{expt} (Ref. 1). For each projectile-target combination, the first row represents the present calculation (using P_{esc} and σ_{ww} from Ref. 4) and the second row is that of Ref. 4, which differs slightly from the values listed in that reference due to a small error (Ref. 9). Note also that for ^{20}Ne on ^{12}C the correct energy should be 1.05 GeV/nucleon (Ref. 1).

Projectile	Target	T_{lab} (GeV/nucleon)	b (fm)	σ (mb)	P_{esc}	σP_{esc} (mb)	σ_{ww} (mb)	$\sigma P_{esc}+\sigma_{ww}$ (mb)	σ_{expt} (mb)
^{12}C	^{238}U	2.1	10.7	252		165		189	173±22
			10.8	203	0.654	133	24	157	
^{20}Ne	^{238}U	2.1	11.2	273		177		240	192±16
			11.4	215	0.650	140	63	203	
^{12}C	^{197}Au	2.1	10.2	212		140		180	178±7
			10.3	188	0.659	124	40	164	
^{20}Ne	^{197}Au	2.1	10.7	234		153		257	268±11
			10.9	200	0.654	131	104	235	
^{40}Ar	^{197}Au	1.8	11.6	230		149		444	463±30
			11.9	220	0.648	143	295	438	
^{56}Fe	^{197}Au	1.7	12.1	228		147		716	707±52
			12.5	230	0.645	148	569	717	
^{139}La	^{197}Au	1.26	13.8	262		167		2225	2130±120
			14.4	266	0.636	169	2058	2227	
^{238}U	^{197}Au	0.96	15.1	325		205		4353	NA
			15.8	292	0.630	184	4148	4332	
^{16}O	^{197}Au	60	10.4	227		149	218	367	400±20
			10.6	195	0.656	128		346	
^{16}O	^{197}Au	200	10.4	227		149	281	430	560±30
			10.6	195	0.656	128		409	
^{12}C	^{89}Y	2.1	8.5	173		118		135	115±6
			8.4	144	0.682	98	17	115	
^{20}Ne	^{89}Y	2.1	9.0	191		129		171	160±7
			9.0	155	0.676	105	42	147	
^{40}Ar	^{89}Y	1.8	9.9	192		128		243	283±11
			10.0	173	0.668	116	115	231	
^{56}Fe	^{89}Y	1.7	10.4	192		127		349	353±14
			10.6	183	0.664	122	222	344	
^{12}C	^{59}Co	2.1	7.8	159		111		119	89±5
			7.6	125	0.695	87	8	95	
^{20}Ne	^{59}Co	2.1	8.3	176		121		142	132±7
			8.2	136	0.689	94	21	115	
^{56}Fe	^{59}Co	1.7	9.7	181		122		235	194±9
			9.8	163	0.675	110	113	223	
^{139}La	^{59}Co	1.26	11.4	214		142		518	450±30
			11.7	195	0.663	129	376	505	
^{12}C	^{12}C	2.1	5.7	116		88		89	60.9±0.6
			5.3	78	0.755	59	0.51	60	
^{20}Ne	^{12}C	1.05	6.3	130		97	1.0	98	78±2
			5.9	89	0.746	66		67	
^{56}Fe	^{12}C	1.7	7.6	141		103		110	94±2
			7.5	114	0.727	83	7	90	
^{139}La	^{12}C	1.26	9.4	173		123		147	148±2
			9.4	143	0.711	102	24	126	

single nucleon can be removed via the nuclear force. The *maximum* value of this impact parameter should correspond to the minimum value b_{min} used in the EM cross-section calculation. It is this maximum value which is listed in Table I. However, we wish to emphasize that this impact parameter is *not* used in our nuclear optical-model calculations. (We integrate over b.) It is calculated simply to provide an independent estimate of the appropriate value of b_{min} to be used for the EM calculations.

We now come to a detailed discussion of our results which are presented in Table I as the first row for each projectile-target combination. Also listed as the second row are the BCV results. (See Ref. 9 for an important comment.) First note the extremely good agreement between our impact parameters and those of BCV. Note that they are *both significantly different* from those obtained using the naive formula $1.2(A_p^{1/3}+A_T^{1/3})$ fm and thus we now strongly recommend that the BCV parametrization of b_{min} be used for future EM calculations. (This has always been used in the past by Hill *et al.*[1]) Second, note the comparison between our optical-model neutron removal cross section σ and that of BCV (fifth column of Table I). The agreement is good although generally our results are somewhat larger than BCV, especially for neutron emission from ^{12}C, perhaps due to the fact that we use realistic nuclear densities whereas BCV use a geometrical parametrization of their optical model. At this point we wish to emphasize that the good agreement between the present work and that of BCV for both b and σ was obtained *without* adjusting any parameters to force agreement. Finally we have used the FSI formula for P_{esc} and the EM cross sections of BCV to arrive at the cross section $\sigma P_{esc}+\sigma_{WW}$ which is to be compared to experiment. (BCV did not calculate σ_{WW} for ^{16}O and ^{197}Au at 60 and 200 GeV/nucleon and thus we include our own calculation in Table I.) It can be seen that both the present work and that of BCV give comparable good agreement with experiment. In particular, whereas previously the worst discrepancy between theory and experiment for the EM cross section[3] occurred for ^{197}Au, there is now excellent agreement except for the 200-GeV/nucleon data. This fact strongly supports the BCV hypothesis that the EM discrepancies have more to do with nuclear theory than with WW formulation. However, not all problems are solved and some new disagreements arise. Some reasons for these may be due to neglect of electric quadrupole excitations,[2,10] errors in the photonuclear data used as input to σ_{WW}, or uncertainties in the treatment of FSI. In our studies we noted that the calculated cross sections are *very* sensitive to the value of P_{esc} and we regard this as the major uncertainty in the BCV work. Another reasonable value[11] for P_{esc} such as 0.5 gives significantly different results which also generally agree with the experimental data.

In summary, the present work has resolved some of the earlier discrepancies between theory and experiment for EM cross sections by determining the nuclear cross section for one neutron removal, adding it to the EM cross section, and comparing the sum to the originally measured total cross section. Our conclusions are in agreement with those of Benesh, Cook, and Vary.[4] Furthermore, we have independently verified that the BCV impact parameter is the appropriate one to use in EM calculations.

The authors wish to thank Ferdous Kahn for help with the computer program. J.W.N. was supported by the National Aeronautics and Space Administration (NASA) under Grant No. NAG-1-1134.

[1] J. C. Hill, F. K. Wohn, J. A. Winger, and A. R. Smith, Phys. Rev. Lett. **60**, 999 (1988); J. C. Hill, F. K. Wohn, J. A. Winger, M. Khayat, K. Leininger, and A. R. Smith, Phys. Rev. C **38**, 1722 (1988); A. R. Smith, J. C. Hill, J. A. Winger, and P. J. Karol, *ibid.* **38**, 210 (1988).

[2] C. A. Bertulani and G. Baur, Phys. Rep. **163**, 299 (1988).

[3] J. W. Norbury, Phys. Rev. C **40**, 2621 (1989).

[4] C. J. Benesh, B. C. Cook, and J. P. Vary, Phys. Rev. C **40**, 1198 (1989).

[5] L. W. Townsend, J. W. Wilson, F. A. Cucinotta, and J. W. Norbury, Phys. Rev. C **34**, 1491 (1986); L. W. Townsend, Can. J. Phys. **61**, 93 (1983).

[6] H. De Vries, C. W. De Jager, and C. De Vries, At. Data Nucl. Data Tables **36**, 495 (1987); **14**, 479 (1974).

[7] J. Gosset, H. H. Gutbrod, W. G. Meyer, A. M. Poskanzer, A. Sandoval, R. Stock, and G. D. Westfall, Phys. Rev. C **16**, 629 (1977).

[8] J. W. Wilson, L. W. Townsend, and F. F. Badavi, Nucl. Instrum. Methods Phys. Res. B **18**, 225 (1987).

[9] J. P. Vary, private communication. The cross section in the second and fourth columns of Tables II–VII of Ref. 4 are slightly different from the numbers one obtains using the formulas of that reference due to a small error. The correct values are listed in Table I of the present work.

[10] J. W. Norbury, Phys. Rev. C **41**, 372 (1990); **42**, 711 (1990).

[11] L. F. Oliveira, R. Donangelo, and J. O. Rasmussen, Phys. Rev. C **19**, 826 (1979).

Electric quadrupole excitations in relativistic nucleus-nucleus collisions

John W. Norbury
Department of Physics, Rider College, Lawrenceville, New Jersey 08648
(Received 16 November 1989; revised manuscript received 09 April 1990)

Calculations are presented for electric quadrupole excitations in relativistic nucleus-nucleus collisions. The theoretical results are compared to an extensive data set and it is found that electric quadrupole effects provide substantial corrections to cross sections, especially for heavier nuclei.

I. INTRODUCTION

The search for a fundamentally new state of matter in the form of a quark-gluon plasma[1] has stimulated the production of very high-energy nuclear beams. The hope is to observe the quark-gluon plasma in a relativistic nucleus-nucleus collision. At the Berkeley Bevalac a variety of light nuclei such as ^{12}C, ^{16}O, and ^{20}Ne can be accelerated up to energies of 2.1 GeV/nucleon and heavier nuclei such as ^{139}La and ^{238}U can be accelerated to 1.26 and 0.96 GeV/nucleon, respectively. At the Brookhaven National Laboratory, ^{16}O and ^{28}Si beams are available at 14.6 GeV/nucleon and at the CERN Super Proton Synchrotron (SPS) in Geneva, beams of ^{16}O and ^{32}S are both produced at 60 and 200 GeV/nucleon. The relativistic heavy-ion collider (RHIC) is expected to produce two *colliding* beams at 100 GeV/nucleon to give a total *center-of-mass* energy of 200 GeV/nucleon, which corresponds to a single beam energy of 21 TeV/nucleon. Grabiak[2] has pointed out that nuclear beams of 3.5 and 8 TeV/nucleon may be possible at the CERN Large Hadron Collider (LHC) or the Superconducting Super Collider (SSC). By way of comparison, the majority of galactic rays have energies[3] of about 1 GeV/nucleon, with a range[3] typically from 10 MeV/nucleon to 1 TeV/nucleon. However, the JACEE (Japanese-American Cooperative Emulsion Experiment) collaboration[4] has made observations as high as 1000 TeV/nucleon.

Nucleus-nucleus reactions proceed mainly through either the strong or electromagnetic (EM) interactions. Historically, strong interaction processes have been the main object of study,[5] however, with the availability of the above high-energy nuclear beams there has been a resurgence of interest in EM interactions in relativistic nucleus-nucleus collisions.[6]

The primary theoretical tool for studying these relativistic EM processes has been via the Weizsäcker-Williams (WW) method[6,7] of virtual quanta. The nucleus-nucleus total EM reaction cross section is

$$\sigma = \int N_{\mathrm{WW}}(E_\gamma)\sigma(E_\gamma)dE_\gamma \ , \tag{1}$$

where E_γ is the virtual photon energy, $N_{\mathrm{WW}}(E_\gamma)$ is the WW virtual photon spectrum, and $\sigma(E_\gamma)$ is the photonuclear reaction cross section. For high accuracy it is important to use experimental photonuclear data for $\sigma(E_\gamma)$. (For an excellent compilation of photoneutron data see Ref. 8.) However, a more exact formulation of σ involves a breakdown into the various EM multipolarities such as electric dipole ($E1$), electric quadrupole ($E2$), magnetic dipole ($M1$), etc. The most important contributions to σ are from $E1$ and $E2$ so that

$$\sigma = \sigma_{E1} + \sigma_{E2}$$
$$= \int [N_{E1}(E_\gamma)\sigma_{E1}(E_\gamma) + N_{E2}(E_\gamma)\sigma_{E2}(E_\gamma)]dE_\gamma \ , \tag{2}$$

where $N_{Ei}(E_\gamma)$ is the virtual photon spectrum of a particular multipolarity due to the projectile nucleus and $\sigma_{Ei}(E_\gamma)$ is the photonuclear reaction cross section of the target nucleus. Bertulani and Baur[6] have derived expressions for $N_{Ei}(E_\gamma)$ and found that the electric dipole spectrum is the same as the WW spectrum, i.e., $N_{E1}(E_\gamma) = N_{\mathrm{WW}}(E_\gamma)$. Furthermore, at very high projectile energies *all* $N_{Ei}(E_\gamma)$ and $N_{Mi}(E_\gamma)$ are equal so that Eq. (1) is seen to be a very high-energy approximation to all multipolarities included in Eq. (2). Bertulani and Baur[6] have made a crude estimate of the EM cross section using Eq. (2) but they pulled $N_{E1}(E_\gamma)$ and $N_{E2}(E_\gamma)$ outside the integral and evaluated them at a single energy and used sum rules to evaluate $\int \sigma_{Ei}(E_\gamma)dE_\gamma$. A more accurate calculation can be performed if one uses experimental data for the photonuclear cross section and evaluates the full integral numerically without removing the energy dependence in the photon spectra. Thus I undertook a more exact study[9] leaving Eq. (2) as it stands and using experimental data for the photonuclear cross sections by defining

$$\sigma_{E1}(E_\gamma) \equiv \sigma_{\mathrm{expt}}(E_\gamma) - \sigma_{E2}(E_\gamma) \ , \tag{3}$$

where $\sigma_{\mathrm{expt}}(E_\gamma)$ is the *experimentally* measured photonuclear cross section and $\sigma_{E2}(E_\gamma)$ is a *theoretical* calculation based on a Lorentzian shape for the electric giant quadrupole resonance (GQR). Details for this procedure can be found in Ref. 9. As was noted in that reference, the above procedure yields very accurate values for the sum $\sigma_{E1}+\sigma_{E2}$ (which is to be compared to nucleus-nucleus reaction experiments) even though the GQR parameters are uncertain. The basic reason for this, as can be seen from Eq. (3), is that an under (over) estimate in $\sigma_{E2}(E_\gamma)$ will give an over (under) estimate in $\sigma_{E1}(E_\gamma)$, so that the combined $\sigma_{E1}+\sigma_{E2}$ in Eq. (2) will not change very much.

In Ref. 9 a detailed study of $E1$ and $E2$ was undertak-

en for the reaction ^{89}Y(RHI,X)^{88}Y, where RHI refers to various relativistic heavy ions and X is anything. It was found that the $E2$ effects account for a considerable fraction of the cross section, and that inclusion of $E2$ [via Eq. (2)] provides improved agreement with experiment over the WW method. Given this situation, it was decided to compare this theoretical approach to as much experimental data as possible. Thus, the present work involves a comparison to neutron emission from ^{89}Y, ^{197}Au, and ^{59}Co and neutron and proton emission from ^{12}C, ^{16}O, and ^{18}O which includes both electric dipole and quadrupole effects. This complements earlier work[7] which involved an extensive comparison of the WW theory to experiment.

II. CALCULATIONAL METHOD

The basic calculational method is outlined in Ref. 9 and the discussion will not be repeated here. Also, Ref. 7 includes a very detailed summary of which photonuclear data were used for $\sigma_{\text{expt}}(E_\gamma)$ in Eq. (3). The same data is used in the present work. All isoscalar GQR parameters were taken from the compilation of Refs. 10 and 21 and are listed in Table I. As mentioned in the Introduction, even though these parameters are somewhat uncertain, the total EM cross section $\sigma_{E1}+\sigma_{E2}$ is expected to be very accurate[9] due to the subtraction procedure of Eq. (3). The most inaccurate results would be expected for the ^{12}C, ^{16}O, and ^{18}O GQR parameters where the isoscalar GQR is fragmented into several components.[10] Only a single Lorentzian[9] was used in the present work. However, σ_{E2} is found to be quite small for these nuclei (see below) so that my conclusion that the calculated $\sigma_{E1}+\sigma_{E2}$ is accurate remains valid.

For the nuclei ^{12}C, ^{16}O, and ^{18}O, proton (p) emission occurs as well as neutron (n) emission. Thus, Eq. (3) needs to be modified to incorporate the branching ratio. I assume that the excited nucleus decays *only* by proton or neutron emission and that the (photon) energy-dependent neutron branching ratio is defined as

$$f_n(E_\gamma)\equiv\frac{\sigma_{\text{expt}}(E_\gamma,n)}{\sigma_{\text{expt}}(E_\gamma,n)+\sigma_{\text{expt}}(E_\gamma,p)} . \tag{4}$$

This is simply a statement that the fraction of neutrons emitted at a given energy is determined by dividing the experimental neutron cross section by the total cross section at the same energy. The total cross section is given as the sum of the neutron and proton cross sections. Thus,

$$\sigma_{E2}(E_\gamma,n)=f_n(E_\gamma)\sigma_{E2}(E_\gamma) , \tag{5}$$

where $\sigma_{E2}(E_\gamma)$ is the photonuclear GQR cross section. Thus, for proton and neutron emission Eq. (3) becomes

$$\sigma_{E1}(E_\gamma,n)=\sigma_{\text{expt}}(E_\gamma,n)-f_n(E_\gamma)\sigma_{E2}(E_\gamma) \tag{6a}$$

and

$$\sigma_{E1}(E_\gamma,p)=\sigma_{\text{expt}}(E_\gamma,p)-[1-f_n(E_\gamma)]\sigma_{E2}(E_\gamma) . \tag{6b}$$

Equations (4)–(6) were used for nucleon emission from ^{12}C, ^{16}O, and ^{18}O. For ^{59}Co, the (γ,p) cross section is not available and so a constant value of $f_n=0.7$ (suggested from Ref. 11) was used. For ^{89}Y and ^{197}Au I used $f_n=1.0$.

TABLE I. Isoscalar giant quadrupole resonance (GQR) parameters taken from the compilation of Refs. 10 and 21. E is the GQR resonance excitation energy, Γ is the full-width at half maximum, and f is the fractional depletion of the energy weighted sum rule. (The GQR of light nuclei are fragmented into several peaks, so that the parameters below represent an estimated average value.)

Nucleus	E (MeV)	Γ (MeV)	f
^{12}C	22.0[a]	6.0[a]	0.3[a]
^{16}O	22.0[b]	6.0[a]	0.4[c,d]
^{18}O	24.0[e]	6.0[a]	0.4[a]
^{59}Co	16.3[b]	5.6[b]	0.61[b]
^{89}Y	13.8[b]	3.2[b]	0.55[c]
^{197}Au	10.8[e]	2.9[b]	0.95[c]

[a]Estimate.
[b]Best value from Table 4 of Ref. 10.
[c]From Fig. 23 of Ref. 10.
[d]From Fig. 17 of Ref. 21.
[e]E is calculated from 63 $A^{-1/3}$.

III. RESULTS AND DISCUSSION

The calculated results are listed in Table II, along with the experimental results of various groups.[12–16] $\sigma_{E1}+\sigma_{E2}$ is the calculated result to be compared with the data σ_{expt}. Also listed are the results of WW calculations.[7] In all cases two theoretical cross sections are listed. The first is calculated using an expression for the minimum impact parameter as

$$b_{\min}=R_{0.1}(T)+R_{0.1}(P) , \tag{7}$$

where $R_{0.1}$ represents the 10% charge-density radius[7] of the target or projectile. The second theoretical cross section listed in parentheses in Table II uses $b_{\min}$ given by Hill *et al.*[14–16] as

$$b_{\min}=r_0[A_P^{1/3}+A_T^{1/3}-X(A_p^{-1/3}+A_T^{-1/3}] , \tag{8}$$

where $r_0=1.34$ fm and $X=0.75$. (Note that there is a small difference between some of my WW calculations and those of Hill *et al.*[14–16] due to a small term which they had inadvertently forgotten.[19,20])

There are several features readily apparent from Table II.

(i) $\sigma_{E1}+\sigma_{E2}$ is *always* larger than σ_{WW}. However, for nucleon emission from ^{12}C, ^{16}O, and ^{18}O this difference is never larger than about 4%, but for neutron emission from ^{59}Co, ^{89}Y, and ^{197}Au the difference is much larger varying between about 7–15 %.

(ii) For nucleon emission from ^{12}C and ^{16}O both $\sigma_{E1}+\sigma_{E2}$ and σ_{WW} agree with experiment for both choices of $b_{\min}$.

(iii) For nucleon emission from ^{18}O both $\sigma_{E1}+\sigma_{E2}$ and σ_{WW} disagree with experiment for both choices of $b_{\min}$. σ_{WW} actually gives slightly better agreement but not by a significant amount.

TABLE II. Calculated results, $\sigma_{E1}+\sigma_{E2}$ and σ_{WW}, compared to experiment (Refs. 12–16). Two theoretical cross sections are listed. The first set uses b_{min} given by Eq. (7) and the second set (in parentheses) uses b_{min} given by Eq. (8). All choices of experimental photonuclear data used as input follow Ref. 7.

Projectile	$R_{0.1}(P)$ (fm)	Target	$R_{0.1}(T)$ (fm)	Energy (GeV/nucleon)	Final state	σ_{expt} (mb)	σ_{WW} (mb)	σ_{E1} (mb)	σ_{E2} (mb)	$\sigma_{E1}+\sigma_{E2}$ (mb)
^{12}C	3.30	Pb	7.83	2.1	^{11}C	51±18	47 (51)	46 (50)	1 (1)	47 (51)
^{12}C	3.30	Pb	7.83	2.1	^{11}B	50±25	68 (74)	68 (73)	2 (2)	70 (75)
^{12}C	3.30	Pb	7.83	1.05	^{11}C	39±24	28 (31)	28 (31)	1 (1)	29 (32)
^{12}C	3.30	Pb	7.83	1.05	^{11}B	50±25	42 (47)	42 (46)	1 (2)	43 (48)
^{16}O	3.68	Pb	7.83	2.1	^{15}O	50±24	59 (64)	58 (63)	2 (2)	60 (65)
^{16}O	3.68	Pb	7.83	2.1	^{15}N	96±26	111 (120)	110 (119)	3 (4)	113 (123)
^{12}C	3.30	Ag	6.37	2.1	^{11}C	21±10	18 (20)	18 (20)	0 (0)	18 (20)
^{12}C	3.30	Ag	6.37	2.1	^{11}B	18±13	26 (29)	26 (29)	1 (1)	27 (30)
^{12}C	3.30	Ag	6.37	1.05	^{11}C	21±10	11 (13)	11 (13)	0 (0)	11 (13)
^{12}C	3.30	Ag	6.37	1.05	^{11}B	25±19	17 (20)	17 (19)	1 (1)	18 (20)
^{16}O	3.68	Ag	6.37	2.1	^{15}O	26±13	23 (25)	22 (25)	1 (1)	23 (26)
^{16}O	3.68	Ag	6.37	2.1	^{15}N	30±16	42 (46)	42 (46)	1 (2)	43 (48)
^{12}C	3.30	Cu	5.45	2.1	^{11}C	10±7	8 (9)	8 (9)	0 (0)	8 (9)
^{12}C	3.30	Cu	5.45	2.1	^{11}B	4±8	11 (12)	11 (12)	0 (0)	11 (12)
^{12}C	3.30	Cu	5.45	1.05	^{11}C	9±8	5 (6)	5 (6)	0 (0)	5 (6)
^{12}C	3.30	Cu	5.45	1.05	^{11}B	5±8	8 (9)	8 (9)	0 (0)	8 (9)
^{16}O	3.68	Cu	5.45	2.1	^{15}O	9±8	10 (11)	10 (11)	0 (0)	10 (11)
^{16}O	3.68	Cu	5.45	2.1	^{15}N	15±8	18 (20)	17 (19)	1 (1)	18 (20)
^{12}C	3.30	Al	4.09	2.1	^{11}C	0±5	2 (2)	2 (2)	0 (0)	2 (2)
^{12}C	3.30	Al	4.09	2.1	^{11}B	0±5	3 (3)	3 (3)	0 (0)	3 (3)
^{12}C	3.30	Al	4.09	1.05	^{11}C	1±6	1 (2)	1 (2)	0 (0)	1 (2)
^{12}C	3.30	Al	4.09	1.05	^{11}B	1±7	2 (2)	2 (2)	0 (0)	2 (2)
^{16}O	3.68	Al	4.09	2.1	^{15}O	0±5	2 (3)	2 (3)	0 (0)	2 (3)
^{16}O	3.68	Al	4.09	2.1	^{15}N	−1±9	4 (5)	4 (5)	0 (0)	4 (5)
^{12}C	3.30	C	3.30	2.1	^{11}C	−2±5	0.4 (0.5)	0.4 (0.5)	0 (0)	0.4 (0.5)
^{12}C	3.30	C	3.30	2.1	^{11}B	−1±4	0.6 (0.7)	0.6 (0.7)	0 (0)	0.6 (0.7)
^{12}C	3.30	C	3.30	1.05	^{11}C	−2±5	0.3 (0.4)	0.3 (0.4)	0 (0)	0.3 (0.4)
^{12}C	3.30	C	3.30	1.05	^{11}B	−2±5	0.5 (0.6)	0.5 (0.6)	0 (0)	0.5 (0.6)
^{16}O	3.68	C	3.30	2.1	^{15}O	−1±4	0.5 (0.6)	0.5 (0.6)	0 (0)	0.5 (0.6)
^{16}O	3.68	C	3.30	2.1	^{15}N	−1±4	1 (1)	1 (1)	0 (0)	1 (1)
^{18}O	3.78	Ti	5.00	1.7	^{17}O	8.7±2.7	15 (16)	15 (16)	0 (1)	15 (17)
^{18}O	3.78	Ti	5.00	1.7	^{17}N	−0.5±1.0	3 (3)	3 (3)	0 (0)	3 (3)
^{18}O	3.78	Pb	7.83	1.7	^{17}O	136±2.9	155 (165)	154 (164)	4 (4)	158 (168)
^{18}O	3.78	Pb	7.83	1.7	^{17}N	20.2±1.8	28 (31)	27 (30)	2 (2)	29 (32)
^{18}O	3.78	U	8.09	1.7	^{17}O	140.8±4.1	191 (202)	189 (200)	5 (5)	194 (205)
^{18}O	3.78	U	8.09	1.7	^{17}N	25.1±1.6	34 (37)	34 (36)	2 (2)	36 (38)
^{12}C	3.30	^{197}Au	7.56	2.1	^{196}Au	75±14	38 (40)	37 (38)	6 (7)	43 (45)
^{20}Ne	4.00	^{197}Au	7.56	2.1	^{196}Au	153±18	100 (105)	97 (101)	16 (18)	113 (119)

TABLE II. (*Continued*).

Projectile	$R_{0.1}(P)$ (fm)	Target	$R_{0.1}(T)$ (fm)	Energy (GeV/nucleon)	Final state	σ_{expt} (mb)	σ_{WW} (mb)	σ_{E1} (mb)	σ_{E2} (mb)	$\sigma_{E1}+\sigma_{E2}$ (mb)
^{40}Ar	4.72	^{197}Au	7.56	1.8	^{196}Au	348±34	289 (297)	280 (287)	46 (49)	326 (336)
^{56}Fe	5.24	^{197}Au	7.56	1.7	^{196}Au	601±54	565 (578)	547 (560)	90 (94)	637 (654)
^{139}La	6.89	^{197}Au	7.56	1.26	^{196}Au	1970±130	2076 (2089)	2006 (2009)	357 (361)	2363 (2380)
^{16}O	3.68	^{197}Au	7.56	60	^{196}Au	280±30	215 (218)	208 (211)	14 (15)	222 (226)
^{16}O	3.68	^{197}Au	7.56	200	^{196}Au	440±40	278 (281)	270 (273)	15 (16)	285 (289)
^{12}C	3.30	^{89}Y[a]	6.02	2.1	^{88}Y	9±12	12 (13)	12 (13)	1 (1)	13 (14)
^{20}Ne	4.00	^{89}Y[a]	6.02	2.1	^{88}Y	43±12	32 (35)	31 (34)	3 (4)	34 (38)
^{40}Ar	4.72	^{89}Y[a]	6.02	1.8	^{88}Y	132±17	90 (96)	88 (94)	9 (10)	97 (104)
^{56}Fe	5.24	^{89}Y[a]	6.02	1.7	^{88}Y	217±20	175 (185)	171 (181)	16 (18)	187 (199)
^{12}C	3.30	^{59}Co	5.33	2.1	^{58}Co	6±9	7 (8)	7 (7)	0 (1)	7 (8)
^{20}Ne	4.00	^{59}Co	5.33	2.1	^{58}Co	32±11	18 (20)	18 (20)	1 (1)	19 (21)
^{56}Fe	5.24	^{59}Co	5.33	1.7	^{58}Co	88±14	98 (105)	96 (104)	7 (7)	103 (111)
^{139}La	6.89	^{59}Co	5.33	1.26	^{58}Co	280±40	339 (358)	333 (352)	24 (26)	357 (378)

[a]For ^{89}Y calculations are presented using the photonuclear data of Lepretre (Ref. 17), multiplied by 0.82, as suggested, by Berman *et al.* (Ref. 18).

(iv) For neutron emission from ^{197}Au, $\sigma_{E1}+\sigma_{E2}$ is significantly closer to experimental values than σ_{WW} is, although for most cases it still lies outside the error bars. An exception, however, is a much poorer agreement for ^{139}La (see also Refs. 19 and 20). Significant discrepancies with ^{197}Au data have been noted previously for WW theory.[7]

(v) For neutron emission from ^{89}Y, $\sigma_{E1}+\sigma_{E2}$ is in much better agreement with experiment than σ_{WW} is. This is especially true for the ^{40}Ar and ^{56}Fe projectiles.

(vi) For ^{59}Co, $\sigma_{E1}+\sigma_{E2}$ is again better for ^{20}Ne, although slightly worse for ^{56}Fe. As above, the agreement for the ^{139}La projectile is significantly poorer.

Finally, the earlier results of Bertulani and Baur can be compared for single neutron emission from ^{59}Co, ^{89}Y, and ^{197}Au targets with ^{12}C, ^{20}Ne, ^{40}Ar, and ^{56}Fe projectiles (see Table II and Ref. 6). Surprisingly the results of Ref. 6 give better agreement with experiment than Table II for ^{12}C and ^{20}Ne on ^{197}Au and also for ^{40}Ar on ^{89}Y. However, for ^{40}Ar and ^{56}Fe on ^{197}Au and ^{56}Fe on ^{59}Co, Table II gives far superior agreement with experiment. Otherwise other comparisons are comparable. However, it should be emphasized that there are substantial differences between Ref. 6 and Table II. In particular, *all* dipole and quadrupole cross-section values are significantly larger than the present work.

IV. SUMMARY AND CONCLUSIONS

Calculations have been made for nucleon emission via EM dissociation in relativistic nucleus-nucleus collisions. Results are presented for the Weizsäcker-Williams theory and also for separate electric dipole and quadrupole components. The theories have been compared to an extensive data set. It is found that electric quadrupole ($E2$) effects are not significant for proton and neutron emission from ^{12}C, ^{16}O, or ^{18}O. However, $E2$ contributions are substantial for neutron emission from ^{59}Co, ^{89}Y, and ^{197}Au, generally leading to improved agreement between theory and experiment. Notable disagreements occur for ^{139}La projectiles (1.26 GeV/nucleon) where the theoretical $\sigma_{E1}+\sigma_{E2}$ are too big. Quadrupole effects improve the theoretical results for ^{16}O projectiles at 60 and 200 GeV/nucleon, although the theoretical cross sections are still too small.

In general, it has been found that electric quadrupole effects are an important component in nucleus-nucleus collisions and that these effects can be calculated accurately.

Note added in proof: Some additional references on electric quadrupoles are R. Fleischhauer and W. Scheid, Nucl. Phys. A **493**, 583 (1989); **504**, 855 (1989); A. Goldberg, *ibid.* **420**, 636 (1984). Also note that Eq. (4) of Ref. 9 should have E_{GQR} in the numerator instead of E.

ACKNOWLEDGMENTS

I wish to thank Larry Townsend for useful discussions and Gayle Norbury for help with the photonuclear data. This work was supported in part by NASA Grant No. NAG-1-797 and NAG-1-1134.

[1]K. Kajantie and L. McLerran, Annu. Rev. Nucl. Part. Sci. **37**, 293 (1987).
[2]M. Grabiak, B. Muller, W. Greiner, G. Soff, and P. Koch, J. Phys. G **15**, L25 (1989).
[3]J. A. Simpson, Annu. Rev. Nucl. Part. Sci. **33**, 323 (1983).
[4]W. V. Jones, Y. Takahashi, B. Wosiek, and O. Miyamura, Annu. Rev. Nucl. Part. Sci. **37**, 71 (1987); J. Wdowczyk and A. W. Wolfendale, *ibid.* **39**, 43 (1989).
[5]W. G. Lynch, Annu. Rev. Nucl. Part. Sci. **37**, 493 (1987).
[6]C. A. Bertulani and G. Baur, Phys. Rep. **163**, 299 (1988); G. Baur and C. A. Bertulani, Phys. Rev. C **34**, 1654 (1986).
[7]J. W. Norbury, Phys. Rev. C **40**, 2621 (1989). The last entry in column 5 of Table I should read 335 ± 49 and not 73 ± 13.
[8]S. S. Dietrich and B. L. Berman, At. Data Nucl. Data Tables **38**, 199 (1988).
[9]J. W. Norbury, Phys. Rev. C **41**, 372 (1990).
[10]F. E. Bertrand, Annu. Rev. Nucl. Sci. **26**, 457 (1976).
[11]J. W. Norbury, F. A. Cucinotta, L. W. Townsend, and F. F. Badavi, Nucl. Instrum. Methods Phys. Res. B **31**, 535 (1988).
[12]H. H. Heckman and P. J. Lindstrom, Phys. Rev. Lett. **37**, 56 (1976).
[13]D. L. Olson, B. L. Berman, D. E. Greiner, H. H. Heckman, P. J. Lindstrom, G. D. Westfall, and H. J. Crawford, Phys. Rev. C **24**, 1529 (1981).
[14]M. T. Mercier, J. C. Hill, F. K. Wohn, C. M. McCullough, M. E. Nieland, J. A. Winger, C. B. Howard, S. Renwick, D. K. Matheis, and A. R. Smith, Phys. Rev. C **33**, 1655 (1986).
[15]J. C. Hill, F. K. Wohn, J. A. Winger, and A. R. Smith, Phys. Rev. Lett. **60**, 999 (1988).
[16]J. C. Hill, F. K. Wohn, J. A. Winger, M. Khayat, K. Leininger, and A. R. Smith, Phys. Rev. C **38**, 1722 (1988).
[17]A. Lepretre, H. Beil, R. Bergere, P. Carlos, A. Veyssiere, and M. Sugawara, Nucl. Phys. **A175**, 609 (1971).
[18]B. L. Berman, R. E. Pywell, S. S. Dietrich, M. N. Thompson, K. G. McNeill, and J. W. Jury, Phys. Rev. C **36**, 1286 (1987).
[19]J. W. Norbury, Phys. Rev. C **39**, 2472 (1989).
[20]J. C. Hill and F. K. Wohn, Phys. Rev. C **39**, 2474 (1989).
[21]J. Speth and A. van der Woude, Rep. Prog. Phys. **44**, 46 (1981).

STOPPING POWERS AND CROSS SECTIONS DUE TO TWO-PHOTON PROCESSES IN RELATIVISTIC NUCLEUS-NUCLEUS COLLISION

Wang K. Cheung and John W. Norbury

Physics Dept., Rider College

Lawrenceville, NJ 08648

List of Symbols

A_u	photon field
$\vec{B}$	magnetic field
b	impact parameter between two nuclei
c	velocity of light
$-\frac{dE}{dx}$	stopping power
$\vec{E}$	electric field
e^+, e^-	positrons, electrons
$F(\omega_1, \omega_2)$	two-photon distribution function associated with photons of frequencies ω_1 and ω_2
$\hat{f}$	Fourier transform of a function f of one variable
$\|f>$	final state
G_F	Fermi coupling constant
h_f	coupling between Higgs and fermion
$\|i>$	initial state
$K_0(x), K_1(x)$	modified Bessel functions of order 0 and 1
k_i	momentum of a photon
L	two-photon luminosity function
$\mathcal{L}_{\text{int}}$	interaction lagrangian
$\mathcal{L}_{\text{int}}^{(e)}$	interaction lagrangian for coupling between a fermion field and the photon field
$\mathcal{L}_{\text{int}}^{(h)}$	interaction lagrangian for coupling between a fermion field and a Higgs field
l^+, l^-	charged leptons

m	mass
m_e	mass of electron
m_f	mass of a fermion
m_l	mass of lepton
$N(\omega, b)$	photon frequency distribution at frequency ω and distance b from the nucleus emitting the photons
$n(\omega, b)$	number of photons per unit frequency interval per unit area at frequency ω and distance b from the nucleus emitting the photons
$P(b)$	probability for producing a particle pair when two nuclei collide at impact parameter b
p_h	momentum of a Higgs particle
p_-, p_+	momenta of charged particles
q_f	fermion charge
S	S-matrix
$S^{(n)}$	n-th order term of S-matrix
$\vec{s}$	Poynting vector
s^+, s^-	charged scalars
s_-, s_+	polarizations of charged leptons
T	time ordering
T_0	normalization time
$\bar{u}(p_-, s_-), v(p_+, s_+)$	lepton and anti-lepton spinors associated with momenta p_-, p_+ and polarizations s_-, s_+
v	velocity
V^+, V^-	charged vectors

W	mass of produced system of particle(s)
W^+, W^-	charged W-bosons
H^0	neutral Higgs scalar
Z	nucleus with charge Z
α	fine structure constant
Γ	width of a particle
γ	$(1 - v^2/c^2)^{-1/2}$, Lorentz factor associated with velocity v
γ_μ	Dirac γ matrices
ϵ_i	photon polarization
Λ_i	mass of photon
ρ	number of nuclei per unit volume
σ	cross section
$\sigma_{\gamma\gamma}(\omega_1, \omega_2)$	photon-photon cross section associated with photons of frequencies ω_1 and ω_2
$\psi(x)$	lepton field operator
Ω	normalization volume
ω	frequency of photon

1. Introduction

The radiation dose received from high energy galactic cosmic rays (GCR) is a limiting factor in the design of long duration space flights and the building of lunar and martians habitats. It is of vital importance to have an accurate understanding of the interactions of GCR in order to assess the radiation environment that astronauts will be exposed to.

Most previous studies have concentrated on strong interaction process in GCR. However there are also very large effects due to electromagnetic (EM) interactions. EM studies have previously concentrated on single photon exchange leading to nucleon removal. However two-photon processes also occur which lead to the production of lepton pairs with cross sections of the order of *kilobarns*. Also at high energy the stopping powers from these processes can exceed that due to atomic collisions. Thus even though very high energy GCR are not as abundant as lower energy GCR they still must be considered due to the fact that the cross sections and stopping powers are so much larger than normal.

In this report we describe our first efforts at understanding these EM production processes due to two-photo collisions. More specifically, we shall consider particle production processes in relativistic heavy ion collisions (RHICs) through two-photon exchange. Examples of this broad category of processes include:

$$Z_1 Z_2 \rightarrow Z_1 Z_2 l^+ l^- \tag{1.1a}$$

$$Z_1 Z_2 \rightarrow Z_1 Z_2 s^+ s^- \tag{1.1b}$$

$$Z_1 Z_2 \rightarrow Z_1 Z_2 V^+ V^- \tag{1.1c}$$

$$Z_1 Z_2 \rightarrow Z_1 Z_2 H^0 \tag{1.1d}$$

in which $l^+ l^-$ denote charged leptons, $s^+ s^-$ denote charged scalars, $V^+ V^-$ denote charged vector particles, and H^0 is a neutral Higgs scalar.

We shall limit our consideration to cases in which the colliding nuclei are identical, so that $Z_1 = Z_2 = Z$. An important Feynman diagram that contributes to (1.1a), (1.1b), and (1.1c) is shown in the following figure (fig. 1).

For process (1.1d), an important diagram is shown in figure 2, in which the triangular loop receives contributions from quarks, leptons and W gauge bosons. These processes are important for the following reasons (ref. 1).

(1) These kind of processes become increasingly important as energy of the colliding nuclei increases, since their cross sections increase with energy. Thus their contributions to the stopping power of high energy ions also become more important at high energies.

(2) These processes can be channels for production of charged particles, e.g., l^+l^-, W^+W^-, and neutral particles such as Higgs bosons, and various mesons.

(3) For high Z nuclei these processes can be used for studying non-perturbative effects in the electromagnetic interaction.

(4) They must be taken into account in the study of strong interaction effects in heavy ion collisions since they can lead to important background events, and must be taken into account also in the design of experimental set up, since they can lead to significant beam loss.

Section 2 of this report gives a brief survey of a few major approaches used in the calculations for these processes. Section 3 examines some results of our calculations. We then point out briefly some open questions and make a few concluding remarks in Section 4.

The purpose of this report is threefold. (1) It gives a simple, elementary introduction to this field. (2) It provides sample calculations for illustrating the approach we use. (3) The background and techniques developed here can be used as a general base for launching further and more specialized studies into this field.

While it is not our main goal here to obtain new and original results, some of our results are possibly new, and are as yet not available in the literature.

2. A Brief Survey of Different Approaches

In this section, we briefly list a few major approaches used in calculating cross sections for the kind of processes we are interested in. The first approach has been discussed in

references 2 and 3. In this approach, each colliding nucleus is replaced by an equivalent spectrum of photons. Each nucleus is considered to move in a straight line, unperturbed by the interaction. At a distance b from the line of motion of a nucleus, a spectrum of photons is generated, whose frequency distribution has the form:

$$N(\omega,b)=\frac{Z^2\alpha}{\pi^2}\left(\frac{\omega}{\gamma v}\right)^2\left(\frac{c}{v}\right)^2\left[K_1^2(x)+\frac{1}{\gamma^2}K_0^2(x)\right] \tag{2.1a}$$

where

$$x\equiv\frac{\omega b}{\gamma v} \tag{2.1b}$$

K_0, K_1 are modified Bessel functions, see reference 4, Sections 3.7 and 15.4.

The cross section for this process can be written as an integral of a photon distribution function multiplied by a photon-photon cross section.

$$\sigma=\int\frac{d\omega_1}{\omega_1}\int\frac{d\omega_2}{\omega_2}F(\omega_1,\omega_2)\sigma_{\gamma\gamma}(\omega_1,\omega_2), \tag{2.2a}$$

where

$$\begin{aligned}F(\omega_1,\omega_2)=2\pi\int_{b_{1\mathrm{mn}}}^{\infty}b_1db_1\int_{b_{2\mathrm{mn}}}^{\infty}b_2db_2\int_0^{2\pi}d\phi N(\omega_1,b_1)\\ \times N(\omega_2,b_2)\theta(b'-R_1-R_2)\end{aligned} \tag{2.2b}$$

and

$$b'=\left(b_1^2+b_2^2-2b_1b_2\cos\phi\right)^{1/2} \tag{2.2c}$$

where ω_1 and ω_2 are the frequencies of the photons emitted by the nuclei, b_1 and b_2 are the distances of the nuclei from the point where the photons collide. Details can be found in Appendix A. Various differential cross sections can be derived from these equations. First we consider $\frac{d\sigma}{dW^2}$ where W is the mass of the produced charged particle pair. We note that $W^2=4\omega_1\omega_2$. Hence we can equate in (2.2a)

$$\sigma=\int\frac{d\omega_1}{\omega_1}\int\frac{dW^2}{W^2}F\left(\omega_1,\frac{W^2}{4\omega_1}\right)\sigma_{\gamma\gamma}\left(\omega_1,\frac{W^2}{4\omega_1}\right), \tag{2.2a}$$

and

$$\frac{d\sigma}{dW^2} = \frac{1}{W^2}\int \frac{d\omega_1}{\omega_1} F\left(\omega_1, \frac{W^2}{4\omega_1}\right)\sigma_{\gamma\gamma}\left(\omega_1, \frac{W^2}{4\omega_1}\right). \tag{2.3b}$$

Next we define the probability for producing a particle pair $P(b)$ at impact parameter b by

$$P(b) \equiv \frac{1}{2\pi b}\frac{d\sigma}{db} \tag{2.4a}$$

where

$$\frac{d\sigma}{db} = \int \frac{d\omega_1}{\omega_1}\int \frac{d\omega_2}{\omega_2} F(\omega_1,\omega_2)\sigma_{\gamma\gamma}(\omega_1,\omega_2)\delta(b-b'), \tag{2.4b}$$

in which it is understood that the δ function is to be taken inside the triple integral which defines $F(\omega_1,\omega_2)$. The correctness of (2.4) can be checked by integrating both sides of (2.4b) over all values of the impact parameter b, which then yields (2.3a) for the total cross section. $P(b)$ is the probability for the events in which two nuclei collide with each other at impact parameter b, producing a charged particle pair in the process. A quantity L, known as the two-photon luminosity function is defined by (see ref. 2, eqs. (1), (9), and (10))

$$L = \int \frac{d\omega_1}{\omega_1}\int \frac{dW^2}{W^2} F\left(\omega_1, \frac{W^2}{4\omega_1}\right). \tag{2.5a}$$

So

$$\frac{dL}{dW^2} = \frac{1}{W^2}\int \frac{d\omega_1}{\omega_1} F\left(\omega_1, \frac{W^2}{4\omega_1}\right), \tag{2.5b}$$

and

$$\frac{d\sigma}{dW^2} = \frac{dL}{dW^2}\sigma_{\gamma\gamma}(W^2), \tag{2.5c}$$

where we have used the fact that $\sigma_{\gamma\gamma}(\omega_1,\omega_2)$ actually depends only on W^2 so that we can write

$$\sigma_{\gamma\gamma}(\omega_1,\omega_2) = \sigma_{\gamma\gamma}(W^2). \tag{2.6}$$

It is our view that equation (10) of reference 2 is in error, and have duly corrected the error in the above definition of the luminosity function L. For stopping power calculation, we use the formula

$$-\frac{dE}{dx} = \rho\int \frac{d\omega_1}{\omega_1}\int \frac{d\omega_2}{\omega_2}(\omega_1+\omega_2)F(\omega_1,\omega_2)\sigma_{\gamma\gamma}(\omega_1,\omega_2), \tag{2.7}$$

where ρ is the number of nuclei per unit volume.

The second type of approach has been applied to a related set of purely quantum electrodynamic (QED) processes: $e^+e^- \rightarrow e^+e^-l^+l^-$. This process can be calculated within the framework of QED. Cross sections can be obtained numerically by Monte-Carlo integration. Approximate formulas for total cross sections have also been obtained. See references 5 and 6. This kind of approach can be modified to apply to RHIC processes, provided one takes into account properly the effects of nuclear currents. See reference 7, Section II.

In an approach closely related to this second type of approaches, Bottcher treated the colliding nuclei classically, by regarding them as classical charge distributions. The remaining amplitude for the production of charged particle pair is then obtained in the framework of QED. Thus for the case of the reaction $Z_1Z_2 \rightarrow Z_1Z_2l^+l^-$ the total cross section can be written in the form (ref. 8, eq. (10), p. 38):

$$\sigma = \frac{Z_1^2 Z_2^2}{4v^2}(4\pi\alpha)^4 \int \frac{d^3p_- d^3p_+ d^2k_{1\perp}}{(2\pi)^8 2p_{-0}2p_{+0}} f_1^2\left(k_1^2\right) f_2^2\left(k_2^2\right)$$
$$\times \sum_{s_-,s_+} \left| \bar{u}(p_-,s_-)\left[\not{\epsilon}_1 \frac{1}{\not{p}_- - \not{k}_1 - m_l} \not{\epsilon}_2 \right.\right.$$
$$\left.\left. + \not{\epsilon}_2 \frac{1}{\not{p}_- - \not{k}_2 - m_l} \not{\epsilon}_1 \right] v(p_+,s_+) \right|^2, \tag{2.8}$$

where v denotes the velocity of one of the nuclei in the center of momentum frame, p_- and p_+ are the momenta of the produced leptons, s_- and s_+ are their polarizations, $\bar{u}(p_-,s_-)$ and $v(p_+,s_+)$ are the lepton spinors, k_1 and k_2 are the momenta of the exchanged photons, and f_1 and f_2 are the nuclear form factors. For any 4-vector A, the slash notation $\not{A}$ is defined by

$$\not{A} = \sum_{\mu=0}^{3} A_\mu \gamma^\mu, \tag{2.9}$$

where γ^μ are the Dirac γ-matrices, see for instance reference 9, Appendix 2, pages 355–361.

3. Results

In this report, we adopt the approach discussed in references 2 and 3. As samples of our calculations, we present a number of results for the process $^{208}Pb^{208}Pb \rightarrow {}^{208}Pb^{208}Pb\, l^+l^-$, and some others. Most of our calculations are done for colliding beam energies of 3400 Gev and 8000 Gev per nucleon. The impact parameter b varies over the range from 10 fm to 1000 fm. The mass of l^+l^- varies from a threshold equal to $2m_l$ up to about 1000 Gev. In Appendix B we list the photon-photon cross sections for the following processes:

$$\gamma\gamma \rightarrow l^+l^- \tag{3.1a}$$

$$\gamma\gamma \rightarrow s^+s^- \tag{3.1b}$$

$$\gamma\gamma \rightarrow V^+V^- \tag{3.1c}$$

$$\gamma\gamma \rightarrow H^0 \tag{3.1d}$$

The derivations of some of these cross sections are also given there. By using (2.2)–(2.6), we can then obtain various luminosity functions, differential and total cross sections, probabilities, and stopping powers.

Table 1 shows the total cross section for $^{208}Pb^{208}Pb \rightarrow {}^{208}Pb^{208}Pb\, e^+e^-$. We compare our numerical results based on (2.1) and (2.2), with the results based on the approximate formula (ref. 5, eq. (F.1), p. 276)

$$\sigma = \frac{28\left(Z_1 Z_2 \alpha^2\right)^2}{27\pi m_e^2}(l^3 - Al^2 + Bl + C) \tag{3.2}$$

where

$$A \approx 6.36, \quad B \approx 15.7, \quad C \approx -13.8,$$

$$Z = \ln\left(\frac{2p_1 \cdot p_2}{m_1 m_2}\right).$$

Z_i, p_i, and m_i, $i = 1, 2$ are the changes, momenta, and masses of the colliding nuclei.

Table 1

Incident energy/nucleon E (Gev)	Total cross section (fm^2)	
	Our results	Calculated from formula
3400.0		0.2445×10^8
8000.0	0.8382×10^8	0.3333×10^8

Table 2 shows the corresponding stopping power calculations. The energies of the incident particles are given for both the case of colliding beams and also the case of an incident beam colliding with a fixed target.

Table 2

Incident energy/nucleon E (Gev, colliding beams)	Incident energy/nucleon E (Gev, fixed target)	$\frac{1}{\rho} \times \left(-\frac{dE}{dx}\right)$ (Gev fm^2)
0.9636	1.039	0.2496×10^1
0.1367×10^1	3.039	0.1918×10^{-1}
0.2704×10^1	14.64	0.1725×10^{-1}
3400.0	0.2462×10^8	0.8855×10^1
8000.0	0.1363×10^9	0.3131×10^2
For Pb-208, $rho =$		

In figure 3, we give plots of $W^2 \frac{dL}{dW^2}$ as a function of W in different ranges of W. The differential cross section $\frac{d\sigma}{dW^2}$ can be obtained from $\frac{dL}{dW^2}$ by multiplying $\frac{dL}{dW^2}$ by a $\gamma\gamma$ cross section as in (2.5c).

Figures 4a–d show plots of $\sigma_{\gamma\gamma}(W^2)$ for the reactions $\gamma\gamma \to l^+l^-$, $\gamma\gamma \to s^+s^-$, $\gamma\gamma \to V^+V^-$, and $\gamma\gamma \to H^0$.

Figure 5 shows plots of $P(b)$ for the reaction $^{208}Pb^{208}Pb \to {}^{208}Pb^{208}Pb\, e^+e^-$ at different energies.

Figure 6 presents plots of the total cross section for the process $^{208}Pb^{208}Pb \to {}^{208}Pb^{208}Pb\, H^0$.

We have compared some of our results with the published results of Papageorgiu and Baur, and found some good agreement. In the following, we give a sample of such comparisons.

Table 3

	W (Gev)	$W/\sqrt{s}$	$W^2\frac{dL}{dW^2}$	
			Our result	Papageorgiu's result
Incident energy/ nucleon (colliding beams) E = 3400.0 Gev	100.0	0.7070×10^{-4}	0.3152×10^{3}	0.33×10^{3}
	141.4	0.1000×10^{-4}	0.8630×10^{2}	0.90×10^{2}
	212.2	0.1500×10^{-3}	0.1206×10^{2}	0.13×10^{2}
	282.9	0.2000×10^{-3}	0.1990×10^{1}	0.21×10^{1}
E = 8000.0 Gev	19.0	0.5709×10^{-4}	0.6129×10^{3}	0.70×10^{3}
	280.0	0.8413×10^{-4}	0.1708×10^{3}	0.20×10^{3}
	370.0	0.1112×10^{-3}	0.5444×10^{2}	0.60×10^{2}
	460.0	0.1382×10^{-3}	0.1881×10^{2}	0.20×10^{2}
	550.0	0.1653×10^{-3}	0.6866×10^{1}	0.70×10^{1}
	640.0	0.1923×10^{-3}	0.2606×10^{1}	0.28×10^{1}

Table 4

Incident energy/nucleon (colliding beams) E = 3755.6 Gev		
W(Gev)	$\frac{d\sigma}{dW^2}$ (fm^2 Gev^{-2})	
	Our result	Baur's result
0.1200×10^{-2}	0.6188×10^{13}	0.62×10^{13}
0.1414×10^{-2}	0.4923×10^{13}	0.48×10^{13}
0.1732×10^{-2}	0.2777×10^{13}	0.28×10^{13}
0.2000×10^{-2}	0.1714×10^{13}	0.17×10^{13}
0.2200×10^{-2}	0.1222×10^{13}	0.12×10^{13}
0.2400×10^{-2}	0.8894×10^{12}	0.92×10^{12}
0.2600×10^{-2}	0.6607×10^{12}	0.69×10^{12}
0.3000×10^{-2}	0.3846×10^{12}	0.40×10^{12}

Papageorgiu and Baur's results were taken from appropriate graphs in their papers (ref. 2, fig. 3; and ref. 3, fig. 9).

Cross sections are expected to scale roughly as $Z_1^2 Z_2^2$. For our case $Z_1 = Z_2 = Z$. So in order to obtain the corresponding cross sections, luminosity function, or stopping power for different nuclei, one can simply multiply the results we have here by a factor $\frac{Z_1 Z_2^2}{(Z=82)^4}$. Thus if one wants the results for $Al\ Fe$ collision, one can multiply the results presented in this section by the conversion factor $\frac{13^2 56^2}{82^4}$. The different nuclear sizes are expected to affect the results also. However for a rough order of magnitude estimate, such a simple scaling is expected to be reasonably accurate.

4. Open Questions and Conclusions

For small values of b, and m_l, such as $m_l = m_e$, $P(b)$ exceeds 1. This signifies the breakdown of perturbation theory. The question as to how to extract meaningful results

from theory is under active investigation. See reference 10. In our simple approach, we have regarded the nuclei as point charges. By using form factors for the nuclei, the problem of violation of unitarity is expected to be somewhat ameliorated. However this problem still needs to be addressed, because for high Z nuclei, the coupling constant for the electromagnetic interaction is of the order Ze, even with nuclear form factor taken into account, which may therefore still lead to a breakdown of the perturbative approach to cross-section calculation. In a collaboration with Mirek Fatyka of Brookhaven National Laboratory (BNL), we shall investigate production and neutral meson production (such as ϵ^0, η^0) in high energy heavy ion collisions. In these processes, we shall look for possible deviation in the measured rates or cross sections for values calculated by perturbation theory.

In many studies of the type of processes considered here, various approximations are used. We have mentioned the equivalent photon approximation, and the semi-classical approximation. Also, in the approach of references 2 and 3, which we have adopted in this report, the effect due to phase coherence of the electromagnetic field generated by the nuclei has not been properly taken into account. One needs to investigate how valid these approximations are and what the regions of validity are for them.

When one is primarily interested in the kind of electromagnetic processes discussd here, one needs to be able to estimate reliably the background due to strong interaction. Furthermore, there are other electromagnetic processes that also need to be studied, in addition to the ones we have looked at, even though the ones we have considered are among the most important.

In summary, we have given a brief introduction to two-photon exchange processes in high energy heavy ion collisions. Our calculations are based on an approach discussed in references 2 and 3. In view of the significance of this class of processes, and the many open questions that remain to be answered, we believe that further study in these areas will be valuable, not only for gaining a better understanding into these processes themselves, but also for studies and experiments in strong interaction physics.

In the following Appendices, we discuss the derivation of some of the formulas we have used. We look at the equivalent photon approximation in Appendix A and show how this is applied to the two-photon exchange processes in RHICs. Then in Appendix B, derivatives are given for some $\gamma\gamma$ cross sections. Appendix C provides a derivation of fermion contribution to the process $H^0 \to \gamma\gamma$. In Appendix D, we look at the details of how certain integrals encountered in our calculations are evaluated. Finally Appendix E gives a simple derivation of the formula (2.7) used for calculating stopping power.

Appendix A. Equivalent Photon Approximation

Consider a charge of moving along the x-axis. The effect of this charge on another charge located a distance b from the x-axis can be approximately calculated as follows.

By first considering the electromagnetic (EM) field due to q in its own rest frame, and then making a Lorentz transformation to the laboratory frame, it is straight forward to show that the electromagnetic field due to q is given by

$$E_1 = -qv\gamma t(b^2 + \gamma^2 v^2 t^2)^{-3/2} \tag{A.1a}$$

$$E_2 = qb\gamma(b^2 + \gamma^2 v^2 t^2)^{-3/2} \tag{A.1b}$$

$$B_3 = \frac{v}{c}E_2 = q\,\frac{v}{c}\,b\gamma(b^2 + \gamma^2 v^2 t^2)^{-3/2} \tag{A.1c}$$

$$E_3 = B_1 = B_2 = 0 \tag{A.1d}$$

$t = 0$ corresponds to the instant when q passes through the origin. When $v \approx c$, the components E_2 and B_3 can be thought of as the components of a pulse of plane-polarized EM wave travelling along x. The energy flux of this EM field is given by the Boynting vector

$$\vec{S} = \frac{c}{4\pi}\vec{E} \times \vec{B}. \tag{A.2}$$

So ignoring E_1 for the moment, $\vec{S}$ points along x, and its magnitude is

$$|\vec{S}| = \frac{c}{4\pi}\,E_2^2, \tag{A.3}$$

in which we have made the approximation $\frac{v}{c} \approx 1$. Over a unit area, the flow of energy is

$$\int_{-\infty}^{\infty} |\vec{S}|\,dt = \frac{c}{4\pi}\int_{-\infty}^{\infty} E_2^2(t)\,dt. \tag{A.4a}$$

Using Parseval's theorem, we therefore have

$$\int_{-\infty}^{\infty} |\vec{S}|\,dt = \frac{c}{4\pi}\int_{-\infty}^{\infty} |\hat{E}_2(\omega)|^2\,d\omega, \tag{A.4b}$$

where $\hat{E}_2$ is the Fourier transform (FT) of E_2, defined by

$$\hat{f}(\omega) \equiv \frac{1}{\sqrt{2\pi}}\int_{-\infty}^{\infty} f(t)\,e^{-i\omega t}\,dt \tag{A.5}$$

Hence the quantity $\hat{S}_2(\omega)$, defined by

$$\hat{S}_2(\omega) = \frac{c}{4\pi} |\hat{E}_2(\omega)|^2, \tag{A.6}$$

can be thought of as the energy per unit frequency per unit area of the EM field at frequency ω generated by the moving charge q. To obtain the photon number per unit frequency per unit area at frequency ω, we set $n_2(\omega) = \frac{1}{\hbar\omega}\hat{S}_2(\omega)$, since each photon has energy $\hbar\omega$. For the function $N_2(\omega)$, the dependence on the distance b is implicit. To make the dependence on b explicit, we can write instead

$$n_2(\omega, b) = \frac{1}{\hbar\omega}\hat{S}_2(\omega). \tag{A.7}$$

From (A.1b), we obtain

$$\hat{E}_2(\omega) = \frac{q}{bv}\sqrt{\frac{2}{\pi}}\frac{\omega b}{\gamma v} K_1\left(\frac{\omega b}{\gamma v}\right) \tag{A.8}$$

Hence

$$\hat{S}_2(\omega) = \frac{c}{4\pi}\frac{2}{\pi v^2}\left(\frac{q}{b}\right)^2\left(\frac{\omega b}{\gamma v}\right)^2 K_1^2\left(\frac{\omega b}{\gamma v}\right) \tag{A.9}$$

The remaining component E_1, of the EM field can be complemented by a magnetic field so that they can be considered to form a pulse of plane polarized EM wave. The same treatment can be applied to these components, so that the energy spectrum can be similarly obtained as before. The result is

$$\begin{aligned}\hat{S}_1(\omega) = \frac{c}{4\pi}|\hat{E}_1(\omega)|^2 = \frac{c}{4\pi}\frac{1}{\gamma^2}\frac{1}{v^2}\left(\frac{q}{b}\right)^2\frac{2}{\pi}\left(\frac{\omega b}{\gamma v}\right)^2 \\ \times K_o^2\left(\frac{\omega b}{\gamma v}\right)\end{aligned} \tag{A.10}$$

The effect of this pulse is roughly $\frac{1}{\gamma^2}$ that of the first pulse. So at high velocity, the second pulse can be neglected when compared with the first pulse.

In conventional treatment, the two pulses are then simply added together, so that the effect due to the original moving charge q is replaced by a spectrum of photons whose number density is simply the sum of the number densities from the two pulses discussed above. Thus

one set

$$n(\omega,b)=\frac{1}{\hbar\omega}\left[\hat{S}_2(\omega)+\hat{S}_1(\omega)\right]=\frac{1}{\hbar\omega}\frac{c}{4\pi}\frac{1}{v^2}\left(\frac{q}{b}\right)^2\frac{2}{\pi}\left(\frac{\omega b}{\gamma v}\right)^2 \times\left[K_1^2\left(\frac{\omega b}{\gamma v}\right)+\frac{1}{\gamma^2}K_o^2\left(\frac{\omega b}{\gamma v}\right)\right] \tag{A.11}$$

After identifying $q=Ze$, $\frac{e^2}{\hbar c}=\alpha$, and noting

$$\hat{S}_i(-\omega)=\hat{S}_i(\omega)\quad\text{for}\quad i=1,2, \tag{A.12}$$

the photon energy spectrum

$$\begin{aligned}N(\omega,b)&=\hat{S}_1(\omega)+\hat{S}_2(\omega)+\hat{S}_1(-\omega)+\hat{S}_2(-\omega)\\&=\frac{Z^2e^2}{\pi^2}\frac{1}{c}\left(\frac{c}{v}\right)^2\left(\frac{\omega}{\gamma v}\right)^2\left[K_1^2\left(\frac{\omega b}{\gamma v}\right)+\frac{1}{\gamma^2}K_o^2\left(\frac{\omega b}{\gamma v}\right)\right]\\&=\hbar\,\frac{Z^2\alpha}{\pi^2}\left(\frac{c}{v}\right)^2\left(\frac{\omega}{\gamma v}\right)^2\left[K_1^2\left(\frac{\omega b}{\gamma v}\right)+\frac{1}{\gamma^2}K_o^2\left(\frac{\omega b}{\gamma v}\right)\right]\end{aligned} \tag{A.13}$$

Application of Equivalent Photon Approximation to Two-Photon Exchange Processes

When two nuclei Z_1 and Z_2 collide with each other, their EM interactions can be studied in terms of the EM interaction of the spectra of photons emitted by the nuclei. The situation can be pictured as in figure A.2.

The two photons γ_1 and γ_2 are considered as colliding head-on with each other. Taking a cross-sectional view perpendicular to the direction of motion of the nuclei, the situation can be pictured as shown in figure A.3.

From our previous discussion, the number of photons emitted by Z_1 at P, whose frequencies are between ω_1 and $\omega_1+d\omega_1$, is $n(\omega_1,b_1)d\omega_1\ b_1\ db_1\ d\phi_1$, where $n(\omega_1\cdot b_1)$ is defined by (A.11). Similarly, the number of photons incident at P emitted by Z_2 is $n(\omega_2,b_2)d\omega_2\ b_2\ db_2\ d\phi_2$. Therefore the EM cross section for the collision of Z_1 and Z_2 through two-photon exchange can be written as

$$\sigma=\int n(\omega_1,b_1)\ n(\omega_2,b_2)\ \sigma_{\gamma\gamma}(\omega_1,\omega_2)b_1\ db_1\ d\phi_1\ b_2\ db_2\ d\phi_2 \times\ \theta(b-R_1-R_2)d\omega_1\ d\omega_2 \tag{A.14}$$

in which R_1 and R_2 stand for the nuclear radii of Z_1 and Z_2, and the θ-function takes into account that when $b < R_1 + R_2$, the two nuclei overlap, and the EM interaction is swamped by the strong interaction of the nuclei, and so one needs to restrict b to values $> R_1 + R_2$ if one wants to look only at EM interaction.

Since $b = (b_1^2 + b_1^2 - 2b_1 b_2 \cos\phi)^{1/2}$, the integration $\int d\phi_1\ d\phi_2$ in (A.14) can be simplified if one integrates over ϕ_1 and converts the integration over ϕ_2 into an integration over ϕ:

$$\int d\phi_1\ d\phi_2 \to 2\pi \int d\phi \tag{A.15}$$

So (A.14) can be rewritten as

$$\begin{aligned}\sigma = 2\pi \int & n(\omega_1, b_1)\ n(\omega_2, b_2)\ \sigma_{\gamma\gamma}(\omega_1, \omega_2)\theta(b - R_1 - R_2) \\ & \times b_1\ bd_1\ b_2\ db_2\ d\phi\ d\omega_1\ d\omega_2.\end{aligned} \tag{A.16}$$

If one now substitutes for $n(\omega_i, b_i), i = 1, 2$, using (A.11), one obtains (2.2).

Concerning the cutoff for $b1$ and b_2, we observe the following. (A.14) involves an approximation, which consists of replacing the virtual photons emitted by Z_1 and Z_2 with real photons γ_1 and γ_2. This approximation is valid only if the masses of the virtual photons Λ_1 and Λ_2 are small compared to the mass of the produced system W. (See ref. 4, Sections 6.1 and 6.7). By the uncertainty relations, $\Lambda_i = \frac{1}{b_i}, i = 1, 2$. Hence in order for the approximation in (A.13) to be valid, we must have $\Lambda_i < W$, or $\frac{1}{b_i} \lesssim W$. Therefore,

$$b_i \gtrsim \frac{1}{W} \tag{A.17}$$

If b_i does not satisfy (A.17), contribution to the cross section is small, and is generally considered negligible. See reference 5, Sections 6.1 and 6.2, and reference 11, Sections 7, 7.1–7.3. Another consideration for the values of b_i is that since we are interested in the effects of each nucleus acting as a single entity rather than as a collection of nucleons acting independently of each other, i.e., we are interested in the coherent effects of the collection of nucleons, we need to restrict

$$b_i > R_i. \tag{A.18}$$

So for reactions in which the Compton wavelength of the produced system is smaller than the nuclear radii, i.e., $\frac{1}{W} < R_i$, we can set the minimum of b_i by

$$b_{imn} = R_i. \tag{A.19}$$

This is the case for $\mu^+\mu^-$ and $\tau^+\tau^-$ pair function. But for e^+e^- pair production, the Compton wavelength of an electron $\frac{1}{m_e}$ is $>R_i$. So we set the minimum of b_i by

$$b_{imn} = \frac{1}{W}. \tag{A.20}$$

Appendix B

First we list the cross sections for the processes in (3.1): $\gamma\gamma \to l^+l^-, \gamma\gamma \to s^+s^-, \gamma\gamma \to V^+V^-$, and $\gamma\gamma \to H^o$. (See ref. 2, eqs. (14)–(17), pp. 159, 160; and ref. 12, eqs. (10), (11), p. 95.)

$$\sigma(\gamma\gamma \to l^+l^1) = \frac{4\pi\alpha^2}{W^2}\left[2(1+y_l-\frac{1}{2}y_l^2)\ln\left(\frac{1}{\sqrt{y_l}}+\sqrt{\frac{1}{y_l}-1}\right) - (1+y_l)\sqrt{1-y_l}\right], \tag{B.1a}$$

$$\sigma(\gamma\gamma \to s^+s^1) = \frac{2\pi\alpha^2}{W^2}\left[(1+y_s)-\sqrt{1-y_s}-2y_s\left(1-\frac{1}{2}\,y_s\right)\ln\left(\frac{1}{\sqrt{y_s}}+\sqrt{\frac{1}{y_s}-1}\right)\right], \tag{B.1b}$$

$$\sigma(\gamma\gamma \to V^+V^1) = \frac{8\pi\alpha^2}{W^2}\left[\frac{1}{t_v}\left(1+\frac{3}{4}t_v+3t_v^2\right)\Lambda-3t_v(1-2t_v)\ln\left(\frac{1+\Lambda}{1-\Lambda}\right)\right], \tag{B.1c}$$

where

$$y_l = \frac{4m_\rho^2}{W^2}, \quad y_s = \frac{4m_s^2}{W^2}, \tag{B.2a}$$

$$t_v = \frac{m_v^2}{W^2}, \quad \Lambda = \sqrt{1-4t_v}. \tag{B.2b}$$

W is the total energy of the two photons in the center of momentum frame.

$$\sigma(\gamma\gamma \to H^0) = \frac{8\pi^2}{m_H}\Gamma\,\delta(W^2-m_H^2) \tag{B.3}$$

where Γ can be written as (ref. 12, eq. (10), p. 95)

$$\Gamma = \frac{\alpha^2 G_F m_H^3}{8\pi^3\sqrt{2}}\,|I|^2, \tag{B.4}$$

and I in turn has the form (ref. 12, eqn. (11), p. 95)

$$I = \sum_q q^2\, I_q + \sum_l I_l + I_w, \tag{B.5a}$$

$$I_q = 3\left[2\lambda_q + \lambda_q(4\lambda_q - 1)f(\lambda_q)\right], \tag{B.5b}$$

$$I_l = 2\lambda_l + \lambda_l(4\lambda_l - 1)f(\lambda_l), \tag{B.5c}$$

$$I_W = 3\lambda_W(1 - 2\lambda_W)f(\lambda_W) - 3\lambda_W - \frac{1}{2}, \tag{B.5d}$$

where for

$$\lambda > \frac{1}{4}, \quad f(\lambda) = -2\left(\arcsin\frac{1}{2\sqrt{\lambda}}\right)^2, \tag{B.6a}$$

and for

$$\lambda < \frac{1}{4}, f(\lambda) = \frac{1}{2}\left(\ln\frac{\eta^+}{\eta^-}\right)^2 - \frac{\pi^2}{2} + i\pi \ln\frac{\eta^+}{\eta^-}, \tag{B.6b}$$

$$\eta^{\pm} = \frac{1}{2} \pm \sqrt{\frac{1}{4} - \lambda} \tag{B.6c}$$

The subscripts q, l, and W stand for quark, lepton and W-boson, respectively.

$$\lambda_i \equiv \frac{m_i^2}{m_h^2}, \quad \text{for} \quad i = q, l, W, \tag{B.7}$$

and m_i are the rest masses of the coresponding particles. m_h is the rest mass of H^0.

In the following, we give the derivatives of the cross sections for the processes

$$\gamma\gamma \to s^+s^-, \tag{B.8}$$

$$\gamma\gamma \to l^+l^-. \tag{B.9}$$

We also give a derivation of the relationship between σ and Γ for the process

$$\gamma\gamma \to H^0 \tag{B.10}$$

$$\gamma\gamma \to s^+s^-.$$

The lagrangian for the system, including EM interaction, can be written as

$$\mathcal{L}_{\rm cm} = -\left(\frac{\partial}{\partial x_\mu} + ieA_\mu\right)\phi^+\left(\frac{\partial}{2x^\mu} - ieA^\mu\right)\phi - m^2\phi^+\phi \tag{B.11}$$

in which ϕ denotes a scalar field operator, A_μ denotes the photon field, $\mu = 0,1,2,3$. We use the convention that repeated indices are summed over, so that for example,

$$A_\mu A^\mu = A_o A^o + A_1 A^1 + A_2 A^2 + A_3 A^3 \tag{B.12a}$$

$$= A_o A_o - A_1 A_1 - A_2 A_2 - A_3 A_3. \tag{B.12b}$$

This lagrangian can be separated into a free part, and an interaction part, so that

$$\mathcal{L}_{\rm int} = ie\left(\phi^+ A^\mu \frac{\partial\phi}{\partial x^\mu} - \frac{\partial\phi^+}{\partial x_\mu} A_\mu\phi\right) + e^2 A^\mu A_\mu \phi^+\phi. \tag{B.13}$$

The S-matrix element that contributes to (B.8) can be written in the form

$$< p-; p+|S^{(1)} + S^{(2)}|\ k_1,\epsilon_1; k_2,\epsilon_2 > \tag{B.14}$$

in which $p^\pm$ denotes the momenta of $S^\pm$, k_1, ϵ_i are the momenta and polarization vectors of the photons, $i = 1,2$, and $S^{(2)}$ is defined by

$$S^{(2)} = \frac{i^2}{2}\, T \int \mathcal{L}_{\rm int}(x_1)\mathcal{L}_{\rm int}\ (x_2)\ d^4x_1\ d^4x_2, \tag{B.15}$$

where T denotes the time-ordering operator. Contribution from $S^{(2)}$ can be represented by the diagrams.

Using (B.13) and (B.15), and standard techniques of field theory, one obtains

$$\begin{aligned} &< p_-;\ p_+|S^{(2)}|k_1,\epsilon_1; k_2,\epsilon_2 > \\ &= ie^2(2\pi)^4(2p_{-o}\cdot 2p_{+o}\cdot 2k_{10}\cdot 2k_{20})^{-\frac{1}{2}}\ \Omega^{-2} \\ &\quad\times\left[\frac{\epsilon_1^\mu(k_\mu + p_{-\mu})\epsilon_2^\nu(p_{+\nu} - k_\nu)}{k^2 - m^2 + i\epsilon} + \frac{\epsilon_2^\mu(k'_\mu + p_{-\mu})\epsilon_1^\nu(p_{+\nu} - k'_\nu)}{k'^2 - m^2 + i\epsilon}\right] \\ &\quad\times\delta^4(p_- + p_+ - k_1 - k_2), \end{aligned} \tag{B.16}$$

where $k \equiv p_- - k_1 = k_2 - p_+$, $k' \equiv p_- - k_2 = k_1 = p_+$, Ω is the normalization volume, and ϵ denotes an infinitessimal quantity.

Likewise $S^{(1)}$ is defined by

$$S^{(1)} = i\,T \int \mathcal{L}_{\rm int}(x)\; d^4k, \tag{B.17}$$

and

$$\begin{aligned} < p_-; p_+ | S^{(1)} | k_1, \epsilon_1; k_2, \epsilon_2 > &= ie^2 (2\pi)^4 (2p_{-o} \cdot 2p_{+o} \cdot 2k_{10} \cdot 2k_{20})^{-1/2} \\ &\times \Omega^{-2}\; 2\epsilon_1 \cdot \epsilon_2\; \delta^4(p_- + p_+ - k_1 - k_2). \end{aligned} \tag{B.18}$$

The diagram representing this matrix element is shown in figure B.2.

The total cross section is obtained by squaring (B.14), averaging over photon polarizations ϵ_1 and ϵ_2, integrating over phase space, and finally dividing by the photon flux. Hence we have

$$\begin{aligned} \sigma = \int \frac{1}{4} \sum_{\epsilon_1, \epsilon_2} \left| < p_-; p_+ \right| S^{(1)} + S^{(2)} \left| \; k_1, \epsilon_1; k_2, \epsilon_2 > \right|^2 \frac{d^3p_- d^3p_+}{(2\pi)^6} \\ \times \Omega^2 \times \frac{\Omega}{2c} \times \frac{1}{T_o}, \end{aligned} \tag{B.19}$$

in which T_o is the normalization time. Substituting (B.16) and (B.18) into (B.19), we obtain

$$\begin{aligned} \sigma &= e^4 a^2 \int f(\theta)\; \delta^4\,(p_- + p_+ - k_1 - k_+)\; \frac{\Omega T_o}{(2\pi)^4}\; \frac{d^3p - d^3p_+}{(2\pi)^6} \frac{\Omega^3}{2cT_o} \\ &= \frac{e^4\; a^2 \Omega^4}{(2\pi)^4 \cdot 2c \cdot (2\pi)^6}\; (p_{-o}^2 - m^2)^{1/2}\; \frac{p_{-o}}{2} \int_0^\pi f(\theta)\; \sin\,\theta\; d\theta \times 2\pi. \end{aligned} \tag{B.20}$$

where

$$\begin{aligned} f(\theta) \equiv \frac{1}{4} \sum_{\epsilon_1, \epsilon_2} \Bigg[&\frac{\epsilon_1 \cdot (k + p_-) \epsilon_2 \cdot (p +- k)}{k^2 - m^2 + i\epsilon} \\ &+ \frac{\epsilon_2 \cdot (k' + p_-) \epsilon_1 \cdot (p_+ - k')}{k'^2 - m^2 + i\epsilon} + 2\epsilon_1 \cdot \epsilon_2 \Bigg]^2, \end{aligned} \tag{B.21}$$

$$a \equiv (2\pi)^4\; (2p_{-o} \cdot 2p_{+o} \cdot 2k_{10} \cdot 2k_{20})\; ^{-1/2}\; \Omega^{-2}, \tag{B.22}$$

and θ is the angle between $\vec{p}_-$ and the z-axis. We shall work in the center of momentum frame of the two photons, and use the fact that for real photons,

$$\epsilon_1 \cdot k_1 = \epsilon_2 \cdot k_2 = 0. \tag{B.23}$$

After some algebraic manipulation, we obtain

$$f(\theta) = \beta^4 \sin^4\theta \left[\frac{1}{(1-\beta\cos\theta)^2} + \frac{2}{(1-\beta\cos\theta)(1+\beta\cos\theta)} + \frac{1}{(1+\beta\cos\theta)^2}\right] + 2 - 2\beta^2\sin^2\theta\left[\frac{1}{1-\beta\cos\theta} + \frac{1}{1+\beta\cos\theta}\right],$$

in which

$$\beta \equiv \frac{|\vec{p}_-|}{p_{-o}}. \tag{B.24}$$

(B.20) can be simplified by carrying out the integration over θ, so that

$$\int_0^\pi f(\theta)\,\sin\theta\,d\theta = 4(2-\beta^2) + 2(\beta^2+1)(\beta^2-1)\frac{1}{\beta}\ln\left|\frac{1+\beta}{1-\beta}\right|, \tag{B.25}$$

and hence

$$\sigma = \frac{e^4 a^2 \Omega^4}{(2\pi)^{10}\cdot 2c}\,\frac{p_{-o}^2}{2}\,\beta \times 2\pi \times \left[4(2-\beta^2) + 2(\beta^2+1)(\beta^2-1)\frac{1}{\beta}\ln\left|\frac{1+\beta}{1-\beta}\right|\right]. \tag{B.26}$$

Using the definition of a in (B.22), we then obtain

$$\sigma = e^4\ (2\pi)^8\Omega^{-4}\frac{1}{16p_{-o}^4}\frac{\Omega^4}{(2\pi)^{10}\times 2c} \times \frac{p_{-o}^2}{2} \times 2\pi \times \left[4(2-\beta^2)\beta + 2(\beta^2+1)(\beta^2-1)\ln\left|\frac{1+\beta}{1-\beta}\right|\right] \tag{B.27a}$$

$$= \frac{e^4}{(2\pi)^2}\frac{1}{16p_{-o}^2}\frac{1}{4c} \times 2\pi \times \left[4(2-\beta^2)\beta + 2(\beta^2+1)(\beta^2-1) \times \ln\left|\frac{1+\beta}{1-\beta}\right|\right]. \tag{B.27b}$$

In the "natural units" in which one sets $\hbar = c = 1$, this result can be written in the form

$$\sigma = \frac{e^4}{(4\pi)^2}\frac{1}{4p_{-o}^2} \times 2\pi \left[(2-\beta^2)\beta + (\beta^2+1)(\beta^2-1) \times \frac{1}{2}\ln\left|\frac{1+\beta}{1-\beta}\right|\right]. \tag{B.28}$$

In terms of the variables $y \equiv \frac{4m^2}{W^2}, W \equiv p_{-o} + p_{+o} = 2p_{-o}$, we can write

$$\sigma = \alpha^2 \times \frac{1}{W^2} \times 2\pi \left[(1+y)\sqrt{1-y} - (2-y)y\ln\left|\frac{1}{\sqrt{y}} + \sqrt{\frac{1}{y}-1}\right|\right] \tag{B.29}$$

in which $\alpha \equiv \frac{e^2}{4\pi}$ is the fine structure constant. This result is the same as the one obtained by Papageorgiu (ref. 2, eq. (15), p. 159). $\gamma\gamma \longrightarrow l^+l^-$. For this case the interaction lagrangian can be written in the form

$$\mathcal{L}_{\text{int}} = -e\,\bar{\psi}(x)\,\not{A}(x)\psi(x), \tag{B.30}$$

in which $\psi(x)$ denotes the lepton field operator. $\not{A}(x) = A_\mu(x)\gamma^\mu$ and γ^μ, $\mu = 0, 1, 2, 3$, are the Dirac γ-matrices. (See ref. 9, Appendix 2, p. 335–361.) $\bar{\psi}(x) = \psi^\dagger(x)\gamma_o$, where $\psi^\dagger(x)$ is the hermitian conjugate of $\psi(x)$. The second order team in the S-matrix is defined by (B.15), with $\mathcal{L}_{\text{int}}(x)$ defined by (B.30). The initial and final states can be denoted as

$$\left|i>\right. = \left|k_1, \epsilon_1; k_2, \epsilon_2>\right., \tag{B.31a}$$

$$\left|f>\right. = \left|p_-, S_-; p_+, S_+>\right., \tag{B.31b}$$

in which we have already defined $k_j, \epsilon_j, j = 1, 2$ as the photon momenta and polarization. $p_\pm, p_\pm$ are the momenta and spins of l^+ and l^- respectively. Following the notations of reference 9, appendix 2, we can write the S-matrix element $< f\left|S^{(2)}\right|i >$ as

$$< f\left|S^{(2)}\right|i > = -e^2 a\left[\bar{u}(p_-, S_-)\,\not{\epsilon}_1 \frac{i(\not{k}+m)}{k^2-m^2+i\epsilon}\,\not{\epsilon}_2\, v(p_+, S_+)\right.$$

$$\left. + \bar{u}(p_-, S_-)\,\not{\epsilon}_2 \frac{i(\not{k}^{11}+m)}{k'^2-m^2+i\epsilon}\,\not{\epsilon}_1\, v(p_+, S_+)\right]\,\delta^4(p_- + p_+ - k_1 - k_2),$$

where

$$k \equiv p_- - k_1 = k_2 - p_+,\ k' \equiv p_- - k_2 = k_1 - p_+, \tag{B.32}$$

$$a \equiv (2\pi)^4 \, (2p_{-o} \cdot 2p_{+o} \cdot 2k_{10} \cdot 2k_{20})^{-1/2} \Omega^{-2},$$

$u(p_-, S_-)$ and $V(p_+, S_+)$ are the spinor wave-functions associated with l^- and l^+. This S-matrix element can also be represented diagrammatically by Figures. (B.1a) and (B.1b). The total cross section is given by a formula similar to (B.19):

$$\sigma = \int \frac{1}{4} \sum_{\substack{\epsilon_1, \epsilon_{(2)}, \\ S_-, S_+}} \left| < f \right| S^2 \left| i > \right|^2 \frac{d^3p_- d^3p_+}{(2\pi)^6} \, \Omega^2 \frac{\Omega}{2c} \frac{1}{T_o} \,. \tag{B.33}$$

Performing the sum over the photon and lepton spins, we can write

$$\sum_{\substack{\epsilon_1, \epsilon_2, \\ S_-, S_+}} \left| < f \middle| S^{(2)} \middle| i > \right|^2 = \sum_{\epsilon_1, \epsilon_2} e^4 a^2 \delta^4 (p_- + p_+ - k_1 - k_2) \frac{\Omega T_o}{(2\pi)^4} \{ (k^2 - m^2 + i\epsilon)^{-}2$$

$$\times Tr \lfloor (\not{p}_- + m) \not{\epsilon}_1 \, i(\not{k} + m) \not{\epsilon}_2 (\not{p}_+ - m) \not{\epsilon}_2 (-i)(\not{k} + m) \not{\epsilon}_1 \rfloor$$

$$+ (k^2 - m^2 + i\epsilon)^{-1} (k'^2 - m^2 + i\epsilon)^{-1} \, Tr \left[(\not{p}_- + m) \not{\epsilon}_1 (k + m) \not{\epsilon}_2 (\not{p}_+ - m) \not{\epsilon}_1 (\not{k}' + m) \not{\epsilon}_2 \right]$$

$$+ (k^2 - m^2 + i\epsilon)^{-1} (k'^2 - m^2 + i\epsilon)^{-1} \, Tr \left[(\not{p}_- + m) \not{\epsilon}_2 (\not{k}' + m) \not{\epsilon}_1 (\not{p}_+ - m) \not{\epsilon}_2 (\not{k} + m) \not{\epsilon}_1 \right]$$

$$+ (k'^2 - m^2 + i\epsilon)^{-2} \, Tr \left[(\not{p}_- + m) \not{\epsilon}_2 (k' + m) \not{\epsilon}_1 (p_+ - m) \not{\epsilon}_1 (\not{k}' + m) \not{\epsilon}_2 \right] \}, \tag{B.34}$$

in which Tr denotes the trace operator. We use m instead of m_l to denote the lepton mass. From (B.34), it can be seen that the sum in (B.34) can be naturally divided into four terms:

$$T_1 \equiv Tr \left[(\not{p}_- + m) \not{\epsilon}_1 (\not{k} + m) \not{\epsilon}_2 (\not{p}_+ - m) \not{\epsilon}_2 (\not{k} + m) \not{\epsilon}_1 \right], \tag{B.35a}$$

$$T_2 \equiv Tr \left[(\not{p}_- + m) \not{\epsilon}_1 (\not{k} + m) \not{\epsilon}_1 (\not{p}_+ - m) \not{\epsilon}_1 (\not{k}' + m) \not{\epsilon}_2 \right], \tag{B.35b}$$

$$T_3 \equiv Tr \left[(\not{p}_- + m) \not{\epsilon}_2 (\not{k}' + m) \not{\epsilon}_1 (\not{p}_+ - m) \not{\epsilon}_2 (\not{k} + m) \not{\epsilon}_1 \right], \tag{B.35c}$$

$$T_4 \equiv Tr \left[(\not{p}_- + m) \not{\epsilon}_2 (\not{k}' + m) \not{\epsilon}_1 (\not{p}_+ - m) \not{\epsilon}_1 (\not{k}' + m) \not{\epsilon}_2 \right]. \tag{B.35c}$$

Hence we can write

$$\sum_{\substack{\epsilon_1, \epsilon_2, \\ S_-, S_+}} \left| < f \middle| S^{(2)} \middle| i > \right|^2 = e^4 a^2 \delta^4 (p_- + p_+ - k_1 - k_2) \, \frac{\Omega T_o}{(2\pi)^4}$$

$$\times \sum_{\epsilon_1,\epsilon_2}\{(k^2-m^2+i\epsilon)^{-2}\,T_1+(k^2-m^2+i\epsilon)^{-1}(k'^2-m^2+ie)^{-1}\,(T_2+T_3)$$
$$+(k'^2-m^2+i\epsilon)^{-2}T_4\}. \tag{B.36}$$

After some straight forward though tedious mathematics, one arrives at the following:

$$\frac{1}{4}\sum_{\epsilon_1,\epsilon_2} T_1 = 8k_{10}^4(1-\beta\cos\theta)\left(1+\frac{m^2}{k_{10}^2}+\frac{2m^2}{k_{10}^2}\beta\cos\theta+\beta^3\cos^3\theta\right)-8m^4, \tag{B.37}$$

$$\frac{1}{4}\sum_{\epsilon_1,\epsilon_2} T_2 = \frac{1}{4}\sum_{\epsilon_1,\epsilon_2} T_3 = 8k_{10}^4\beta^2(1-\cos^2\theta)\left[1-\beta^2(1-\cos^2\theta)\right], \tag{B.38}$$

$$\frac{1}{4}\sum_{\epsilon_1,\epsilon_2} T_4 = 8k_{10}^4(1+\beta\cos\theta)\left(1+\frac{m^2}{k_{10}^2}-\frac{2m^2}{k_{10}^2}\,\beta\cos\theta-\beta^3\cos^3\theta\right)-8m^4, \tag{B.39}$$

where $\beta \equiv \frac{|\vec{p}_-|}{p_{-o}}$. From (B.33) and (B.36) we obtain

$$\sigma = e^4(2\pi)^8(2k_{10})^{-4}\Omega^{-4}\,\frac{\Omega T_o}{(2\pi)^4}\,\frac{\Omega^3}{(2\pi)^6}\,\frac{1}{2cT_o}$$
$$\times\int\left\{\frac{1}{4}\sum_{\epsilon_1,\epsilon_2}[(k^2-m^2+i\epsilon)^{-2}T_1+(k^2-m^2+i\epsilon)^{-1}(k'^2-m^2+i\epsilon)^{-1}\,(T_2+T_3)\right.$$
$$\left.+(k'^2-m^2+i\epsilon)^{-2}T_4]\right\}d^3p_-d^3p_+\delta^4(p_-+p_+-k_1-k_2)$$
$$=\frac{e^4}{(2\pi)^2}\,\frac{1}{16k_{10}^4}\frac{1}{2c}\beta k_{10}^2\times\int\left\{\frac{1}{4}\sum_{\epsilon_1,\epsilon_2}[(k^2-m^2+i\epsilon)^{-2}T_1\right.$$
$$\left.+(k^2-m^2+i\epsilon)^{-1}(k'^2-m^2+i\epsilon)^{-1}(T_2+T_3)+(k'^2-m^2+i\epsilon)^{-2}T_4]\right\}$$
$$\times\frac{1}{2}\sin\theta\,d\theta\times 2\pi. \tag{B.40}$$

Now we use

$$k^2-m^2=-2k_{10}^2(1-\beta\cos\theta), \tag{B.41}$$

$$k'^2-m^2=-2k_{10}^2(1+\beta\cos\theta), \tag{B.42}$$

together with (B.37), (B.38), and (B.39) to arrive at

$$\int_0^\pi \frac{1}{4}\sum_{\epsilon_1,\epsilon_2}(k^2-m^2+i\epsilon)^{-2}T_1\ \sin\theta\ d\theta = \int_0^\pi \frac{1}{4}\sum_{\epsilon_1,\epsilon_2}(k'^2-m^2+i\epsilon)^{-2}T_4\sin\theta\ d\theta$$

$$= -\frac{4}{3}\beta^2 - 4 - 8\frac{m^2}{k_{10}^2} + 2(2+3\frac{m^2}{k_{10}^2})\frac{1}{\beta}\ln\left|\frac{1+\beta}{1-\beta}\right| - \frac{4m^4}{k_{10}^4}\frac{1}{1-\beta^2}, \tag{B.43}$$

$$\int_0^\pi \frac{1}{4}\sum_{\epsilon_1,\epsilon_2}(k^2-m^2+i\epsilon)^{-1}(k'^2-m^2+i\epsilon)^{-1}T_2\sin\theta\ d\theta$$

$$= \int_0^\pi \frac{1}{4}\sum_{\epsilon_1,\epsilon_2}(k^2-m^2+i\epsilon)^{-1}(k'^2-m^2+i\epsilon)^{-1}T_3\sin\theta\ d\theta$$

$$= 8(1-\beta^2) + \frac{4}{3}\beta^2 - \frac{2}{\beta}(2-\beta^2)(1-\beta^2)\ln\left|\frac{1+\beta}{1-\beta}\right|. \tag{B.44}$$

So from (B.43) and (B.44) we have

$$\begin{aligned}
&\int_0^\pi \frac{1}{4}\sum_{\epsilon_1,\epsilon_2}[(k^2-m^2+i\epsilon)^{-2}T_1 + (k^2-m^2+i\epsilon)^{-1}(k'^2-m^2+i\epsilon)^{-1}\ (T_2+T_3)\\
&\quad +\ (k'^2-m^2+i\epsilon)^{-2}T_4]\sin\theta\ d\theta\\
&= -8(2-\beta^2) + \frac{4}{\beta}[2+3(1-\beta^2)-(2-\beta^2)-(1-\beta^2)]\ln\left|\frac{1+\beta}{1-\beta}\right|.\\
&= -8(1+y) + \frac{16}{\beta}\left(1+y-\frac{y^2}{2}\right)\ln\left|\frac{1}{\sqrt{y}} + \sqrt{\frac{1}{y}-1}\right|,
\end{aligned} \tag{B.45}$$

where $y \equiv \frac{4m^2}{W^2} = 1-\beta^2$. Putting this into (B.40), we have

$$\begin{aligned}
\sigma &= \frac{e^4}{(2\pi)^2}\frac{1}{16k_{10}^4}\frac{1}{2c}\beta k_{10}^2 \times 8\left[-(1+y) + \frac{2}{\beta}\left(1+y-\frac{y^2}{2}\right)\right.\\
&\quad \left.\times \ln\left|\frac{1}{\sqrt{y}} + \sqrt{\frac{1}{y}-1}\right|\right] \times \frac{2\pi}{2}\\
&= \frac{e^4}{(4\pi)^2}\frac{1}{W^2} \times 4\pi\left[-(1+y)\sqrt{1-y} + 2\left(1+y-\frac{y^2}{2}\right)\ln\left|\frac{1}{\sqrt{y}} + \sqrt{\frac{1}{y}-1}\right|\right]\\
&= \frac{\alpha^2}{W^2} \times 4\pi\left[-(1+y)\sqrt{1-y} + 2\left(1+y-\frac{y^2}{2}\right)\ln\left|\frac{1}{\sqrt{y}} + \sqrt{\frac{1}{y}-1}\right|\right],
\end{aligned} \tag{B.46}$$

in "natural" units. This result is the same as the one obtained by Papageorgiu (ref. 2, eq. (14), p. 159).

We now consider the process $\gamma\gamma \to S^o$ in which S^o is a neutral scalar. Using p_s to denote the momentum of S^o, the cross section for this process can be written as

$$\sigma = \int \frac{1}{4} = \sum_{\epsilon_1,\epsilon_2} \Big| < p_s \Big| S \Big| k_1, \epsilon_1; k_2, \epsilon_2 > \Big|^2 \frac{d^3 p_s}{(2\pi)^3}\ \Omega \times \frac{\Omega}{2c} \times \frac{1}{T_o}, \tag{B.47}$$

in which S denotes the S-matrix. For the reverse decay process $S^o \to \gamma\gamma$, the width Γ can be written in the form

$$\Gamma = \frac{1}{T_o} \int \sum_{\epsilon_1,\epsilon_2} \Big| < k_1, \epsilon_1; k_2, \epsilon_2 \Big| S \Big| p_s \Big|^2 \frac{d^3 k_1\ d^3 k_2}{(2\pi)^6}\ \Omega^2 \tag{B.48}$$

From conservation of momentum, we can write

$$< p_s \Big| S \Big| k_1, \epsilon; k_2, \epsilon_2 > = < p_s \Big| T \Big| k_1, \epsilon_1; k_2, \epsilon_2 > \delta^4(p_s - k_1 - k_2) \tag{B.49}$$

From (B.47) and (B.49) we now have

$$\sigma = \frac{1}{4} \sum_{\epsilon_1,\epsilon_2} \Big| < p_s \Big| T \Big| k_1, \epsilon_1; k_2, \epsilon_2 > \Big|^2 \delta(p_{so} - k_{10} - k_{20}) \times \frac{1}{(2\pi)^3} \frac{\Omega^2}{2cT_o} \frac{\Omega T_o}{(2\pi)^4} \tag{B.50a}$$

$$= \frac{1}{8c} \frac{\Omega^3}{(2\pi)^7} \sum_{\epsilon_1,\epsilon_2} \Big| < p_s \Big| T \Big| k_1, \epsilon_1; k_2, \epsilon_2 > \Big|^2 \delta(p_{so} - 2k_1 \tag{B.50b}$$

In (B.50), we assume that we are working in the next frame of S^o. Likewise (B.48) can also be rewritten in the form

$$\Gamma = \frac{1}{T_o} \sum_{\epsilon_1,\epsilon_2} \Big| < k_1, \epsilon_1; k_2, \epsilon_2 \Big| T \Big| p_s > \Big|^2 \frac{k_{10}^2}{2} \times 4\pi \times \frac{\Omega^2}{(2\pi)^6} \frac{\Omega T_o}{(2\pi)^4}$$

$$= \frac{\Omega^3}{(2\pi)^9}\ k_{10}^2 \sum_{\epsilon_1,\epsilon_2} \Big| < k_1, \epsilon_1; k_2, \epsilon_2 \Big| T \Big| p_s > \Big|^2 \tag{B.51}$$

From time-reversal invariance, we know that

$$\sum_{\epsilon_1,\epsilon_2} \Big| < k_1, \epsilon_1; k_2, \epsilon_2 \Big| T \Big| p_s > \Big|^2 = \sum_{\epsilon_1,\epsilon_2} \Big| < p_s \Big| T \Big| k_1, \epsilon_1; k_2, \epsilon_2 > \Big|^2. \tag{B.52}$$

Therefore from (B.50) and (B.51) we now have

$$\sigma = \frac{1}{8c}\,(2\pi)^2\,\Gamma \times \frac{1}{k_{10}^2}\,\delta(p_{so} - 2k_{10}). \tag{B.53}$$

In the next frame of S^o,

$$\sigma = (2\pi)^2\Gamma\frac{1}{k_{10}}\,\delta(m_s^2 - 4k_{10}^2) = \frac{8\pi^2}{m_s}\Gamma\delta(m_s^2 - S), \tag{B.54}$$

in which S is the square of the total momentum $(k_1 + k_2)^2$. For $\gamma\gamma \rightarrow H^o$ in which H^o is a neutral Higgs particle, Γ can be written in the form given by (B.4)$\frac{1}{n}$ (B.7).

Appendix C. Fermion Contribution to $\Gamma(H^o \to \gamma\gamma)$.

In this appendix, we derive the Fermion contribution to the decay width of the decay of a Higgs particle $H^o \to \gamma\gamma$. For this case the interaction lagrangian can be written as (ref. 13, eqs. (22.58), (22.78), pp. 676, 682)

$$\mathcal{L}_{\rm int}(x) = \mathcal{L}^{(e)}_{\rm int}(x) + \mathcal{L}^{(h)}_{\rm int}(x), \tag{C.1a}$$

where

$$\mathcal{L}^{(e)}_{\rm int}(x) = q_f \bar{\psi}_f \not{A}(x)\psi_f(x), \mathcal{L}^{(h)}_{\rm int}(x) = h_f \bar{\psi}_f(x)\eta(x)\psi_f(x). \tag{C.1b}$$

$\psi_f(x)$ is the fermion field operator, $A_\mu(x)$ the photon field operator, and $\eta(x)$ the scalar Higgs field operator. q_f denotes the charge of the fermion, and h_f the coupling between the Higgs scalar and the fermion. The process $H^o \to \gamma\gamma$ is third order in the interaction, so that the relevant term in the S-matrix is

$$S^{(3)} = \frac{\mathrm{i}^3}{3!}\, T\left[\int \mathcal{L}_{\rm int}(x,)\mathcal{L}_{\rm int}(x_2)\mathcal{L}_{\rm int}(x_3)\; d^4x,\; d^4x_2\; d^4x_3\right] \tag{C.2}$$

The initial and final states can be denoted as

$$|i> = |p_h>, \text{ and } |f>= |k_1,\epsilon_1;k_2,\epsilon_2>, \tag{C.3}$$

in which p_h denotes the momentum of the Higgs scalar, $k_j, \epsilon_j, j = 1,2$, are the momenta and polarizations of the the photons.

We use m_f and m_h to denote the masses of the fermion and Higgs scalar. The width for the process is given by

$$\Gamma = \frac{1}{T_o}\frac{1}{4}\int \sum_{\epsilon_1,\epsilon_2} \left| < k_1,\epsilon_1;k_2,\epsilon_2 \middle| S^{(3)} \middle| p_h > \right|^2 \frac{d^3k_1\; d^3k_2}{(2\pi)^6}\, \Omega^2. \tag{C.4}$$

The S-matrix element can be represented by the diagrams:

Employing standard techniques of field theory, we find

$$< k_1,\epsilon_1;k_2,\epsilon_2\Big|\ S^{(3)}\Big|p_h > = -q_f^2 h_f (2ph_o\cdot 2k_{10}\cdot 2k_{20})^{-1/2}\ \Omega^{-3/2}$$
$$\times \int d^4p_1 \Big\{ \Big[(p_1-k_1)'^2 - m_f^2 + i\epsilon\Big]^{-1}\ T_r\Big[(\not p_1+m_f)\ \not\epsilon_1(\not p_1-\not k_1+m_f)\ \not\epsilon_2(\not p_1-\not k_1-\not k_2+m_f)\Big]$$
$$+\Big[(p_1-k_2)^2-m_f^2+i\epsilon\Big]^{-1}\ T_r\Big[(\not p_1+m_f)\ \not\epsilon_2(\not p_1-\not k_2+m_f)\ \not\epsilon_1(\not p_1-\not k_1-\not k_2+m_f)\Big]\Big\}$$
$$\times (p_1^2-m_f^2+i\epsilon)^{-1}\Big[(p_1-k_1-k_2)^2-m_f^2+i\epsilon\Big]^{-1}\ \delta^4(k_1+k_2-p_h). \qquad \text{(C.5)}$$

We can separate the two terms on the right hand side of (C.5) and let $S^{(3)} = S_1^{(3)} = S_2^{(3)}$, so that

$$< k_1,\epsilon_1;k_2,\epsilon_2\Big|\ S_1^{(3)}\Big|p_h > = -q_f^2 h_f (2p_{h_o}\cdot 2k_{10}\cdot 2k_{20})^{-1/2}\ \Omega^{-3/2}\delta^4(k_1+k_2-p_h)$$
$$\times \int d^4p_1\Big[(p_1-k_1)^2-m_f^2+i\epsilon\Big]^{-1}\ (p_1^2-m_f^2+i\epsilon)^{-1}$$
$$\times\Big[(p_1-k_1-k_2)^2-m_f^2+\ i\epsilon\Big]^{-1} T_1^{(3)}, \qquad \text{(C.6a)}$$

where

$$T_1^{(3)} \equiv T_r\Big[(\not p_1+m_f)\ \not\epsilon_1(\not p_1-\not k_1+m_f)\ \not\epsilon_2(\not p_1-\not k_1-\not k_2+m_f)\Big], \qquad \text{(C.6b)}$$

and

$$< k_1,\epsilon_1;k_2,\epsilon_2\Big|\ S_1^{(3)}\Big|h> = -q_f^2 h_f (2p_{h_o}\cdot 2k_{10}\cdot 2k_{20})^{-1/2}\ \Omega^{-3/2}\delta^4(k_1+k_2-p_h)$$
$$\times \int d^4p_1\Big[(p_1-k_1)^2-m_f^2+i\epsilon\Big]^{-1}\ \Big[p_1^2-m_f^2+i\epsilon\Big]^{-1}$$
$$\times \Big[(p_1-k_1-k_2)^2-m_f^2+\ i\epsilon\Big]^{-1} T_2^{(3)}, \tag{C.7}$$

where

$$T_2^{(3)} \equiv T_r\Big[(\not p_1+m_f)\ \not\epsilon_2(\not p_1-\not k_2+m_f)\ \not\epsilon_1(\not p_1-\not k_1-\not k_2+m_f)\Big]. \tag{C.8}$$

The evaluation of the matrix elements (C.6) and (C.6) are quite similar. So we need only consider (C.6) in detail for illustration. By evaluating the trace in (C.6b), and using the fact that in the center of momentum frame of the two photons,

$$\epsilon_1\cdot k_1=\epsilon_1\cdot k_2=\epsilon_2\cdot k_1=\epsilon_2\cdot k_2=0, \tag{C.9}$$

and also

$$k_1^2=k_2^2=0, \tag{C.10}$$

for real photons, we find

$$T_1^{(3)} = 4m_f(4p_1\cdot\epsilon_1 p_1\cdot\epsilon-\epsilon_1\cdot\epsilon_2 p_1^2)+8m_f\epsilon_1\cdot\epsilon_2 p_1\cdot k_1$$
$$+4m_f(-k_1\cdot k_2+m_f^2)\epsilon_1\cdot\epsilon_2. \tag{C.11}$$

Now we use a standard technique of Feynman parameterization (ref. 14, Section 3.2, pp. 160–197).

$$(p_1^2-m^2+i\epsilon)^{-1}\Big[(p_1-k_1)^\alpha-m^\alpha+i\epsilon\Big]\Big[(p_1-k_1-k_2)^2-m^2+i\epsilon\Big]^{-1}$$
$$=2\int_0^1 dx\int_0^{1-x} dy\Big[(p_1-Q)^2+p_1^2\Big]^{-3} \tag{C.12a}$$

where

$$Q^\mu \equiv xk_1^\mu+y(k_1^\mu+k_2^\mu), \tag{C.12b}$$

$$p_1^2 \equiv -Q^2 - m_f^2 + k_1^2 x + (k_1 + k_2)^2 y + i\epsilon$$
$$\equiv -Q^2 - m_f^2 + 2k_1 \cdot k_2 y + i\epsilon. \tag{C.12c}$$

Now (C.6) can be rewritten in the form

$$< k_1, \epsilon_1; k_2, \epsilon_2 \Big| S_1^3 \Big| p_h > = -q_f^2 h_f (2p_{h_o} \cdot 2k_{10} \cdot k_{20})^{-1/2} \Omega^{-3/2} \delta^4 (k_1 + k_2 - p_h)$$
$$\times 2 \int_0^1 dx \int_0^{1-x} dy \int d^{\,4} p_1 \Big[(p_1 - Q)^2 + p_1^2 \Big]^{-3} T_1^{(3)}. \tag{C.13}$$

From (C.11) and (C.13), it is apparent that in order to evaluate (C.13) we need to compute the following integrals:

$$I_2^{\mu\nu} \equiv \int dx\, dy\, d^4 p_1\, p_1^\mu p_1^\nu \Big[(p_1 - Q)^2 + p_1^2 \Big]^{-3}, \tag{C.14}$$

$$I_1^\mu \equiv \int dx\, dy\, d^4 p_1\, p_1^\mu \Big[(p_1 - Q)^2 + p_1^2 \Big]^{-3}, \tag{C.15}$$

$$I_o \equiv \int dx\, dy\, d^4 p_1 \Big[(p_1 - Q)^2 + p_1^2 \Big]^{-3}. \tag{C.16}$$

These integrals can be computed using the method of dimensional regularization in which one first computes the following integrals:

$$I_2^{\mu\nu}(n) \equiv \int dx\, dy\, d^n p_1\, p_1^\mu p_1^\nu \Big[(p_1 - Q)^2 + p_1^2 \Big]^{-3}, \tag{C.17}$$

$$I_1^\mu(n) \equiv \int dx\, dy\, d^n p_1\, p_1^\mu \delta \Big[(p_1 - Q)^2 + p_1^2 \Big]^{-3}, \tag{C.18}$$

$$I_o(n) \equiv \int dx\, dy\, d^n p_1 \delta \Big[(p_1 - Q)^2 + p_1^2 \Big]^{-3}, \tag{C.19}$$

in which n is a real number, which in the final result are allowed to approach 4. Details of this process is given in Appendix D.

From the results in Appendix D, we find

$$\int d^4 p_1 \frac{4p_1^\mu p_1^\nu - p_1^2 g^{\mu\nu}}{\Big[(p_1 - Q)^2 + p_1^2 \Big]^3} = -i \frac{\pi^2}{2} \frac{1}{p_1^2} \Big[g^{\mu\nu} (p_1^2 - Q^2) + 4Q^\mu Q^\nu \Big], \tag{C.20}$$

$$\int d^4 p_1 \frac{p_1^\mu}{\Big[(p_1 - Q)^2 + p_1^2 \Big]^3} = -i \frac{\pi^2}{2} \frac{Q^\mu}{p_1^2}, \tag{C.21}$$

and

$$\int d^4p_1 \frac{1}{\left[(p_1-Q)^2+p_1^2\right]^3} = -i\,\frac{\pi^2}{2}\,\frac{1}{p_1^2}. \tag{C·22}$$

Define

$$J_1 \equiv \int d^4p_1 \left[(p_1-k_1)^2-m_f^2+i\epsilon\right]^{-1}\left(p_1^2-m_f^2+i\epsilon\right)^{-1} \times \left[(p_1-k_1-k_2)^2-m_f^2+i\epsilon\right]^{-1} \times T_1^{(3)}. \tag{C·23}$$

By using (C·9)–(C·12), (C·20)–(C·23), we find

$$J_1 = -i\pi^2 \int_0^1 dx \int_0^{1-y} dy\, \frac{1}{p_1^2}\left[4m_f\left(p_1^2-Q^2\right) + 8m_f Q\cdot k_1 + 4m_f\left(-k_1\cdot k_2+m_f^2\right)\right]\epsilon_1\cdot\epsilon_2. \tag{C·24}$$

Using the definitions of p_1 and Q in (C·11) and (C·12), we can simplify (C·24) to

$$J_1 = -i\pi^2\, 2m_f\, \epsilon_1\cdot\epsilon_2 \int_0^1 dx \int_0^{1-x} dy\, \frac{4y(1-x-y)-1}{y(1-x-y)-\lambda+i\epsilon}, \tag{C·25}$$

where $\lambda \equiv \frac{m_f^2}{2k_1\cdot k_2} = \frac{m_f^2}{m_h^2}$.

The integral in (C·25) can be done after some changes of integration variables and applying some techniques in complex analysis. The result is

$$J_1 = -i\pi^2\, 2m_f\, \epsilon_1\cdot\epsilon_2 J_0, \tag{C·26}$$

where for $\lambda = \frac{m_f^2}{m_h^2} > \frac{1}{4}$,

$$J_0 = 2 - 2\left(4\lambda-1\right)\left[\arcsin\left(\frac{1}{\sqrt{4\lambda}}\right)\right]^2, \tag{C·27a}$$

and for $\lambda \le \frac{1}{4}$,

$$J_0 = 2 + \left(4\lambda-1\right)\left\{-\frac{\pi^2}{2} + \frac{1}{2}\left[\ln\left|\frac{\frac{1}{2}+\sqrt{\frac{1}{4}-\lambda}}{\frac{1}{2}-\sqrt{\frac{1}{4}-\lambda}}\right|\right]^2 - i\pi\ln\left|\frac{\frac{1}{2}+\sqrt{\frac{1}{4}-\lambda}}{\frac{1}{2}-\sqrt{\frac{1}{4}-\lambda}}\right|\right\}. \tag{C·27b}$$

From (C·5), (C·6), (C·23) and (C·26) we have therefore

$$< k_1, \epsilon_1; k_2,\ \epsilon_2 | S_1^{(3)} | p_h > = -q_1^2\ h_f \left(2p_{h_o} \cdot 2k_{10} \cdot 2k_{20}\right)^{-1/2} \Omega^{-3/2} J_1 \delta^4 \left(k_1 + k_2 - p_k\right)$$
$$= -q_f^2\ h_f \left(2p_{h_o} \cdot 2k_{10} \cdot 2k_{20}\right)^{-1/2} \Omega^{-3/2} \delta^4 \left(k_1 + k_2 - p_h\right)$$
$$\times \left(-i\pi^2 \times 2m_f \times \epsilon_1 \cdot \epsilon_2\ J_0\right). \qquad \text{(C·28)}$$

It is straight forward to check that

$$< k_1, \epsilon_1; k_2, \epsilon_2 | S_2^{(3)} | p_h > = < k_1, \epsilon_1; k_2, \epsilon_2 | S_1^{(3)} | p_h. \qquad \text{(C·29)}$$

Therefore using (C·3)–(C·8) and (C·28),

$$\Gamma = \frac{1}{T_0}\ \frac{1}{4} \int \sum_{\epsilon_1, \epsilon_2} 4q_f^4\ h_f^2 \left(2p_{h_o} \cdot 2k_{10} \cdot 2k_{20}\right)^{-1} \Omega^{-3} \delta^4 \left(k_1 + k_2 - p_h\right)$$
$$\times \pi^4 \times 4m_f^2 \times \left(\epsilon_1 \cdot \epsilon_2\right)^2 |J_o|^2 \times \frac{\Omega T_o}{(2\pi)^4}\ \frac{d^3k_1 d^3k_2 \Omega^2}{(2\pi)^6}. \qquad \text{(C·30)}$$

Now

$$\sum_{\epsilon_1, \epsilon_2} \left(\epsilon_1 \cdot \epsilon_2\right)^2 = 2, \quad 2k_{10} = 2k_{20} = p_{h_o} = m_h, \qquad \text{(C·31)}$$

Therefore

$$\Gamma = \frac{q_f^4 h_f^2}{(2\pi)^{10}} \times 2 \times \frac{\pi^4 m_f^2}{m_h^3} \times 2\ |J_o|^2 \int d^3k_1 \delta \left(k_{10} + k_{20} - p_{h_o}\right)$$
$$= \frac{1}{16 \times (2\pi)^5}\ q_f^4\ h_f^2\ m_h \lambda\ |J_o|^2, \qquad \text{(C·32)}$$

h_f is related to the Fermi coupling constant G_F by $h_f^2 = m_f^2 \times 2\sqrt{2} G_F$ (ref. 13, Section 22.2, eqs. (22.58), (22.70), and (22.83), pp. 676, 679, 684)

$$\Gamma = \frac{1}{16 \times (2\pi)^5}\ q_f^4 \times 2\sqrt{2} G_F\ m_h^3\ \lambda^2\ |J_o|^2$$
$$= |\frac{q_f}{e}|^4\ \frac{\alpha^2 G_F}{8\sqrt{2}\pi^3}\ m_h^3 \lambda^2\ |J_o|^2. \qquad \text{(C·33)}$$

We note that $\frac{q_f}{e}$ is the charge of the fermion in units of the electron charge. Our result agrees with that in the literature. (See ref. 12, eqs. (10) and (11), p. 95.) We note that the sign of the imaginary part of J_o in (C·27b) is opposite to that of reference 12, equation (11).

However, since only $|J_o|^2$ enters into quantities of physical interest, such as Γ and σ, therefore this difference in sign of the imaginary part of J_o is not significant.

Appendix D. Evaluation of certain integrals.

In this appendix, we outline the procedures involved in evaluating the integrals in (C·14)–(C·19).

The following integrals can be evaluated by standard methods of calculus.

$$\int_0^\infty \frac{u^m du}{(u^2+M^2)^\ell} = C_{m,\ell} \times M^{-2\ell+m+1}, \tag{D·1}$$

provided m is even, $m \geq 0$, ℓ is an integer ≥ 0, $\ell \geq \frac{m}{2}+1$, and the coefficients $C_{m,\ell}$ are defined by

$$C_{m,\ell} = \frac{(\ell-\frac{m}{2}-1)!}{(\ell-1)!}\left(\frac{m-1}{2}\cdot\frac{m-3}{2}\cdots\frac{3}{2}\cdot\frac{1}{2}\right) \times \int_0^{\frac{\pi}{2}} (\cos\theta)^{2\ell-m-2}\, d\theta \tag{D·2}$$

If ℓ is a half-integer, (D·1) still applies with

$$C_{m,\ell} = \left[(\ell-1)(\ell-2)\ldots\left(\ell-\frac{m}{2}\right)\right]^{-1}\left(\frac{m-1}{2}\cdot\frac{m-3}{2}\cdots\frac{1}{2}\right) \times \int_0^{\frac{\pi}{2}} (\cos\,\theta)^{2\ell-m-2}\, d\theta. \tag{D·3}$$

Using methods of complex analysis, we can show that the same formula (D·1) applies if M is replaced by iM in (D·1).

$$\int d^n p (p^2+M^2)^{-\alpha} = \int_{-\infty}^{\infty} dp_o \int_0^\infty |\vec{p}|^{n-2} d|\vec{p}|\ (p_o^2-|\vec{p}|^2+M^2)^{-\alpha}\Omega_{n-2}^{(0)}, \tag{D·4}$$

where $\Omega_n^{(0)}$ denotes the surface area of the n-dimensional unit sphere. Now using (D·1), we find

$$\begin{aligned}\int d^n p (p^2+M^2)^{-\alpha} &= \int_{-\infty}^{\infty} dp_o (-1)^\alpha C_{n-2,\alpha}(-p_o^2-M^2)^{-\alpha+\frac{n-1}{2}}\Omega_{n-2}^{(0)} \\ &= 2(-1)^{\frac{n-1}{2}} C_{n-2,\alpha} C_{0,\alpha-\frac{n-1}{2}}\Omega_{n-2}^{(0)} M^{-2\alpha+n}.\end{aligned} \tag{D·5}$$

From (D·5), it is straight forward to compute

$$\int d^n p \left(p^2 + 2p \cdot Q + M^2\right)^{-\alpha} = \int d^n p \left[(p+Q)^2 + M^2 - Q^2\right]^{-\alpha}$$
$$= 2(-1)^{\frac{n-1}{2}} C_{n-2,\alpha} C_{0,\alpha-\frac{n-1}{2}} \Omega^{(0)}_{n-2} \left(M^2 - Q^2\right)^{-\alpha+\frac{n}{2}}. \quad \text{(D·6)}$$

Now we can evaluate

$$\int d^n p \, p_\mu \left(p^2 + 2p \cdot Q + M^2\right)^{-\alpha} = \frac{-1}{2(\alpha-1)} \frac{\partial}{\partial Q^\mu} \int d^n p \left(p^2 + 2p \cdot Q + M^2\right)^{-\alpha+1}$$
$$= (-1)^{\frac{n+1}{2}} \frac{2\left(\alpha - 1 - \frac{n}{2}\right)}{\alpha - 1} C_{n-2,\alpha-1}$$
$$\times C_{0,\alpha-\frac{n+1}{2}} \times \Omega^{(0)}_{n-2} \left(M^2 - Q^2\right)^{-\alpha+\frac{n}{2}} Q_\mu. \quad \text{(D·7)}$$

Using similar techniques we can evaluate

$$\int d^n p \, p_\mu p_\nu \left(p^2 + 2p \cdot Q + M^2\right)^{-\alpha} = (-1)^{\frac{n+3}{2}} \left(\alpha - 2 - \frac{n}{2}\right) (\alpha-1)^{-1} (\alpha-2)^{-1}$$
$$\times C_{n-2,\alpha-2} \, C_{0,\alpha-\frac{n+3}{2}} \, \Omega^{(0)}_{n-2} \left(M^2 - Q^2\right)^{-\alpha+1+\frac{n}{2}}$$
$$\times \left[g_{\mu\nu} + \left(M^2 + Q^2\right)^{-1} \left(-\alpha + 1 + \frac{n}{2}\right)\right.$$
$$\left. \times \left(-2Q_\mu Q_\nu\right)\right], \quad \text{(D·8)}$$

and

$$\int d^n p \, p^2 \left(p^2 + 2p \cdot Q + M^2\right)^{-\alpha} = (-1)^{\frac{n+3}{2}} \left(\alpha - 2 - \frac{n}{2}\right) (\alpha-1)^{-1} (\alpha-2)^{-1}$$
$$\times C_{n-2,\alpha-2} C_{0,\alpha-\frac{n+3}{2}} \Omega^{(0)}_{n-2} \left(M^2 - Q^2\right)^{-\alpha+1+\frac{n}{2}}$$
$$\times \left[n = 2\left(\alpha - 1 - \frac{n}{2}\right) \left(M^2 - Q^2\right)^{-1} Q^2\right], \quad \text{(D·9)}$$

in which $q_{\mu\nu}$ is the metric tensor

$$g_{oo} = -g_{11} = -g_{22} = -g_{33} = 1, \quad \text{(D·10)}$$

and all $g_{\mu\nu}$ with $\mu \neq \nu$ are 0.

We also note the following:

$$\int_0^\infty \frac{u^m}{(u^2+M^2)^\alpha}\,du = \frac{-1}{\alpha-1}\frac{\partial}{\partial M^2}\int_0^\infty \frac{u^m}{(u^2+M^2)^{\alpha-1}}du \tag{D·11}$$

Therefore, by using (D·1), we find

$$C_{m,\alpha} = \left(\alpha - 1 - \frac{m+1}{2}\right)(\alpha-1)^{-1}C_{m,\alpha-1}. \tag{D·12}$$

We can now use these results to evaluate

$$\begin{aligned}
&\int d^n p_1 \left(4p_1^\mu p_1^\nu - p_1^2 g^{\mu\nu}\right)\left[(p_1-Q)^2+p_1^2\right]^{-\alpha} \\
&= (-1)^{\frac{n+3}{2}}\left(\alpha-2-\frac{n}{2}\right)(\alpha-1)^{-1}(\alpha-2)^{-1}C_{n-2,\alpha-2}C_{0,\alpha-\frac{n+3}{2}}\Omega^{(0)}_{n-2} \\
&\quad\times\left[g^{\mu\nu}(4-n)\left(p_1^2+Q^2\right)\left(p_1^2\right)^{-\alpha+\frac{n}{2}} - 4(4-n)Q^\mu Q^\nu\left(p_1^2\right)^{-\alpha+\frac{n}{2}}\right].
\end{aligned} \tag{D·13}$$

Using (D·12) in (D·13), we find

$$\begin{aligned}
&\int d^n p_1 \left(4p_1^\mu p_1^\nu - p_1^2 g^{\mu\nu}\right)\left[(p_1-Q)^2+p_1^2\right]^{-\alpha} \\
&= (-1)^{\frac{n+3}{2}}\left(\alpha-1-\frac{n}{2}\right)^{-1}C_{n-2,\alpha}C_{0,\alpha-\frac{n-1}{2}}\Omega^{(0)}_{n-2} \\
&\quad\times\left[g^{\mu\nu}(4-n)\left(p_1^2+Q^2\right)\left(p_1^2\right)^{-\alpha+\frac{n}{2}} - 4(4-n)Q^\mu Q^\nu\left(p_1^2\right)^{-\alpha+\frac{n}{2}}\right].
\end{aligned} \tag{D·14}$$

Setting $\alpha = 3$, and taking the limit as $n \to 4$, we find

$$\begin{aligned}
&\int d^n p_1 \left(4p_1^\mu p_1^\nu - p_1^2 g^{\mu\nu}\right)\left[(p_1-Q)^2+p_1^2\right]^{-\alpha} \\
&= (-1)^{\frac{7}{2}}\times 2\Omega^{(0)}_2\frac{1}{p_1^2}\left[g^{\mu\nu}\left(p_1^2-Q^2\right)+4Q^\mu Q^\nu\right]C_{2,3}C_{0,\frac{3}{2}} \\
&= -i\,\frac{\pi^2}{2}\,\frac{1}{p_1^2}\left[g^{\mu\nu}\left(p_1^2-Q^2\right)+4Q^\mu Q^\nu\right].
\end{aligned} \tag{D·15}$$

In similar fashion we find

$$\begin{aligned}
\int d^n p_1 p_1^\mu\left[(p_1-Q)^2+p_1^2\right]^{-d} &= (-1)^{\frac{n+1}{2}}2\left(\alpha-1-\frac{n}{2}\right)(\alpha-1)^{-1}C_{n-2,\alpha-1} \\
&\quad\times C_{0,\alpha-\frac{n+1}{2}}\,\Omega^{(0)}_{n-2}\left(p_1^2\right)^{-\alpha+\frac{n}{2}}(-Q^\mu) \\
&= (-1)^{\frac{n+1}{2}}\,2C_{n-2,\alpha}\,C_{0,\alpha-\frac{n-1}{2}}\Omega^{(0)}_{n-2}\,\left(p_1^2\right)^{-\alpha+\frac{n}{2}}(-Q^\mu).
\end{aligned} \tag{D·16}$$

Therefore,

$$\int d^4p_1\, p_1^\mu \left[(p_1-Q)^2+p_1^2\right]^{-3} = -i2C_{2,3}\, C_{0,\frac{3}{2}}\, \Omega_2^{(0)} \frac{1}{p_1^2}\, Q^\mu$$
$$= -i\,\frac{\pi^2}{2}\,\frac{Q^\mu}{p_1^2}. \qquad \text{(D·17)}$$

Finally,

$$\int d^4p_1 p_1^\mu \left[(p_1-Q)^2+p_1^2\right] = 2(-1)^{3/2} C_{2,3}\, C_{0,\frac{3}{2}}\, \Omega_2^{(0)} \frac{1}{p_1^2}$$
$$= -i\,\frac{\pi^2}{2}\,\frac{1}{p_1^2}. \qquad \text{(D·18)}$$

Appendix E. Stopping Power

Consider the reaction

$$Z_1 Z_2 \rightarrow Z_1 Z_2 X, \tag{E·1}$$

in which X represents one or more particles produced in the process. Let Z_1 be an incident particle, and Z_2 represent a fixed target, whose density is ρ (number of nuclei per unit volume). Let σ denote the cross section for the process (E·1), and E_x the energy of the system X. If we disregard the effect due to recoil of Z_2, then by the conservation of energy, the energy loss of Z_1 is equal to E_x. Consider a slab of the target Z_z of cross-sectional area A and thickness Δx.

Figure E.1

The number of Z_2 nuclei in this slab is $\rho A \Delta x$. The cross section for an incident particle Z_1 to collide with a Z_2, producing X is given by

$$\Delta\sigma = \rho A \Delta x \, \frac{d\sigma}{dE_x} \, dE_x, \tag{E·2}$$

where we assume the energy of the produced system X to be between E_x and $E_x + dE_x$.

Therefore the probability for this process is

$$P(E_x)dE_x = \frac{\Delta\sigma}{A} = \rho\Delta x \, \frac{d\sigma}{dE_x} \, dE_x, \tag{E·3}$$

in which $P(E_x)$ represents the probability density for the process. Therefore the total energy loss by the incident particle Z_1 per unit length is given by

$$-\frac{dE}{dx} = \lim_{\Delta x \to 0} \frac{1}{\Delta x} \int E_x P(E_x) \, dE_x \tag{E·4a}$$

$$= \rho \int E_x \, \frac{d\sigma}{dE_x} \, dE_x. \tag{E·4b}$$

The $-$ sign in (E·4) signifies the fact that energy is lost by Z_1 in the process, so that the change in its energy dE is negative. (See ref. 15, eq (6·4), page 741.

For two-photon processes of this kind that we have considered

$$E_x = w_1 + w_2, \tag{E·5}$$

in which again we use the "natural units" for which $\hbar = 1$. The cross section is given by (2·2a). By switching the variables of integration from w_1, w_2 to w_1, E_x, and using the fact

$$dw_1 \, dw_2 = dw_1 \, dE_x, \tag{E·6}$$

which can be obtained from (E·5), (E·4b) can be written in the form

$$-\frac{dE}{dx} = \rho \int \frac{dw_1}{w_1} \int \frac{dE_x}{E_x - w_1} E_x \, F(w_1, \, E_x - w_1) \times \sigma_{\gamma\gamma}(w_1, \, E_x - w_1) \tag{E·7a}$$

$$= \rho \int \frac{dw_1}{w_1} \int \frac{dw_2}{w_2} (w_1 + w_2) \, F(w_1, \, w_2) \sigma_{\gamma\gamma}(w_1, \, w_2) \tag{E·7b}$$

(E·7b) is the same as (2·7).

References

1. Fatyga, M.; and Norbury, J. W.: An Experiment to Study Strong Electromagnet Fields at RHIC. Proceedings of the Fourth Workshop on Experiments and Detectors for a Relativistic Heavy Ion Collider, Brookhaven National Laboratory, July 1990, pp. 345–368.
2. Papageorgiu, E.: Two-photon Physics With Ultra-High-Energy Heavy-Ion Beams. Phys. Lett. B, vol. 250, no. 1,2, Nov. 1990, pp. 155–160.
3. Baur, G.; and Ferreira Filho, L. G.: Coherent Particle Production at Relativistic Heavy-ion Colliders Including Strong Absorption Effects. Nucl. Phys. A, vol. 518, 1990, pp. 786–800.
4. Jackson, J. D.: Classical Electrodynamics, John Wiley & Sons, Inc., 1975.
5. Budnev, V. M.; Ginzburg, I. F.; Meledin, G. V.; and Serbo, V. G.: The Two-Photon Particle Production Mechanism. Physical Problems. Applications. Equivalent Photon Approximation. Phys. Rep., vol. 15, 1975, pp. 181–282.
6. Vermasseren, J. A. M.: Two-Photon Processes at Very High Energies. Nucl. Phys. B, vol. 229, 1983, pp. 347–371.
7. Bottcher, C.; and Strayer, M. R.: Electron Pair Production From Pulsed Electromagnetic Fields in Relativistic Heavy-Ion Collisions. Phys. Rev. D, vol. 39, no. 5, March 1989, pp. 1330–1341.
8. Wu, J. S.; Bottcher, C.; and Strayer, M. R.: Coherent Particle Production in a Classical Field Approximation. Phys. Lett. B, vol. 252, no. 1, Dec. 1990, pp. 37–42.
9. Commins, E. D.: Weak Interactions. McGraw Hill, Inc., 1973.
10. Rhoades-Brown, M. J.; and Weneser, J.: Higher Order Effects on Pair Creation by Relativistic Heavy Ion Beams. Brookhaven National Laboratory preprint BNL-45629, Dec. 1990.
11. Bertulani, C. A.; and Baur, G.: Electromagnetic Processes in Relativistic Heavy Ion Collisions. Phys. Rep., vol. 163, nos. 5 & 6, June 1988, pp. 299–408.

12. Papageorgiu, E.: Coherent Higgs-Bosons Production in Relativistic Heavy-Ion Collisions. Phys. Rev. D, vol. 40, no. 1, July 1989, pp. 92–100.

13. Lee, T. D.: Particle Physics and Introduction to Field Theory. Harwood Academic Publishers, 1981.

14. Frampton, P. H.: Gauge Field Theories. The Benjamin/Cummings Publishing Company, Inc., 1987.

15. Bertulani, C. A.; and Baur, G.: Electromagnetic Processes in Relativistic Heavy Ion Collisions. Nucl. Phys. A, vol. 458, 1986, pp. 725–744.

Figure Captions

Figure 1. A Feynman diagram for the processes $Z_1Z_2 \to Z_1Z_2l^+l^-, Z_1Z_2 \to Z_1Z_2s^+s^-$ and $Z_1Z_2 \to Z_1Z_2V^+V^-$.

Figure 2. A Feynman diagram for the process $Z_1Z_2 \to Z_1Z_2H^0$.

Figure 3. Plots of $W^2 \frac{dL}{dW^2}$.

Figure 4. a–d: $\sigma_{\gamma\gamma}(W^2)$ for the reactions $\gamma\gamma \to l^+l^-, \gamma\gamma \to s^+s^-$, $\gamma\gamma \to V^+V^-$ and $\gamma\gamma \to H^0$.

Figure 5. Plots of P(b) for the reaction $^{208}Pb^{208}Pb \to {}^{208}Pb^{208}Pbe^+e^-$ at different energies.

Figure 6. Plots of the total cross section for the process $^{208}Pb^{208}Pb \to {}^{208}Pb^{208}PbH^0$.

Figure A.1: Electromagnetic fields generated by a charge q moving along the x-axis.

Figure A.2: Protons emitted by two colliding nuclei, viewed along direction of motion of the nuclei in their center of momentum frame.

Figure A.3: Cross-sectional view of the collision of two nuclei.

Figure B.1a–b: Second order Feynman diagrams for the process $\gamma\gamma \to s^+s^-$.

Figure B.2: First order Feynman diagram for the process $\gamma\gamma \to s^+s^-$.

Figure C.1a–b: Feynman diagrams representing fermion contribution to the process $H^0 \to \gamma\gamma$.

Figure E.1: A beam of particles Z_1 incident on a fixed target Z_2.

NASA Technical Memorandum 4262

Corrections to the Participant-Spectator Model of High-Energy Alpha-Particle Fragmentation

Francis A. Cucinotta, Lawrence W. Townsend,
and John W. Wilson
Langley Research Center
Hampton, Virginia

John W. Norbury
Rider College
Lawrenceville, New Jersey

National Aeronautics and
Space Administration
Office of Management
Scientific and Technical
Information Division

1991

Symbols and Notation

Particles and fragments:

a, b	projectile fragments
N	nucleon
n	neutron
P	projectile
p	proton
T	target
v	virtual particle
X	final target state
α	alpha particle

Symbols:

A_i	mass number of particle i
B	slope parameter
D_i	energy of particle i in center-of-mass frame
$D(p, q)$	dispersion integral (eq. (20))
E_i	energy of particle i
FSI	final-state interactions
f_{iT}	scattering amplitude of fragment i
i	imaginary number
K	phase space factor
K_i	4-momentum of virtual particle i
K_s, K_p	defined in equations (9) and (12)
$\mathbf{k}_i$	momentum of virtual particle i
$\mathbf{k}_{ij}$	relative momentum of virtual particles i and j
$\mathbf{k}$, $\mathbf{k}'$	intermediate-state relative momenta (eqs. (17) and (18))
m_i	mass of particle i
P_i	4-momentum of particle i
$\mathbf{p}_i$	momentum of particle i
$\mathbf{p}_{ij}$	relative momentum of particles i and j
p_{lab}	laboratory momentum, MeV
$\mathbf{Q}$	total momentum transfer
$\mathbf{R}_i$	momentum of particle i in center-of-mass frame
T_D^1, T_D^2	double-scattering contribution to transition matrix
T_s, T_p	contributions to transition matrix from spectator and participant terms
$\tilde{T}_s, \tilde{T}_p$	distorted transition matrix contributions
t_{ij}	full transition amplitudes for interaction between particles i and j
V	normalization volume
Y_s, Y_p	defined in equations (10) and (13)
α	$= -2\mu_{ab}\epsilon_s$
β_{ij}	relative velocity between particles i and j
ϵ	infinitesimal energy
ϵ_s	separation energy
θ_i	emission angle of particle i
θ_{lab}	laboratory emission angle, deg
μ_{ij}	reduced mass of particles i and j
ρ	ratio of the real to imaginary parts of the forward scattering amplitudes
σ	cross section, mb
Φ	relative cluster momentum distribution
$\tilde{\Phi}$	distorted relative cluster momentum distribution
ϕ	overlap function
Ω_i	solid angle of emission of particle i

Abstract

The participant-spectator model of nuclear fragmentation is described in terms of pole graphs from direct reaction theory. Corrections to the model for more than one projectile fragment scattering on the target are considered using a triangle graph model. Results for alpha-particle fragmentation at 1 GeV/A indicate that corrections to the participant-spectator model are significant, as indicated by the large interference effects found between the pole and triangle graph terms in the double- and single-differential cross sections.

Introduction

The description of biological damage from galactic cosmic rays (GCR) ultimately depends on the track structure of energetic ions in tissue (refs. 1 and 2). Risk assessment for deep space missions requires accurate transport codes for determining the differential flux of ions behind natural and protective radiation shielding. Previous studies (refs. 3 and 4) have indicated the importance of the nuclear fragmentation data base in developing such transport codes. Nuclear fragmentation drastically alters the composition of ion fields, and its proper description is essential for track structure models or any fluence-based risk system.

For high-energy reactions, the participant-spectator model (ref. 5) describes the dominant peripheral channels where only a small number of projectile fragments are produced. These move in the forward direction with velocities near that of the projectile. The nuclear abrasion process occurs for large impact parameters when the overlapping volumes of the projectile and target nuclei, called participants, are sheared off in the collision. The remaining portion of the projectile, the spectator, is assumed to receive only a small momentum transfer in the collision. The spectator fragment may be in an intermediate excited state (prefragment stage), decaying to the final fragment through particle evaporation in the ablation step of the reaction. In contrast to the peripheral breakup channels, there are central collisions when almost complete overlap of projectile and target volumes leads to a multiplicity of fragments in a wide cone of emission angles.

In previous work (refs. 6 and 7), we have considered the diagram approach to direct reaction theory (ref. 8) for describing the abrasion step in terms of dispersion pole diagrams. In this work, we consider corrections to the pole diagrams for two-body dissociation in order to estimate contributions when more than one projectile fragment interact strongly (participate) in the reaction. The direct reaction graphs with singularities closest to the physical values of the fragment variables give the dominant contributions to the cross sections. For the direct reaction approach to be useful, only a few dispersion graphs should contribute over the kinematical region of interest. In references 6 and 7, we showed that the single-pole diagram corresponding to the participant-spectator assumption saturates the production cross section only if the mass of the fragment of interest is much larger than that of the participant fragments. For the lightest nuclei, and for some dissociation channels for heavier projectiles, fragments with comparable mass are produced in a single channel. Rescattering corrections may then become important and are investigated herein for ^{4}He projectiles (alpha particles) fragmenting on ^{1}H targets. For heavier systems, the multiple scattering approach considered here is expected to be modified by using the high-energy optical model (refs. 9 and 10) to properly account for distortion and cascade effects and by treating the ablation step according to the methods in reference 11.

Pole Diagrams

Consider the two-body dissociation of a projectile P fragmenting on a target T:

$$P + T \rightarrow a + b + X \tag{1}$$

where X is the final target state, and a and b are the projectile fragments. The transition matrix T_{fi} for this reaction is related to the momentum distribution for producing the fragment a by

$$\frac{d\sigma}{d\mathbf{p}_a} = \frac{V^3}{(2\pi)^5 \beta_{PT}} \int d\Omega_b \, K |T_{fi}|^2 \tag{2}$$

where β is the relative velocity in the initial state, K is the phase space factor, and V is the normalization volume; a summation over all final target states X is implied. In the overall center-of-mass frame (CM),

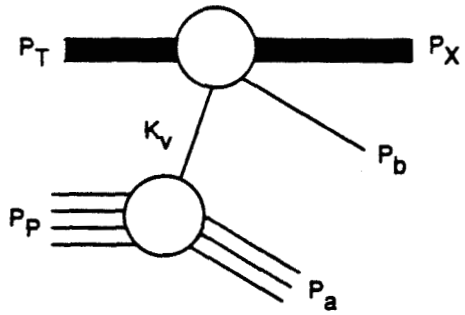

Figure 1. Spectator term for projectile fragmentation.

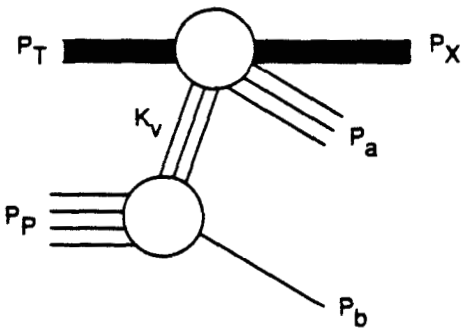

Figure 2. Participant term for projectile fragmentation.

assuming azimuthal symmetry about the beam direction, we have

$$K = \frac{p_b^2 E_b E_X}{p_b(E_b + E_X) + p_a E_b \cos(\theta_a + \theta_b)} \tag{3}$$

The pole diagram for the spectator contribution (Serber term), where the observed fragment is assumed to avoid interaction with the target, is shown in figure 1. A first correction to the spectator model is to reverse the roles of the participant and spectator, with the observed fragment interacting with the target as shown in figure 2. These terms have simple poles at the value of the interacting fragment's mass (ref. 8) and both contribute at small $\mathbf{p}_a$ if the masses, m_a and m_b, are comparable (refs. 6 and 7). Here the singularities of both graphs are relatively close to the physical region. Similar conclusions are expected if the Treiman-Yang criterion (ref. 12) is used to test the spectator pole term. The spectator contribution to the transition matrix is written

$$T_s = \phi\left(\mathbf{p}_a - \frac{A_a}{A_P}\mathbf{p}_P\right) t_{bT}(\mathbf{Q}) \tag{4}$$

and the participant contribution is written

$$T_p = \phi\left(-\mathbf{p}_b + \frac{A_b}{A_P}\mathbf{p}_P\right) t_{aT}(\mathbf{Q}) \tag{5}$$

where ϕ is the overlap function for the virtual dissociation of the projectile, $\mathbf{Q}$ is the total momentum transfer, and t_{iT} is the full transition amplitude for the fragment-target interaction. In equations (4) and (5), we are using the high-energy (on-shell) approximation, and all amplitudes are evaluated at the initial energy. Note that the total momentum transfer is

$$\mathbf{Q} = \mathbf{p}_T - \mathbf{p}_X = \mathbf{p}_a + \mathbf{p}_b - \mathbf{p}_P \tag{6}$$

and the relative momentum of the fragments is

$$\mathbf{p}_{ab} = \frac{1}{A_P}(A_b\mathbf{p}_a - A_a\mathbf{p}_b) \tag{7}$$

The amplitudes appearing in the pole diagrams are transformed to their proper CM frames using relativistic kinematics and the Moller invariants such that

$$T_s = \frac{-2\pi}{V}\sqrt{K_s}\sqrt{Y_s}\,\phi(\mathbf{R}_a)\, f_{bT}(\mathbf{R}_\mathbf{Q}) \tag{8}$$

where f is the scattering amplitude,

$$\sqrt{K_s} = \left[\frac{D_T D_b D_X (D_P - D_a)}{E_T E_b E_X (E_P - E_a)}\right]^{1/2}\left[\frac{\mathbf{R}_{bT}(D_b + D_X)}{\beta_{bT} D_b D_X}\right]^{1/2} \tag{9}$$

and

$$\sqrt{Y_s} = \left[\frac{m_P D_a (m_P - D_a)}{E_P E_a (E_P - E_a)}\right]^{1/2} \tag{10}$$

For the participant term, we have

$$T_p = \frac{-2\pi}{V}\sqrt{K_P}\sqrt{Y_P}\,\phi(-\mathbf{R}_b)\, f_{aT}(\mathbf{R}_\mathbf{Q}) \tag{11}$$

where

$$\sqrt{K_p} = \left[\frac{D_T D_a D_X (D_P - D_b)}{E_T E_a E_X (E_P - E_b)}\right]^{1/2}\left[\frac{\mathbf{R}_{aT}(D_a + D_X)}{\beta_{aT} D_a D_X}\right]^{1/2} \tag{12}$$

and

$$\sqrt{Y_p} = \left[\frac{m_P D_b (m_P - D_b)}{E_P E_b (E_P - E_b)}\right]^{1/2} \tag{13}$$

In equations (8) through (13), D and $\mathbf{R}$ denote energies and momenta in the proper CM frame, which may differ for each amplitude.

The contribution of the pole terms to the momentum distribution is now written

$$\frac{d\sigma}{d\mathbf{p}_a} = \frac{1}{\beta_{PT}}\int d\Omega_b\, K\Big|-\sqrt{K_s Y_s}\,\Phi(\mathbf{R}_a)\, f_{bT}(\mathbf{R}_\mathbf{Q}) - \sqrt{K_p Y_p}\,\Phi(-\mathbf{R}_b)\, f_{aT}(\mathbf{R}_\mathbf{Q})\Big|^2 \tag{14}$$

where we have defined the relative cluster momentum distribution

$$\Phi(\mathbf{R}) = \frac{\sqrt{V}}{(2\pi)^{3/2}}\phi(\mathbf{R}) \tag{15}$$

Final-State Interactions

The fragments a and b are expected to interact following their separation, and their relative momentum vector is expected to have a relatively small value. The diagrams for final-state interactions (FSI) between projectile fragments are shown in figures 3 and 4. Following references 13 to 15, we use a separable potential model that incorporates orthogonality between the bound and scattering states of the projectile fragments and that is appropriate for small $\mathbf{p}_{ab}$. Note that orthogonality is violated if an optical potential is employed, since the same potential is not employed to describe the bound and scattering states.

For figure 3, we write

$$T_s^{\mathrm{FSI}} = t_{bT}(\mathbf{Q})\frac{V}{(2\pi)^3}\int d\mathbf{k}'\frac{2\mu_{ab}\,\phi(\mathbf{k})\,t_{ab}(\mathbf{k},\mathbf{k}')}{\mathbf{p}_{ab}^2 - \mathbf{k}'^2 + i\epsilon} \tag{16}$$

where μ is reduced mass and we define the intermediate-state relative momenta

$$\mathbf{k} = \frac{1}{A_P}\left(A_b\mathbf{k}_a - A_a\mathbf{k}_v\right) \tag{17}$$

and

$$\mathbf{k}' = \frac{1}{A_P}\left(A_b\mathbf{k}_a - A_a\mathbf{k}_b\right) \tag{18}$$

Following references 13 to 15, we use the separable potential model for t_{ab} such that equation (16) is reduced to

$$T_s^{\mathrm{FSI}} = \frac{2\pi}{V}\sqrt{K_s}\sqrt{Y_s}\,\Phi(\mathbf{R}_{ab})\frac{D\left(\mathbf{R}_{ab}, 2\frac{A_a}{A_P}\mathbf{R}_{\mathbf{Q}}\right)}{D(\mathbf{R}_{ab},0)}f_{bT}(\mathbf{R}_{\mathbf{Q}}) \tag{19}$$

where the dispersion integral is defined in reference 14 as

$$D(p,q) = \int d\mathbf{k}\frac{\Phi(\mathbf{k}+\mathbf{q}/2)\,(\alpha^2+k^2)\,\Phi(\mathbf{k})}{p^2-k^2+i\epsilon} \tag{20}$$

and α is related to the a-b separation energy ϵ_s through $\alpha^2 = -2\mu_{ab}\epsilon_s$. The dispersion integral is evaluated in analytic form for typical phenomenological forms of the overlap functions.

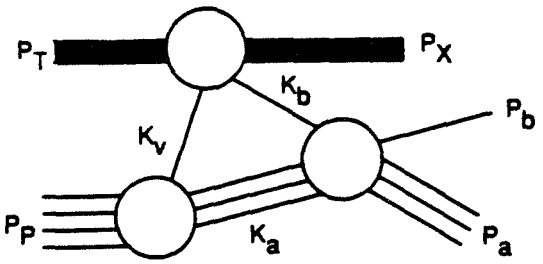

Figure 3. Spectator term with final-state interaction.

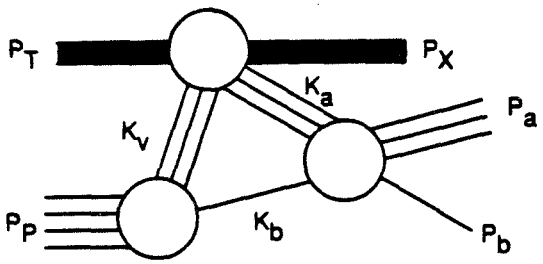

Figure 4. Participant term with final-state interaction.

We now define a distorted momentum distribution given by

$$\tilde{\Phi}(\mathbf{R}_a,\mathbf{R}_{ab}) = \Phi(\mathbf{R}_a) - \Phi(\mathbf{R}_{ab})\frac{D(\mathbf{R}_{ab}, 2\frac{A_a}{A_P}\mathbf{R}_{\mathbf{Q}})}{D(\mathbf{R}_{ab},0)} \tag{21}$$

and the distorted spectator term

$$\begin{aligned}\tilde{T}_s &= T_s + T_s^{\mathrm{FSI}} \\ &= \frac{-2\pi}{V}\sqrt{K_sY_s}\,\tilde{\Phi}(\mathbf{R}_a,\mathbf{R}_{ab})\,f_{bT}(\mathbf{Q})\end{aligned} \tag{22}$$

Similarly for the participant contribution

$$\begin{aligned}\tilde{T}_p &= T_p + T_p^{\mathrm{FSI}} \\ &= \frac{-2\pi}{V}\sqrt{K_pY_p}\,\tilde{\Phi}(\mathbf{R}_b,\mathbf{R}_{ab})\,f_{aT}(\mathbf{Q})\end{aligned} \tag{23}$$

Evaluation of these terms for model inputs is discussed subsequently. The pole model with FSI for the fragment momentum distribution is now written as in equation (14) with the distorted terms discussed above replacing the relative cluster momentum distributions.

Double-Scattering Corrections

The corrections to the pole diagrams for scattering by a second projectile fragment on the target are shown in figures 5 and 6. Figures 7 and 8 show further contributions from FSI between a and b. The contributions from the graphs in figures 7 and 8 are expected to be difficult to evaluate, since

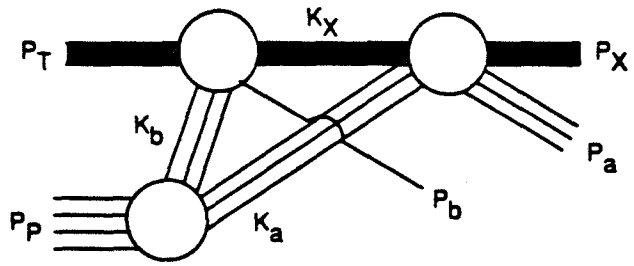

Figure 5. Rescattering correction for spectator term for projectile fragmentation.

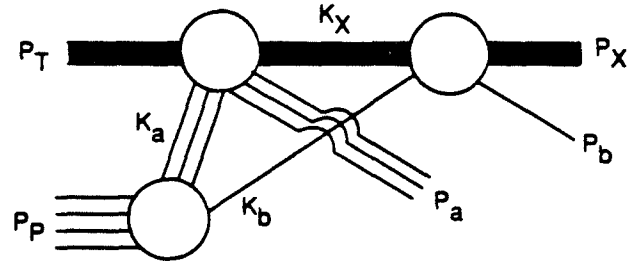

Figure 6. Rescattering correction for participant term for projectile fragmentation.

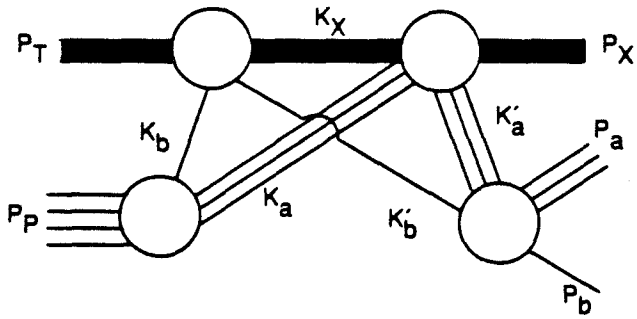

Figure 7. Rescattering correction for spectator term with final-state interaction.

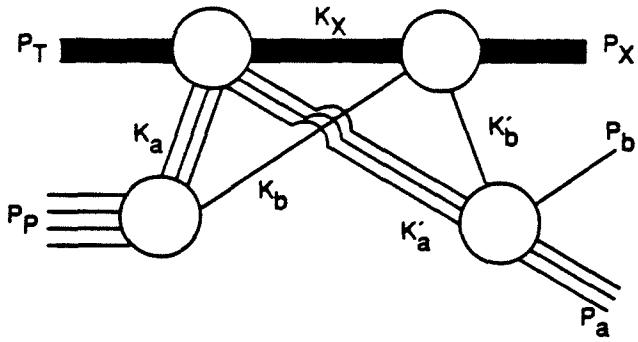

Figure 8. Rescattering correction for participant term with final-state interaction.

the complications of a three-body propagator cannot be avoided, even in the cluster model employed herein. The contributions from the double-scattering diagrams of figures 5 and 6 are estimated using the high-energy propagator derived in reference 9.

Define the relative momenta for figure 5 to be

$$\mathbf{p}_{aX} = \frac{1}{A_T + A_a}\left(A_a \mathbf{p}_X - A_T \mathbf{p}_a\right) \tag{24}$$

and

$$\mathbf{k}_{aX} = \frac{1}{A_T + A_a}\left(A_a \mathbf{k}_X - A_T \mathbf{k}_a\right) \tag{25}$$

and the momentum transfers to be

$$\mathbf{q}_1 = \mathbf{p}_T - \mathbf{k}_X \tag{26}$$

and

$$\mathbf{q}_2 = \mathbf{k}_X - \mathbf{p}_X \tag{27}$$

with

$$\mathbf{k}_{aX} = \mathbf{p}_{aX} + \mathbf{q}_2 \tag{28}$$

We write the double-scattering contribution to the transition matrix of figure 5 as

$$T_D^1 = \frac{V}{(2\pi)^3}\int d\mathbf{k}_{aX}\frac{2\mu_{aT}\, t_{bT}(\mathbf{q}_1)\,\phi(\mathbf{k}_{ab})\, t_{aT}(\mathbf{q}_2)}{\mathbf{p}_{aX}^2 - \mathbf{k}_{aX}^2 + i\epsilon} \tag{29}$$

Ignoring the noninvariance of the amplitudes on the right side of equation (29), we approximate this expression by

$$T_D^1 \approx \frac{1}{\pi V \mu_{bT}}\int d\mathbf{q}_2 \times \frac{f_{bT}(\mathbf{Q} - \mathbf{q}_2)\,\phi\left(\mathbf{p}_a - \frac{A_a}{A_P}\mathbf{p}_P - \mathbf{q}_2\right) f_{aT}(\mathbf{q}_2)}{-\mathbf{q}_2^2 - 2\mathbf{p}_{aX}\cdot\mathbf{q}_2 + i\epsilon} \tag{30}$$

Treating only the singularities of the propagator and using contour integration, we reduce equation (30) to

$$T_D^1 \cong \frac{4\pi i p_{aX}}{V\mu_{bT}}\int_0^\pi \sin\zeta\cos\zeta\, d\zeta\, f_{bT}(\mathbf{Q} - \mathbf{x}) \times \phi\left(\mathbf{p}_a - \frac{A_a}{A_P}\mathbf{p}_P - \mathbf{x}\right) f_{aT}(\mathbf{x}) \tag{31}$$

where

$$\mathbf{x} = -2p_{aX}\cos\zeta\,\hat{\mathbf{q}}_2 \tag{32}$$

and $\hat{\mathbf{q}}_2$ is a unit vector.

The singularity structure of the overlap function is ignored here, since only first estimates of the double-scattering corrections are considered. In a

similar manner, we find the double-scattering contribution to the transition matrix of figure 6:

$$T_D^2 \cong \frac{4\pi i p_{bX}}{V \mu_{aT}} \int_0^\pi \sin\zeta \cos\zeta \, d\zeta \, f_{aT}(\mathbf{Q} - \mathbf{y}) \times \phi\left(-\mathbf{p}_b + \frac{A_b}{A_P}\mathbf{p}_P + \mathbf{y}\right) f_{bT}(\mathbf{y}) \quad (33)$$

where

$$\mathbf{p}_{bX} = \frac{1}{A_T + A_b}(A_b \mathbf{p}_X - A_T \mathbf{p}_b) \quad (34)$$

and

$$\mathbf{y} = -2 p_{bX} \cos\zeta \, \hat{\mathbf{q}}_2 \quad (35)$$

The approximations to the double-scattering terms given by equations (31) and (33) are evaluated numerically using the inputs described subsequently.

Results and Discussion

We now apply our model to ^{3}He production from 1 GeV/A alpha particles scattering on ^{1}H targets. The treatment of the summation over target states for composite targets is not discussed in this report. General properties of the overlap functions for single nucleon knockout have been reported by Berggren (ref. 16). For the ^{3}He-n overlap, a sum of Yukawa terms is assumed to be

$$\Phi(\mathbf{p}) = \sum_{i=1}^{2} \frac{a_i}{p^2 + \alpha_i^2} \quad (36)$$

with $\alpha_1 = \alpha$, and the normalization is

$$\int |\Phi(\mathbf{p})|^2 d\mathbf{p} = |Z|^2 \quad (37)$$

where $|Z|^2$ is the total probability of finding the two fragments in the projectile. Note from reference 16 that $|Z|^2 < 1$. For ^{3}He-n, $\alpha_1 = 0.846$ fm^{-1} and from reference 15, $\alpha_2 = 1.12$ fm^{-1}, $a_1 = 1$, and $a_2 = -1$. For $|Z|^2$, we use 0.9. Values in the literature for $|Z|^2$ range from 0.6 to 0.9 depending on the method of determination. The dispersion integral is then found to be

$$D(p,q) = \frac{4\pi}{q} \sum_{i,j} a_i a_j \left\{ \tan^{-1}\left(\frac{q/2}{\alpha_i^2 - \alpha_j^2}\right) + \frac{1}{2}\left(\frac{p^2 + \alpha_1^2}{p^2 + \alpha_j^2}\right)\left[\tan^{-1}\left(\frac{\alpha_i q}{\alpha_i^2 + p^2 - \frac{q^2}{4}}\right)\right] + \frac{i}{2}\ln\left[\frac{\alpha_i^2 + (p + q/2)^2}{\alpha_j^2 + (p - q/2)^2}\right]\right\} \quad (38)$$

with

$$D(p,0) = 4\pi \sum_{i,j} a_i a_j \frac{1}{\alpha_i + \alpha_j}\left[1 + \frac{\alpha_1^2 + p^2}{(\alpha_i - ip)(\alpha_j - ip)}\right] \quad (39)$$

We note that solutions of this dispersion integral differ in references 13 through 15.

At high energies we use diffractive approximations to the a-T and b-T scattering amplitudes. For neutron-proton scattering, this is

$$f_{bT}(\mathbf{q}) = \frac{\sigma(\rho + i)k_{NN}}{4\pi} e^{-1/2Bq^2} \quad (40)$$

with the NN scattering parameters listed in table 1. For ^{3}He-proton scattering, we use the Glauber approximation result (ref. 17):

$$f_{aT}(\mathbf{q}) = \sum_{j=1}^{3} \binom{3}{j} (-1)^j \left[\frac{\sigma(1 - i\rho)}{2\pi(R^2 + 2B)}\right]^{j-1} \times \frac{\sigma(1 - i\rho)}{2j} e^{-w_j q^2} \quad (41)$$

where

$$w_j = \frac{6B + (3 - j)R^2}{12j} \quad (42)$$

with the radius $R = 1.51$ fm.

Table 1. NN Parameters at 1 GeV

	σ, mb	B, fm^2	ρ
np	43.7	0.26	-0.26
pp	47.6	.24	-.09

Results for the double-differential cross section at several laboratory angles are shown in figures 9 to 11. The experimental data of reference 18 are shown in figures 10 and 11. The dashed line is the spectator term, equation (22); the dotted line the participant term, equation (23); the dash-dot line the coherent sum of the spectator and participant terms; and the solid line the coherent sum of participant-spectator terms and the double-scattering terms of equations (31) and (33). Single-scattering results include FSI. The double-scattering terms are observed to contribute in a nonnegligible way at 0°. This makes a simple extraction using the distorted-wave-born-approximation of the overlap function from small angle data, as was suggested in reference 19, invalid. The double-scattering approximations of equations (31) and (33) do not neglect the longitudinal

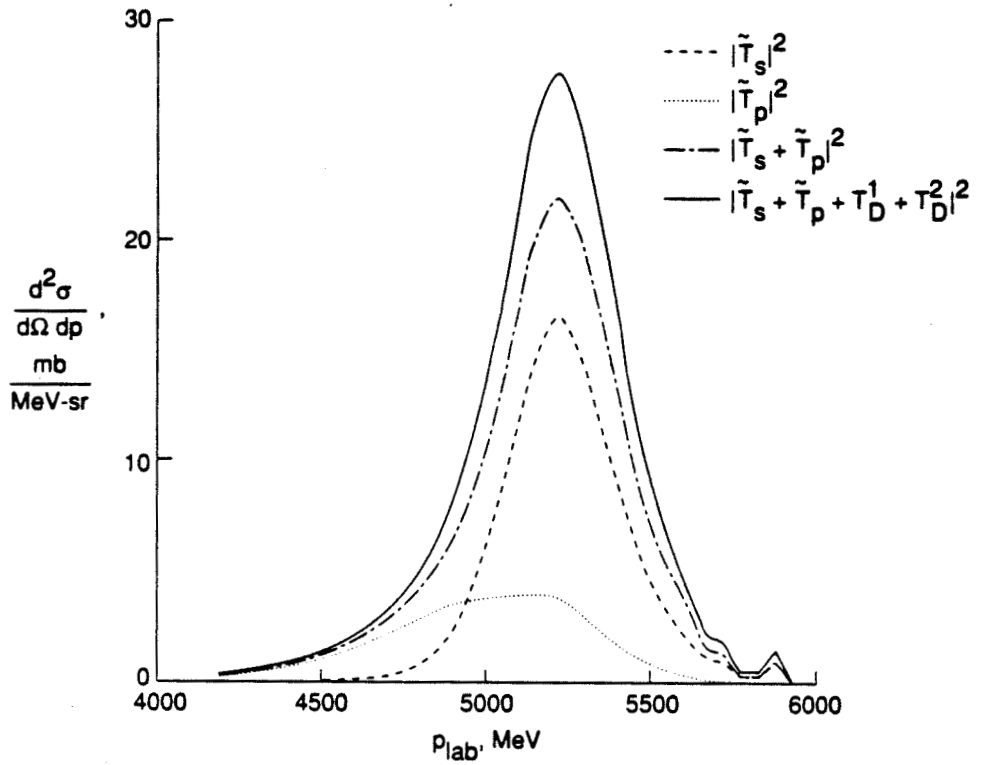

Figure 9. Double-differential cross section at $\theta_{lab} = 0°$ for $\alpha + {}^1H \rightarrow {}^3He$ at 1.02 GeV/A.

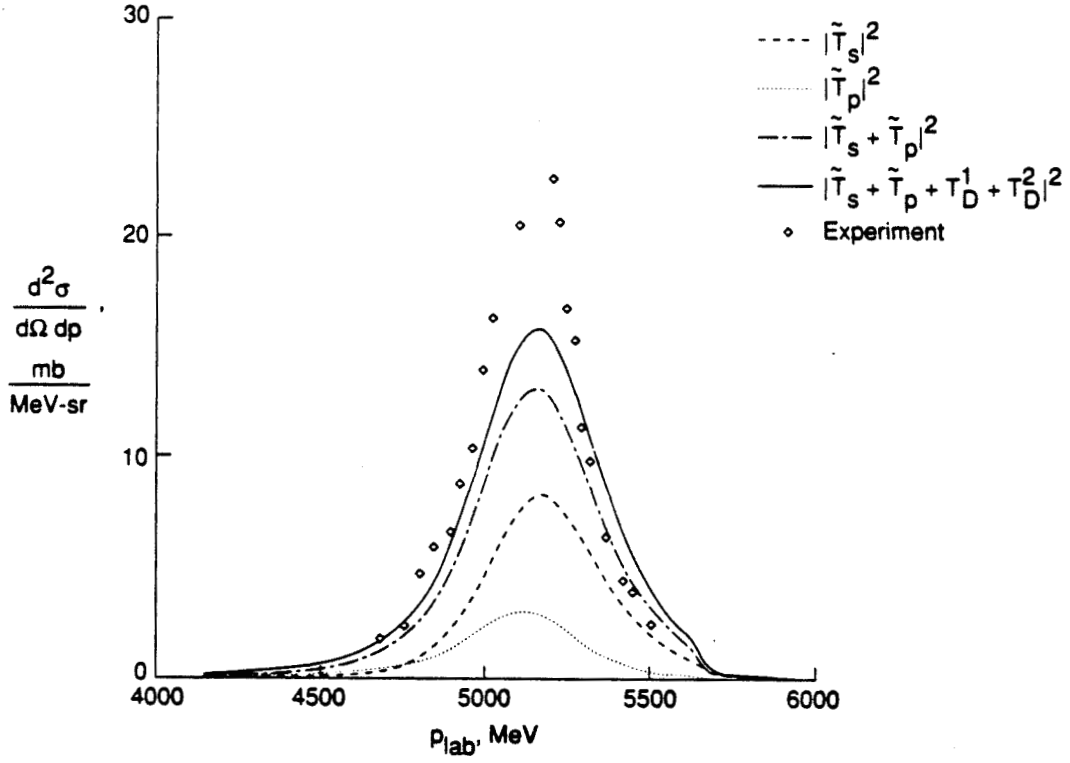

Figure 10. Double-differential cross section at $\theta_{lab} = 0.65°$ for $\alpha + {}^1H \rightarrow {}^3He$ at 1.02 GeV/A. Experimental data from reference 18.

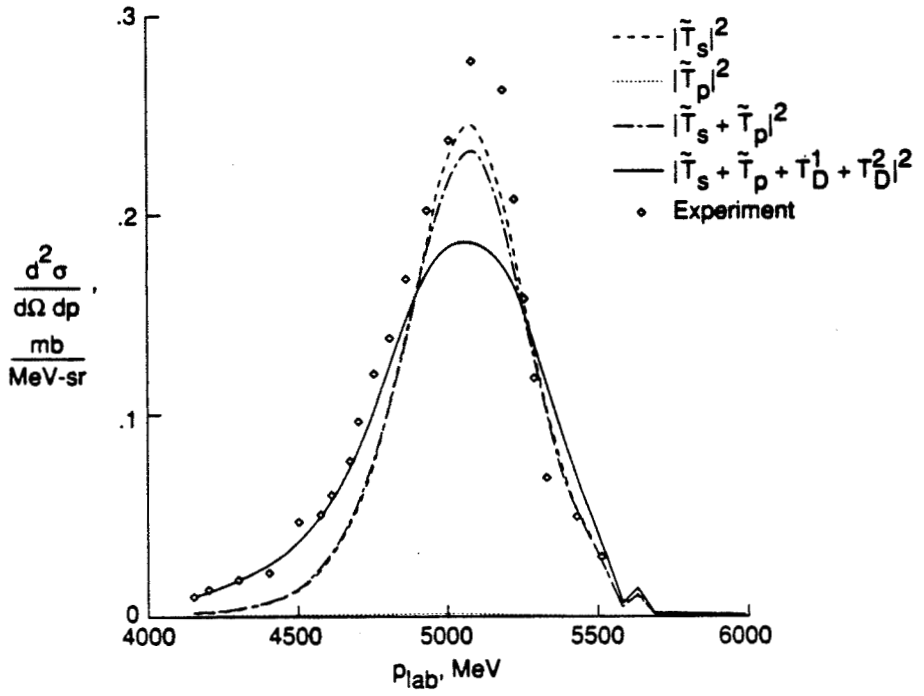

Figure 11. Double-differential cross section at $\theta_{lab} = 4.07°$ for $\alpha + {}^1H \rightarrow {}^3He$ at 1.02 GeV/A. Experimental data from reference 18.

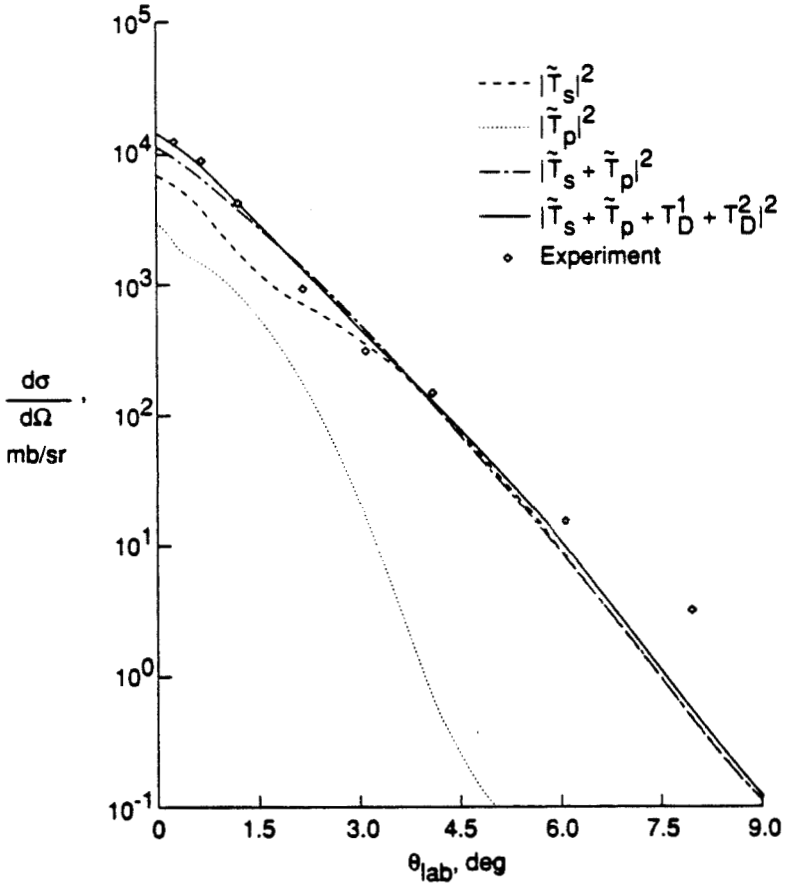

Figure 12. Angular distribution for $\alpha + {}^1H \rightarrow {}^3He$ at 1.02 GeV/A. Experimental data from reference 18.

momentum transfer and therefore lead to a good prediction of the position of the peak in the cross section with increasing angle (as seen in fig. 11 at $\theta_{lab} = 4.07°$). We note that in the Glauber model of alpha-particle breakup of reference 20, the downshift in the momentum distribution must be treated in an ad hoc manner.

Interference effects between the various scattering terms are found in all results. The spectator and participant terms interfere constructively for all angles considered. The energy-dependent parameters ρ_{np} and ρ_{pp} determine the interference effects to a large degree. Prescription for the on-shell fragment-target interaction energy could then be used to study the interference effects in more detail. The singularity structure of the overlap function and FSI effects on the double-scattering terms need to be studied in order to make conclusions about the magnitude and interference contributions of the double-scattering terms.

In figure 12, the angular distribution for ^{3}He production is shown in the laboratory system. The importance of the participant and double-scattering terms is seen at all angles. We expect that the small differences between our calculations and the data at the smallest angles between 1.5° and 4.5° could be reduced if the phases between the various terms were treated correctly. We underestimate the data at the largest angles, which may be because of contributions not treated here, such as intermediate-state deuteron production, charge exchange, and pion production. Results for the total production cross section are given in table 2. Good agreement is found with experiment when all scattering terms are included.

Table 2. ^{3}He Production Cross Section in α + ^{1}H Reaction at 1 GeV/A

	σ, mb
Experiment (ref. 18)	24.1 ± 1.9
$\lvert\widetilde{T}_s\rvert^2$	12.2
$\lvert\widetilde{T}_p\rvert^2$	3.3
$\lvert\widetilde{T}_s + \widetilde{T}_p\rvert^2$	20.7
$\lvert\widetilde{T}_s + \widetilde{T}_p + T_D^1 + T_D^2\rvert^2$	22.7

Conclusions

A first approximation to the double-scattering correction to the participant-spectator model of fragmentation was found to be important in describing alpha-particle breakup. Interference effects between single- and double-scattering graphs were found to determine the overall magnitude and shape of the double- and single-differential production cross sections. The prescription for the on-shell projectile cluster-target amplitude energy should be considered to study the interference effects in more detail. The singularity structure of the projectile dissociation overlap function should be considered to improve the results given here. Good agreement with experiment for the total production cross section was found for the single projectile energy considered. Extensions of this work are expected to contribute to the development of a nuclear cross section data base for galactic cosmic ray transport codes.

NASA Langley Research Center
Hampton, VA 23665-5225
March 12, 1991

References

1. Curtis, Stanley B.: Effects of Low and High LET Radiation on Neoplastic Transformation in Cells and the Importance of Single Track Effects in Space. *Terrestrial Space Radiation and Its Biological Effects,* Percival D. McCormack, Charles E. Swenberg, and Horst Bücker, eds., Plenum Press, 1988, pp. 153–161.

2. Cucinotta, Francis A.; Katz, Robert; Wilson, John W.; Townsend, Lawrence W.; Nealy, John E.; and Shinn, Judy L.: *Cellular Track Model of Biological Damage to Mammalian Cell Cultures From Galactic Cosmic Rays.* NASA TP-3055, 1991.

3. Wilson, J. W.; Townsend, L. W.; and Badavi, F. F.: Galactic HZE Propagation Through the Earth's Atmosphere. *Radiat. Res.,* vol. 109, no. 2, Feb. 1987, pp. 173–183.

4. Townsend, L. W.; and Wilson, J. W.: An Evaluation of Energy-Independent Heavy Ion Transport Coefficient Approximations. *Health Phys.,* vol. 54, no. 4, Apr. 1988, pp. 409–412.

5. Goldhaber, Alfred S.; and Heckman, Harry H.: High Energy Interactions of Nuclei. *Annual Review of Nuclear and Particle Science, Volume 28,* J. D. Jackson, Harry E. Gove, and Roy F. Schwitters, eds., Annual Reviews Inc., 1978, pp. 161–205.

6. Cucinotta, Francis A.: Theory of Alpha-Nucleus Collisions at High Energies. Ph.D. Thesis, Old Dominion Univ., 1988.

7. Cucinotta, F. A.; Townsend, L. W.; and Norbury, J. W.: Corrections to Pole Diagrams in ^{4}He Fragmentation at 1 GeV/A. *Bull. American Phys. Soc.,* vol. 34, no. 4, Apr. 1989, p. 1138.

8. Shapiro, I. S.: Some Problems in the Theory of Nuclear Reactions at High Energies. *Sov. Phys. Uspekhi,* vol. 10, no. 4, Jan.–Feb. 1968, pp. 515–535.

9. Wilson, John W.: Composite Particle Reaction Theory. Ph.D. Diss., College of William and Mary in Virginia, June 1975.

10. Thies, Michael: Quantum Theory of Inelastic Multiple Scattering in Phase Space. *Ann. Phys. (NY)*, vol. 123, no. 2, Dec. 1979, pp. 411–441.

11. Norbury, John W.; Townsend, Lawrence W.; and Deutchman, Philip A.: *A T-Matrix Theory of Galactic Heavy-Ion Fragmentation*. NASA TP-2363, 1985.

12. Shapiro, I. S.; Kolybasov, V. M.; and Augst, G. R.: Treiman-Yang Criterion for Direct Nuclear Reactions. *Nucl. Phys.*, vol. 61, no. 3, Jan. 1965, pp. 353–367.

13. Kolybasov, V. M.; and Ksenzov, V. G.: Role of Secondary Rescattering in the Reaction $D(\pi^-, \pi^- p)n$ at High Energies. *Sov. J. Nucl. Phys.*, vol. 22, no. 4, July–Dec. 1975, pp. 372–378.

14. Aladashvili, B. S.; Germond, J. F.; Glagolev, V. V.; Nioradze, M. S.; Siemiarczuk, T.; Stepaniak, J.; Streltsov, V. N.; Wilkin, C.; and Zielinski, P.: Final-State Interaction in the High-Energy Proton-Deuteron Break-Up Reaction. *J. Phys. G.*, vol. 3, no. 1, 1977, pp. 7–20.

15. Chevallier, M.; Fäldt, G.; Hallgren, A.; Jonsson, S.; Badelek, B.; Burq, J. P.; Chemarin, M.; Dahlgren, S.; Grafström, P.; Hagberg, E.; Ille, B.; Kullander, S.; Lambert, M.; Nassalski, J.; Querrou, M.; and Vazeille, F.: Quasi-Elastic Pion-Helium Scattering at 5 GeV/c. *Nucl. Phys.*, vol. A343, no. 3, July 21, 1980, pp. 449–467.

16. Berggren, Tore: Overlap Integrals and Single-Particle Wave Functions in Direct Interaction Theories. *Nucl. Phys.*, vol. 72, no. 2, Oct. 1965, pp. 337–351.

17. Glauber, R. J.; and Matthiae, G.: High-Energy Scattering of Protons by Nuclei. *Nucl. Phys.*, vol. B21, no. 1, Aug. 1, 1970, pp. 135–157.

18. Bizard, G.; Le Brun, C.; Berger, J.; Duflo, J.; Goldzahl, L.; Plouin, F.; Oostens, J.; Van Den Bossche, M.; Vu Hai, L.; Fabbri, F. L.; Picozza, P.; and Satta, L.: ^{3}He Production in ^{4}He Fragmentation on Protons at 6.85 GeV/c. *Nucl. Phys.*, vol. A285, no. 3, Aug. 1, 1977, pp. 461–468.

19. Fujita, T.; and Hüfner, J.: Momentum Distributons After Fragmentation in Nucleus-Nucleus Collisions at High Energy. *Nucl. Phys.*, vol. A343, no. 3, July 21, 1980, pp. 493–510.

20. Bizard, G.; and Tekou, A.: Interpretation of the ^{4}He Dissociation at High Energy. *Nuovo Cimento*, vol. 51A, no. 1, May 1, 1979, pp. 114–130.

NASA
National Aeronautics and Space Administration

Report Documentation Page

1. Report No.	2. Government Accession No.	3. Recipient's Catalog No.
NASA TM-4262		

4. Title and Subtitle	5. Report Date
Corrections to the Participant-Spectator Model of High-Energy Alpha-Particle Fragmentation	May 1991
	6. Performing Organization Code

7. Author(s)	8. Performing Organization Report No.
Francis A. Cucinotta, Lawrence W. Townsend, John W. Wilson, and John W. Norbury	L-16883

9. Performing Organization Name and Address	10. Work Unit No.
NASA Langley Research Center Hampton, VA 23665-5225	199-04-16-11
	11. Contract or Grant No.

12. Sponsoring Agency Name and Address	13. Type of Report and Period Covered
National Aeronautics and Space Administration Washington, DC 20546-0001	Technical Memorandum
	14. Sponsoring Agency Code

15. Supplementary Notes

Francis A. Cucinotta, Lawrence W. Townsend, and John W. Wilson: Langley Research Center, Hampton, Virginia.
John W. Norbury: Rider College, Lawrenceville, New Jersey.

16. Abstract

The participant-spectator model of nuclear fragmentation is described in terms of pole graphs from direct reaction theory. Corrections to the model for more than one projectile fragment scattering on the target are considered using a triangle graph model. Results for alpha-particle fragmentation at 1 GeV/A indicate that corrections to the participant-spectator model are significant, as indicated by the large interference effects found between the pole and triangle graph terms in the double- and single-differential cross sections.

17. Key Words (Suggested by Author(s))	18. Distribution Statement
Nuclear fragmentation Inclusive momentum distribution Participant-spectator models	Unclassified—Unlimited Subject Category 73

19. Security Classif. (of this report)	20. Security Classif. (of this page)	21. No. of Pages	22. Price
Unclassified	Unclassified	12	A03

NASA FORM 1626 OCT 86

NASA-Langley, 1991

For sale by the National Technical Information Service, Springfield, Virginia 22161-2171

NASA Reference Publication 1257

1991

Transport Methods and Interactions for Space Radiations

John W. Wilson and Lawrence W. Townsend
Langley Research Center
Hampton, Virginia

Walter Schimmerling
Lawrence Berkeley Laboratory
University of California
Berkeley, California

Govind S. Khandelwal and Ferdous Khan
Old Dominion University
Norfolk, Virginia

John E. Nealy, Francis A. Cucinotta,
Lisa C. Simonsen, and Judy L. Shinn
Langley Research Center
Hampton, Virginia

John W. Norbury
Rider College
Lawrenceville, New Jersey

National Aeronautics and Space Administration
Office of Management
Scientific and Technical Information Program

Contents

AN INTRODUCTION TO USING THE FORTRAN PROGRAMS PROVIDED WITH

COMPUTATIONAL NUCLEAR PHYSICS 1
NUCLEAR STRUCTURE
K. LANGANKE, J.A. MARUHN AND S.E. KOONIN (EDS.)
SPRINGER-VARLAG BERLIN GERMANY 1991

Matthew A. Boytos and John W. Norbury
Department of Physics
Rider College
Lawrenceville NJ 08648

INTRODUCTION

The authors of Computational Nuclear Physics have provided along with their text an excellent set of well-written, ready-to-run Fortran programs that should prove useful in many disciplines of theoretical nuclear physics.

The purpose of this document is to provide, simply, a synopsis of the programs and their use for those who wish to begin working on the computer immediately. We will attempt to provide some background on each program before going into the specific details of how to get the program running and make its results useful.

A separate section is devoted to each chapter (and program set) in the text. Within each section, there are five headings. A brief description of what will be found in each follows.

Abstract — A short summary of what the program(s) will do, and brief instructions on their use.
Files — A listing of the files provided by the authors and their content and use.
Compiling, linking and running — A comprehensive set of instructions giving the specifics on installing the code(s).
Obtaining results — A section of hints, notes and procedures to help users make effective use of the code(s).
Tutorial — A detailed, step-by-step procedure for installing the code and running an example calculation.

This guide is not meant to be a replacement for the text, and thus we will not present information (such as tables, charts) that is present in the text except where necessary.

All on the procedures given are general with the exception of the tutorial which is specific to VAX/VMS. The particular examples we give were checked for accuracy on a VAX 4000 using VAX/VMS 5.3 and VAX Fortran.

When we refer to a specific file path, the characters ' ... ' mean the file specification necessary to reach the level where the specific files we refer to have been installed in your system.

A suggestion: It is useful to have a separate subdirectory for each chapter in the text. An easy way to do this is with a system something like this:

chapter 1 [...KOONIN.CHAPTER_1]

and so on for each of the 10 chapters. This will simplify keeping track of the many files that most of the programs use. Also , keep in mind that as a package, the programs require at least 10.0 MBytes disk space to be used effectively. Be sure that this amount is available before beginning to avoid delays. We will point out when a particular program uses either large amounts of disk space or cpu time. Finally we have ensured that all programs run without errors on a Vax.

CHAPTER 1

THE NUCLEAR SHELL MODEL

• ABSTRACT

The codes consist of four separate programs. The first two, FDSMCFP and PD are used to calculate coefficients needed by the two main codes, FDSM and FDTR. FDSMCFP and PD need only be run one time and as long as the data files are retained, one need only generate an appropriate input file and run the program (FDSM or FDTR) of interest.

• FILES

FDSMCFP.FOR - This is the Fortran code for the segment that generates the coefficients of fractional parentage (CFPs).

PD.FOR - Fortran code to generate the Hamiltonian operator matrix elements

LIB.FOR - A Fortran library of often used subroutines

FDU0.FOR - Part 1 of the actual shell model code

FDTR.FOR - Part 2 of the shell model code (computes transitions)

FDSM.INP - A sample input file

FDTR.INP - A sample input file for transition calculations

• COMPILING, LINKING AND RUNNING

Note: In order to use the programs in this chapter, 5.0 Mbytes of disk space are required. The IMSL Fortran library is also required.

Begin by compiling the above five Fortran source codes separately. Next, link FDSM.OBJ, FDSMCFP.OBJ, PD.OBJ and FDTR.OBJ to LIB.OBJ and the IMSL library. (They should *not* be linked to each other. See the tutorial.)

The first time these programs are used, FDSMCFP and PD will need to be run. These take only a few minutes of cpu time, with the exception of FDSMCFP's second run, which will take about 120 minutes of cpu time to complete.

First, run FDSMCFP giving it 'SO8' input in response to 'symmetry' prompt. Then, run it again (in batch mode) using 'SP6' input, which will, as stated before, require about 2 hours of cpu time. Then, when the job has finished, run PD twice, once for 'SO8' and once for 'SP6'. These runs will produce several output files. Keep these files as they are required for all subsequent runs of FDU0 and FDTR.

The programs FDU0 and FDTR take input from files named FDU0.INP and FDTR.INP. All input is done in one block format. Output is in the form of a comprehensive output file named FDTR.OUT or FDU0.OUT.

• OBTAINING RESULTS / NOTES

As stated previously, all input and output to/from the FDU0 and FDTR codes is via data files using a text format. The input file is in block form. Note that the dollar sign must be in the second column or else an input conversion error will occur.

An effective way to keep track of files is to write a separate input file for each problem you will be solving, then copy this file to either FDU0.INP or FDSM.INP and execute the program. When finished, copy the output file to a separate output file for each project.

A comprehensive description of the input parameters is provided in the text. The author provides a sample input data file which can be used to verify the programs output and to serve as the basis for experimenting with the parameters.

• **TUTORIAL**

Compile the five Fortran source code files.

```
$ FORTRAN FDSMCFP.FOR
$ FORTRAN PD.FOR
$ FORTRAN LIB.FOR
$ FORTRAN FDU0.FOR
$ FORTRAN FDTR.FOR
```

Each of the four program object files is now linked to the library object file as well as the IMSL library. (They should *not* be linked to each other.)

```
$ LINK FDSMCFP.OBJ, LIB.OBJ, IMSL/LIBRARY
$ LINK PD.OBJ, LIB.OBJ, IMSL/LIBRARY
$ LINK FDU0.OBJ, LIB.OBJ, IMSL/LIBRARY
$ LINK FDTR.OBJ, LIB.OBJ, IMSL/LIBRARY
```

The FDSMCFP program is run first to generate a file of coefficients. Run it first for 'SO8' symmetry, then as a batch job for the 'SP6' symmetry as this will take about 2 hours cpu time.

```
$ RUN FDSMCFP.EXE
SO8
```

Note that SO8 must be entered in UPPERCASE letters. This will create 4 new files named SO8P.DAT, SO8JSIZE.DAT,SO8CFP.DAT and SO8JSIZE.TAB.

A typical batch file would be

```
$ RUN FDSMCFP.EXE
SP6
```

Note that SP6 must be entered in UPPERCASE letters.

This will create 4 new files named SP6P.DAT, SP6JSIZE.DAT,SP6CFP.DAT and SP6JSIZE.TAB. These are needed as input for FDU0 and FDTR.

When the job has finished running, run PD for both 'SO8' and 'SP6' symmetries.

To run the main codes using the sample input file, simply type

```
$ RUN FDU0.EXE
```

and then to compute the transitions

```
$ RUN FDTR.EXE
```

The output will be written to files named FDSM.OUT and FDTR.OUT in a text format.

CHAPTER 2

THE SKYRME-HARTREE-FOCK MODEL OF THE NUCLEAR GROUND STATE

• ABSTRACT

The Skyrme-Hartree-Fock method is implemented in a single Fortran program SKHAFO. The code uses an iterative solution. A sample input file for the 17 [O] nucleus is provided.

• FILES

SKHAFO.FOR - Fortran source code for the Hartree-Fock analysis
FOR005.DAT - Sample input file

• COMPILING, LINKING AND RUNNING

There are no special requirements; simply compile the single source code file, link the object file and run the program.

• OBTAINING RESULTS / NOTES

All input and output is done using files. The input file must be named FOR005.DAT. Output is written to files named FOR006.DAT and FOR011.DAT. As with several of the programs in the text, a convenient method of processing data sets is to rename input files to FOR005.DAT, run the program and then rename the output to another file for safe keeping.

Comprehensive descriptions of the input parameters are provided in the text.

Do not be concerned with what may be interpreted as error messages in the output file that refer to for the PAIR routine, indicating termination of the calculation without convergence in the first few iterations. There is no reason to be concerned about this as the PAIR routine converges well in the later iterations.

• TUTORIAL

The first steps are to compile and link the program.

```
$ FORTRAN SKHAFO.FOR
$ LINK SKHAFO.FOR
```

Since a sample input file named FOR005.DAT is provided, simply run the program by typing $ RUN SKHAFO.EXE

The output is written to two files, FOR006.DAT and FOR011.DAT.

CHAPTER 3

THE CRANKED NILSSON MODEL

• ABSTRACT

The main code for this chapter is NICRA.

• FILES

NICRA.FOR - The Nilsson Cranker Fortran source code
APPEN.TEX - Text file giving example output and hints
INPUT1.DAT INPUT2.DAT - Two example input files for the study of 160 [Yb]
NICRAPAR.FOR - Include file of parameters
NICRAINC.FOR - Include file of common block statements

• COMPILING, LINKING AND RUNNING

While the basic installation procedure is simple enough, there a few fine points that may need attention.

The first of these is the file NICRAPAR.FOR. This file is included in the code via an include statement to the compiler and determines the dimension of several variables. The value here to be concerned about is the maximum number of shells. The default value is set at 6 shells. For a different number of shells, see the table below.

Before you set the number of shells to the maximum, keep in mind the size of the executable module that results!

The value for the variable MAXDIM to change in the file is shown in the table.

MAX N	MAX DIM	MODULE SIZE
4	22	0.1 MBytes
5	34	0.2
6	50	0.3
7	70	0.4
8	95	0.6
9	125	0.9
10	161	1.5
11	203	2.2
12	252	3.2

Secondly, if your system is not a VAX you will need to rewrite the include statements in NICRA.FOR.

• OBTAINING RESULTS / NOTES

As the program is written. NICRA expects to receive input from the terminal. A much more effective method is to run the program as a batch job, inserting the batch commands into the input file. Output is written to a text file.

The best method to use to run the program for different data set is to write a small batch file, then add it to you data sets before submitting the job. Processing takes about 2-15 minutes of cpu time depending on the number of shells and other parameters.

The amount and type of output the program produces can be controlled by changing values in the input file of the variables IN_LEV and LEV_PRINT.

A listing of input parameters as well as a sample input file appear in the text for reference.

The authors provide two examples in the files INPUT1.DAT and INPUT2.DAT. The first example shows how to construct a single particle diagram that is a plot of single orbitals as a function of angular speed of rotation. About 5 minutes of cpu time is required for this calculation using the values for LEV_PRINT in INPUT1.DAT file. The plot in Fig. 3.3 in the text can be produced simply enough by making a copy of the output file, formatting the necessary data correctly with labels and commands for TELL-A-GRAF or another similar graphics package.

The second example is an investigation of the triaxiality of the nucleus of 160 [Yb] as a function of spin. This run takes approximately 25 minutes of cpu time to complete. The graphs appearing in Fig. 3.4 can be produced in the same manner as the previous example.

• TUTORIAL

In this example we will run the program using the default number of shells, MAXN=6. The instructions to use more or fewer shells are given above. First, set the default directory to chapter 3 and compile the Fortran file NICRA.FOR. Then link the resulting object file. There is no need to worry about including the files NICRAPAR.FOR and NICRAINC.FOR as this is done automatically for VAX systems via include statements in the main code.

```
$ FORTRAN NICRA.FOR
$ LINK NICRA.OBJ
```

Note that the other codes should *not* be compiled because they are done via an INCLUDE statement as mentioned above.

Because the programs need a large amount of input data entered, it is best to run them as a batch job with the command $ RUN NICRA placed at the top of INPUT1.DAT. Then change its name say to BAT.COM and submit it as a batch job.

The second example can be run in the same way as the first. It is a good idea to use a different set of files for each run.

CHAPTER 4

THE RANDOM-PHASE-APPROXIMATION FOR COLLECTIVE EXCITATIONS

• ABSTRACT

The main code for this chapter is RPA.

• FILES

RPA.FOR - Fortran source code for the program

• COMPILING, LINKING AND RUNNING

This is most likely the easiest to use program in the text. Simply compile it, link it and run it. Input is read from the keyboard, output goes to the terminal.

• OBTAINING RESULTS / NOTES

When the program has been started, it waits for input. Simply type the input data on you terminal using the format given in table 4.1 in the text. The output will appear on the terminal also. The session can be captured for later review/analysis of output by using set host to record in a log file.

• TUTORIAL

Set the default directory to chapter 4, compile and link the program RPA.

```
$ FORTRAN RPA.FOR
$ LINK RPA.OBJ
```

Then start the program and input the parameters. The values shown are for the example of 16 [O] given by the author.

```
$ RUN RPA
0.25,50
16,8
1,3,1,0
-1,0,0,0
10,0.5
-1100,15000,0.5,0.93
1,0,40,1,1
0
```

CHAPTER 5

THE PROGRAM PACKAGE PHINT FOR IBA CALCULATIONS

• ABSTRACT

In the IBA model two different bosons are considered: the s- and d-boson. The program PCIBAXW calculates excitation energies and wave functions; PCIBAEM calculates electromagnetic transitions; CFPGEN is the code to generate coefficients of fractional parentage (CFPs).

• FILES

PCIBAXW.FOR - Main program and some subroutines in Fortran for calculation excitation energies and wave functions

PCIBAEM.FOR - Electromagnetic transition matrix elements and probabilities main code

CFPGEN.FOR - Main Fortran code for generating CFP file

PCIBALIB.FOR - Library of subroutines commonly used by codes

ANGMOM.FOR - Routines for calculating angular-momentum recoupling brackets

DIAG.FOR - Routine for the diagonalization of a real symmetric matrix

PCIBAEM.OUT - Sample output files PCIBAXW.OUT

• COMPILING, LINKING AND RUNNING

The six Fortran source files, PCIBAXW.FOR, PCIBAEM.FOR, CFPGEN.FOR, PCIBALIB.FOR, ANGMOM.FOR and DIAG.FOR, should first be compiled separately resulting in six object files. Next link the object files as shown:

PCIBAXW.OBJ to DIAG.OBJ, PCIBALIB.OBJ and ANGMOM.OBJ

PCIBAEM.OBJ to PCIBALIB.OBJ and ANGMOM.OBJ

CFPGEN.OBJ to ANGMOM.OBJ

At this point the result should be three executable files.

• OBTAINING RESULTS / NOTES

All three programs are set up to accept input from the terminal and write their output to a file. The author of the code has provided full prompting for each input data item, making the programs easy to use. A table describing the input parameters is given in the text.

Program output is written to a file with the name of the program followed by .OUT . Before running the two main programs, run CFPGEN to create the file PHINT.CFP. For applications, run PCIBAXW to generate spectra followed by PCIBAEM to generate transitions rates. The authors provide sample output files.

Since output is written to the same file, the scheme of renaming the output file will be necessary to save results for future use.

How to calculate for a single nucleus:

1. Determine the number of bosons. The number of bosons is equal to the number of fermion pairs outside a closed shell. As an example, take 104 46 [Pd] 58. Here,

Neutrons: -4 fermions +2 bosons

Protons : +8 fermions +4 bosons

Total : +6 bosons

2. Determine the strategy: which limiting case? For a more rotational-like spectrum it is better to use multi-pole operators while for a vibrational case the appropriate method is not to use the multipoles but to

define the Hamiltonian in terms of HBAR, C, F and G.

3. Fit the parameters in the Hamiltonian Make a first guess of the parameters using the analytic formula given in the text.

4. You are now ready to run PCIBAEM. Several recipes for these runs are given in the text.

• **TUTORIAL**

Begin by compiling the six Fortran source code files.

```
$ FORTRAN PCIBAXW.FOR
$ FORTRAN PCIBAEM.FOR
$ FORTRAN CFPGEN.FOR
$ FORTRAN PCIBALIB.FOR
$ FORTRAN ANGMOM.FOR
$ FORTRAN DIAG.FOR
```

After the six object files have been generated, link the files as shown here.

```
$ LINK PCIBAXW.OBJ, DIAG.OBJ, PCIBALIB.OBJ, ANGMOM.OBJ
$ LINK PCIBAEM.OBJ, PCIBALIB.OBJ, ANGMOM.OBJ
$ LINK CFPGEN.OBJ, ANGMOM.OBJ
```

Next, you will need to run CFPGEN to create the file PHINT.CFP

```
$ RUN CFPGEN.EXE
```

In this last section, a sample input for PCIBAXW and PCIBAEM is shown. The programs are completely self-prompting and therefore easy to use. Only the responses are shown. These examples can be found on pp93-97 of the text.

EXAMPLE 1 : USING PCIBAXW
[R] means press RETURN or ENTER

```
$ RUN PCIBAXW.EXE
N [R]
7 [R]
Y [R]
0.5 [R]
[R]
-0.1 [R]
[R]
[R]
[R]
[R]
[R]
[R]
[R]
Y [R]
4 [R]
```

EXAMPLE 2 : USING PCIBAEM

In this example note that E2 must be entered in UPPERCASE letters.

```
$ RUN PCIBAEM.EXE
E2 [R]
[R]
2 [R]
1 [R]
0 [R]
```

-2 [R]
1 [R]
0 [R]
100 [R]
S [R]

Note: Pressing return [R] in response to a prompt instructs the program to use the default value for that parameter (see the text for the default values).

CHAPTER 6

NUMERICAL APPLICATIONS OF THE GEOMETRIC COLLECTIVE MODEL

• ABSTRACT

The main code for this chapter is GCM.

• FILES

GCM.FOR - Fortran source file for main program

ANGP.DAT - Data file provided that contains the parameters for the Hamiltonian

ANGQ.DAT - Data file provided that contains corresponding values of matrix elements for quadrupole operator.

INPUT.DAT - Sample input file for calculations with 186 [Os]

PARA.DAT - Parameters data file of Hamiltonian

• COMPILING, LINKING AND RUNNING

To run the GCM code, the IMSL Fortran library is required.

Compiling and linking the code is fairly straightforward. There is one source file GCM.FOR which should be compiled and the object file linked to the IMSL library. The program is then ready to use.

• OBTAINING RESULTS / NOTES

The program expects to read the files ANGP.DAT and ANGQ.DAT from units 20 and 21. Thus, you should copy these files as shown below:

copy ANGP.DAT to FOR020.DAT copy ANGQ.DAT to FOR021.DAT

As the example is set up, the code expects to read Hamiltonian parameters from unit 40. These parameters, which for the example are provided in the file PARA.DAT, can be read or calculated depending on the value of the variable IFPARA in the first line of the input file. To use the example as it stands, copy PARA.DAT to FOR040.DAT.

The program expects to read input from the terminal, and thus it is suggested to run the program as a batch job using the input from a file to avoid typing errors since the program doesn't provide much in the way of error correction. Create a batch file to run the program, then append the given input file to it.

Output from the program is written to a file named OUTPUT.DAT, which includes a rudimentary graph meant for line printers. However, data from the output file can be used with relative ease to create plots of the type shown in the text by using TELL-A-GRAF or a similar graphics package.

• TUTORIAL

We will begin by setting the default directory and compiling the Fortran code. Then the object file is linked to the IMSL library.

```
$ FORTRAN GCM.FOR
$ LINK GCM.OBJ, IMSL/LIBRARY
```

Next, the input data files must be copied into appropriate Fortran unit files.

```
$ COPY ANGP.DAT FOR020.DAT
$ COPY ANGQ.DAT FOR021.DAT
$ COPY PARA.DAT FOR040.DAT
```

As the final step before running the program, create a batch file and append the input file to it. This will allow you to run the code for the 186 [Os] example given in the text.

Create a batch file named, for instance, GCM_FIRST_TRY.BAT, using a editor It should contain

```
$ RUN GCM
$ APPEND INPUT.DAT GCM_FIRST_TRY.BAT
```

Now run the program and the output is written to OUTPUT.DAT Remember that we are running it in batch mode.

```
$ SUBMIT/LOG_FILE=[...KOONIN.CHAPTER_6]GCM.LOG/NOPRINTER GCM_FIRST.BAT
```

The SUBMIT qualifiers used should be familiar by now.

CHAPTER 7

THE RELATIVISTIC IMPULSE APPROXIMATION

• ABSTRACT

The main codes for this chapter are TIMORA, FOLDER and HOOVER.

• FILES

TIMORA.FOR - Fortran code for the first section of the procedure that generates scalar and bayeron densities for neutrons and protons.

FOLDER.FOR - The Fortran code for the second section of the procedure that processes the densities into Dirac scalar and vector optical potentials.

HOOVER.FOR - Fortran code for the final program segment that takes input from FOLDER and adds coulomb potentials and computes the observable scattering.

TIMORA.INP FOLDER.INP - Example Input and output files provided by the author

• COMPILING, LINKING AND RUNNING

The three Fortran codes should be compiled and linked separately. To ensure correct results it is suggested that the three programs be run as described below.

• OBTAINING RESULTS / NOTES

First, run the program TIMORA. It will display the status of the run on the terminal. Next, run FOLDER, which will advance the solution a second step. Then, as a final step, run HOOVER. The total cpu time required to complete the run using the sample input data in the text was about 5 minutes.

It is up to the user to decide whether to run the codes in a batch file or interactively. It might be beneficial to run the programs all as a single batch job when large input data sets are to be processed or else there are large calculations to be done as these can require anywhere from 15 minutes to about 4 hours cpu time for any reasonable calculations that might be desired.

• TUTORIAL

As usual, set the default directory, then compile and link the three *separate* code segments.

```
$ FORTRAN TIMORA.FOR
$ FORTRAN FOLDER.FOR
$ FORTRAN HOOVER.FOR
$ LINK TIMORA.OBJ
$ LINK FOLDER.OBJ
$ LINK HOOVER.OBJ
```

The second step after the programs have been compiled and linked is to run them in order. Results are displayed on the terminal as the programs run to let the user know the status of the programs, any final output is written to data files in a text format.

So, now simply run the programs.

```
$ RUN TIMORA.EXE
$ RUN FOLDER.EXE
$ RUN HOOVER.EXE
```

CHAPTER 8

THREE-BODY BOUND-STATE CALCULATIONS

• ABSTRACT

The main code for this chapter is TRIMOD. This is the only chapter where we have modified our codes. We have done this so that they run with the IMSL library rather than the NAG library.

• FILES

TRIMOD.FOR - Source code for the Fortram program

• COMPILING, LINKING AND RUNNING

As the code was orginally written, the NAG Fortran library is required. Since it is apparantly not widely-used in the United States, we have modified the code to use IMSL procedures instead. The basic modifications included substituting the IMSL Gaussian quadrature subroutine for the NAG version used in the original code. The other NAG routine used was one that solved a linear system with multiple right hand sides. Since there was no directly corresponding routine in the IMSL library, we used IMSL's LU-factorization routine first, then used a loop to solve each right-hand-side using a single RHS linear system solve procedure. This is implimented with the subroutine MRHSLS added to the end of the code.

• OBTAINING RESULTS / NOTES

The program writes output to the screen. In order to save this for future use, it is convenient to use the SET HOST command with the qualifier /LOG_FILE= in order to capture the output in a specific file.

• TUTORIAL

First set the default directory, then compile the code and link it to the IMSL Fortran library.

```
$ FORTRAN TRIMOD.FOR
$ LINK TRIMOD,IMSL/LIB
$ RUN TRIMOD.EXE
```

CHAPTER 9

VARIATIONAL MONTE-CARLO TECHNIQUES IN NUCLEAR PHYSICS

• ABSTRACT

The main code for this chapter is VARMC.

• FILES

VARMC.FOR - Fortran source code file for the simulation program
VARMCH3.IN - A sample input file provided by the author
VARMCH3.OUT - An example output file provided by the author

• COMPILING, LINKING AND RUNNING

The actual procedure for getting the code installed is relatively simple: the source code is compiled to give an object code file which is then linked to give the executable program.

• OBTAINING RESULTS / NOTES

All input to the program is through the file VARMCH3.INP Program output is written to several data files in a text format. See the text for a full description of the input parameters.

• TUTORIAL

First, select the default directory and compile, then link the program file.

```
$ FORTRAN VARMC.FOR
$ LINK VARMC.OBJ
```

Now you are ready to use the program. It should be run in batch mode with the command $ RUN VARMC placed at the top of the VARMCH3.IN file. Also the header in this file MUST be removed in order for the program to run properly. Rename the whole file to JOB.COM and then submit as a batch job.

CHAPTER 10

ELECTRON-SCATTERING FORM FACTORS AND NUCLEAR TRANSITION DENSITIES

• ABSTRACT

The main codes for this chapter are ELHO, MAHO, WSAXE and WSAXM.

• FILES

The first four files here are source code for the four main programs

PROGRAM FILE	WAVE FUNCTION	TYPE OF TRANSITIONS
ELHO.FOR	HARMONIC OSC	ELECTRONIC
MAHO.FOR	HARMONIC OSC	MAGNETIC
WSAXE.FOR	WOODS-SAXON	ELECTRONIC
WSAXM.FOR	WOODS-SAXON	MAGNETIC

ELLIB.FOR - Library of math subroutines required by most of the code

The authors have also included several sample input files to allow the programs to be run right away. The user will need to supply data for WSAXE and WSAXM to run the example for these.

• COMPILING, LINKING AND RUNNING

The Fortran source code files are compiled separately and then the files are linked as follows:

ELHO.OBJ is linked to ELLIB.OBJ
MAHO.OBJ is linked to ELLIB.OBJ
WSAXM.OBJ is linked to ELLIB.OBJ
WSAXE.OBJ is linked to ELLIB.OBJ

Input is expected to be read from the terminal, which makes the use of batch processing convenient; output is done with data files in text format.

As we have described in previous section, the most convenient method to use in running the prograams is to append the input data set to a standard batch file.

• OBTAINING RESULTS / NOTES

Since the codes require that input come from the terminal, running the programs in the batch mode using the input files added (appended) to the batch file is the easiest method to obtain results with the minimum of fuss.

• TUTORIAL

Begin by setting the default directory, then compiling and linking the program segments.

```
$ FORTRAN ELHO.FOR
$ FORTRAN MAHO.FOR
$ FORTRAN WSAXE.FOR
$ FORTRAN WSAXM.FOR
$ FORTRAN ELLIB.FOR
$ LINK ELHO.OBJ, ELLIB.OBJ
$ LINK MAHO.OBJ, ELLIB.OBJ
```

```
$ LINK WSAXE.OBJ, ELLIB.OBJ
$ LINK WSAXM.OBJ, ELLIB.OBJ
```

Then run ELHO and MAHO First, you will need to create batch files for this purpose. Call them, for example, JOB1.COM and JOB2.COM

The file JOB1.COM should contain

```
$ RUN ELHO
```

and likewise, the file JOB2.COM should have the corresponding commands

```
$ RUN MAHO
```

To use the example data files, append them to the batch files.

```
$ APPEND ELHO.INP JOB1.COM
$ APPEND MAHO.INP JOB2.COM
```

Then submit each job to run ELHO and MAHO.

See the text for descriptions of the required input data for running WSAXE and WSAXM. They are run using the same procedures as shown above.

BNL-52262
UC-414
(High Energy Physics
DOE/OSTI-4500—R75)

Fourth Workshop on Experiments and Detectors for a Relativistic Heavy Ion Collider

July 2-7, 1990

Edited by M. Fatyga and B. Moskowitz

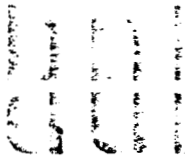

BROOKHAVEN NATIONAL LABORATORY
ASSOCIATED UNIVERSITIES, INC.
UPTON, LONG ISLAND, NEW YORK 11973

UNDER CONTRACT NO. DE-AC02-76CH00016 WITH THE
UNITED STATES DEPARTMENT OF ENERGY

An Experiment to Study Strong Electromagnetic Fields at RHIC.

M.Fatyga

Physics Department
Brookhaven National Laboratory
Upton,NY 11973

and

John W.Norbury

Department of Physics
Rider College
Lawrenceville, NJ 08648

ABSTRACT

We present a description of an experiment which can be used to search for effects of strong electromagnetic fields on the production of e^+e^- pairs in the elastic scattering of two heavy ions at RHIC. A very brief discussion of other possible studies of electromagnetic phenomena at RHIC is also presented.

1. Introduction.

When two high energy heavy ions approach one another to a distance comparable to their nuclear radius, electromagnetic fields of high intensity will be created. The presence of these fields will result in a wide range of electromagnetic processes, involving both the production of particles and photoexcitations of nuclei. The significance of such phenomena for a physics program at RHIC is threefold: first, the production of particles by electromagnetic fields will naturally accompany all central or semi-central collisions. Electromagnetic processes must be carefully considered as a possible background in some investigations of central collisions. Second, two very abundant electromagnetic processes constitute the primary limitation to the lifetime of stored beams at RHIC. One of them is a nuclear decay following the electromagnetic excitation of the giant dipole resonance, and the second one is a creation of an e^+e^- pair accompanied by the capture of an electron in the atomic level of one of the ions. [1] Third, (last but not least) it is of significant interest to study the physics of particle production by strong electromagnetic fields. Even conventional QED calculations indicate that collisions of heavy ions at RHIC will produce unique electromagnetic phenomena which cannot be studied by any other means. Of particular interest seems to be the production of e^+e^- pairs by energetic heavy ions. This process can no longer be described by perturbative methods, since the S-matrix for single e^+e^- pair production violates unitarity bounds. [2] Non-perturbative approaches to QED can be studied in this system through measurements of the pair multiplicity (as well as other properties of pairs) in collisions with small impact parameters. Finally, one must not exclude the possibility that new, as yet unknown phenomena due to strong fields can be observed in collisions of heavy ions. In the remainder of this paper we will present an outline of some experimental concepts which can be used to study the physics of strong electromagnetic fields with relativistic heavy ions.

2. Experimental concepts.

2.1 Definitions.

Let us consider a symmetric collision of two ions with a charge Z, a mass number A, an energy per nucleon corresponding to the lorentz factor γ, and with an impact parameter b. Using the impact parameter b, we will divide all collisions into three categories:
if R is the nuclear radius of either ion,
$b < 2R$ is a hard hadronic collision in which at least one nucleon in each ion was shifted out of of the beam rapidity range.
$b > 2R$ is a collision without a nuclear contact. Only electromagnetic phenomena can occur in such a collision.
$b = 2R$ is a nuclear grazing collision in which no nucleons are lost from the beam rapidity range, but both ions interacted strongly. This type of a collision can leave one or both ions in an excited state, and it can also lead to the production of particles through a two pomeron exchange.

2.2 Experimental studies of electromagnetic phenomena.

The primary difficulty in using heavy ions to study electromagnetic phenomena lies in a proper selection of collisions without a nuclear contact. A true electromagnetic event has quite low multiplicity and should not present one with any particular instrumental problems. One must expect however, that potentially serious problems may appear at the trigger level. A typical electromagnetic trigger carries a small amount of energy when compared to the total energy which is available in a collision. Hence, a trigger on the electromagnetic process must be restrictive (clever) enough not to be overwhelmed by a background due to hadronic interactions. A triggering scheme must be based on the primary trigger which selects the desired process and a set of veto detectors which reject spurious triggers due to hadronic events. More violent hadronic interactions can be easily detected with the use of a multiplicity detector of some sort. Events with a smaller multiplicity (close to the nuclear grazing collision) can perhaps be vetoed by forward calorimeters detecting beam rapidity nucleons emitted in a process of a particle decay of

excited ions. This type of veto must be applied judiciously, due to the high probability of exciting one or both ions electromagnetically. We will discuss these issues in more detail later in the paper.

2.3 Controlling the intensity of the field.

The intensity of electromagnetic fields which are created in a collision is controlled by three parameters: charges of ions (Z), their lorentz γ, and impact parameter (b). Two of these three parameters (Z, γ) can be varied quite trivially (in principle at least), by varying the charge of a beam and/or its energy. The ability to study electromagnetic phenomena as a function of Z and γ with a single apparatus is one of the most attractive features of RHIC. Such a study will allow one to vary the average strength of the field in a controlled manner, thus observing the onset of phenomena which are associated with strong fields. As an example, let us consider the production of e^+e^- in a collision without a nuclear contact. In fig.1 we show a perturbative calculation of the probability of producing a pair in a collision with the impact parameter equal to the compton wavelength of the electron (b=385fm). [3] A solid arrow points to the maximum energy at RHIC (this calculation assumes a fixed target reference frame). For the U+U collision the calculated probability exceeds unity, thus implying that the perturbative calculation can no longer describe this phenomenon correctly. At the same time the probability for producing a pair in Zr+Zr collision is well below unity, which implies that for beams with lower charges the perturbative approach is valid. By varying the charge of the beam one can study a transition from a perturbative to a non-perturbative regime in a production of e^+e^- pairs. A similar transition can be induced by lowering the energy of a heavy beam. The dotted arrow in fig.1 points to the value of γ which corresponds to 1/5 of the maximum energy at RHIC. At this energy even in U+U collision the perturbative estimate does not violate the unitarity bounds. Hence, one can study a similar transition between a perturbative and a non-perturbative regime using different means.

2.4 Controlling the impact parameter.

The dependence of electromagnetic cross sections on the charge and the energy of a beam is a powerful tool with which one can study some aspects of non-perturbative QED. This tool is likely to be insufficient however, if one wants to search for new phenomena induced by strong fields. Since the electromagnetic interaction is a long range interaction, processes like the production of particles or photonuclear excitations occur within a wide range of impact parameters. To be more quantitative, let us consider again an example of the e^+e^- pair production. In fig.2 we show the dependence of e^+e^- cross section on the impact parameter in U+U and p+p collisions. [4] The impact parameter scale is expressed in the units of the compton wavelength of the electron (385fm). We observe that the calculated cross section in U+U collision is nearly flat (slightly decreasing) in the region 15fm-385fm, while the maximum field intensity must vary by nearly three orders of magnitude in the same interval of b (with weaker fields favored by the phase space). Hence, if one would like to look for effects of strong fields which go beyond the present QED predictions, some method of selecting collisions with a small impact parameter seems necessary.

Conceptually, the most direct method of tagging a collision with its impact parameter would be to measure the transverse momentum transfer to both ions. Since relativistic heavy ions follow essentially classical Rutherford trajectories these two quantities can be related to each other. Unfortunately, a measurement of the transverse momentum transfer in an elastic collision of heavy ions appears to be extremely difficult (probably impossible). The maximum momentum transfered to each ion in gold on gold collisions is approximately 1.1GeV/c, while the incident momentum of each ion is nearly 20000 GeV/c (at relativistic energies the transverse momentum transfer is nearly independent of the incident energy). This means that the maximum deflection angle due to the Rutherford scattering is less than .06mrad, too small to be measured. Some other, more indirect method of tagging collisions with the impact parameter must be found.

In this paper we will discuss an indirect method of measuring an impact parameter which is based on the measurement of a cross section for a coincidence between two electromagnetic processes. Such measurements are not feasible at presently available energies due to prohibitively low coincidence rates. The situation will be far more favorable at RHIC

energies however, as probabilities for some electromagnetic processes approach unity. As a first example let us consider a measurement of the coincidence between $\mu^+\mu^-$ pairs and e^+e^- pairs in a collision of two gold ions at $\gamma = 100$ (a collision without a nuclear contact). Suppose, that we trigger the experiment on a single pair of muons and measure its invariant mass. Having established a trigger, we detect all electrons which were produced in the same event. We can now vary the invariant mass of a muon pair, observing that massive pairs can only be created in a collision with a small impact parameter. To illustrate this point quantitatively, let us assume that we detect a pair with mass M at the rapidity zero. Using the Weizsacker-Wiliams approximation one can estimate the range of impact parameters within which this pair could have been created. The upper limit of this range is given by:

$$b_{max} = \frac{2\gamma hc}{2\pi M} \tag{2.1}$$

If one sets a detection threshold for the minimum mass of

$$M_{min} = 4M_{0,\mu}$$

where $M_{0,\mu}$ is a rest mass of a muon, the maximum impact parameter b_{max} is equal to 95fm. Hence, a trigger pair with the invariant mass equal to $4M_{0,\mu}$ would span the 14fm-95fm range of impact parameters. The lower limit of this range is determined by the requirement of a collision without the nuclear contact. Through the same approximation one can estimate the maximum mass of a $\mu^+\mu^-$ pair to be $2.9GeV/c^2$. A trigger on such massive pairs will therefore select collisions with the smallest impact parameter ($b_{min} = 2R$, where R is a radius of an ion). One should stress, that by requiring a trigger pair of a given mass one does not select a single value of the impact parameter, but a range of impact parameters from the minimum ($b_{min} = 2R$) to the b_{max} which was defined in Eq. (2.1) .

As a second example let us consider an experiment in which $\mu^+\mu^-$ pairs are measured in coincidence with beam rapidity neutrons on either side of the interaction diamond. Beam rapidity neutrons can be emitted in a process of a decay of an excited beam ion. An excitation can be induced electromagnetically or through a nuclear grazing collision. For the purpose of this discussion we will assume that electromagnetic and nuclear components can be accurately separated. Implications of this assumption will be discussed later.

We present calculations concerning two types of events which include beam rapidity neutrons. First, an event in which only one neutron is detected on either side of the interaction region, with no neutron on the complementing side. This type of an event will be denoted as T(1n,0n). Second, an event in which two neutrons are detected, one on each side of the interaction region. This type of an event will be denoted as T(1n,1n). In fig 3 we show probabilities of the both types of events, P[T(1n,0n)] and P[T(1n,1n)], plotted against the impact parameter. We observe two features of these distributions: (a) in collisions with a small impact parameter both P[T(1n,0n)] and P[T(1n,1n)] are large, 50% and 20% respectively. Consequently, these two channels are suitable as an element of a coincidence measurement. (b) Both probabilities depend very differently on the impact parameter. P[T(1n,0n)] changes *roughly* like $\frac{1}{b^2}$, while P[T(1n,1n)] changes like $\frac{1}{b^4}$.

A measurement of $\mu^+\mu^-$T(1n,0n) and $\mu^+\mu^-$T(1n,1n) channels can be viewed as a first step in a separate study of a dependence of the $\mu^+\mu^-$ pair production and electromagnetic excitation of nuclei on the impact parameter. Since both these processes should be calculable within a perturbative formalism, we do not select (or declare) any of them as a trigger process. It is a consistency check, which can nevertheless reveal new phenomena in case a discrepancy is observed. One can go further and study channels T(2n,0n),T(2n,1n),T(2n,2n), etc..... . These channels will introduce even stronger bias towards collisions with a small impact parameter, albeit at the cost of introducing growing experimental problems. First, the absolute value of a probability of inducing a more complex decay will be decreasing, which will decrease the coincidence rate. Second, as the probability of an electromagnetic excitation decreases one must worry more about the background due to the same decay induced in a nuclear grazing collision. These problems should be addressed in future studies (calculations) in order to examine the feasibility of a more extensive program.

2.5 Quality of a trigger.

Several times in the preceding discussion we have referred to possible problems with the quality of a trigger. Before proceeding to describe an experimental apparatus, we will discuss the problem of a trigger quality in more general terms.

A trigger for an electromagnetic process must consist of two parts, the first one to select the desired process and the second one in the form of veto detectors which attempt to

discriminate against hadronic interactions. For example, in the case of $\mu^+\mu^-e^+e^-$ measurement the primary trigger would be defined as two and only two penetrating tracks in the muon region. Veto detectors would probably consist of crude multiplicity detectors covering forward and central regions. The quality of this trigger rests on the identification of muon tracks and a completeness of veto detectors. Although various tests of the performance of such a trigger can be devised, the final test of its quality must be accomplished by measuring the dependence of a trigger rate on the charge of a beam and/or its energy. A precise calculation of the Z dependence of trigger rates should be possible, as long as the rate of a trigger process can be calculated with perturbative methods.

A similar test can be applied to the emission of nucleons from excited ions. The calculation of the dependence of a cross section on the charge of a beam is not as straightforward as in the case of particle production. The main difficulty lies in the fact that the change in the charge of a beam implies simultaneous changes in the nuclear structure which must be taken into account in all calculations. These difficulties are less severe when cross sections are measured as a function of the beam energy, rather than the beam charge. Hence, the dependence of a cross section on the beam energy seems to be the most appropriate test of a trigger quality in this case.

In summary, the issue of a trigger quality definitely requires further study, mainly through Monte Carlo simulations. We note however, that direct experimental tests of this quality can (and should) be performed. Once again, it is apparent that the ability to study the same process with beams of different charge and energy is a very important feature of RHIC.

3. An outline of the apparatus.

The apparatus which will be *sketched* in this section is designed to perform three basic measurements which were discussed in previous sections: massive $\mu^+\mu^-$ or e^+e^- trigger pairs, low energy e^+e^- pairs and beam rapidity nucleons. The actual design of an experiment requires far more work than has been done thus far. In most instances we will simply outline problems which must be studied further, rather than provide ready solutions.

3.1 Low energy electrons.

We begin with a discussion of what seems to be the most difficult task, namely detecting low energy electrons. The kinetic energy spectrum of electrons (positrons) which are produced in a heavy ion collision peaks at energies between 1 and 2 MeV. Hence, a complete measurement of non-perturbative QED phenomena in a heavy ion collision requires a serious effort to detect electrons and positrons down to very low energies. Two features of a collider make it a particularly complicated task at RHIC. First, the length of the interaction diamond (22cm RMS) complicates the geometry and the acceptance of a detector. This length combined with the absence of a target constraint makes tracking of low energy electrons very difficult. Second, due to the stringent vacuum requirements inside the beam pipe ($10^{-10}Tr$) it is very difficult to put detectors directly into the beam vacuum. A silicon strip detector is perhaps the only presently available type of a detector which does not cause a conflict vith vacuum requirements. As an alternative solution one can use a thin beam pipe made of a low Z material and position a detector immediately outside the beam pipe. Although the latter choice is probably more practical both solutions should be studied seriously. In fig.4 we show a schematic view of an electron detection region. It consists of an interaction diamond and two adjacent regions of a magnetic field in which more energetic electrons are bent away from the beam and analyzed. One may also consider applying a weak magnetic field to the region of the interaction diamond. The purpose of such a field would be to bend all electrons and positrons out of the beam. Since low energy electrons (positrons) have quite broad angular distributions, it is not clear whether this field is really needed. This question must be studied further. Angular distributions become more focused with respect to the beam axis as the energy of an electron (positron) increases. Hence, one needs two regions of the magnetic field (one on each side of the interaction diamond) to bend more energetic electrons (positrons) out of the beam. The magnetic field will also provide some opportunity for the momentum analysis, albeit an uncertainty due to the absence of a target constraint.

The primary objective of the low energy region should be to measure the multiplicity of e^+e^- pairs and energy distributions of electrons and positrons. It is obviously desirable to measure other kinematic variables like an invariant mass distribution of e^+e^- pairs

or transverse momenta of singles and pairs. The feasibility of measuring an invariant mass spectrum depends to a large degree on the actual multiplicity of pairs. If it is true that multiple pairs are created in a collision, any measurement of the invariant mass will be difficult due to a combinatorial background. It will also be very difficult to measure transverse momenta of electrons (positrons) due to problems which were described above. A detector which is chosen to meet these objectives should have a good granularity as well as a capability to measure the total energy of individual electrons. A simple range detector composed of layers of scintillator tiles (perhaps separated by thin absorber plates) would seem a good choice in the low energy region. Crystals of CsI can be used to detect energetic electrons above 100MeV or so (a trigger pair). The choice of a granularity depends on the expected multiplicity of pairs which is still an object of some controversy (and may remain so until the measurement is done). Consequently, it is difficult to say at this time what granularity is really needed. In fig.5 we show a schematic design of a simple range detector. The design of the low energy electron spectrometer requires much more work than has been done thus far. One of the issues which must be carefully looked at is the feasibility of tracking in the intermediate energy range (5-10MeV). Some less conventional designs of the spectrometer should also be considered.

3.2 A trigger pair.

A trigger pair can be a massive e^+e^- pair or a $\mu^+\mu^-$ pair. There are some technical advantages to the use of an e^+e^- rather than a $\mu^+\mu^-$ pair. These advantages are partially offset by a potential for a combinatorial background when multiple pairs of electrons are produced. This ambiguity can be reduced to an arbitrarily low level however, by imposing a lower limit on the invariant mass of a trigger pair. The probability of producing two massive pairs in a single event will then be very low. The technical advantage of an electron pair is in the fact that the total energy of an electron can be measured in a shower detector. The detector can be relatively small, since electromagnetic showers are both short and narrow. This facilitates both the total energy measurement and a particle identification. The electron can be tracked prior to entering the total absorption detector, giving one more complete and precise information about its kinematic variables than a muon would. It is obviously very interesting to have a capability to trigger both on electron and on muon

pairs and compare the two results in the limit of a high invariant mass of a trigger pair. In fig.6 we show a scheme for a combined measurement of a trigger pair and low energy electron-positron pairs. This design is based on the assumption that the transverse momentum of a high energy muon or electron is small when compared to its longitudinal momentum. A high momentum electron (muon) propagates nearly undisturbed through the first region of a weak magnetic field and is analyzed in the downstream region with a stronger field. The detection of an electron should involve tracking backed by a small electromagnetic calorimeter. Muons must be identified by a range detector, perhaps coupled with a detection of a muon decay. At the limit of the invariant mass range of a trigger pair one expects two back to back electrons (muons) with the momentum of the order of 1.4 GeV/c. The identification of an electron above a few hundred Mev poses no problems if one uses a suitable total energy detector (eg. CsI crystals) to identify its electromagnetic shower. A positive identification of muons in this energy range (and particularly their separation from pions) may be difficult. Even so, the suppression of a background due to hadronic interactions should be feasible by requiring two and only two penetrating tracks, one on each side of the beamline. According to our earlier discussion the quality of the trigger can be examined experimentally. One should also mention the fact, that the increase in the invariant mass of a trigger pair is coupled to some broadening of angular distributions of single electrons (muons). Consequently, one may be forced to modify the simple design which is shown in fig.6 to avoid losses of experimental acceptance for high mass pairs. As with most other experimental issues in this paper, the detection of a trigger pair requires further study.

3.3 Detecting beam rapidity nucleons.

Detecting beam rapidity nucleons at RHIC should not be particularly difficult. Neutrons can be detected at zero degrees behind the first bending magnet, while protons will emerge from the beam at twice the bending angle of the beam, also after the first bending magnet. If one assumes a maximum transverse momentum of a neutron to be 400 MeV/c (a conservative assumption), then at a distance of 20 meters from the interaction region all neutrons are still confined within a circle 16cm in diameter. Hence, beam rapidity neutrons remain well focused even at large distances from the interaction region. The most

appropriate technique for detecting a neutron with an energy of 100GeV is a hadronic calorimeter. The main purpose of this calorimeter should be to count the number of neutrons in an event. Even if an overall energy resolution of such a detector is about 20%, one can still count beam rapidity neutrons without much trouble. A two neutron peak would be separated from a one neutron peak by more than five standard deviations, quite enough for a reliable classification of the event. In reality, one should expect the energy resolution to be better than 20%. A good hadronic calorimeter (available today) can offer an energy resolution of 5% at an energy of 100GeV. The fermi momentum distribution will broaden the laboratory energy distribution of a neutron to about 12% of its average value. Hence, even if one assumes that the instrumental energy resolution is a factor of three worse than the 5% quoted above, one still arrives at the overall width of the energy spectrum equal to 19% of the average value. The separation can be further improved if one uses a segmented calorimeter, so that a simple pattern recognition can be used. A similar discussion applies to beam rapidity protons.

3.4 Event rates and multiple interactions per bunch crossing.

The cross section for producing a $\mu^+\mu^-$ pair in an extremely peripheral collision of two gold ions at $\gamma = 100$ is approximately 300 mb. At the design luminosity of $2 * 10^{26} cm^{-2} sec^{-1}$ one expects 60 $\mu^+\mu^-$ pairs per second. Triggering on the invariant mass interval which corresponds to 1% of the total cross section one still expects .6 pairs per second, a respectable trigger rate.

Since the cross section for producing e^+e^- pairs is very large, one must worry about the possibility of multiple interactions per one bunch crossing. The geometric cross section for a passage of two ions within a distance smaller than 385fm is of the order of 5kb, which corresponds to .22 of an interaction per bunch crossing. Hence, the probability of two interactions of this kind in a single bunch is of the order of 5%. In this simple estimate we assume that coherent effects in a crossing of two beam bunches are not important (this assumption needs some further investigation). One should also say, that the 5% estimate is probably somewhat low, since e^+e^- pairs can be produced at impact parameters which are larger than 385fm. The probability to produce a pair drops quite rapidly with the

impact parameter however, making this region of impact parameters less significant. More theoretical work on the impact parameter dependence of the e^+e^- pair production may be needed to improve our estimates. In practice, it will be quite important to compare measurements taken with beams of varying luminosity, to make sure that no significant contamination due to multiple interactions is present.

4. Summary.

4.1 Summary of the experimental program.

In this section we will summarize the experimental program which was outlined thus far.

1. A measurement of the $\mu^+\mu^-e^+e^-$ channel can provide an insight into non-perturbative aspects of e^+e^- pair production, as well as allow one to search for new phenomena in strong fields. All QED calculations predict that the multiplicity of e^+e^- pairs depends very weakly on the impact parameter in a collision, as long as the impact parameter is smaller than 385fm. This result can actually be tested by measuring the multiplicity of e^+e^- pairs as a function of the invariant mass of a $\mu^+\mu^-$ pair. Any significant variation (particularly an increase) in the multiplicity of e^+e^- pairs when the mass of a $\mu^+\mu^-$ pair increases would point to the possibility of new phenomena in e^+e^- pair production. We note, that massive e^+e^- pairs can also be used as a trigger. It would seem very worthwile to repeat the same measurement with $\mu^+\mu^-$ and e^+e^- pairs as a trigger. In the limit of a large invariant mass of a trigger pair both measurements should produce identical results. Any strong field phenomenon should depend very sensitively on the combined charges of beams. Hence, it is essential to repeat this measurement with a variety of beams and study its results as a function of the charge of a beam.

2. A measurement of the coincidence between $\mu^+\mu^-$ or e^+e^- pairs and beam rapidity nucleons can be viewed as a trigger study for the previous experiment, or as an independent study of the dependence of dilepton production and electromagnetic excitation of nuclei on the impact parameter. A coincidence measurement provides a consistency test between the two processes. The failure of this test can be interpreted as a signature of new phenomena in either one of the two processes. Further measurements would be necessary to understand

such a failure. It is again essential to do the experiment with a variety of beams and a: several beam energies.

A measurement of the coincidence between two electromagnetic processes provides one with the equivalent of a *minimum bias*, indirect trigger on collisions with small impact parameters. One can interpret a $\mu^+\mu^-$ pair as a minimum bias trigger for the study of e^+e^- pairs. Using this trigger one can study properties of the *average* e^+e^- pair created in a collision with a small impact parameter. If one searches for rare events due to strong fields, this experimental method becomes insufficient. One must then construct a trigger which explicitely searches for such events. Events with an abnormally high multiplicity of e^+e^- pairs can be an example of a rare event.

4.2 Other possibilities.

There are other experiments in the general area of extremely peripheral collisions of relativistic heavy ions which are of interest, but have not been discussed in this paper.

It has been suggested by E.Teller [5] that strong magnetic fields which are created in heavy ion collisions without the nuclear contact can lead to the enhanced production of mesons. His suggestion was motivated by the earlier work of J.Schwinger, [6] who speculated that quarks can have a magnetic charge in addition to their known electric charge. Best candidates for such studies would probably be simple non-flavored mesons like π^0,η,η_c. An anomalous dependence of cross sections for producing these mesons on the charge of a beam could then indicate a new mechanism of meson production due to strong fields. The measurement of a coincidence between mesons and e^+e^- pairs (and/or electromagnetic decays of nuclei) can provide further insights into the impact parameter dependence of meson production.

4.3 Conclusions.

We have discussed some possibilities of studying the physics of strong electromagnetic fields in extremely peripheral collisions of relativistic heavy ions. A physics motivation for these studies ranges from confirming already predicted non-perturbative phenomena in QED processes, to searches for new phenomena due to strong electromagnetic fields. Because of the long range nature of the electromagnetic interaction it seems necessary to

find a way in which an experiment can be triggered on collisions with a small impact parameter. One such method which is based on the coincidence between two electromagnetic processes has been presented in this paper.

It seems that the general area of the physics of extremely peripheral collisions of relativistic heavy ions has a potential to develop into an experimental program at RHIC. This program is quite distinct from the study of central collisions both in terms of its goals and instrumental requirements. Peripheral events have a relatively low multiplicity, with accurate triggering as the main experimental problem. In contrast, triggering is not a problem in studies of central collisions. Backgrounds due to high multiplicities of produced particles are the greatest obstacle in these experiments. Some of the measurements which relate to peripheral interactions can be done parasitically, using detectors which are designed with central collisions in mind. Given the differences in essential requirements however, it would seem most effective to construct modest, dedicated experiments for the study of peripheral interactions rather than attempt parasitic measurements with large detectors. For example, most detectors avoid particle tracking in the immediate vicinity of the interaction diamond due to the background of charged pions. This is a nonexistent problem in peripheral collisions, where some form of tracking close to the interaction region is actually very desirable. For the same reason of enormous charged particle multiplicity, most detectors tend to have high granularity and be located at large distance from the interaction diamond (to reduce the occupancy rate). Again, from the point of view of peripheral interactions such a design is needlessly complex and expensive. Last but not least, physics goals of both programs are quite different, and one probably should avoid mixing them in a single experiment.

We hope that the area of extremely peripheral collisions of relativistic heavy ions will become an integral part of the physics program at RHIC.

References.

1. Conceptual Design of the Relativistic Heavy Ion Collider
   Brookhaven National Laboratory Internal Rep. 52195
   May 1989.
2. Can RHIC be used to test QED? - Workshop Proceedings
   ed. M.Fatyga, M.J.Rhoades-Brown, M.J.Tannenbaum
   Brookhaven National Laboratory Report 52247
   April 20-21, 1990.
3. C.A.Bertulani and G.Baur, Phys.Rep. 163(1988) 299.
4. C.Bottcher, M.R.Strayer, J.S.Wu, A.K.Kerman, M.J.Rhoades-Brown in:
   Can RHIC be used to test QED? - Workshop Proceedings
   ed. M.Fatyga, M.J.Rhoades-Brown, M.J.Tannenbaum
   Brookhaven National Laboratory Report 52247
   April 20-21, 1990.
5. E.Teller, Proc. of the 9th International Conference on the Application of Accelerators in Research and Industry, ed. J.L.Duggan North Holland Amst. 1986.
6. J.Schwinger, Science v165, N3895(1969)757.

Acknowledgments

We would like to thanks all members of the QED study group for useful discussions. In particular we wish to thank Drs. C.A.Bertulani and M.J.Rhoades-Brown.
This work supported in part by NASA Research Grant NAG-1-1134 and DOE contract DE-AC02-76CH00016.

Figure Captions.

Fig.1 A perturbative calculation of the probability for e^+e^- pair production in a collision with the impact parameter 385fm (Ref. 3).

Fig.2 The cross section for e^+e^- pair production as a function of the impact parameter in U+U and p+p collision at RHIC. Colliding beams at $\gamma = 100$ (Ref. 4).

Fig.3 Probabilities of removing a neutron from one ion only (P[T(1n,0n)]) and removing one neutron from each ion (P[T(1n,1n)]) in a collision of two Au nuclei with $\gamma = 100$ (colliding beams). Both probabilities are plotted against the impact parameter.

Fig.4 A schematic view of the low energy electron region.

Fig.5 A schematic view of the low energy electron detector.

Fig.6 A schematic view of the combined measurement of a trigger pair and low energy electrons.

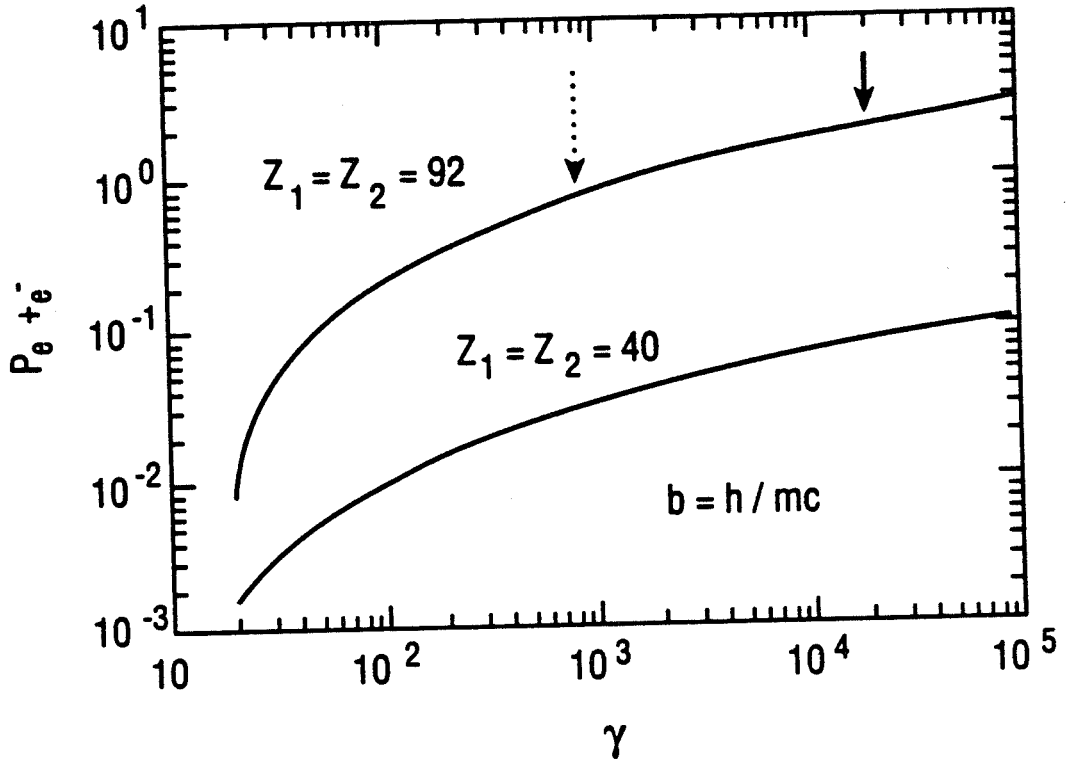

Fig. 1

Fatyga 1a 8/90 IR

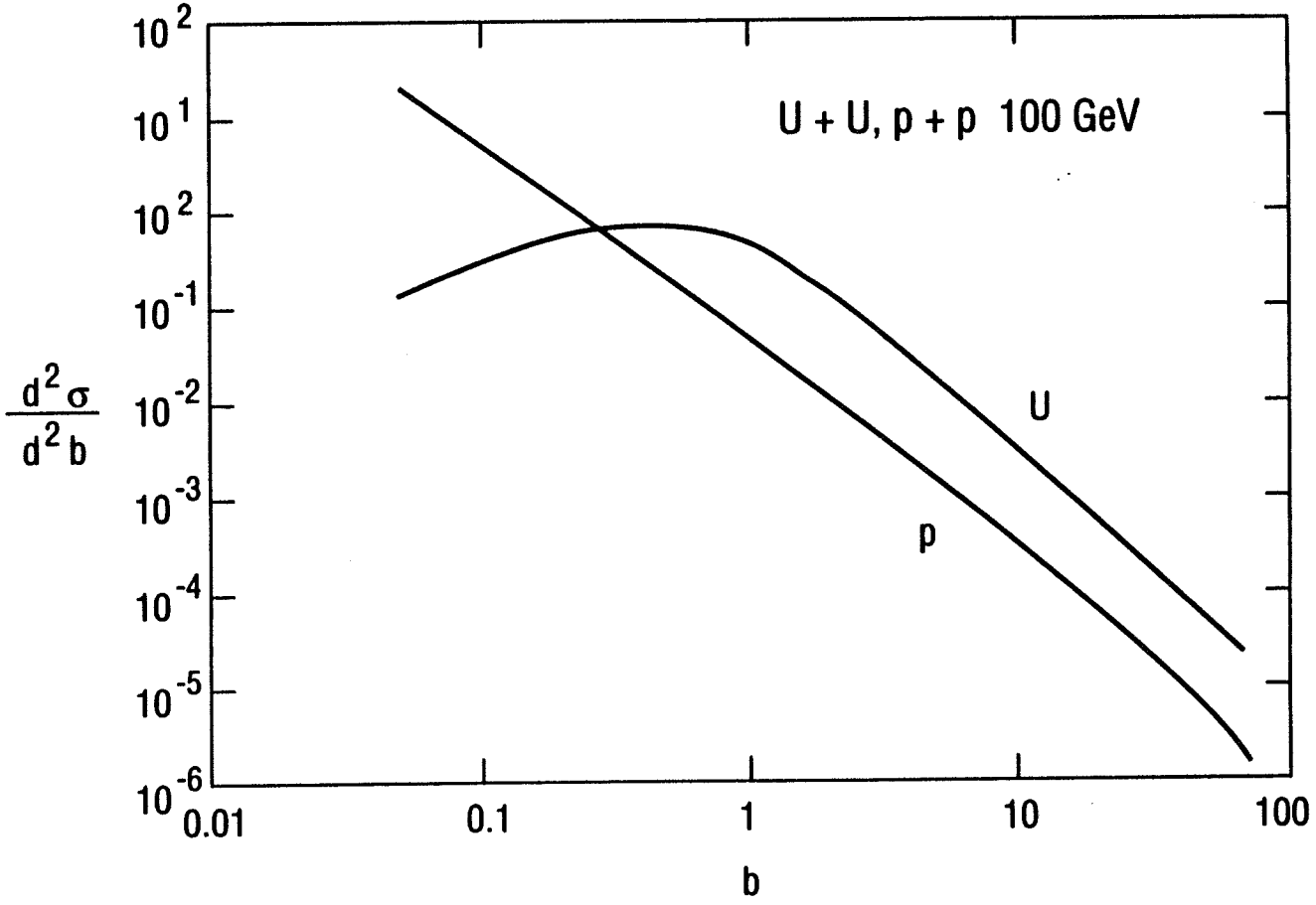
U + U, p + p 100 GeV
U
p
$\frac{d^2\sigma}{d^2b}$
10^2
10^1
10^2
10^{-1}
10^{-2}
10^{-3}
10^{-4}
10^{-5}
10^{-6}
0.01
0.1
1
10
100
b

Fig. 2

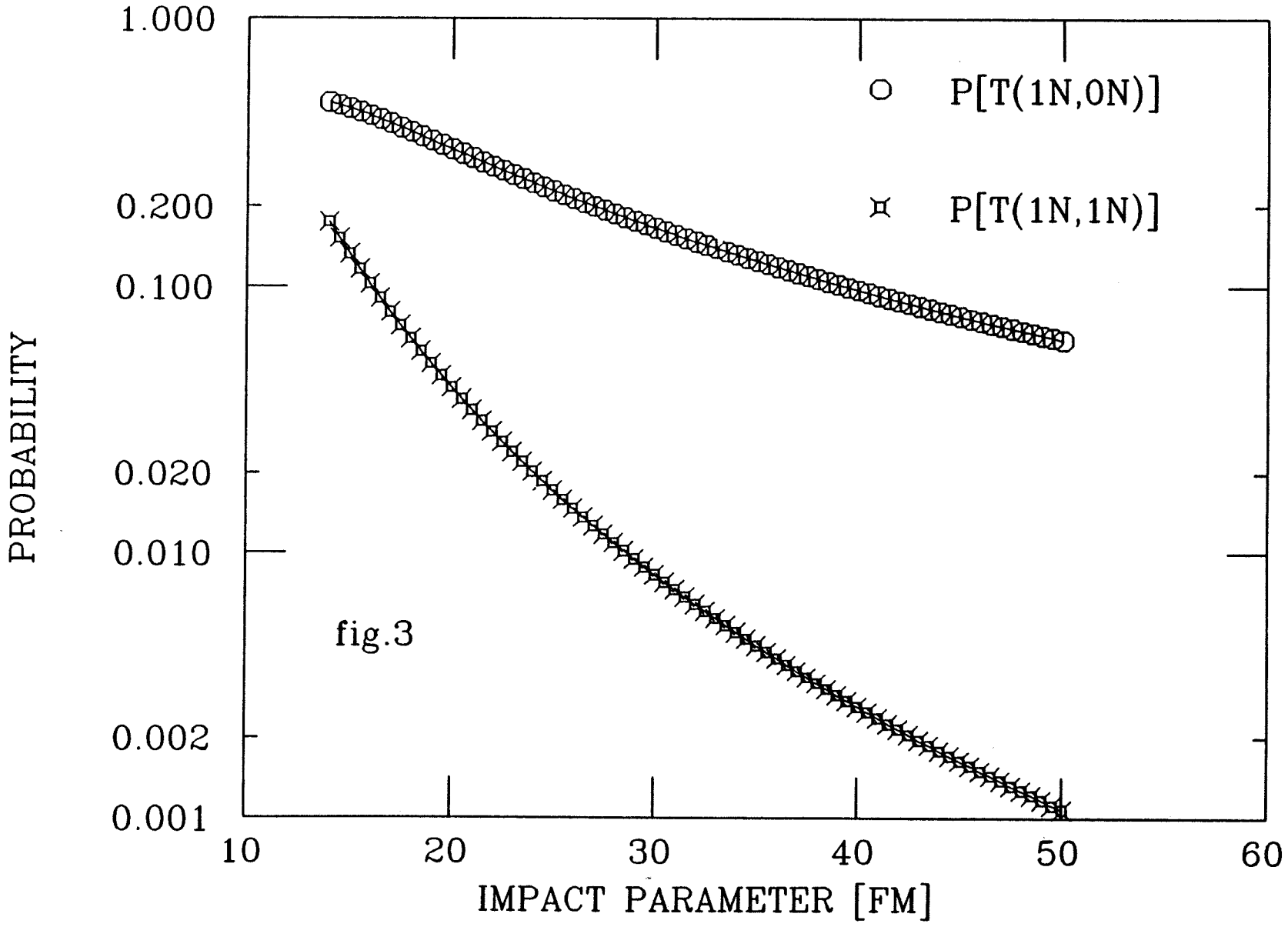
1.000
0.200
0.100
0.020
0.010
0.002
0.001
PROBABILITY
P[T(1N,0N)]
P[T(1N,1N)]
10
20
30
40
50
60
IMPACT PARAMETER [FM]

fig.3

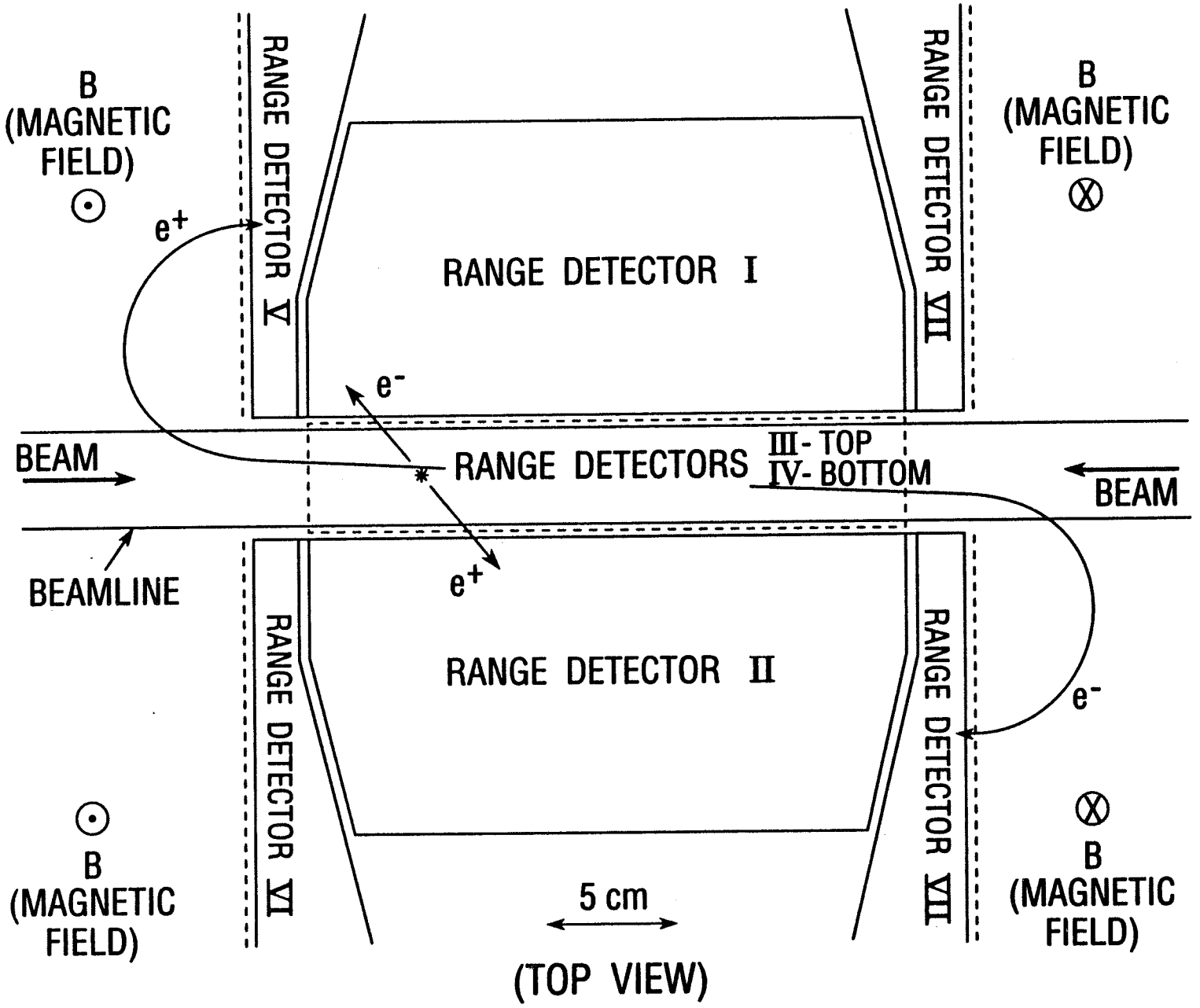

Fig. 4

Fatyga 4-1 8/90 IR

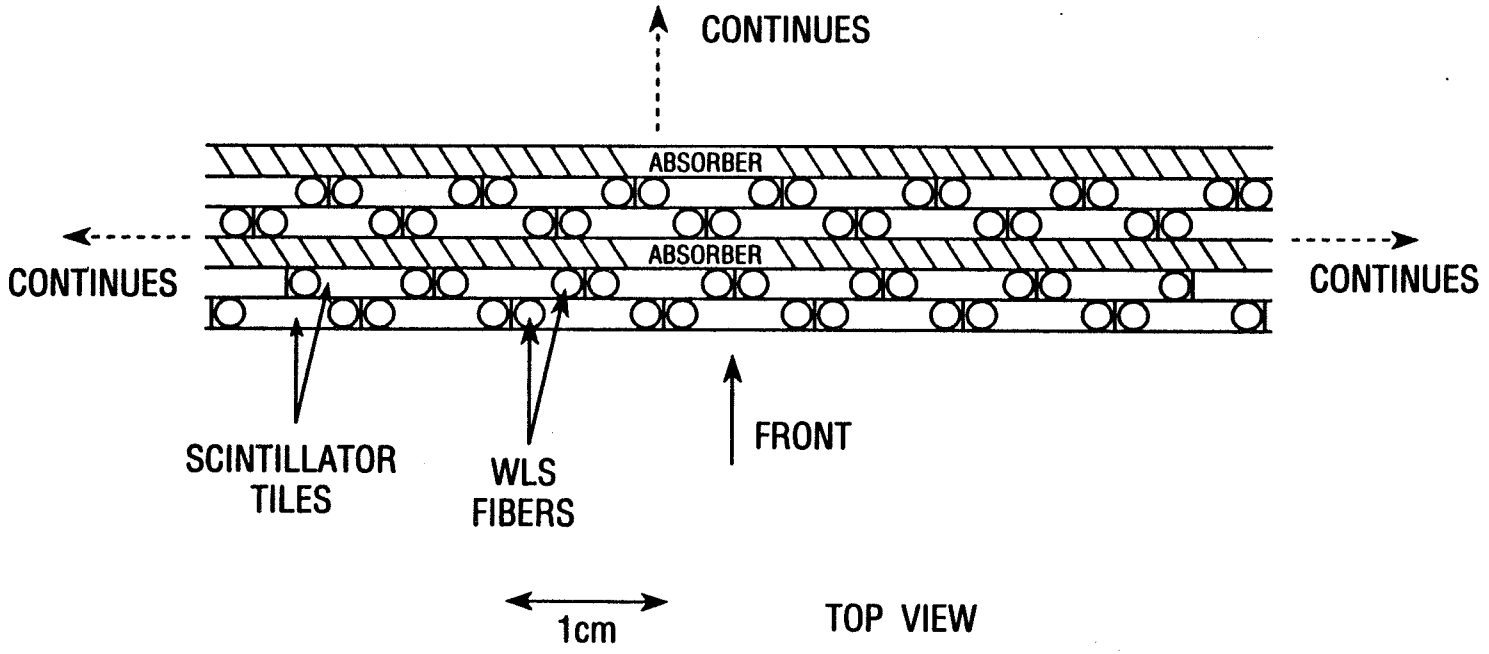
CONTINUES
ABSORBER
ABSORBER
CONTINUES
CONTINUES
SCINTILLATOR TILES
WLS FIBERS
FRONT
1cm
TOP VIEW

Fig. 5

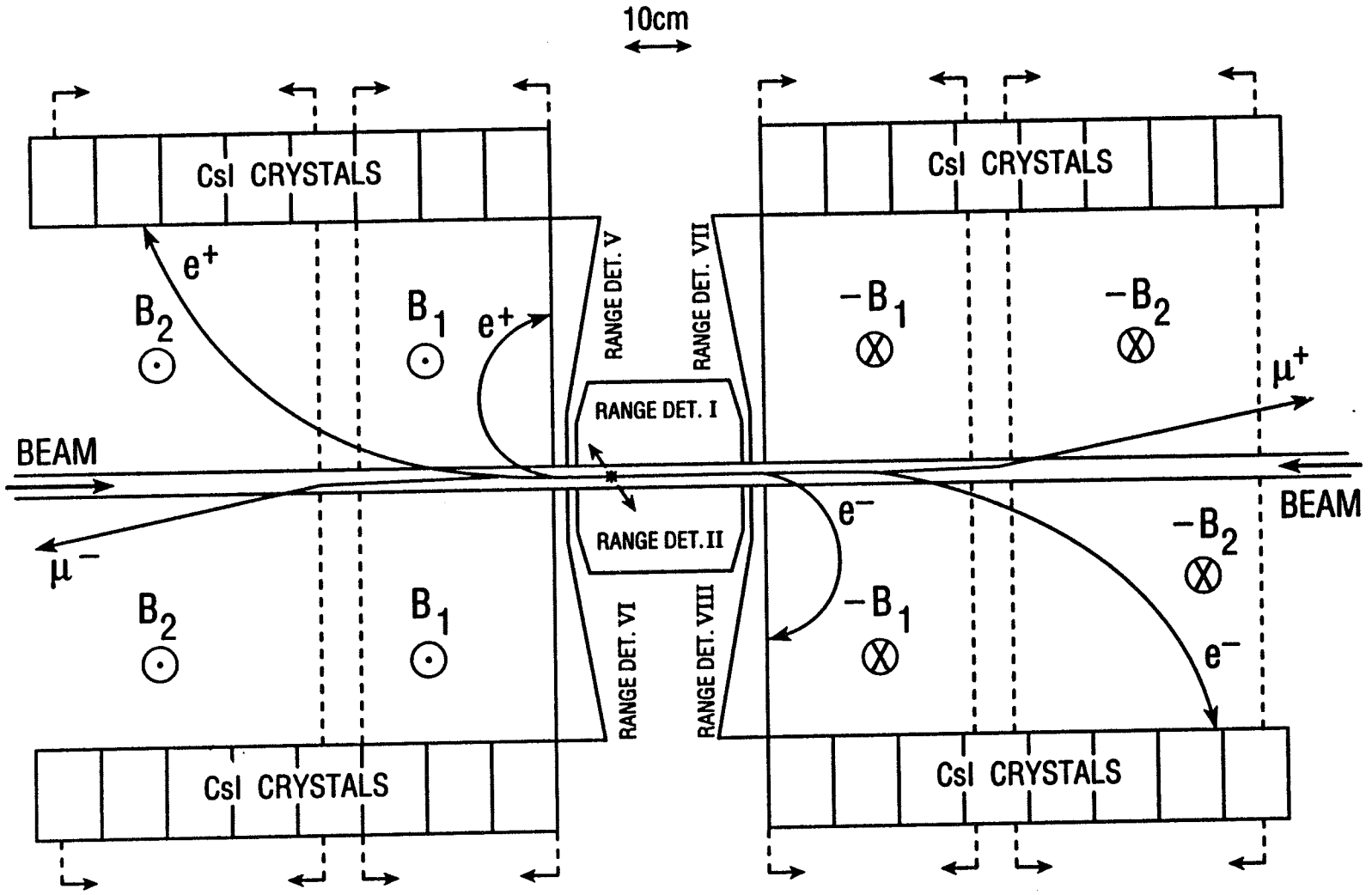

$B_1 = 0.1 - 0.2$ T

$B_2 = 1 - 2$ T

TOP VIEW

Fig. 6

FATYGA 6-1 8/90 IR

A Letter of Intent for an Experiment to Study Strong Electromagnetic Fields at RHIC via Multiple Electromagnetic Processes.

M.Fatyga

Physics Department
Brookhaven National Laboratory
Upton,NY 11973

and

John W.Norbury

Department of Physics
Rider College
Lawrenceville, NJ 08648

ABSTRACT

An experimental program at RHIC which is designed to study non-perturbative aspects of electrodynamics is outlined. Additional possibilities for new studies of electrodynamics via multiple electromagnetic processes are also described.

1. Introduction

This letter is being submitted in response to the call for letters of intent for small experiments at RHIC. In it, we present an outline of an experimental program which is designed to study multiple electromagnetic processes in the quasi-elastic scattering of relativistic heavy ions. By quasi-elastic scattering we mean these events in which particles are produced out of the vacuum due to electromagnetic interactions alone. Two beam ions are required to pass one another within a distance which is greater than the sum of their nuclear radii. We believe that such measurements belong to the exclusive domain of relativistic heavy ion colliders and constitute a unique test of electrodynamics under the conditions of strong electromagnetic fields. Following the submission of the letter we intend to work on the design of an apparatus. To this end, John Norbury is presently working on calculations which will establish a set of parametrized probability distributions for various electromagnetic processes. These parametrizations will include the dependence of probabilities on an invariant mass of di-lepton pairs, the rapidity of pairs or mesons and the impact parameter in a collision. Following the completion of this work, we should be able to establish fast event generators which can then be used for realistic Monte Carlo simulations of an apparatus. By formulating a program of measurements we are also hoping to increase the theoretical activity in this area. We will work towards appraising our theoretical colleagues about opportunities which will be presented by RHIC in this domain. We are anxious to receive as much theoretical feedback as possible.
Finally, we are very interested in hearing the opinion of the Committee on the merits of our proposal. Encouragement would be most helpful in searching for new collaborators.

Having had to work with a very short deadline, we would like to apologize for all of the defects and shortcomings of this letter. It has been put together in haste. We will be glad to answer any questions that the committee may have after reading it.

2. Physics Motivation

It has been recognized for some time now, that relativistic heavy ions can be treated as a good source of virtual photons due to the enhancement of a virtual photon flux (per ion) by a factor which is *approximately* equal to the square of a charge of an ion. [1] The cross sections for two-photon processes in a heavy ion collider are greater than those in e^+e^- machines by a factor which is *approximately* equal to the beam charge to the fourth power. It also has been pointed out however, that this gain in flux of virtual photons is largely offset by limitations in the luminosity of heavy ion machines. [2] In fact, this loss in luminosity is about equal in magnitude to the gain in the flux of virtual photons. Therefore (it was concluded), heavy ions do not offer any significant advantage in the magnitude of cross sections for two photon processes. At the same time, significant new difficulties due to hadronic backgrounds are introduced . We have no quarrel with these assertions. There exists however, an *entire class* of interesting processes exclusive to Relativistic Heavy Ion Colliders which involve a production of particles by electromagnetic fields. These are multiple electromagnetic processes, in which two or more distinct objects (lepton pairs, neutral hadrons, hadron pairs) are created through the electromagnetic polarization of a vacuum. If one approximates the probability of a double process by the convolution of probabilities for simple two photon processes, the cross section for a double electromagnetic process depends on the charge of beams like Z^8. Consequently, relativistic heavy ion colliders have no competition from other machines in this field of study. The purpose of this section is to discuss the physics significance of such processes as well as the program of measurements for exploring opportunities in this area. Specifically, we will discuss a production of multiple lepton pairs (e^+e^- and $\mu^+\mu^-$), a production of π^0 or η^0 in coincidence with e^+e^- pairs and a coincidence of all these processes with beam rapidity neutrons (protons) which are emitted due to a Giant Dipole Excitation of beam ions.

2.1. e^+e^- pair production

The production of e^+e^- pairs in the quasi-elastic scattering of relativistic heavy ions will exhibit strong non-perturbative effects. In fact, it has been shown by many authors,

that the perturbative estimate of the probability to produce a pair violates unitarity at low invariant masses. [3] It seems particularly attractive to study these effects at RHIC, due to its variety of available beams. All the effects of strong fields can in essence be turned on and turned off by a mere change of beams. Most calculations of a non-perturbative pair production emphasize masses just above a production threshold ($(1-2)\frac{MeV}{c^2}$), concluding that strong non-perturbative effects can be seen predominantly in the production of pairs with very low invariant masses. From an experimental point of view, such an observation implies that it would be necessary to measure electron pairs at extremely low invariant masses (and perhaps trigger a measurement on them) in order to explore the non-perturbative regime. We will seek to demonstrate that in a properly designed experiment this region of non-unitarity can be extended up to invariant masses of the order of $(10-20)\frac{MeV}{c^2}$. As an added benefit, we will show that such an experiment can be provided with a relatively background-free trigger.

In a perturbative approximation, the probability to produce a pair with an invariant mass M and at an impact parameter b is a function of the product Mb. One therefore observes, that if the unitarity is violated in the production of a threshold pair at an impact parameter equal to the compton wavelength of an electron (385fm), one expects the same violation of unitarity in a production of pairs with invariant masses of the order of $20\frac{MeV}{c^2}$ at the smallest allowed impact parameter prior to the nuclear contact (15.2fm for gold+gold collision). In fig.(1) we show a Weizsacker-Williams calculation of the probability to produce an e^+e^- pair in a gold+gold collision at top RHIC energy (100GeV/nucleon), and at a minimum allowed impact parameter. [4] This calculation clearly shows a violation of unitarity in the production of pairs with invariant masses of the order of $10\frac{MeV}{c^2}$. However, there remains a significant difficulty in applying this observation to a realistic measurement. First, a *minimum bias* $10\frac{Mev}{c^2}$ pair can be produced in a wide range of impact parameters. As an illustration, in Fig(2) we show the impact parameter dependence of the probability to produce a $10\frac{MeV}{c^2}$ pair. It is clear that the decrease of the probability due to an increase of an impact parameter is quite slow. This slow drop will cause a minimum bias cross section to be dominated or at least severely contaminated by less interesting distant collisions, simply because of a phase space ($2\pi bdb$) factor. Moreover, it may be very difficult to trigger an experiment in a collider environment on pairs of a low mass.

To remedy both difficulties, we designed a measurement which allows for the selection of collisions with a small impact parameter and simultaneously provides a distinct and a relatively background free trigger. Namely, we propose to trigger the experiment on a high invariant mass e^+e^- pair and measure all other pairs associated with such an event. A veto on hadronic interactions can be provided by two multiplicity detectors positioned in a forward-backward direction. A leading hadronic background at the trigger level should be a topological equivalent of a minimum bias p-p collision. Harder hadronic interactions will produce large multiplicities and should not be difficult to suppress. When an invariant mass of a trigger pair approaches that of a WW limit (about $3\frac{GeV}{c^2}$ at RHIC at a minimum allowed impact parameter), only collisions with small impact parameters will be selected. Moreover, there should be no particular difficulties in triggering an experiment on a single pair in a few hundred Mev range of invariant masses. By varying the invariant mass of a trigger pair one can change the range of impact parameters being selected, thus studying an evolution of e^+e^- pair production with a varying strength of electromagnetic fields. Since we have the freedom of choosing the charge of beams, the same evolution can be studied by independent means (changing the charge of beams). For a completeness of this discussion, one should point out that an interpretation of the coincidence measurement which was described here is still dependent on our understanding of the impact parameter dependence of the probability to produce a trigger pair. At high invariant masses such probability distributions should be calculable reliably via perturbative approximations. *In addition*, there exists a set of auxiliary, supporting measurements which will test the accuracy of our predictions. A list of such measurements with a rudimentary description of their interpretation will be provided later in this letter.

In summary, we propose to use a massive e^+e^- pair as an experimental trigger on elastic heavy ion collisions at impact parameters close to the nuclear contact. Such a trigger should allow us to study a fully non-perturbative production of e^+e^- pairs at fairly high invariant masses.

We believe that there exists yet another regime of invariant masses in which measurements of a production of multiple e^+e^- pairs is of interest. Namely, we are considering a study of the production of two or more pairs in an invariant mass range of $(20-100)\frac{MeV}{c^2}$. A motivation for such a study is relatively simple. Let us observe, that the compton wavelength

which is associated with a pair in this range of masses is in a $4 - 20fm$ range. Hence, formation times of such pairs are not much smaller than the collision time, and volumes necessary to produce them are also large. For these two reasons, we believe that higher order corrections to the probability to produce two pairs (relative to a simple convolution of first order probabilities) will be most pronounced in the $20 - 100\frac{MeV}{c^2}$ range of invariant masses. We will study a feasibility of such a measurement through Monte Carlo simulations in a near future. In this letter, we will only evaluate event rates by using a convolution of probability distributions for a single pair which were obtained in a first order perturbative approximation.

2.2. π^0,η^0 in coincidence with e^+e^-

As a logical extension of a multiple pair measurement, we will now consider a process in which a neutral meson is produced in coincidence with e^+e^- pairs. In the first step, one would like to verify that the dependence of total integrated cross sections for the production of π^0 and η^0 on the charge of beams shows no anomalies. The observation of an anomaly could indicate a change in the rate of production of strange quarks relative to up and down quarks when the strength of electromagnetic fields increases. In the second step, one measures the probability that an e^+e^- pair is produced in coincidence with a meson. One also measures the properties of such pairs, namely their invariant mass and rapidity distributions. An interpetation of the coincidence rates can be twofold. First, they probe the impact parameter dependence of the probability to produce π^0 and an η^0. Pairs of a relatively low invariant mass will be particularly sensitive to the shape of these distributions. Second, when the invariant mass of an electron pair increases up to the $40 - 100\frac{MeV}{c^2}$ range, the energy density which is necessary to produce such a pair becomes comparable to that of a π^0 or even an η^0. Consequently, an observation of an anomaly in these coincidence rates could indicate an interference between the formation of a meson and the formation of an electron pair. Once again we will invoke an argument, that the relatively large compton wavelength of an electron pair in this mass range implies that an overlap between formation times and formation volumes of a meson and a pair is likely. One should also note that the preceding measurement of a multiple pair production can

be used as a calibration measurement of sorts which will facilitate an understanding of the coincidence between pairs and mesons.

2.3. An electromagnetic excitation of the Giant Dipole Resonance

Finally, we discuss yet another coincidence experiment that can accompany all the measurements which were discussed above. Namely, in an elastic collision of relativistic heavy ions, either one of the two ions can experience an excitation of the Giant Dipole Resonance due to an interaction with the electromagnetic field of its counterpart in a collision. A leading de-excitation mode is the emission of a neutron or a proton with an energy of the order of a few MeV in the center of mass system of an ion. Such a free nucleon appears in the laboratory system with a beam rapidity, thus having a kinetic energy which is centered on 100GeV at a top RHIC energy. Beam rapidity neutrons can be quite easily detected in a zero degrees calorimeter positioned downstream from the first bending magnet, whereas protons can be detected after the same bend at an angle which is a bit larger than twice the bending angle of the beam. In fig(3) we show a probability to detect a beam rapidity neutron as a function of the impact parameter in a collision. The functional form of this probability distribution can be very well approximated by the form $P(b) = \frac{P_0}{b^2}$. We can see that in a gold+gold collision at the minimum allowed impact parameter a probability of emitting a single neutron from either ion is of the order of 40%. This large probability implies that coincidences with beam rapidity neutrons will be frequent for all processes. We will now show how such a coincidence measurement can be used to constrain calculations of the impact parameter dependence of the probability to produce a trigger pair in a multiple pair measurement. To illustrate the method, let us assume that a calculation of a probability to produce the neutron is correct. We will further assume that the probability to produce an e^+e^- pair of a high invariant mass (defined as a trigger pair in a multiple pair measurement) is described by a $P(b) = \frac{P_0}{b^n}$ formula, where n is an adjustable parameter (to be deduced from a measurement). For simplicity , we will limit the discussion to pairs with rapidity zero. In fig(4) we show the probability to observe a neutron in coincidence with a pair for three values of a parameter n, where $n = 0, 2, 4$. This probability is plotted against a parameter $A = \frac{b_{max}}{b_{min}}$, where b_{min} is the minimum

allowed impact parameter, and b_{max} is related to an invariant mass of a pair due to an adiabatic cutoff of the virtual photon spectrum in a Weizsacker-Williams approximation (b_{max} in units of [fm]):

$$b_{max} = \frac{2 * \gamma * 197.3}{M}$$

It is quite clear, that such a coincidence measurement has a significant level of sensitivity to the functional form of the probability to produce a pair. Naturally, the actual functional form of the probability distribution can be more complicated than $\frac{1}{b^n}$. We assumed such a simple form to illustrate the sensitivity of this method. In the final analysis, the best available calculation for both probability distributions (for a neutron emission and for a production of a pair) must be used in calculation and then compared to a measurement. A complete experiment requires a consistency test for three independent observables: the total cross section for an emission of a neutron, the cross section for producing an electron pair of an invariant mass M, and the cross section for a coincidence between a neutron and a pair. All three observables should be measured with beams of different charges and energies.

An emission of a single beam rapidity neutron will be accompanying all processes which were discussed in previous sections, and with a high probability of occurence. It can be treated as an additional factor in efforts to understand multiple electromagnetic processes.

2.4. A summary of proposed measurements.

Let us list now a set of measurements which should allow for a reasonably exhaustive analysis of phenomena which were discussed above:

- the total cross section for e^+e^- pairs as a function of the charge and energy of beams.

- the invariant mass and rapidity distributions of e^+e^- pairs as a function of the charge and the energy of beams.

- the total cross section for π^0 and η^0 as a function of the charge and the energy of beams.

- the rapidity distribution of π^0 and η^0 as a function of the charge and the energy of beams.

- the multiple pair production with a trigger pair of a large invariant mass. All measurements should be done in a widest possible range of beam charges and energies (cross sections will be vanishing very fast with decreasing charge and energy of the beams).

- the multiple pair production with two (or more) pairs in a $(20-100)\frac{MeV}{c^2}$ range of invariant masses. All measurements should be done in a widest possible range of beam charges and energies (cross sections will be vanishing very fast with decreasing charge and energy of the beams).

- the $\pi^0 e^+ e^-$ and $\eta^0 e^+ e^-$ coincidence cross sections. Invariant mass and rapidity distributions of pairs, a comparison between pairs accompanying π^0 and pairs accompanying η^0. All measurements should be done in a widest possible range of beam charges and energies (cross sections will be vanishing very fast with decreasing charge and energy of beams).

3. Estimates of count rates.

3.1. Assumptions

A number of assumptions will be made to calculate event rates for the purpose of this letter:

1. all probabilities and cross sections are obtained by a simple convolution of first order probabilities (usually obtained in a Weizsacker-Williams approximation).
2. a following formula is being used to calculate cross sections for multiple processes:

$$\sigma_{mp} = P_1(b_{min}) * P_2(b_{min}) * ...P_i(b_{min}) * 7.6\ [barns]$$

're $P_i(b_{min})$ isthe probability of a single process at the minimum allowed impact parameter. A deriviation of this formula is given in an appendix 1.

3. all rate estimates refer to a collision of two gold ions at an energy of 100GeV/nucleon at a luminosity of $2 * 10^{26} cm^{-2} s^{-1}$. [5]

3.2. Multiple e^+e^- pairs

The following approximate formula was used to calculate the probability to produce a single pair of an invariant mass M_i at the minimum allowed impact parameter b_{min}:

$$P_i(M) = \frac{10^2}{M_i^2}$$

where M_i is an invariant mass expressed in MeV. This probability is normalized to unity at $M_i = 10\frac{MeV}{c^2}$ (Fig(1)), and describes the probability of producing a pair in an interval of invariant masses $[M_i(1-\alpha), M_i(1+\alpha)]$, with $\alpha = 0.05$. Consequently, the probability to produce n pairs at a minimum allowed impact parameter is:

$$P_n = \frac{10^{2n}}{M_1^2 * M_2^2 * ....M_i^2}$$

A deriviation of these formulas is provided in an appendix 2. A summary of results is presented in three figures, Fig(5) - Fig(7). In Fig.(5) we show the event rate for two pair events, with the mass of one of the two pairs fixed at $100\frac{MeV}{c^2}$ and the second one taken as a variable. In Fig.(6) we show the event rate for events with two pairs, each within an invariant mass range which is centered on $M_0 = 100\frac{MeV}{c^2}$, plotted against a parameter α describing a width of a mass range for each pair. Hence, each pair has a mass

within a range $[M_0(1 \mp \alpha), M_0(1 - \alpha)]$. Finally, in Fig.(7) we show event rates for events with 2 pairs of the same invariant mass, with α fixed at a value of $\alpha = 0.05$. The event rate is plotted against a value of invariant masses ($M_1 = M_2 = 20, 30, 40, 50, ... \frac{MeV}{c^2}$). Since no acceptance cuts were put into these calculations, event rates should be treated as an upper limit (within limitations of our approximations). One might add, that changing the beam to uranium (from gold), would increase all rates by approximately a factor of 2.5.

3.3. Events with π^0 and η^0

In fig(8) we show the results of a calculation of event rates for events with one neutral meson (π^0, η^0) and an e^+e^- pair. Event rates are plotted against the invariant mass of an e^+e^- pair.

4. Technical considerations

4.1. Triggering

In the following section we discuss an outline of trigger configurations which can satisfy the requirements of measurements which were proposed in previous sections. Monte Carlo studies of trigger configurations will continue until the final proposal can be formulated. First, let us remind the reader that we wish to limit our measurements to quasi-elastic collisions of relativistic heavy ions, *with no hadronic interactions*. A successfull trigger will be capable of vetoing all hadronic interactions. Events of interest are characterized by the low multiplicity, as well as the survival of both ions completely (or at least nearly) intact. We must allow for some exceptions to the last requirement due to decays of electromagnetically induced nuclear resonances. These resonances will be dominated by the Giant Dipole Resonance which can result in an emission of a neutron or a proton at a beam rapidity.

As an example of a trigger configuration let us first discuss a study of multiple e^+e^- pairs, with one pair of a large invariant mass. A trigger setup for this measurements should

include following elements:

- One massive e^+e^- pair in which a total energy measurement is coupled to a simple tracking arrangement.

- No multiplicity being detected on either side of an interaction region. Shapes and locations of multiplicity vetoes should be chosen so that a maximum rejection is obtained for a minimum bias p-p collision. Detector arrangements used for luminosity measurements in p-p or p-pbar colliders can be used as an example of such a veto.

- At most one beam rapidity neutron or a beam rapidity proton can be seen on either side of an interaction region. Neutrons can be detected by hadronic calorimeters positioned at zero degrees past the first bending magnet, downstream from an interaction region. Protons can be detected at twice the deflection angle of a beam past the same first bending magnet. It should be noted that at high energies one may have to allow for events with two beam rapidity nucleons emitted from a single ion. Although a probability of such events occuring due to electromagnetic interaction alone should be very low, one may choose to study events with two (or more) nucleons as a function of a beam energy to make sure that no significant bias is introduced by rejecting two-nucleon events.

- A crude multiplicity veto around the interaction vertex can be added to veto on central collisions which do not activate downstream multiplicity vetoes. We feel that a veto of this kind would be redundant, but a possibility of adding it will be studied further.

As an invariant mass of a trigger pair decreases towards a $(10 - 100)\frac{Mev}{c^2}$ range, one expects increasing difficulties in triggering. Various designs of a trigger must be studied to cope with these difficulties. At this time we can only list some elements of a trigger setup

which should definitely be considered:

A segmented electromagnetic calorimeter with a low noise (probably crystals with photomultipliers) capable of detecting low energy depositions at a trigger level. A simulataneous requirement of a total energy and a hit multiplicity can then be imposed. An independent multiplicity detector should accompany this setup as a third element in a trigger. Standard hadronic vetoes are alwys imposed.

Triggering on the intermediate mass range will be one of the main objects of study in a design of an electron spectrometer for this experiment.

5. Compatibility with large experiments

At this time we believe that our program of measurements is not compatible with large experiments which are being designed to search for the quark-gluon plasma. Reasons for a poor compatibility can be summarized as follows:

5.1. Differences in the transverse momentum acceptance

Most designs that we are familiar with involve significant p_t thresholds for all produced objects (di-leptons or mesons). These thresholds are introduced in an attempt to hold down costs and avoid a need for a 2π detector coverage in ϕ. A study of electromagnetic phenomena must use a detector system with an acceptance which is centered on $p_t = 0$. Having said this, we do not imply that a study of this kind requires a very elaborate detector system. We must stress again, that an event structure which we are considering here is much simpler than that of a central collision. We are considering events with a low multiplicity (hence a low occupancy rate), without a problem of discriminating against an intense pion background. These two requirements seem to be primary factors in determining costs of an experimental apparatus for a study of central collisions.

5.2. An energy range for single particles.

The dynamic range for energies of single particles in our apparatus is very different from the dynamic range in a typical RHIC experiment. With the exception of a massive trigger pair, we are interested in electrons and photons in the few to few hundred MeV energy range. In a multiple pair measurement a specialized low energy electron spectrometer is probably called for. In a photon measurement a crystal detector positioned close to the beam line with a maximum possible coverage in solid angle should be considered. Both the electron and the photon parts of an apparatus must be succesfully merged. Although a careful study of the design of an apparatus must be performed before final conclusions are reached, it is our intuition that the set of requirements which is necessary for a good measurement of electromagnetic processes will be contradictory to those imposed by large experiments. We are particularly refering to dead material surrounding the beamline, as well as space constraints imposed by magnets and other elements of a very complex apparatus.

6. Summary

In conclusion, we have submitted this letter of intent with following goals in mind:

- To demonstrate that it is possible to design an experiment in which non-perturbative production of e^+e^- pairs can be studied in the $(10-20)\frac{MeV}{c^2}$ energy range, rather than $(1-2)\frac{MeV}{c^2}$ energy range. We understand that detecting electrons of such low energies still poses a significant technical challenge. At the same time, a ten-fold increase in the energy of electrons significantly improves prospects for tracking and reduces problems which are associated with multiple scattering. We believe that the physics payoff is worth the effort.

- To demonstrate that many new possibilities will exist in a study of electromagnetic phenomena in the $(10-100)\frac{MeV}{c^2}$ range of invariant masses, and sufficient event

rates exist to consider experiments in this area. Such a field of a study also represents a unique domain of relativistic heavy ion colliders.

- Finally, we would like to obtain the advice and the opinion of the Committee, whether such a direction of study can be supported at RHIC. All the work which served as a basis for this letter had been accomplished with marginal resources. Before committing significantly more time to the preparation of an experimental design, we would like to get a better understanding of the prospects for submitting a successfull proposal in this area. Given some encouragement from the committee we will work towards developing the final design of an apparatus. We will also seek new collaborators.

We are convinced that the physics motivation for this proposal is compelling. Electrodynamics constitutes one of the pillars of modern physics. We should take advantage of any opportunity to devise meaningful new tests of our understanding of electromagnetic phenomena. understanding of it should be taken advantage of. In our opinion, relativistic heavy ion colliders will provide us with such new opportunities, perhaps leading to the creation of a completely new field of study.

Appendix I.

A rate calculation for multiple electromagnetic processes

In order to allow for the expeditious calculation of rates for this letter we derived few formulas based on simplifying assumptions:

Let us consider two electromagnetic processes, each with a probability distribution with respect to an impact parameter which is described by a formula $P_i = \frac{1}{b^{n_i}}$, $i = 1, 2$. A cross section for a convolution of these two processes can be calculated as follows:

$$\sigma_{mp} = \int_{b_{min}}^{b_{max}} \frac{P_1}{b^{n1}} \frac{P_2}{b^{n2}} 2\pi b db \tag{I.1}$$

where b_{min} is a minimum allowed impact parameter prior to the nuclear contact, b_{max} is a maximum impact parameter determined by an adiabatic cutoff for one of the two processes (whichever is smaller).

The result of an integration can be expressed as follows:

$$\sigma_{mp} = \frac{P_1 * P_2 * 2\pi}{(n_1 + n_2 - 2)} * \kappa \tag{I.2}$$

with

$$\kappa = \left[\frac{1}{b_{min}^{n_1+n_2-2}} - \frac{1}{b_{max}^{n_1+n_2-2}} \right] \tag{I.3}$$

For simplicity, we now assume that b_{max} is much larger than b_{min}, a true statement for most of the processes which we consider. Under this assumption we can rewrite the result as:

$$\sigma_{mp} = \frac{P_1}{b_{min}^{n_1}} * \frac{P_2}{b_{min}^{n_2}} * \frac{2}{n_1 + n_2 - 2} * \pi b_{min}^2 \tag{I.4}$$

An expression πb_{min}^2 desrcibes a total hadronic cross section, which for gold+gold collision is approximately equal to 7.6 barns. For final rate estimates we take $n_1 = n2 = 2$ for all processes considered (an approximation again. In reality, n is somewhat less than 2). We believe that our rate estimates should be good to within a factor of two. More exact rate estimates will be performed for a proposal, based on calculations which are now in progress.

Appendix II.

The dependence of e^+e^- probabilities on the invariant mass.

The dependence of the probability to produce an e^+e^- pair on its invariant mass can be well described by a $\frac{1}{M^3}$ dependence. This dependence is well illustrated in fig.(9), where the probability to produce a pair is integrated over a fixed interval of invariant masses, $1\frac{Mev}{c^2}$. To make our discussion more realistic from the experimental point of view, we chose to present these probabilities in a somewhat modified form. Namely, we integrate the probability to produce a pair of an invariant mass M_0 over a mass interval which is described by a fraction of M_0. In other words, we integrate over an invariant mass range $[M_0(1-\alpha); M_0(1+\alpha)]$, where α is a parameter. Hence, we obtain:

$$P_\alpha = \int_{M_0(1-\alpha)}^{M_0(1+\alpha)} \frac{1}{M^3} dM \tag{II.1}$$

which leads to:

$$P_\alpha = \frac{2}{M_0^2}\left[\frac{\alpha}{(1-\alpha^2)^2}\right] \tag{II.2}$$

In most rate estimates $\alpha = 0.05$ was taken. A typical dependence of results on the value of α is shown in fig.(6) . The reader should bear in mind that using our formulas with large values of a parameter α may be somewhat misleading, due to a very steep dependence of probabilities on the invariant mass. For example, a rate estimate for events with two $100\frac{MeV}{c^2}$ pairs, using $\alpha = 0.4$, will be dominated by events with two $60\frac{MeV}{c^2}$ pairs. A value of α should be adjusted to fit a particular physics topic which is being discussed, as well as capabilities of the experimental apparatus.

For the purpose of rate estimates in this letter we normalized a probability to produce a $10\frac{MeV}{c^2}$ pair, at a minimum allowed impact parameter, to unity. We use $\alpha = 0.05$ in this approximation. The actual value of a probability which was obtained via a Weizsacker-Williams calculation is 1.04.

Appendix III.

An average mass of the coincident pair. A simple example

To provide the reader with an example of qualitative features of the multiple pair measurement we made a *simple* estimate of an average mass of the coincident pair as a function of the invariant mass of the trigger pair. First, we assume that the average mass of a pair produced in a collision with the impact parameter b is:

$$M_b = \frac{M_0}{b}$$

with M_0 adjusted so that $M_b = 10\frac{MeV}{c^2}$ at $b = b_{min}$. Second, we calculate the average mass of a coincident pair by using a probability distribution for the trigger pair which is expressed as $P_e = \frac{1}{b^2}$. The average mass of a coincident pair can then be calculated as follows:

$$M_c = \left[\int_{b_{min}}^{b_{max}} \frac{P_e}{b^2}\frac{M_0}{b} 2\pi b db\right] * N^{-1} \qquad \text{(III.1)}$$

where

$$N = \int_{b_{min}}^{b_{max}} \frac{P_e}{b^2} 2\pi b db \qquad \text{(III.2)}$$

and b_{max} is determined by the adiabatic cutoff in the Weizsacker-Williams spectrum of virtual photons:

$$b_{max} = \frac{2 * \gamma * 197.3}{M}$$

Results of this calculation are summarized in fig.(10). An average mass of a coincident pair shows a fairly steep dependence on the mass of a trigger pair, thus demonstrating a sensitivity of the coincidence measurement to the range of impact parameters which is spanned by a trigger pair. The actual value of an average mass will be higher than indicated in fig(10). after the perturbative component in mass distribution is taken into account.

References

1. C.A.Bertulani and G.Baur, Phys.Rep. 163(1988) 299 (and references therein)..

2. Can RHIC be used to test QED? - Workshop Proceedings
   ed. M.Fatyga, M.J.Rhoades-Brown, M.J.Tannenbaum
   Brookhaven National Laboratory Report 52247
   April 20-21, 1990.

3. G.Baur;
   C.Bottcher, M.R.Strayer, J.S.Wu, A.K.Kerman, M.J.Rhoades-Brown in:
   W.Scheid;
   Can RHIC be used to test QED? - Workshop Proceedings
   ed. M.Fatyga, M.J.Rhoades-Brown, M.J.Tannenbaum
   Brookhaven National Laboratory Report 52247
   April 20-21, 1990.

4. J.Norbury, W.Cheung , (Rider College) - Unpublished

5. Conceptual Design of the Relativistic Heavy Ion Collider
   Brookhaven National Laboratory Internal Rep. 52195
   May 1989.

Figure Captions

Fig.1) A probability to produce an e^+e^- pair of the invariant mass M_0, calculated for a collision at a minimum allowed impact parameter (prior to the nuclear contact). An invariant mass of a pair is contained within the $(M_0 * 0.95; M_0 * 1.05)$ range. Gold + Gold, 100GeV/nucleon.

Fig.2) A probability to produce an e^+e^- pair of the invariant mass $M_0 = 10\frac{MeV}{c^2}$, plotted as a function of an impact parameter. An invariant mass of a pair is contained within the $(M_0 * 0.95; M_0 * 1.05)$ range. Au + Au, 100GeV/nucleon.

Fig.3) A probability to produce a beam rapidity neutron in an elastic scattering of two gold ions plotted as a function of the impact parameter in a collision. Au + Au, 100GeV/nucleon.

Fig.4) A probability to produce a beam rapidity neutron in a coincidence with a second electromagnetic process, plotted as a function of a ratio between an impact parameter of an adiabatic cutoff for a coincidence process and a minimum allowed impact parameter $(A = \frac{b_{max}}{b_{min}})$. A probability of a second (unspecified) process is assumed to depend on the impact parameter like $\frac{1}{b^n}$. Results of calculations using three different values of the parameter n are showed.

Fig.5) Event rates for events with two e^+e^- pairs. An invariant mass of one pair is fixed at $100\frac{MeV}{c^2}$. Rates are plotted against a value of an invariant mass of a second pair. One day indicates 24 hours of running with a design luminosity of $L = 2 * 10^{26} cm^{-2} s^{-1}$,

Fig.6) Event rates for events with two e^+e^- pairs. An invariant mass of each pair is contained within a range of $(M_0 * (1 + \alpha); M_0 * (1 - \alpha))$, with M_0 fixed at a value of $100\frac{MeV}{c^2}$.Rates are plotted against a value of a parameter α. One day indicates 24 hours of running with a design luminosity of $L = 2 * 10^{26} cm^{-2} s^{-1}$.

Fig.7) Event rates for events with two e^+e^- pairs. An invariant mass of each pair is contained within a range of $(M_0 * (1+\alpha); M_0 * (1-\alpha))$, with α fixed at a value of 0.05. Rates are plotted against a value of a parameter M_0. One day indicates 24 hours of running with a design luminosity of $L = 2 * 10^{26} cm^{-2} s^{-1}$.

Fig.8) Event rates for events with a neutral meson and an e^+e^- pair. An invariant mass of a pair is contained within a range of $(M_0 * (1+\alpha); M_0 * (1-\alpha))$, with α fixed at a value of 0.05. Rates are plotted against a value of a parameter M_0. One day indicates 24 hours of running with a design luminosity of $L = 2 * 10^{26} cm^{-2} s^{-1}$.

Fig.9) A probability to produce an e^+e^- pair of the invariant mass M, calculated for a collision at a minimum allowed impact parameter (prior to the nuclear contact). A probability is plotted against $\frac{1}{M^3}$ to illustrate its dependence on M. An invariant mass of a pair is contained within the 1MeV range. Gold + Gold, 100GeV/nucleon.

Fig.10) A correlation between the masses of a trigger pair and a coincident pair. Gold + Gold, 100GeV/nucleon.

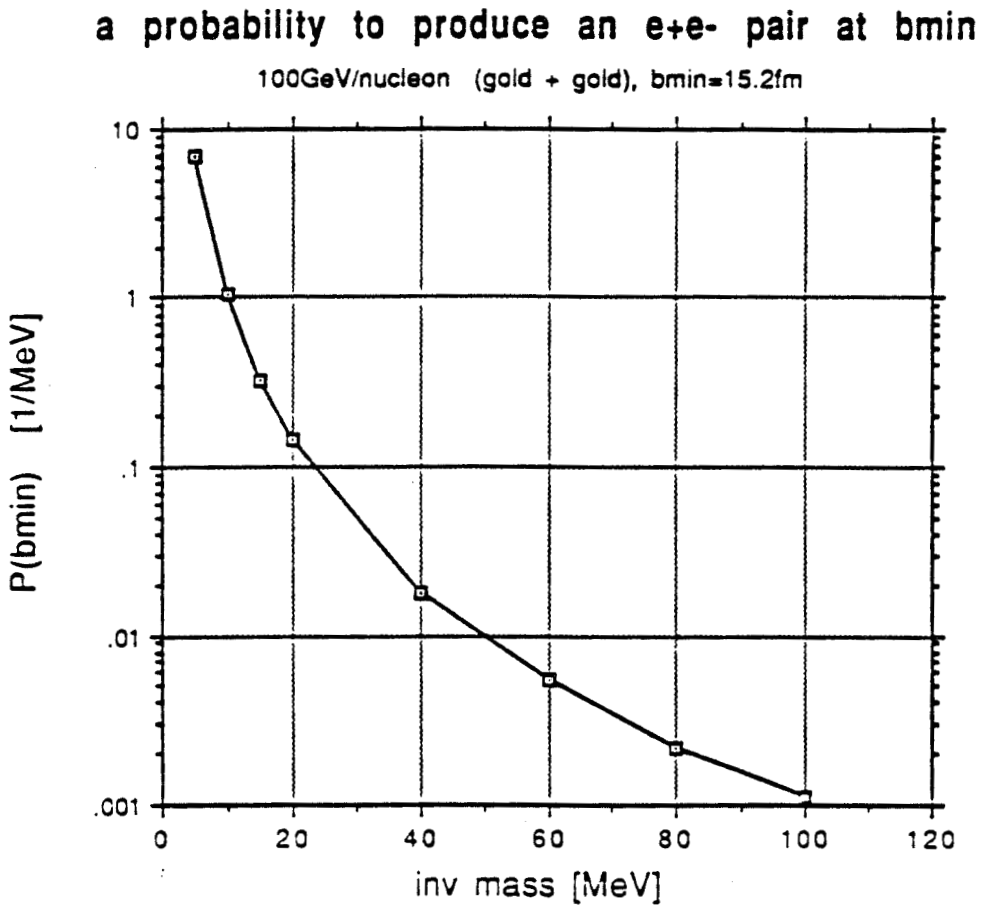
a probability to produce an e+e- pair at bmin
100GeV/nucleon (gold + gold), bmin=15.2fm
P(bmin) [1/MeV]
10
1
.1
.01
.001
0
20
40
60
80
100
120
inv mass [MeV]

fig. 1

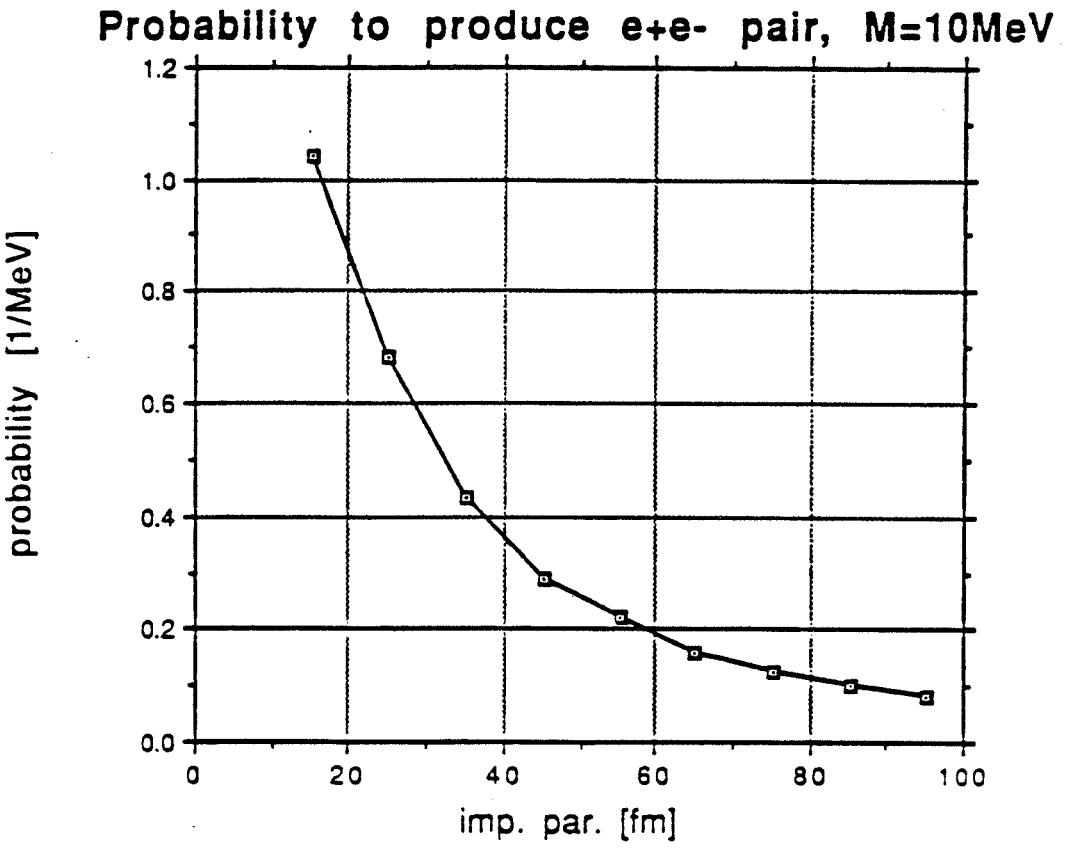
Probability to produce e+e- pair, M=10MeV
probability [1/MeV]
1.2
1.0
0.8
0.6
0.4
0.2
0.0
0
20
40
60
80
100
imp. par. [fm]

fig.2

fig.3

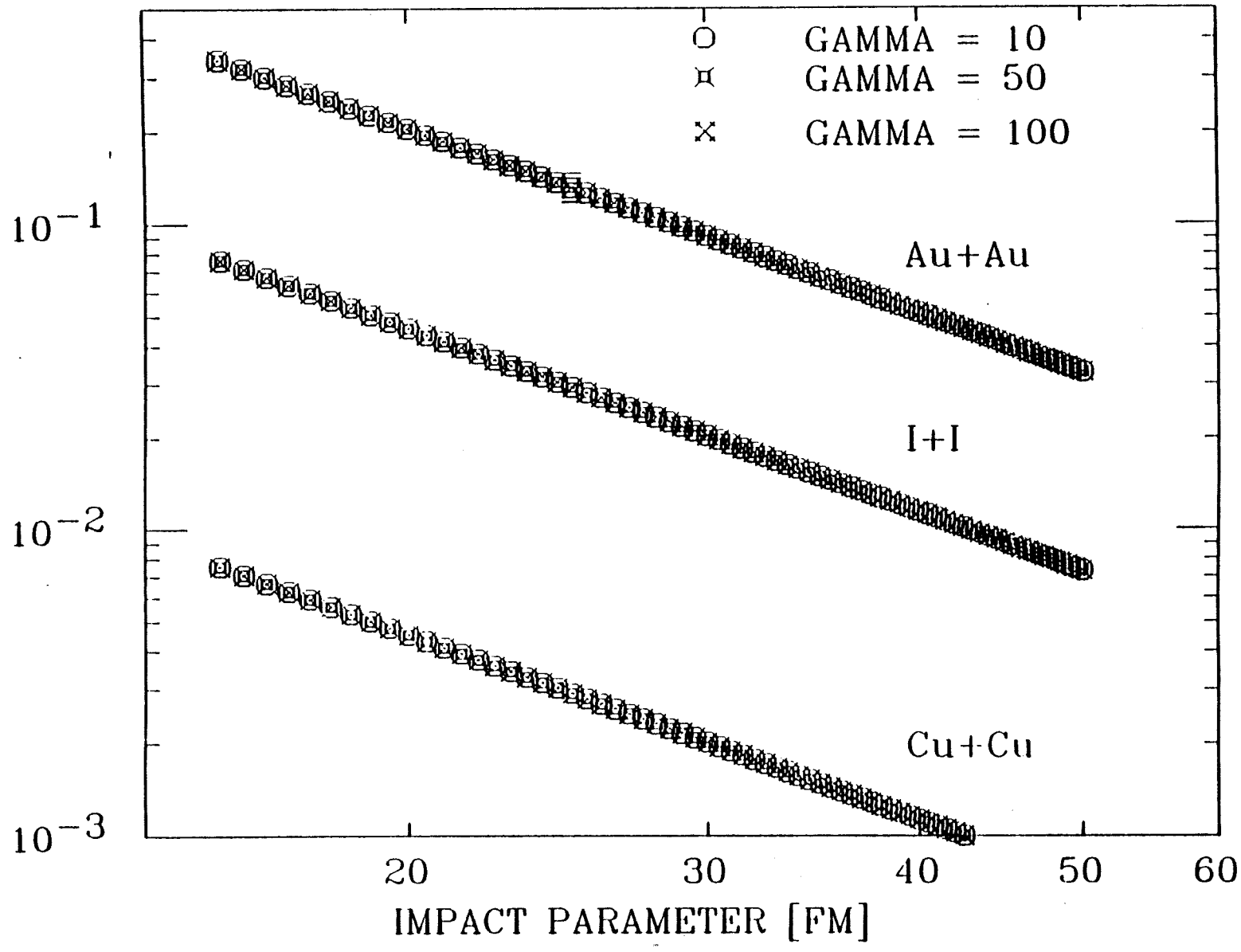
GAMMA = 10
GAMMA = 50
GAMMA = 100
Au+Au
I+I
Cu+Cu
PROBABILITY
10^{-1}
10^{-2}
10^{-3}
20
30
40
50
60
IMPACT PARAMETER [FM]

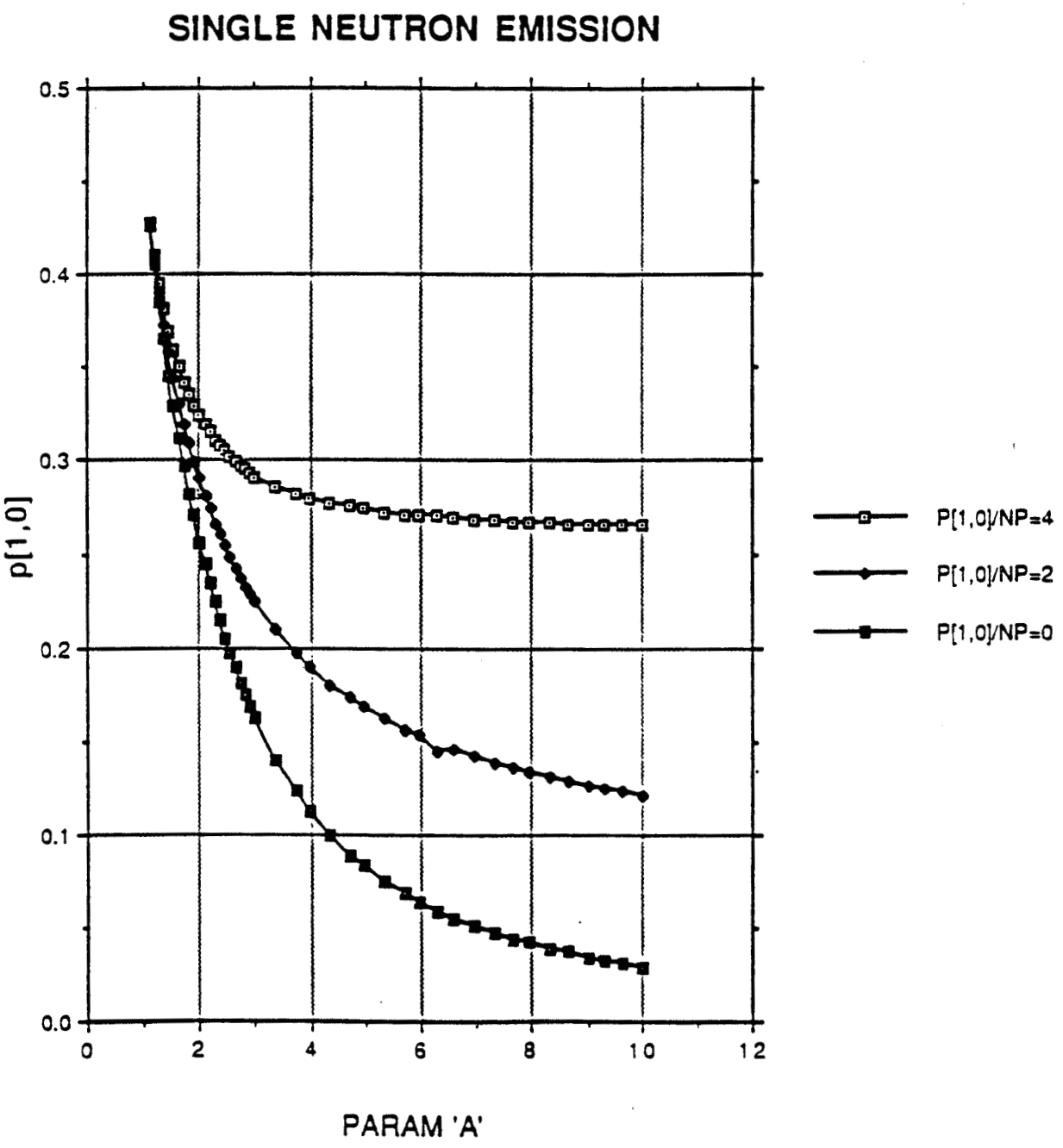
SINGLE NEUTRON EMISSION
0.5
0.4
0.3
0.2
0.1
0.0
p[1,0]
0
2
4
6
8
10
12
PARAM 'A'
P[1,0]/NP=4
P[1,0]/NP=2
P[1,0]/NP=0

fig.4

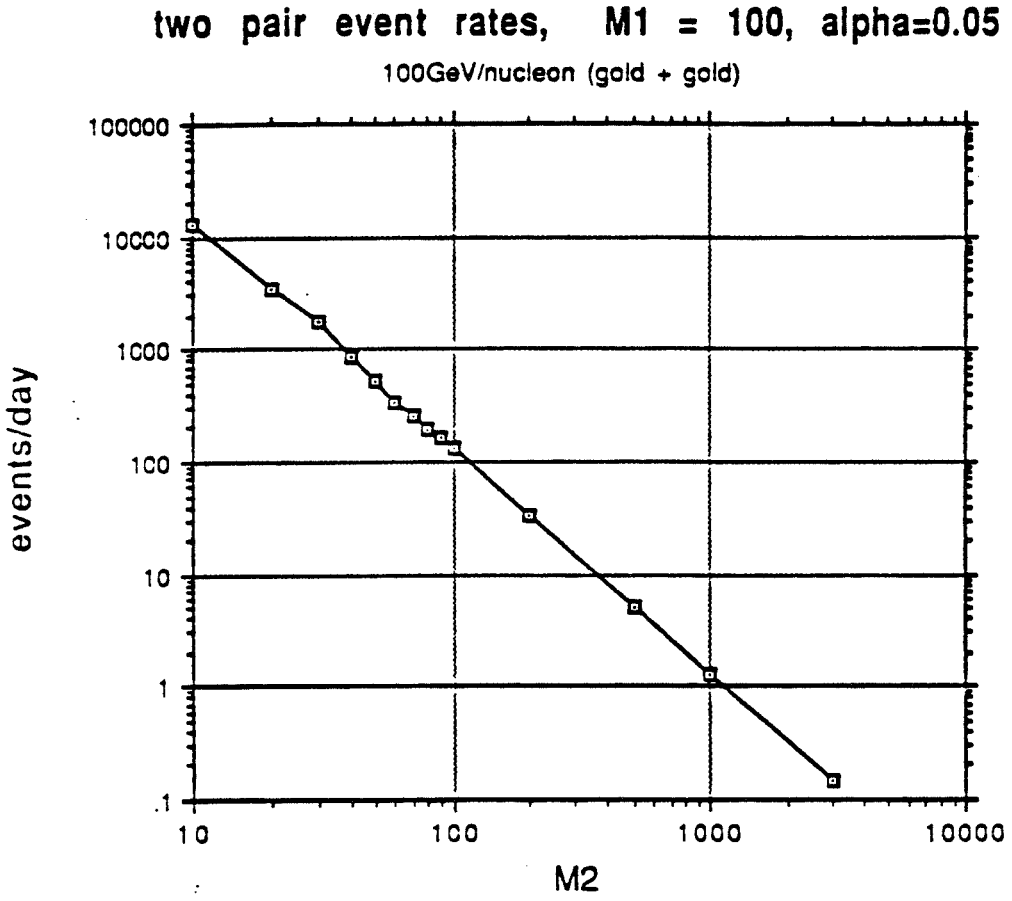
two pair event rates, M1 = 100, alpha=0.05
100GeV/nucleon (gold + gold)
events/day
100000
10000
1000
100
10
1
.1
10
100
1000
10000
M2

fig.5

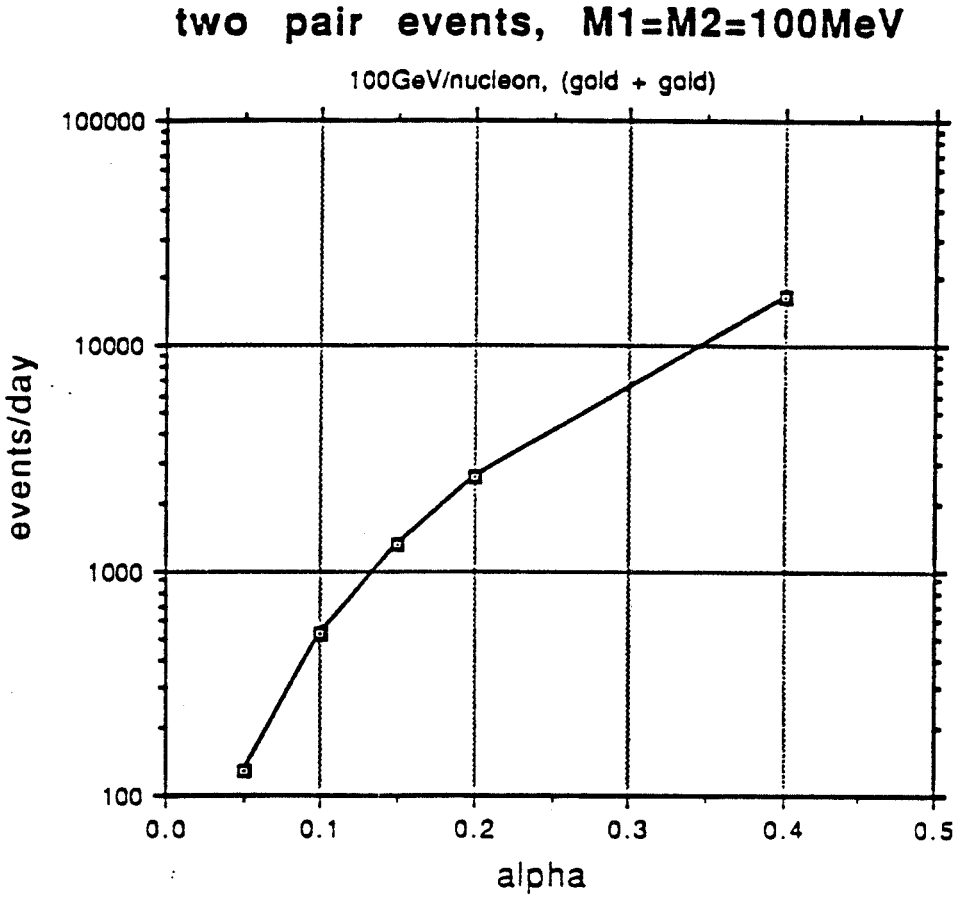
two pair events, M1=M2=100MeV
100GeV/nucleon, (gold + gold)
100000
10000
1000
100
events/day
0.0
0.1
0.2
0.3
0.4
0.5
alpha

fig.6

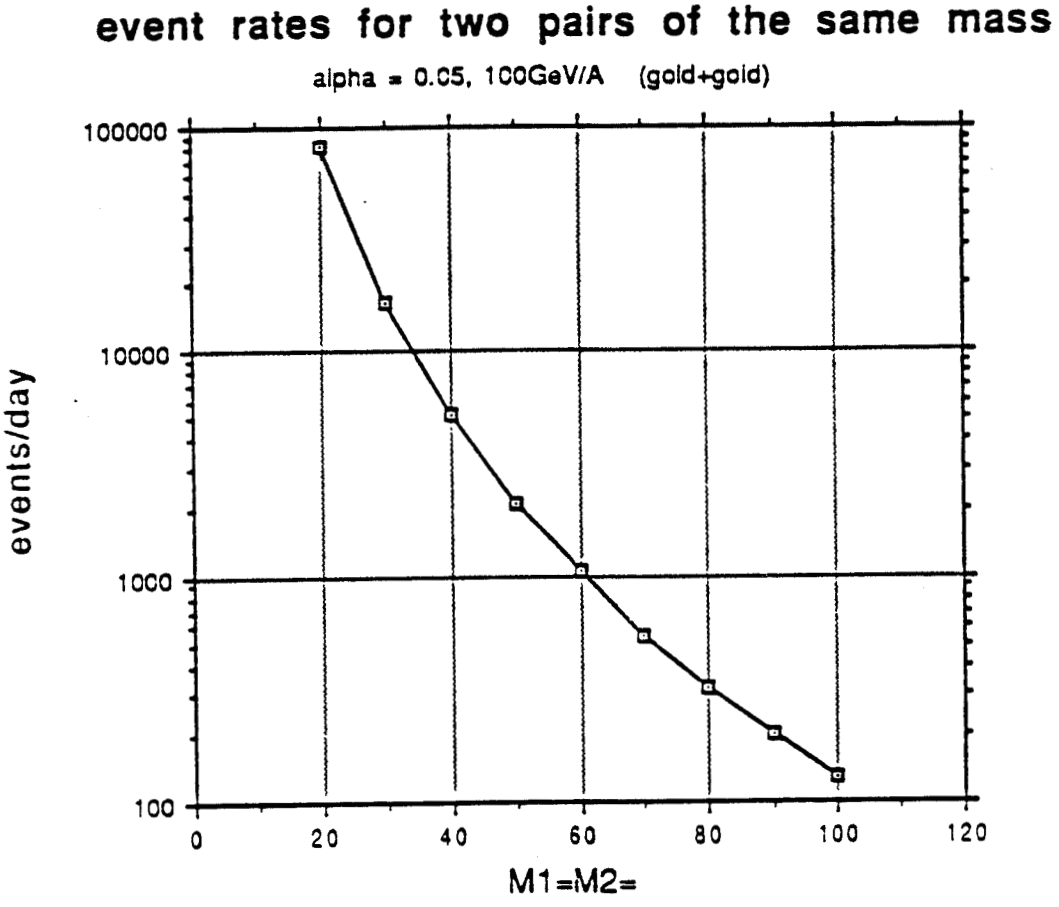
event rates for two pairs of the same mass
alpha = 0.05, 100GeV/A (gold+gold)
events/day
100000
10000
1000
100
0
20
40
60
80
100
120
M1=M2=

fig.7

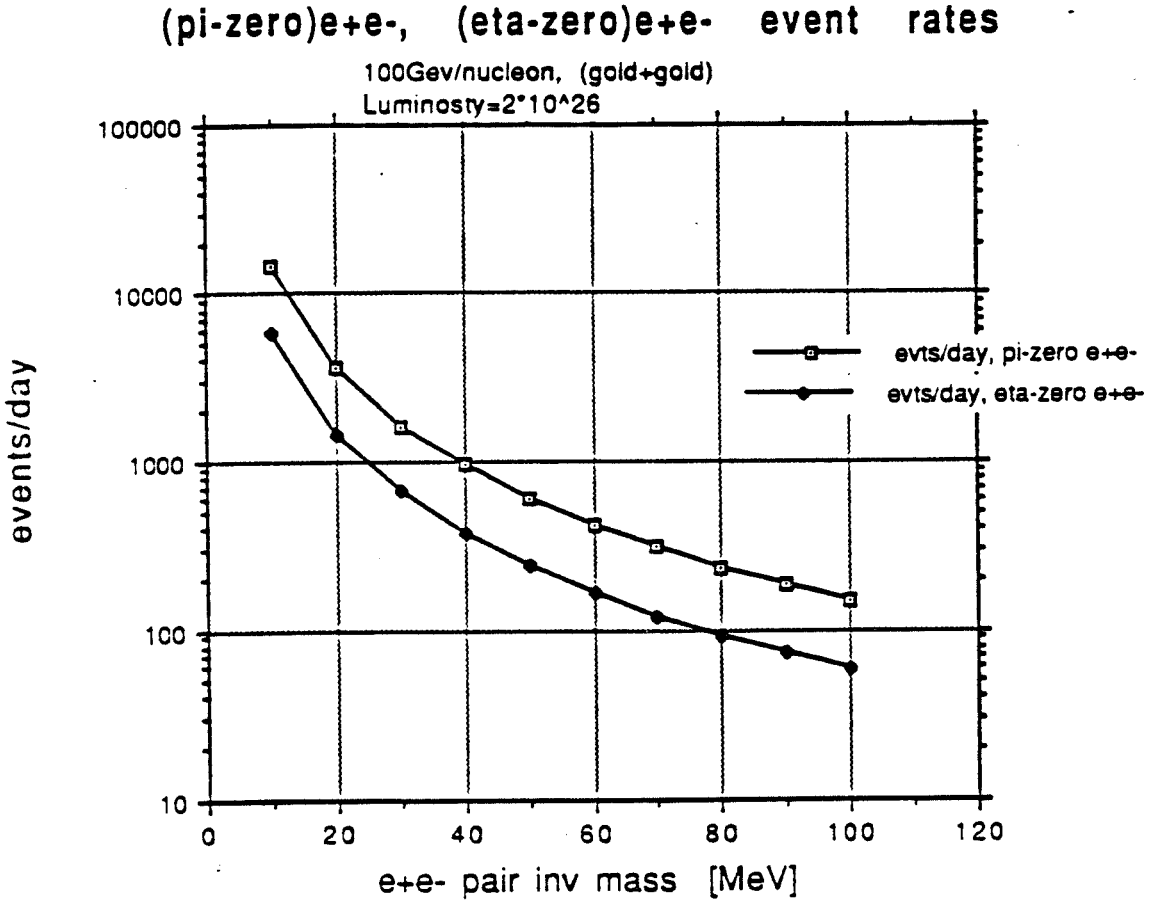
(pi-zero)e+e-, (eta-zero)e+e- event rates
100Gev/nucleon, (gold+gold)
Luminosty=2*10^26
events/day
100000
10000
1000
100
10
0
20
40
60
80
100
120
e+e- pair inv mass [MeV]
evts/day, pi-zero e+e-
evts/day, eta-zero e+e-

fig.8

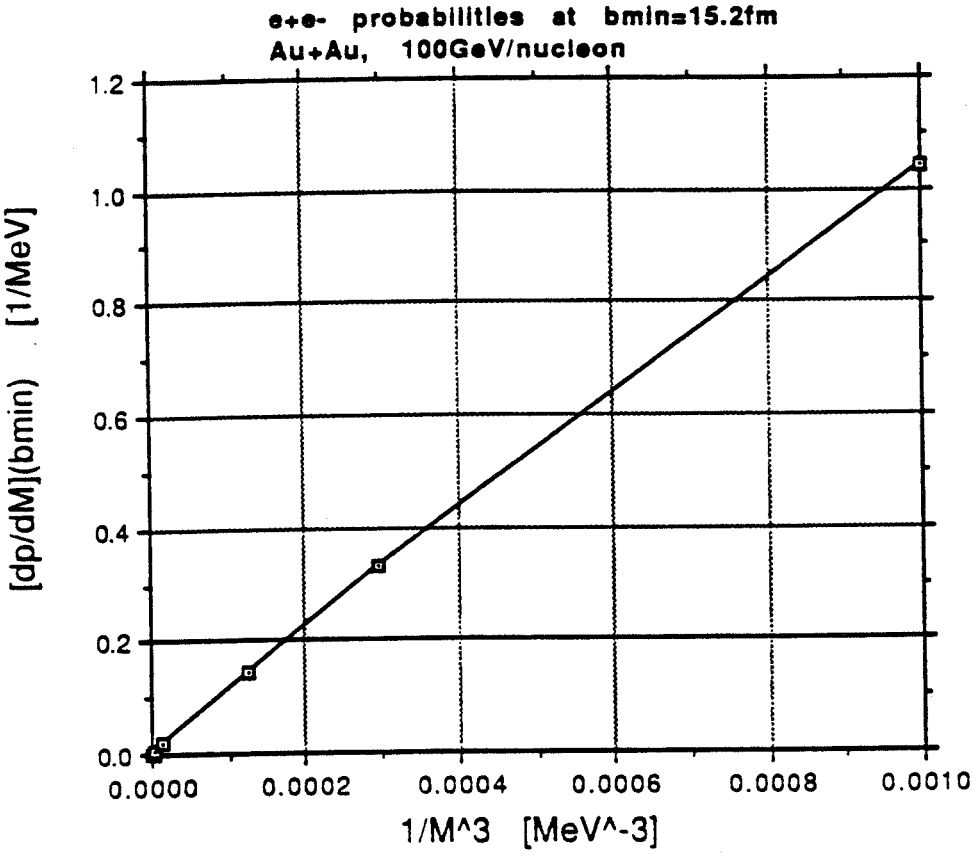
e+e- probabilities at bmin=15.2fm
Au+Au, 100GeV/nucleon
[dp/dM](bmin) [1/MeV]
1.2
1.0
0.8
0.6
0.4
0.2
0.0
0.0000
0.0002
0.0004
0.0006
0.0008
0.0010
1/M^3 [MeV^-3]

fig.9

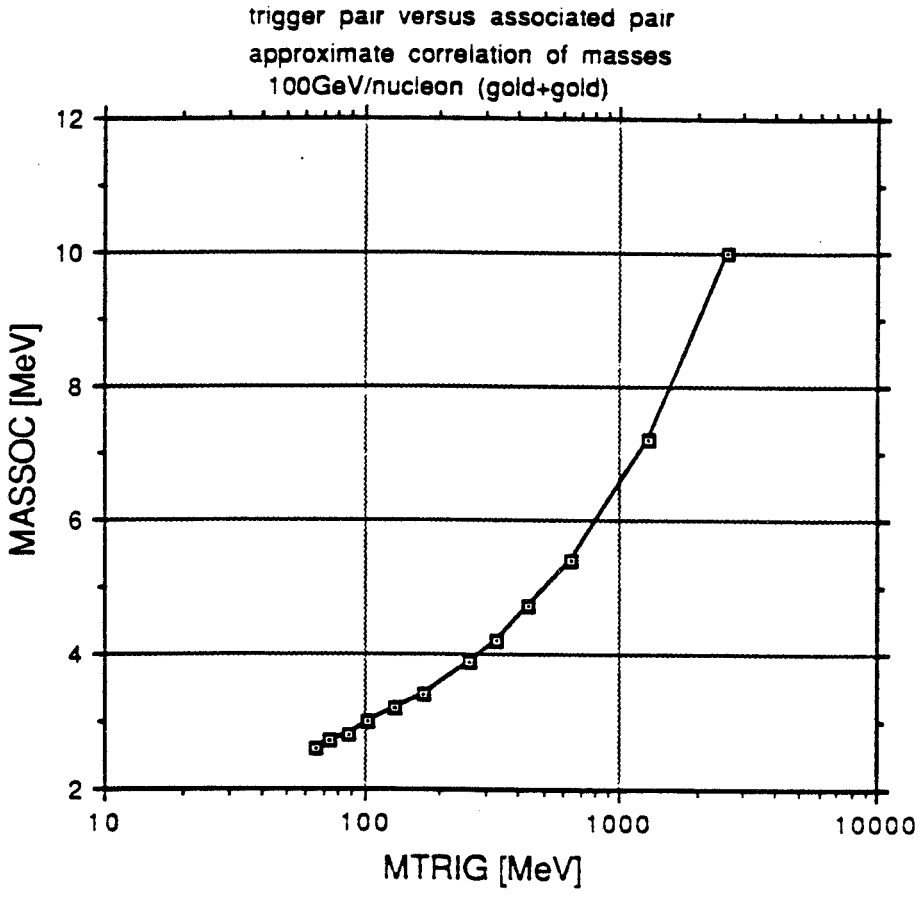
trigger pair versus associated pair
approximate correlation of masses
100GeV/nucleon (gold+gold)
MASSOC [MeV]
MTRIG [MeV]
12
10
8
6
4
2
10
100
1000
10000

fig.10